

Sheffield Hallam University

Arc brazing of austenitic stainless steel to similar and dissimilar metals.

MOSCHINI, Jamie Ian.

Available from the Sheffield Hallam University Research Archive (SHURA) at:

<http://shura.shu.ac.uk/20091/>

A Sheffield Hallam University thesis

This thesis is protected by copyright which belongs to the author.

The content must not be changed in any way or sold commercially in any format or medium without the formal permission of the author.

When referring to this work, full bibliographic details including the author, title, awarding institution and date of the thesis must be given.

Please visit <http://shura.shu.ac.uk/20091/> and <http://shura.shu.ac.uk/information.html> for further details about copyright and re-use permissions.

Adsetts Centre, City Campus
Sheffield S1 1WD

101 968 153 5



Sheffield Hallam University
Learning and IT Services
Adsetts Centre City Campus
Sheffield S1 1WB

REFERENCE

ProQuest Number: 10697398

All rights reserved

INFORMATION TO ALL USERS

The quality of this reproduction is dependent upon the quality of the copy submitted.

In the unlikely event that the author did not send a complete manuscript and there are missing pages, these will be noted. Also, if material had to be removed, a note will indicate the deletion.



ProQuest 10697398

Published by ProQuest LLC (2017). Copyright of the Dissertation is held by the Author.

All rights reserved.

This work is protected against unauthorized copying under Title 17, United States Code
Microform Edition © ProQuest LLC.

ProQuest LLC.
789 East Eisenhower Parkway
P.O. Box 1346
Ann Arbor, MI 48106 – 1346

Arc Brazing of Austenitic Stainless Steel to Similar and Dissimilar Metals

Jamie Ian Moschini

A thesis submitted in partial fulfilment of the requirements of
Sheffield Hallam University
for the degree of Doctor of Philosophy

November 2009

Collaborating Organisations

EPSRC

Outokumpu Stainless Research Foundation

Abstract

There is a desire within both the stainless steel and automotive industries to introduce stainless steel into safety critical areas such as the crumple zone of modern cars as a replacement for low carbon mild steel. The two main reasons for this are stainless steel's corrosion resistance and its higher strength compared with mild steel. It has been anticipated that the easiest way to introduce stainless steel into the automotive industry would be to incorporate it into the existing design. The main obstacle to be overcome before this can take place is therefore how to join the stainless steel to the rest of the car body. In recent times arc brazing has been suggested as a joining technique which will eliminate many of the problems associated with fusion welding of zinc coated mild steel to stainless steel.

Similar and dissimilar parent material arc brazed joints were manufactured using three copper based filler materials and three shielding gases. The joints were tested in terms of tensile strength, impact toughness and fatigue properties. It was found that similar parent material stainless steel joints could be produced with a 0.2% proof stress in excess of the parent material and associated problems such as Liquid Metal Embrittlement were not experienced. Dissimilar parent material joints were manufactured with an ultimate tensile strength in excess of that of mild steel although during fatigue testing evidence of Liquid Metal Embrittlement was seen lowering the mean fatigue load.

At the interface of the braze and stainless steel in the similar material butt joints manufactured using short circuit transfer, copper appeared to penetrate the grain boundaries of the stainless steel without embrittling the parent material. Further microscopic investigation of the interface showed that the penetration could be described by the model proposed by Mullins. However, when dissimilar metal butt joints were manufactured using spray arc transfer, penetration of copper into the stainless steel resulted in embrittlement as discussed by Glickman.

Acknowledgements

The author would like to thank Corus Research and Development, Swinden Laboratories (Rotherham, South Yorkshire) and the Avesta Research Centre (Avesta, Sweden) for their assistance with fatigue testing.

Special thanks to Prof. Alan Smith, Prof. Staffan Hertzman and Dr. David Dulieu for technical guidance, and support.

Thanks also go to the technical staff at Sheffield Hallam University for their guidance throughout the course of the work. In particular Mr R Grant, Mr J Bradshaw, Mr S Magowan, Mr R Tingle, Mr B Didsbury, Mr T O'Hara, Mr J Vickers, Mr M Jackson and Mr S Creasey.

Thanks to Mr S Magowan and Mr D Mallon for their assistance with the practical aspects of impact testing.

Finally thanks go to Mrs S Moschini, Dr E Ashcroft, Mr F Burgin, Dr A Clifton, Ms E Giess, Ms S Pack, Ms K Donovan, Mr D Garrish, Mr A Foster, Mr J Wigley, Mr J Eyre and Mrs M Zagrodnik-Eyre and the author's family for their support and faith in the author's ability when his own was lacking.

Advanced Studies

The following section contains the list of advanced studies undertaken in connection with the course of research.

Publications/Posters

- Arc Brazing of Stainless Steel, Poster Presentation, Materials and Engineering Research Institute Open Day, Sheffield, UK (2004)

Presentations

- Outokumpu Stainless Research Foundation Annual Presentation, Avesta, Sweden (2004, 2005, 2006)
- Sheffield Metallurgical and Engineering Association Lecture Competition, Area Heat, Sheffield, UK (2005)
- Materials and Engineering Institute Seminar, Sheffield, UK (2005)
- Outokumpu Stainless Research Foundation Annual Presentation, Sheffield, UK (2005)

Conferences

- Challenges for Computational Weld Mechanics Research, Trollhättan, Sweden (2005)

Training

- Internal Scanning Electron Microscopy training and competency exam, MERI. (2003)

Secondments

- Six week research secondment to Outokumpu Stainless ARC, Avesta, Sweden. (2006)

Table of Contents

1.0	Introduction	24
1.1	Background	24
1.2	Objective	25
2.0	Literature Review	26
2.1	Parent Materials: Stainless Steel	26
2.1.1	Austenitic Stainless Steels	29
2.1.2	Rephosphorized Zinc Coated Mild Steel.....	33
2.2	Brazing	35
2.2.1	The Arc Brazing Process	38
2.2.2	Advantages and Disadvantages of the Arc Brazing Process	41
2.2.3	Microstructure of Arc Brazed joints.....	46
2.2.4	Gas Metal Arc Brazing Process Variables	48
2.2.4.1	Joint Geometry	48
2.2.4.2	Heat Input	50
2.2.4.3	Shielding Gas.....	52
2.2.4.4	Arc Brazing Filler Material	54
2.3	Residual Stress	57
2.3.1	Residual Stresses in Welding	58
2.4	Fatigue	59
2.4.1	Staircase Fatigue Test.....	59
2.5	Possible Initiation and Failure Modes of Liquid Metal Embrittlement	62
2.6	Summary of Literature	65
3.0	Experimental Procedure	67
3.1	As-Received Material Characterisation: Tensile Testing	67

3.2	Initial Testing of Arc Brazed Similar Metal Butt Joints	68
3.3	Microstructural Characterisation of Arc Brazed Joints with High Joint Efficiency	71
3.3.1	Immersion Test of Stainless Steel into BS:2901 C28 and BS:2901 C9 Braze Alloys.....	72
3.3.2	Microstructural Analysis of Simulated Experimental As-Brazed Alloy	73
3.3.3	Volume Fraction Analysis of Cellular Dendritic Structure	73
3.4	Similar Metal Butt Joints	75
3.4.1	Optimisation of Process Variables to Maximise Joint Tensile Strength	75
3.4.1.1	Optimum Torch Height	75
3.4.1.2	Optimum Torch Velocity.....	75
3.4.1.3	Measuring Arc Characteristics	76
3.4.1.4	Optimisation of Arc Characteristics	77
3.4.1.5	Optimisation of Butt Joint Root Gap.....	78
3.4.1.6	Selection of Braze Filler Material and Shielding Gas Compositions	79
3.4.2	Effect of Braze Seam Geometry on Tensile Properties.....	81
3.4.3	Impact Testing	82
3.4.3.1	Modified Quantitative Chisel Test	82
3.4.4	Fatigue Testing - Similar Metal Butt Joint	86
3.5	Manufacturing Similar Metal Arc Brazed Lap Joints	87
3.6	Dissimilar Butt Joints – Dogal 260RP-x Zinc Coated Mild Steel to AISI 304 Stainless Steel	90

3.6.1	Determination of Process Variables	90
3.6.1.1	Optimisation of Torch Height and Torch Angle	90
3.6.1.2	Optimisation of Torch Velocity.....	90
3.6.1.3	Optimisation of the Arc Characteristics	91
3.6.1.4	Optimisation of Butt Joint Root Gap.....	91
3.6.1.5	Selection of Filler Material.....	91
3.6.2	Fatigue Testing - Dissimilar Metal Butt Joints.....	93
3.7	Scanning Electron Microscopy Measurement of Mullins Grooving	94
3.8	Summary	95
4.0	Results	96
4.1	Material Characterisation	96
4.2	Initial Testing of Similar Metal Butt Joints	97
4.2.1	Comparison of Ultimate Tensile Strengths of Various Combinations of Parent Material, Filler Material and Shielding Gas	97
4.2.2	Microstructural Characterisation of an Arc Brazed Joint with High Joint Efficiency	106
4.2.2.1	Immersion Testing of AISI 304 in Molten BS:2901 C9 Braze Alloy	119
4.2.2.2	Experimental melt of AISI 304 in BS:2901 C28 Molten Filler Metal at 1600°C	121
4.2.2.3	Volume Fraction of Cellular Dendritic Structure in joints produced using BS:2901 C28 filler material and Pure Argon, Argon Containing 1% oxygen and Argon Containing 2% Oxygen Shielding Gases	122
4.3	Similar Metal Butt Joints – AISI 304 to AISI 304	125

4.3.1	Determination of Optimum Process Variables	125
4.3.1.1	Optimisation of Torch Height.....	125
4.3.1.2	Optimisation of Torch Velocity.....	125
4.1.3.3	Optimisation of Arc Characteristics	125
4.3.1.4	Similar Metal Butt Joint Root Gap	126
4.3.1.4.1	Penetration and Aesthetic Quality	126
4.3.1.4.2	Effect of Varying Butt Joint Root Gap on Tensile Properties ..	131
4.3.1.4.3	Microstructural investigation.....	148
4.3.1.5	Selection of Filler Material and Shielding Gas for Similar Metal Butt Joints.	150
4.3.2	Effect of Braze Seam Geometry on the Tensile Properties of Nine Filler Material and Shielding Gas Combinations	158
4.4	Impact Testing of Similar Metal Modified Impact Test Samples	166
4.4.1	Wetting of Parent Material	166
4.4.2	Modified Quantitative Impact Test Result	169
4.5	Similar Metal Lap Joints	174
4.5.1	Tensile Properties	174
4.5.2	Microstructural Investigation of Similar Metal Arc Brazed Lap Joints	179
4.6	Optimisation of Process Parameters for Dissimilar Metal Butt Joints – Dogal 260RP-x to AISI 304	181
4.6.1	Optimisation of Torch Angle and Torch Height	181
4.6.2	Optimisation of Root Gap.....	182
4.6.3	Optimisation of Torch Velocity.....	184

4.6.4	Optimisation of Arc Characteristics	187
4.6.5	Dissimilar Metal Butt Joints Tensile Properties	188
4.7	Fatigue Testing Results for Similar and Dissimilar Metal Joints Using Optimised Arc Brazing Process Parameters	189
4.7.1	Similar Metal Butt Joints.....	189
4.7.2	Dissimilar Metal Butt Joints.....	189
4.8	Mullins Grooving	194
4.8.1	Similar Material Joints.....	194
4.8.2	Dissimilar Material Joint Braze / Stainless Steel Interface	197
4.9	Summary of Results	199
5.0	Discussion of Results	202
5.1	Parent Material Characterisation	202
5.2	Initial Mechanical Testing of Similar Metal Arc Brazed Butt Joints	205
5.2.1	Arc Brazed AISI 304 Grade Similar Metal Butt Joints Using BS:2901 C9 and BS:2901 C28 Filler Materials and Pure Argon and Argon Containing 2% Oxygen Shielding Gases.....	205
5.2.2	Arc Brazed AISI 316 Grade Similar Metal Butt Joints Using BS:2901 C9 and BS:2901 C28 Filler Materials and Pure Argon and Argon Containing 2% Oxygen Shielding Gases.....	206
5.2.3	Microstructural Characterisation of an Arc Brazed Joint with High Joint Efficiency.....	207
5.2.3.1	Immersion of AISI 304 Stainless Steel into BS:2901 C9 Braze Alloy	209
5.2.3.2	Experimental Melting of Stainless Steel into BS:2901 C28 Braze Alloy	210

5.2.3.3	Volume Fraction Analysis of Cellular Dendritic Structure	212
5.3	Determination of Arc Brazing Process Variables	214
5.3.1	AISI 304 Similar Metal Butt Joints	214
5.3.1.1	The Affect of Torch Height on the Arc Brazing Process	214
5.3.1.2	Effect of the Changes in the Composition of the Shielding Gas	215
5.3.1.3	The Effect of Butt Joint Root Gap on Mechanical and Aesthetic Properties of Similar Metal Butt Joints	217
5.3.1.3.1	The Effect of Increasing Butt Joint Root Gap on Aesthetic Appearance of Similar Metal Butt Joints.....	217
5.3.1.3.2	The Effect of Increasing Butt Joint Root Gap on Tensile Properties of Similar Metal Butt Joints	218
5.3.1.4	Selection of Shielding Gas and Filler Material Similar Metal Butt Joints with a Root Gap of 0.5mm	220
5.3.2	Dissimilar Metal Butt Joints – AISI 304 Stainless Steel to Dogal 260 RP-x Zinc Coated Mild Steel.....	222
5.3.2.1	The Affect of Process Variables on the Arc Brazing Process ..	222
5.3.2.1.1	The Effect of Torch Angle and Height on the Wetting and Aesthetic Properties of Dissimilar Material Arc Brazed Butt Joints.....	222
5.3.2.1.2	Optimisation of Root Gap for Dissimilar Metal Butt Joints.....	222
5.3.2.1.3	Optimisation of Torch Velocity for Dissimilar Metal Butt Joints..	223
5.3.2.1.4	Optimisation of Arc Variables for Dissimilar Metal Butt Joints....	223

5.3.2.1.5 Selection of Filler Material for Dissimilar Metal Joints Tensile Specimens.....	224
5.3.2.1.6 Tensile Properties of Dissimilar Metal Joints.....	224
5.4 Effect of Braze Seam Geometry on the Tensile Properties of Similar Metal Butt Joints	226
5.5 Impact Testing of Similar Metal Plug Brazed Joints Manufactured Using BS:2901 C9, BS:2901 C11 and BS:2901 C28 Filler Materials and Pure Argon, Argon Containing 1% Oxygen and Argon Containing 2% Oxygen Shielding Gases	227
5.5.1 Wetting of the Parent Material	227
5.5.2 Modified Quantitative Chisel Test of Arc Brazed Plug Joints .	228
5.6 Fatigue Testing of Similar and Dissimilar Metal Arc Brazed Butt Joints	231
5.7 Arc Brazed Similar Metal Lap Joints	235
5.7.1 Effect of Overlap on the Tensile Properties of Similar Metal Arc Brazed Lap Joints	235
5.7.2 Microstructural Investigation of Wetting of the Parent Material of Arc Brazed Similar Metal Lap Joints	235
5.7.3 Effect of Torch Angle On The Wetting of Parent Material of Similar Metal Arc Brazed Lap Joints	236
5.8 Liquid Metal Embrittlement - Mullins Grooving	238
5.9 Summary of Discussion of Results	243
6.0 Conclusions	249
6.1 Summary	251
7.0 Further Work	253

APPENDIX 1	255
Optimal Process Parameters For the Manufacture of Similar and Dissimilar Metal Butt Arc Brazed Butt Joints Using AISI 304 Parent Material and Various Combination of Filler Material and Shielding Gases	255
Similar Metal Butt Joints:.....	256
Dissimilar Metal Butt Joints	265
APPENDIX 2	267
Volume Fraction Images	267
Sample 65 (BS:2901 C28 filler material argon containing 1% oxygen).	268
Sample 67 (BS:2901 C28 filler material argon containing 1% oxygen).	271
Sample 69 (BS:2901 C28 filler material and argon containing 2% oxygen)	274
References	277

Table of Figures

Figure 2.1 - Comparison of Stress Strain Curves of Stainless Steels ⁶	28
Figure 2.2 - Schaeffler Delong Diagram	29
Figure 2.3 - Schematic diagram of a gas metal arc brazing torch modified from ¹⁵	38
Figure 2.4i - Butt Joint Configuration	48
Figure 2.4ii - Lap Joint Configuration.....	48
Figure 2.5 - Waveforms produced using a pulsed current input. (These waveforms are recorded using arc monitoring equipment (the Arc Logger 10 and Arclog Software manufactured by the Validation Centre)).....	51
Figure 2.6 - Schematic diagram showing that an increasing oxygen content in the shielding gas leads to an increase in thermal conductivity and a decrease in the conductive core of the arc.....	53
Figure 2.7 – Distribution of Residual Stresses in a Welded Butt Joint	58
Figure 2.8 – Gradient used as m in Mullins Model	63
Figure 3.1 - Dimensions of flat test piece.....	67
Figure 3.2a – Unbrazed sample blanks.....	69
Figure 3.2b – Brazed samples.....	69
Figure 3.3 – Schematic Diagram of the BOC HW75 Tractor at Sheffield Hallam University	76
Figure 3.4 – Schematic diagram of the Arc Logger Ten (ALX)	77
Figure 3.5 – Dog bone tensile test piece (butt joint)	79
Figure 3.6 - Plug Braze Lap Shear Specimen.....	83
Figure 3.7 – Modified arc brazed joint, diagram modified from ⁶²	84
Figure 3.8 – Similar Metal Butt Joint Fatigue Test Sample	86
Figure 3.9i – Joint geometry of a single seam lap joint.....	88

Figure 3.9ii – Joint geometry of a double seam lap joint	88
Figure 3.10 – Lap joint dog bone tensile test piece.	88
Figure 3.11 - Orientation of GMAB Torch during Manufacture of Similar Lap Joints	89
Figure 3.12 – Dissimilar Metal Butt Joint Fatigue Test Sample	93
Figure 4.1 - Comparison of tensile strengths for joints constructed from combinations of BS:2901 C9 and BS:2901 C28 filler materials; argon and argon containing 2% oxygen and 316 stainless steel base material.....	102
Figure 4.2 - Comparison of tensile strengths for joints constructed from combinations of BS:2901 C9 and BS:2901 C28 filler materials; argon and argon containing 2% oxygen and 304 stainless steel base material.....	103
Figure 4.3 - Comparison of percentage elongations of joints constructed from combinations of BS:2901 C9 and BS:2901 C28 filler materials; argon and argon containing 2% oxygen and 316 stainless steel base material.	104
Figure 4.4 - Comparison of percentage elongations of joints constructed from combinations of BS:2901 C9 and BS:2901 C28 filler materials; argon and argon containing 2% oxygen and 304 stainless steel base material	105
Figure 4.5 - Optical light micrograph taken at the joint interface of a sample manufactured from AISI 304 stainless steel parent material, brazed with BS:2901 C9 braze alloy and pure argon shielding gas etched in alcoholic ferric chloride. Tensile testing results showed no elongation.	106
Figure 4.6 - Sample manufactured from AISI 304 stainless steel parent material, brazed with BS:2901 C9 braze alloy and pure argon shielding gas etched in alcoholic ferric chloride. Tensile testing results showed no elongation.....	108

- Figure 4.7 – Optical light micrograph taken at the joint interface of a sample manufactured from AISI 304 stainless steel parent material, brazed with BS:2901 C28 braze alloy and argon containing 2% oxygen shielding gas etched alcoholic ferric chloride. 110
- Figure 4.8 – Sample manufactured from AISI 316 stainless steel parent material, brazed with BS:2901 C28 braze alloy and argon containing 2% oxygen shielding gas etched alcoholic ferric chloride, showing a cellular dendritic structure composed of iron within the braze microstructure. 112
- Figure 4.9 - Low magnification image of a sample with low joint efficiency manufactured from AISI 304 stainless steel parent material, brazed with BS:2901 C9 braze alloy and pure argon shielding gas dual etched in alcoholic ferric chloride and electro-etched in 10% oxalic acid. 114
- Figure 4.10 - High magnification using secondary electron imaging of the microstructure of the possible intermetallic region in figure 4.9. 115
- Figure 4.11 - Low magnification scanning electron microscopy secondary electron image of a sample with high joint efficiency manufactured from AISI 304 stainless steel parent material, brazed with BS:2901 C28 braze alloy and argon containing 2% oxygen shielding gas dual etched in alcoholic ferric chloride and electro-etched in 10% oxalic acid. 116
- Figure 4.12 - High magnification scanning electron micrograph (secondary electron image) of the intermetallic region in figure 4.11 dual etched in alcoholic ferric chloride and electro-etched in 10% oxalic acid and x-ray maps showing the distribution of copper and iron. 117
- Figure 4.13i – Secondary electron image of AISI 304 stainless steel strip after immersion in BS:2901 C9 braze alloy. 119

Figure 4.13ii – X-ray maps produced by EDX of image in figure 4.13i showing diffusion of iron, chromium and silicon into the copper of the braze alloy.	120
Figure 4.14 - As polished structure of an alloy composed of 10% 304 stainless steel and 90% BS:2901 C28 braze alloy showing similar cellular dendritic structures to those seen in arc brazed joints.	121
Figure 4.15 – Tensile strength of arc brazed butt joints compared to volume fraction of iron rich cellular dendritic structures present in the microstructure.....	124
Figure 4.16i - Front view of a joint brazed using BS:2901 C28 filler material and argon containing 2% oxygen shielding gas with a 0.1mm root gap.	126
Figure 4.16ii - Rear view of a joint brazed using BS:2901 C28 filler material and argon containing 2% oxygen shielding gas with a 0.1mm root gap	127
Figure 4.17i - Front view of a joint brazed using BS:2901 C28 filler material and argon containing 2% oxygen shielding gas with a 0.6mm root gap	128
Figure 4.17ii - Rear view of a joint brazed using BS:2901 C28 filler material and argon containing 2% oxygen shielding gas with a 0.6mm root gap.....	128
Figure 4.18i - Front view of a joint brazed using BS:2901 C28 filler material and argon containing 2% oxygen shielding gas with a 0.8mm root gap.	130
Figure 4.18ii - Rear view of a joint brazed using BS:2901 C28 filler material and argon containing 2% oxygen shielding gas with a 0.8mm root gap	130
Holes caused by the root gap being too large	130
Figure 4.19 - Comparison of the effect of varying braze root gaps on the tensile strength of butt joints constructed using BS:2901 C28 filler material and argon containing 2% oxygen compared with the as received material tensile strength.	138

- Figure 4.20 - Comparison of the effect of varying braze root gaps on the 0.2% proof stress of butt joints constructed using BS:2901 C28 filler material and argon containing 2% oxygen compared with the as received parent material 0.2% proof stress. 139
- Figure 4.21 - Comparison of the effect of varying braze gaps on the tensile strength of butt joints constructed using BS:2901 C28 filler material and pure argon shielding gas compared with the as received material tensile strength. 140
- Figure 4.22 - Comparison of the effect of varying braze root gaps on the 0.2% proof stress of butt joints constructed using BS:2901 C28 filler material and pure argon shielding gas compared with the as received parent material 0.2% proof stress. 141
- Figure 4.23 - Comparison of the effect of varying braze root gaps on the tensile strength of butt joints constructed using BS:2901 C9 filler material and pure argon shielding gas compared with the as received material tensile strength.. 142
- Figure 4.24 - Comparison of the effect of varying braze root gaps on the 0.2% proof stress of butt joints constructed using BS:2901 C9 filler material and pure argon shielding gas compared with the as received parent material 0.2% proof stress. 143
- Figure 4.25 - Comparison of the effect of varying braze gaps on the tensile strength of butt joints constructed using BS:2901 C9 filler material and argon containing 2% oxygen compared with the as received material tensile strength..... 144
- Figure 4.26 - Comparison of the effect of varying braze gaps on the 0.2% proof stress of butt joints constructed using BS:2901 C9 filler material and argon containing 2% oxygen compared with the as received parent material 0.2% proof stress. 145

Figure 4.27 - Comparison of Filler Material and Shielding Gas Combinations with a 0.5mm Gap Prior to Brazing..... 146

Figure 4.28 - Comparisons of Filler Material and Shielding Gas Combinations with a 0.5mm Gap Prior to Brazing..... 146

Figure 4.29 - Liquid metal embrittlement as found adjacent to sample BGT25c brazed using BS:2901 C28 filler material and pure argon shielding gas shielding gas. 148

Figure 4.30 - Comparison of 0.2% proof stresses for various combinations of filler material and shielding gas for joints using 304 parent material with a root gap of 0.5mm 155

Figure 4.31 – Comparison of the ultimate tensile strength for various combinations of filler material and shielding gas for joints using 304 parent material with a root gap of 0.5mm..... 156

Figure 4.32 - Comparison of extensions at failure for various combinations of filler material and shielding gas for joints using 304 parent material and a root gap of 0.5mm 157

Figure 4.33 - Comparison of maximum loads experienced prior to failure by ground and unground butt joints manufactured using 304 parent material and various combinations of filler material and shielding gas..... 163

Figure 4.34 – Comparison of loads experienced at yield by ground and unground butt joints manufactured using 304 parent material and various combinations of filler material and shielding gas. 164

Figure 4.35 – Comparison of total extensions at failure of ground and unground butt joints manufactured using 304 parent material and various combinations of filler material and shielding gas. 165

Figure 4.36 - Plug braze manufactured using BS:2901 C28 filler material and pure argon shielding gas showing complete wetting of the upper and lower plate... 166	166
Figure 4.37 - Plug braze manufactured using BS:2901 C11 filler material and argon containing 1% oxygen shielding gas showing incomplete wetting of the lower plate. 167	167
Figure 4.38 - Lap shear sample showing braze pull-out failure of an arc brazed plug joint..... 168	168
Figure 4.39 - Lap shear sample showing braze pull-out failure of an arc brazed plug joint..... 168	168
Figure 4.40 – Impact energies achieved for similar metal impact test samples which have been joined using 3 different filler metals, 3 different shielding gas combinations and 6mm and 8mm resistance spot welds..... 173	173
Figure 4.41 - Loads at yield for lap joints manufactured using BS:2901 C28 filler material and argon containing 1% oxygen compared with butt joints manufactured using the same consumables..... 177	177
Figure 4.42 - Maximum loads prior to failure supported by lap joints manufactured from BS:2901 C28 filler material and argon containing 1% oxygen shielding gas compared with butt joints manufactured using the same consumables..... 178	178
Figure 4.43 - Interface between braze material and top sheet of the similar metal lap joint..... 179	179
Figure 4.44 - Interface between braze material and bottom sheet of the similar metal lap joint..... 180	180
Figure 4.45 - Orientation of GMAB Torch during Manufacture of Dissimilar Butt Joints..... 181	181

Figure 4.46 - Braze seam reinforcement with 0.5mm root gap joining AISI 304 grade stainless steel to Dogal 260RP-x.	182
Figure 4.47 - Braze seam reinforcement with 0.6mm gap joining AISI 304 grade stainless steel to Dogal 260RP-x	183
Figure 4.48i - Braze seam reinforcement with $88.9\text{cm}\cdot\text{min}^{-1}$ torch velocity showing a neat, uniform braze seam.....	184
Figure 4.48ii - Rear view of brazed joint with $88.9\text{cm}\cdot\text{min}^{-1}$ torch velocity showing complete penetration by the braze alloy	184
Figure 4.49i - Braze seam reinforcement with $96.5\text{cm}\cdot\text{min}^{-1}$ torch velocity with unacceptable appearance	185
Figure 4.49ii - Rear view of brazed joint with $96.5\text{cm}\cdot\text{min}^{-1}$ torch velocity showing inadequate penetration of the joint.	185
Figure 4.50 – Optical microscopy image of a band at the interface between the mild steel and BS:2901 C28 braze alloy joined using argon containing 1% oxygen shielding gas.	190
Figure 4.51 – SEM Image of band between the BS:2901 C28 braze alloy and mild steel.....	191
Figure 4.52 – Spectrum of Spot Analysis of Area Highlighted in Figure 4.51.	192
Figure 4.53 – Failed dissimilar metal butt joint showing evidence of LME at the interface of the stainless steel and BS:2901 C28 braze alloy.	193
Figure 4.54 - SEM image showing grain boundary grooving of AISI 304 grade stainless steel in a butt joint brazed using BS:2901 C28 filler material and argon containing 1 % oxygen shielding gas.	195

Figure 4.55 - Interface of stainless steel and braze in a dissimilar parent material butt joint manufactured from AISI 304 and Dogal 260RP-x parent materials, BS:2901 C28 filler material and argon containing 1% oxygen shielding gas..... 198

Figure 5.1 - Schaeffler Delong Diagram⁸ showing the expected microstructure for AISI grade 316 stainless steel..... 203

Figure 5.2 - Schaeffler Delong Diagram⁸ showing the expected microstructure for AISI grade 304 stainless steel..... 204

Figure 5.3 – Backscattered electron volume fraction image (at magnification x1000) showing suspected porosity in a braze microstructure manufactured using BS:2901 C28 filler material and argon containing 1% oxygen shielding gas... 213

Figure 5.4 – Optical image of spherical inclusion within the braze microstructure of a joint manufactured using BS:2901 C28 filler material and argon containing 1% oxygen shielding gas. 213

Tables:

Table 2.1 – Mechanical and Thermal Properties of AISI grade 304 and 316 Stainless Steel and Mild Steel.....	45
Table 2.2 – Chemical compositions, ultimate tensile strength and melting point of the filler materials investigated ⁴⁵	56
Table 2.3 - Example of Staircase Fatigue Test Results	60
Table 3.1 - Chemical Compositions of AISI 304 and AISI 316 ³⁶	69
Table 3.2 – Combinations of filler materials and shielding gases tested	80
Table 3.3 - Plug Braze Lap Shear Sample Dimensions.....	83
Table 3.4 – Quantitative Arc Braze impact test samples dimensions.....	84
Table 4.1 - Tensile Properties of AISI 316 and 304 Stainless Steel.....	96
Table 4.2 - Tensile Properties of Arc Brazed Butt Joints.....	101
Table 4.3 – Volume Fraction of iron and chromium rich grains found in the microstructures of arc brazed joints.....	123
Table 4.4 – Optimum torch velocities for respective shielding gases when manufacturing butt joints using AISI 304 parent material.	125
Table 4.5 - Tensile properties of arc brazed butt joints with varying root gaps between 0.4mm and 0.6mm.....	137
Table 4.6 – Comparison of Tensile Properties of Filler Materials and Shielding Gases	154
Table 4.7 - Comparison of Tensile Properties of Unground Butt Joints	162
Table 4.8 - Impact Properties of Arc Plug Brazes	172
Table 4.9 – Tensile Properties of Arc Brazed Lap Joints	176

Table 4.10 - Tensile properties of dissimilar metal arc brazed butt joints manufactured from AISI 304 and Dogal 260RP-x parent materials, BS:2901 C28 filler material and argon containing 1% oxygen shielding gas	188
--	-----

Table 4.11 - Depth of penetration of copper from the braze-stainless steel interface for similar material butt joints brazed using BS:2901 C28 filler material and argon containing 1% oxygen shielding gas.	196
---	-----

1.0 Introduction

1.1 Background

There is a desire within both the stainless steel and automotive industries to introduce stainless steel into safety critical areas, such as the crumple zones, of modern cars as a replacement for low carbon mild steel. The two main reasons for this are stainless steel's corrosion resistance and its higher strength compared with mild steel. It has been anticipated that the easiest way to introduce stainless steel into the automotive industry would be to incorporate it into the existing design. The main obstacle to be overcome before this can take place is, therefore, how to join the stainless steel panels to the rest of the car body.

In recent times in the automotive industry there has been an increasing interest in brazing processes as an alternative joining method to conventional fusion welding. The first reason for this is that, on external joints, brazing processes can offer a better cosmetic finish to the traditional spot welded lap joint¹. The second reason is associated with the difficulties of welding zinc coated mild steel; zinc coated steel is routinely used in the manufacture of cars to provide the requisite corrosion protection in those areas most susceptible to attack. Zinc melts at a temperature of 419°C and turns to vapour 907°C; mild steel, however, does not melt until ~1500°C. The zinc vapour produced during the weld thermal cycle can lead to²:

- *Porosity*
- *Lack of fusion*
- *Increased spatter levels (in gas metal arc welding) due to the unstable arc*

The spatter produced by the unstable arc necessitates increased cleaning of the joint². Gas metal arc welding of galvanised steel also produces fumes which can be damaging to the health of the welder³.

A relatively new and innovative method of joining metals using braze material is the arc brazing process. This uses the heat of an electric arc to melt the filler material. Significant improvements in the levels of control now available in gas metal arc joining offers new opportunities for the application of the arc brazing process to dissimilar metal joining.

A feasibility study into arc brazing has been conducted at Sheffield Hallam University⁴ the results of which show that it is possible to fabricate joints capable of withstanding adequate tensile stresses using the process.

1.2 Objective

To develop an arc brazing process capable of joining stainless steel to itself and to dissimilar metals, with aesthetic and mechanical properties acceptable for use in the automotive industry.

2.0 Literature Review

2.1 *Parent Materials: Stainless Steel*

Iron – Chromium alloys were in use as early as the late 19th century without the realisation of their full potential⁵. The discovery of stainless steel is generally accredited to the Sheffield Metallurgist Harry Brearly. Brearly was working on the development of an abrasive wear resistant material for firearm barrels^{5, 6}. During this work he found a 0.3% C, 13% Cr steel that was both difficult to etch and which did not rust in the laboratory environment⁵.

During the same period researchers in Germany working for the Krupp Company were responding to pressures from the chemical industry for improvements in steel properties⁵. Benno Strauss and Eduard Maurer are credited with the discovery of austenitic stainless steels⁵ and patents on the Cr – Ni materials were registered in 1912⁵.

Despite developments, in the 1950s stainless steels were still regarded as a semi-precious metal and priced accordingly⁵. In the 1960s stainless steel was still produced in small electric arc furnaces in a one stage process that involved melting nickel, ferro-chrome and scrap, with production times in excess of three and half hours⁵.

Advances in technology have meant that since the 1970s stainless steel has been produced in higher volumes in a two stage process. The first stage is the melting of scrap and iron alloys in an electric arc furnace, with high carbon ferro-chrome as the

main source of chromium⁵. The second stage involves refinement of the high carbon melt using either an Argon – Oxygen Decarburizer (AOD) or Blowing Oxygen Under Vacuum (VOD)⁵. Combined with the adoption of continuous casting, substantial cost savings have been made so reducing the price of stainless steel⁵.

There are five main categories of stainless steel:

- Martensitic
- Ferritic
- Austenitic
- Duplex
- Precipitation Hardened

As their names suggest, the first four types of stainless steel have different microstructures and therefore different mechanical properties, as can be seen in figure 2.1.

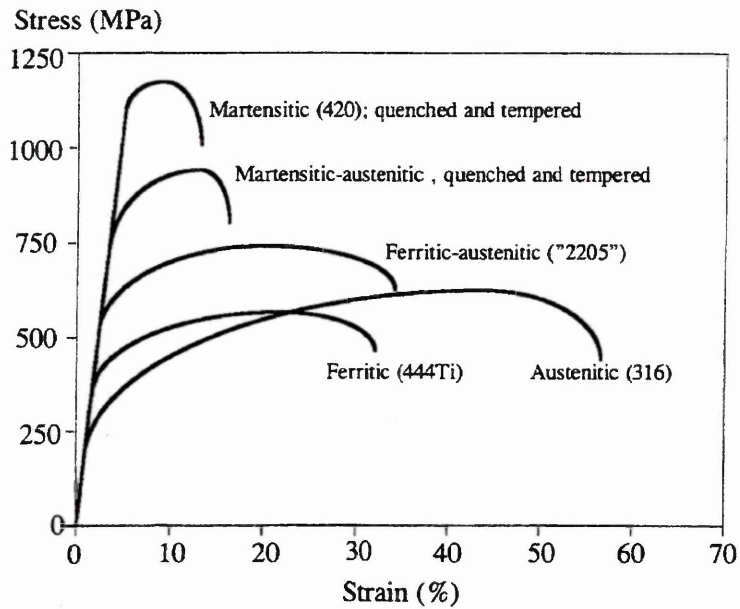


Figure 2.1 - Comparison of Stress Strain Curves of Stainless Steels⁶

The corrosion resistance of stainless steel increases with chromium content from around 11% up to 18%⁶. When in the presence of an oxidising agent, the chromium in the steel reacts creating what is known as a passive layer which prevents further oxidation. As long as the steel is in an oxidising environment, the layer is self repairing⁶.

2.1.1 Austenitic Stainless Steels

The affect that alloying additions have on the microstructure and properties of a given steel can be broadly divided into two, depending on whether they stabilise the austenitic or ferritic phase field. Chromium is a ferrite stabiliser and so promotes a ferritic microstructure. Nickel, on the other hand, is an austenite stabiliser and can promote an austenitic microstructure even at room temperature. All the elements routinely added to stainless steel have been categorised in this way by Schaeffler and an empirical formula and Schaeffler diagram have been produced (fig 2.2). Some elements are considerably more effective at stabilising the austenite phase field and, due to the high price of nickel, other elements such as carbon, nitrogen and manganese may be used to promote the austenite formation⁷.

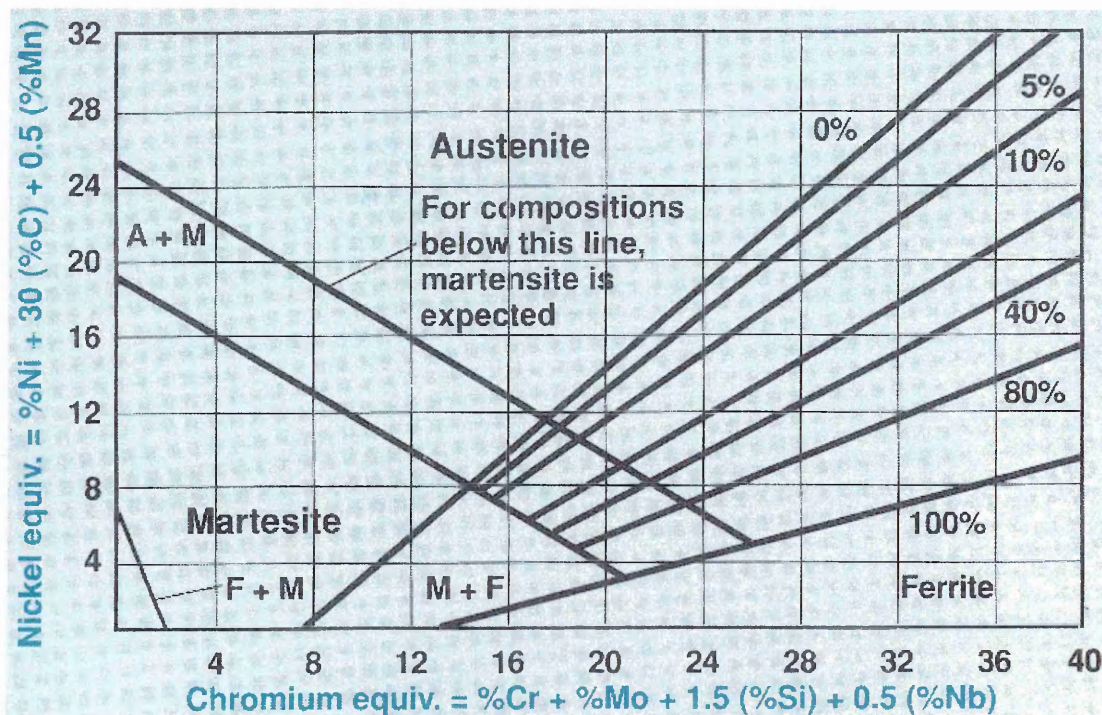


Figure 2.2 - Schaeffler Delong Diagram⁸

Both nitrogen and carbon are very strong austenite stabilisers, and are both interstitial solutes in austenite resulting in them being extremely effective solid solution strengtheners of austenitic stainless steels⁹. However, of these two alloying elements, nitrogen is more useful due to its lower tendency to cause intergranular corrosion, and its beneficial effect on mechanical properties; with as little as 0.25wt% of nitrogen resulting in a doubling of the proof stress of an austenitic stainless steel⁹.

Within the microstructure of austenitic stainless steel the grain size is not as important as twin spacing in controlling the tensile strength of the material¹⁰. This is because of the effect that the stacking fault energy has on work hardening. However, twin spacing has no effect on the proof stress of the material because stacking fault energy has little effect at the low strains around the proof stress value¹⁰. The tensile strength may also be affected by the environment. Contamination near to the surface, from oxidation or carburisation, can result in a reduction in tensile strength in thin sections¹⁰.

Austenitic stainless steel cannot be hardened except by cold working and unlike ferritic steels they are not magnetic⁶. As austenitic stainless steels cannot be hardened by heat treatment¹¹, the thermal cycle of joining process will have little effect on the mechanical properties of the parent material. They are also generally regarded as being readily weldable although they can suffer from a number of detrimental effects such as:

- Hot cracking due to stresses built up during contraction upon solidification^{5, 12}.
- Forms of liquation cracking in the weld metal and heat affected zone (HAZ) if low melting point phases such as borides are present¹².

- Carbide precipitation at grain boundaries¹².

Solidification cracking occurs in weld metal as it is about to solidify. This is a result of the high co-efficient of thermal expansion generating high contraction stresses⁵. The contraction stresses pull the crystals apart whilst still being surrounded in liquid metal resulting in interdendritic cracking⁵. It is therefore promoted by low melting point elements which will remain in the liquid state for longer during solidification⁵.

Sensitisation

Between 500°C and 800°C the chromium in an austenitic stainless steel will start to form chrome carbides (Cr_{23}C_6)¹³ which can lead to embrittlement and intergranular corrosion¹³. The carbides form because the solubility limit of carbon in austenitic stainless steels reduces with temperature. At 1100°C the solubility limit of carbon in stainless steel is 0.5wt%, but with a reduction of 300°C this has reduced to 0.05wt%⁹. Due to their different sizes chromium (atomic no. 24) moves much slower than carbon (atomic no. 6)¹⁴, this means that when carbides are formed at grain boundaries the carbon will have been drawn from all over the grain, whereas the chromium will have been drawn from the regions close to the grain boundary¹⁴. In addition to this for every 6 atoms of carbon there are 23 atoms of chromium required to form the carbides⁹. This local depletion of chromium will prevent the formation of the passive layer¹⁵ and a loss of corrosion resistance leading to intergranular corrosion, which in severe cases can lead to disintegration of the steel⁹.

In production different methods are employed to overcome the problem of carbide formation. By heating the steel to between 1050°C and 1150°C all the carbon will be

The Brazing of Austenitic Stainless Steel to Similar and Dissimilar Metals Literature Review

taken into solution, rapid cooling by quenching will result in a supersaturated austenitic stainless steel as the carbides will not have had time to form at the grain boundaries⁹. Another method is to lower the carbon content of the steel to below 0.03wt%, when all the carbon will be kept in solution^{5, 9}. Finally the use of strong carbide forming elements such as niobium and titanium can be employed^{5, 9}. These carbides are more stable and form more readily than chromium carbides⁹. The thermal cycle of welding and arc brazing will result in areas of the HAZ that will be at the carbide precipitation temperature¹³ and will therefore be at risk from the associated problems of sensitisation.

Finally, austenitic stainless steels have a very high coefficient of thermal expansion. This may lead to severe distortion when joining thin sections of material, particularly when dissimilar metal joining where the materials have significantly different coefficients of thermal expansion.

Compared with ferritic stainless steels, austenitic stainless steels have higher coefficients of thermal expansion, a lower thermal conductivity and lower melting points, resulting in them requiring joining processes with a lower and preferably more localised heat input¹⁶.

2.1.2 Rephosphorized Zinc Coated Mild Steel

Traditionally, mild steel has been the most commonly used material for body panels in the automotive industry. However without the inherent corrosion resistance of materials such as aluminium and stainless steel, coatings have had to be used to inhibit corrosion and prolong the life of the vehicle body. The most common corrosion resisting coating is zinc which acts as a sacrificial anode. The zinc may be applied by electroplating, or hot dipping where the material to be coated is passed through a bath of molten zinc at approximately 460°C.

The protection offered by the zinc coating works in the following way. When the coated steel is exposed to the atmosphere the zinc reacts with the oxygen to form a layer of zinc oxide¹⁷. This in turns reacts with any humidity present to form zinc hydroxide¹⁷. Carbon dioxide from the atmosphere then reacts with the zinc hydroxide to form zinc carbonate¹⁷. The zinc carbonate is highly insoluble in water and so forms a protective barrier on the surface of the steel¹⁷. Unlike a barrier such as paint, the zinc has a secondary form of protection to the steel. In the event of the zinc coating becoming scratched, the electrochemical nature of iron and zinc will result in iron acting as the cathode and zinc acting as the anode, resulting in the zinc corroding preferentially to the iron¹⁷.

Although zinc has a beneficial effect on the anti-corrosion properties of mild steel, it can have a detrimental effect when attempting to join mild steel using conventional fusion welding. Zinc evaporates at 907°C, but the melting point of mild steel is approximately 1530°C¹⁷. This means that as soon as the arc is struck the zinc will start to evaporate resulting in two detrimental problems. Firstly, the zinc in the area

immediately adjacent to the weld will be removed, meaning that it will not have the anti-corrosion properties required^{17, 18}. Secondly, the zinc vapour can have a detrimental effect on the weld metal and on the health of the operator¹⁷.

The presence of phosphorous in low carbon mild steel has generally been considered detrimental¹⁹ as steels with high phosphorous levels are prone to poor surface quality, chemical segregation²⁰ and embrittlement. The presence of phosphorous may also result in hot cracking²¹ and is generally removed from iron during the steel making process²². However, phosphorous is a solid solution strengthener of ferrite²³ and as a result can increase the strength of low carbon mild steel²⁴. For this reason phosphorous is added during secondary steel making²², this removal and subsequent addition of phosphorous results in the term rephosphorized mild steel.

2.2 *Brazing*

Brazing is a joining process that occurs by heating the materials to be joined in the presence of a filler material. The liquidus of the filler material should be above 450°C and below the solidus of the parent materials. If the liquidus of the filler material is below 450°C and below the liquidus of the material to be joined then the process is known as soldering. If the filler metal solidus is above the melting point of the material to be joined, then it is termed welding.

Soldering and brazing, along with forging are some of the oldest methods of permanent joining, with examples dating back to Mesopotamia in 3400BC²⁵. Brazing was developed in the middle ages by friar Teophilus Prezbiter, who advocated the use of pure copper and alloys of copper with silver, tin, lead and gold as filler materials²⁵.

In order to produce a brazed joint the faying surfaces must first be cleaned to ensure that they are free from dirt and grease. Great care must then be taken to assemble the components as the braze material will be distributed by capillary action, therefore the tolerances for the gaps (at the brazing temperature) between the faying surfaces is critical. A flux may be applied for the purposes of improving wetting by reducing the surface tension of the molten filler material²⁶, removing oxides from the surface of the material to be joined and inhibiting the formation of oxides during the heating process. The braze alloy may then be prepositioned or fed into the assembly during the brazing process. The braze must then be heated to a temperature at which the filler material will be molten and flow through the joint, this may be achieved using an oxy-fuel torch or a furnace.

The Brazing of Austenitic Stainless Steel to Similar and Dissimilar Metals Literature Review

Whilst wetting and capillary action are controlled by the same forces they are different phenomenon. Wetting is a function of the forces between the liquid filler metal and the solid parent material²⁷ and it is a measure of how easily a liquid will spread over a solid. For example a combination of solid and liquid with good wetting properties will result in the liquid spreading over the solid more than a combination with poor wetting properties.

When a solid metal is clean the atoms at the edge of the material radiate an attractive force which is effective over a very small distance²⁸. If a second material, which is also has clean edges, is brought into range of the force a union may be made²⁸. Surface inequalities may then be overcome by making one metal liquid²⁸. If two solid metals, with clean surfaces, are placed in close proximity in the presence of a liquid metal and the adhesive force produced is greater than cohesive force of the liquid then the liquid will flow between the closely fitting surfaces, even against the force of gravity²⁷. This phenomenon is known as capillary action.

Brazing offers the possibility of joining materials of various geometries, obtaining joints with high strength and other useful working properties²⁵.

Other than the temperature of the joining operation brazed joints differ from welds in the following ways²⁶:

- The composition of the filler material is significantly different to that of the parent material.
- The strength of the filler material is significantly less than that of the parent material.

- The melting point of the filler material is lower than that of the parent material.

These differences mean that brazing offers the following advantages over fusion welding techniques²⁶:

- Less heating is required, so the process is quicker and more economical and results in less metallurgical damage.
- Virtually all metals may be joined by brazing.
- Brazing is ideally suited for dissimilar metal joining, even if the metals have extremely differing melting points.

As with all manufacturing techniques, brazing has disadvantages as well as advantages. Heating of the joint after manufacture in an attempt to straighten or repair a damaged assembly may inadvertently melt the joint²⁶. Corrosion can also be a problem for brazed components as all brazed joints are made from at least two dissimilar metals in contact (the base and filler material) and therefore in the presence of an aggressive electrolyte may establish a galvanic cell. Finally, the load to failure of a brazed joint is proportional to its cross sectional area which will affect joint design.

2.2.1 The Arc Brazing Process

As mentioned in section 2.2 the heat source in a conventional brazing process may be an oxy-fuel torch or variously heated furnaces and the braze material itself will be pre-positioned or fed in during the process, whilst a flux is used to aid the wetting of the faying surfaces and to protect the braze from atmospheric contamination. Arc brazing differs from conventional brazing in the following ways.

The equipment used for Gas Metal Arc Welding (GMAW), as shown in figure 2.3, can be used to perform Gas Metal Arc Brazing (GMAB) by using the appropriate consumable electrode. The consumable electrode is supplied in the form of a coiled wire which is fed towards the arc during the process.

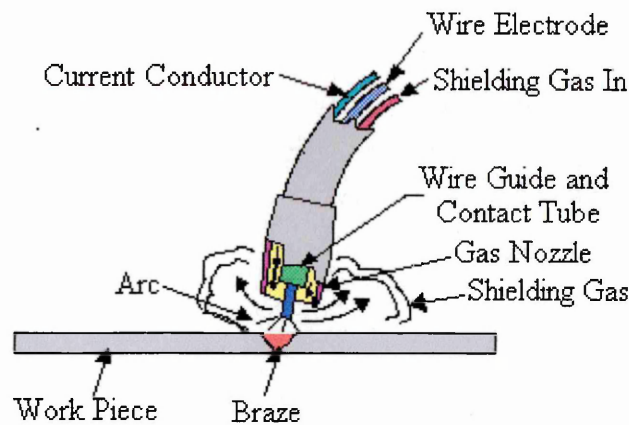


Figure 2.3 - Schematic diagram of a gas metal arc brazing torch modified from¹⁵.

The arc cleans the surface of the material meaning that a flux is not required and the filler material is deposited by Short Circuit Transfer, Globular Transfer or Spray Arc Transfer rather than by capillary action.

Short Circuit Transfer

As the arc is initiated it causes a drop of molten filler metal to grow on the tip of the electrode. As the current passes through the electrode a compressive magnetic force, known as Lorentz force or *magnetic pinch*, is exerted on the wire. The wire feed then causes the drop to contact the work piece and as a result of the short circuit the current increases. The increased current results in an increase in the magnetic pinch force exerted on the electrode and the droplet is detached. This re-initiates the arc and the process is repeated^{15, 29, 30}.

Globular Transfer

Globular transfer takes place when the current is slightly higher than that required for short circuit transfer. The droplet size deposited is greater than the electrode diameter and care must be taken to ensure the arc is long enough to prevent the droplet contacting the work piece before detachment. If the arc is too short the droplet will cause a short circuit which will result in the molten drop disintegrating causing spatter. During globular transfer the droplets are detached at a rate of a few drops per second¹⁵.

Spray Arc Transfer

When the current is above a critical value (transition current) spray arc transfer occurs, below the transition current globular transfer is achieved. The transition current is dependent upon the filler materials melting point; the surface tension of the molten filler material and is inversely proportional to the electrode diameter. Unlike globular transfer the droplet detachment rate is in the order of hundreds per second.

The Droplets are accelerated by the arc forces across the gap to the work piece.

Because the droplets are smaller than the arc gap a short circuit cannot occur¹⁵.

Each of the metal transfer methods can offer advantages and disadvantages. Spray arc transfer offers the most stable arc and the droplets produced are the same diameter as the wire used³¹ producing the neatest brazed seam. However it also produces the highest heat input of all the GMAW metal transfer methods. Globular transfer produces droplets which are larger than the filler material meaning that the process is prone to producing spatter³¹ but uses a lower heat input than spray arc transfer³¹. Short circuit transfer produces the lowest heat input of all the transfer methods, but the arc produced by this method is the most unstable.

2.2.2 Advantages and Disadvantages of the Arc Brazing Process

Arc brazing offers advantages over both conventional brazing and fusion welding techniques for the proposed application. The first of these is with regard to conventional brazing. It is relatively simple to automate a furnace brazing process for small components, however, it is not feasible in the automotive industry. The size and mobility of the equipment required for arc brazing coupled with the localised nature of the heating means that it may be possible to automate the process for larger products, without the need to heat the whole assembly³.

Compared to fusion welding processes, arc brazing offers a relatively low heat input³, this results in a narrow Heat Affected Zone (HAZ) reducing metallurgical damage. There is also less distortion of the parent material and therefore lower residual stresses present in the material^{3, 32, 33}. The lower heat input also produces less spatter improving the aesthetic quality of the joint³⁰.

Arc brazing also offers the advantage with stainless steel that the arc has a cleaning action, removing the passive layer of the parent material² and improving wetting. Therefore no flux is required for the process and a shielding gas is used to protect the joint from atmospheric contamination.

With regard to joining stainless steel to galvanised mild steel, arc brazing results in considerably less burn off of the zinc coating² in the area immediately adjacent to the joint. As stated in section 2.1.2 zinc has a boiling point of 907°C, therefore during

fusion welding processes zinc vapour is produced, this can cause several problems including: porosity within the joint, bond failures, lack of fusion, cracking and it can also cause an unstable arc resulting in increased spatter. The lower melting point of the arc brazing filler material means that a zinc coating thickness of up to 15µm can be tolerated without suffering any of the above metallurgical problems associated with traditional fusion welding processes². The zinc vapours produced can also have detrimental effects on the welder's health, by reducing the zinc burn-off these effects are reduced³.

Arc brazing also produces joints which are easily machined³ and offers the possibility of bonding materials which were originally thought difficult to weld with minimal spatter³. Finally, arc brazed joints do not require pre or post heat treatment often required with traditional welding processes³.

There are also potential problems associated with the arc brazing process. The first of these is Liquid Metal Embrittlement (LME). Joseph, Picat and Barber defined Liquid Metal Embrittlement (LME) as:

*“loss of ductility or brittle fracture in a normally ductile material whilst in the presence of liquid metal”*³⁴.

However embrittlement occurs once the liquid material has solidified so a better definition may be:

“loss of ductility or brittle fracture in a normally ductile material after exposure to liquid metal”.

As well as exposure to liquid metal stress must be present in the material²⁷, this may be residual stress or an externally applied stress. The molten filler material weakens the parent material and cracks form along the grain boundaries²⁷. Only a small amount of liquid metal is required for the onset of Liquid Metal Embrittlement (LME) and it is characterised by a crack propagation rate in the order of several metres per second. The material suffers a loss of tensile strength and may fail below yield point giving no previous warning from deformation³⁴.

The filler material in any brazing process must be dissimilar to the parent metal. Therefore, a galvanic cell may be created if the joint comes into intimate contact with an aggressive electrolyte resulting in the preferential corrosion of the less noble metal.

The proposed application of the process is in the automotive industry, therefore it must be capable of producing joints with impeccable aesthetic qualities. Spatter is associated with the GMAW short circuit transfer method (see section 2.2.1) as it is difficult to maintain a stable arc.

Even though conditions are favourable compared to fusion welding distortion can also cause problems in arc brazing. The severity of the distortion is dependent on several factors:

- Heat Input
- Restraint
- Residual stresses in the parent material
- Properties of the parent material

The heat input in arc brazing is non-uniform and will cause the parent material to contract unevenly. This produces stresses which can be reduced by the material distorting. If the material is restrained this may reduce the distortion, but it may also result in higher residual stresses within the material which will be difficult to relieve and may lead to cracking and premature failure.

During the arc brazing process any residual stresses within the material will be relieved in the area adjacent to the braze. Upon cooling, the distortion will be a result of the stresses caused by uneven expansion and contraction and the residual stresses present prior to the joining operation. Finally, the thermal properties of the parent material are important. A material with a zero co-efficient of thermal expansion will not expand during the heating process and therefore those materials with higher co-efficients of thermal expansion will tend to distort more. The coefficient of thermal expansion of stainless steel is approximately 1 and half times that of mild steel³⁵, as shown in table 2.1, and this must be considered when attempting dissimilar metal joining.

Material	R_m (MPa)	$R_{p0.2}$ (MPa)	Coefficient of Thermal Expansion ($\times 10^{-6} \text{ K}^{-1}$)
AISI grade 304 Stainless Steel	600^{36}	290^{36}	16^{36}
AISI grade 316 Stainless Steel	570^{36}	280^{36}	16^{36}
Mild Steel ⁱ	$380-460^{37}$	$260-320^{37}$	$12-13^{35}$

Table 2.1 – Mechanical and Thermal Properties of AISI grade 304 and 316 Stainless Steel and Mild Steel

ⁱ The mechanical properties displayed are the specific values for Dogal 260RP-x whilst the thermal coefficient of thermal expansion is the generic value for high strength low alloy mild steel.

2.2.3 Microstructure of Arc Brazed joints

There is no current literature on the microstructure of arc brazed stainless steel joints. However, Li et al³⁸ have investigated the evolution of the microstructure of arc brazed galvanised mild steel joints, using a copper based filler material containing 3% silicon in their paper “Growth Mechanisms of Interfacial Compounds in Arc Brazed Galvanised Steel Joints With $\text{Cu}_{97}\text{Si}_3$ Filler”. The work breaks down the growth of the intermetallic compounds into seven stages³⁸:

- *The first stage is as the arc heats the filler material causing it to melt and be distributed between the faying surfaces. Iron atoms then begin to diffuse into the liquid braze material and copper and silicon atoms begin to diffuse into the interfacial zone.*
- *The iron atoms in the braze begin to react with the silicon forming Fe_5Si_3 . A layer of this compound is also found at the interface of the parent and filler material with “branches” of the compound advancing into the braze.*
- *The “branches” advance deeper into the braze and more intermetallic Fe_5Si_3 forms in the braze.*
- *The Fe_5Si_3 layer at the interface thickens and the “branches” are broken by the stirring action of the arc forces.*
- *Some of the broken branches solidify in situ but others are swept further into the braze where they grow into spherical form.*
- *The compound concentrates and grows into starlike form which in turn grow into flowerlike form.*
- *The quantity and dimensions of the spherical, starlike and flowerlike form increase and are dispersed throughout the braze.*

The Brazing of Austenitic Stainless Steel to Similar and Dissimilar Metals Literature Review

In a separate investigation Li et al concluded that it was the presence of the Fe_5Si_3 intermetallic compound that is responsible for the strength of the joint³⁹.

The microstructural evolution of the arc brazed joints produced in this current research work will be examined later.

2.2.4 Gas Metal Arc Brazing Process Variables

2.2.4.1 Joint Geometry

There are two main types of joint configuration normally used with arc brazing.

These are shown in Figures 2.4i and 2.4ii respectively.

Butt Joint

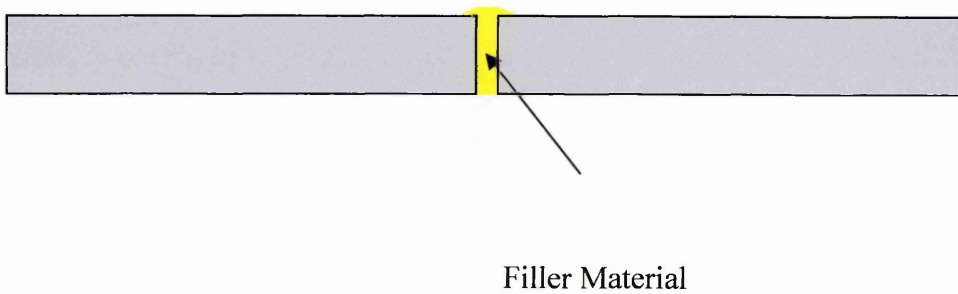


Figure 2.4i - Butt Joint Configuration

Lap Joint

Filler Material

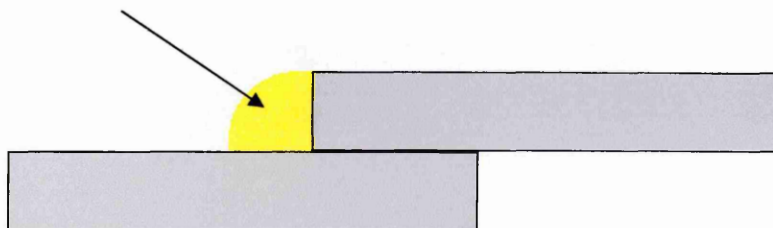


Figure 2.4ii - Lap Joint Configuration

There are seven main process variables for each joint geometry:

- Current
- Voltage
- Torch velocity
- Shielding gas composition
- Shielding gas flow rate
- Torch height
- Torch angle

The importance of these variables is dependent upon the properties of the joint which are to be optimised. For instance an arc brazed joint can only be as strong as the filler material so in terms of strength the filler material composition is the most important variable.

When all other variables are held constant the current will vary with the feed rate¹⁵. If the electrode diameter is increased the current must also be increased to ensure the same feed rate¹⁵. An increased current for the same diameter of filler material will result in a higher deposition rate and therefore a larger seam¹⁵ for the same pass velocity, for this reason the current and the pass velocity are the most important variables when considering joint penetration.

With all other variables held constant the voltage controls the arc length¹⁵. During short circuit transfer the arc length and torch height are important for the aesthetic properties of the joint. If the torch is positioned too close to the workpiece electrode stubbing will occur as there is insufficient time for the molten filler material to be

detached before the electrode contacts the workpiece. If the torch is positioned too far from the workpiece increased levels of spatter will be experienced.

Shielding gas flow rate must be sufficient to cover the joint and therefore prevent contamination from the air. The composition of the shielding gas can affect the arc characteristics, the material transfer mode, the appearance of the joint, the torch velocity and the mechanical properties of the joint. This will be discussed in greater detail in section 2.2.4.3²⁹.

2.2.4.2 Heat Input

Whilst the torch velocity will control the degree of penetration achieved and the current controls the mode of material transfer; the current, voltage and torch velocity are related to the total heat input by equation 2.1

$$H_{NET} = \frac{\eta EI}{v}$$

- Where:
- H_{NET} = The total heat input ($J.s^{-1}$).
 - η = The heat transfer efficiency of the arc.
 - E = The voltage (V).
 - I = The current (A).
 - v = The velocity of the torch ($mm.s^{-1}$).

Equation 2.1

The current can be a constant DC input or it can be pulsed as seen in figure 2.5.

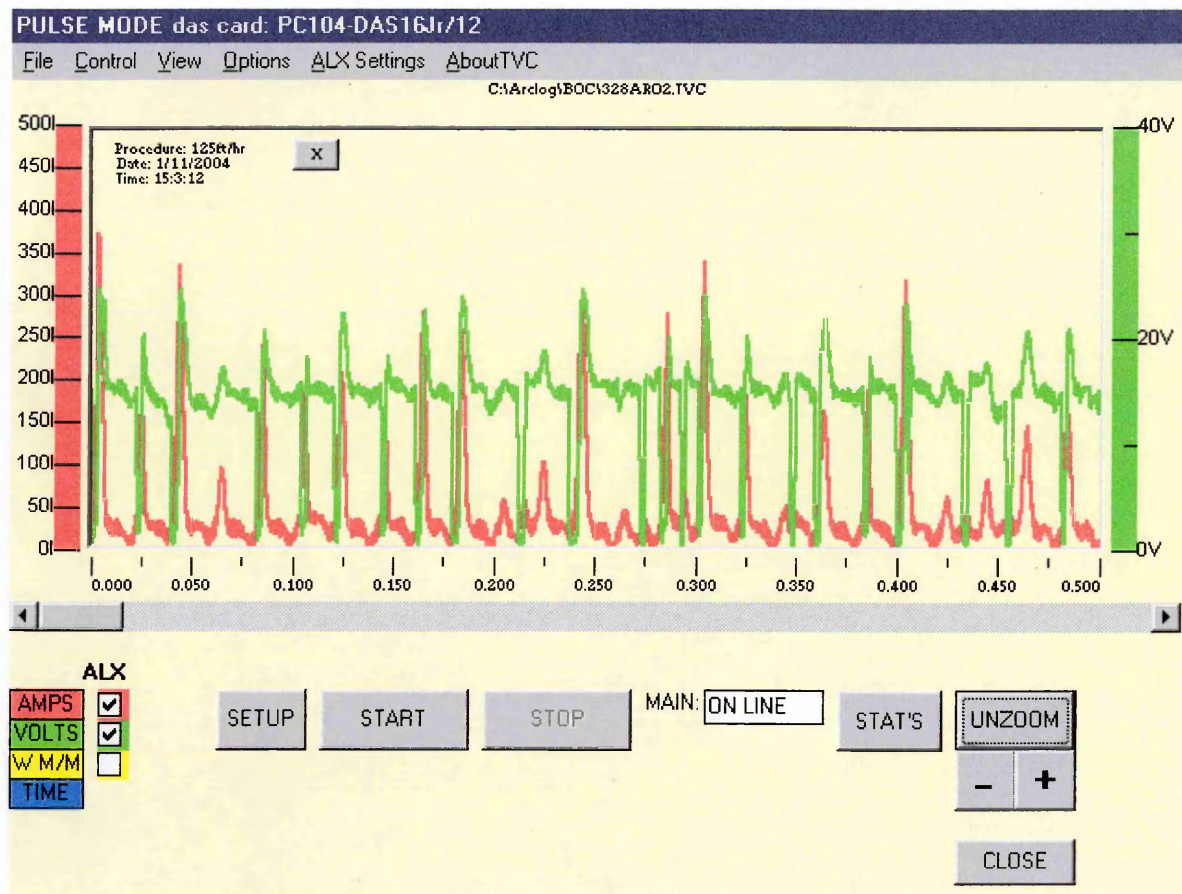


Figure 2.5 - Waveforms produced using a pulsed current input. (These waveforms are recorded using arc monitoring equipment (the Arc Logger 10 and Arclog Software manufactured by the Validation Centre)).

When using a pulsed current it is also possible to vary the base current, the pulse width, frequency, and the peak rise and fall rates. By varying the pulsed arc variables it should be possible to reduce the heat input whilst still maintaining a stable arc.

2.2.4.3 Shielding Gas

The main purpose of the shielding gas is to protect the molten braze from atmospheric contamination. If brazing were simply to be conducted in air, then oxides and nitrides may be formed leading to problems such as porosity and embrittlement. However, shielding gases also have a major effect on other variables such as²⁹:

- *Arc characteristics*
- *The method by which the metal is deposited*
- *Appearance of the joint*
- *Torch velocity*
- *Mechanical properties of the joint*

In order for heat to pass from the arc to the work piece a proportion of the shielding gas must undergo a change of state to plasma⁴⁰. The ease with which an arc can be initiated and the stability of the arc during the brazing process is dependent upon the ionisation potential of the shielding gas and this can be defined as:

"The voltage needed to remove an electron from an atom making it an ion"⁴⁰

The lower the ionisation potential of a gas, the easier it is to initiate an arc and maintain its stability^{30, 34, 40}. The ionisation potential of gases can be altered using gas mixtures^{30, 41} for example the addition of 2% oxygen to argon. With a lower ionisation potential, the material transfer will be less violent resulting in reduced spatter, improving the aesthetic quality of the joint and reducing the process cost (as less filler material is used and less grinding of the joint is required).

The thermal conductivity of the shielding gas is an important property as it influences the total amount of energy supplied during the joining process³⁰. A shielding gas with a high thermal conductivity will increase the braze fluidity, since the viscosity of the braze will decrease with increased temperature, improving both the penetration of the joint and the appearance of the final braze seam^{30, 40}. However, a high thermal conductivity will also lead to a reduction in the diameter of the conducting core of the shielding gas (as shown below in figure 2.6) which increases the voltage, which in turn, leads to instability of the arc⁴².

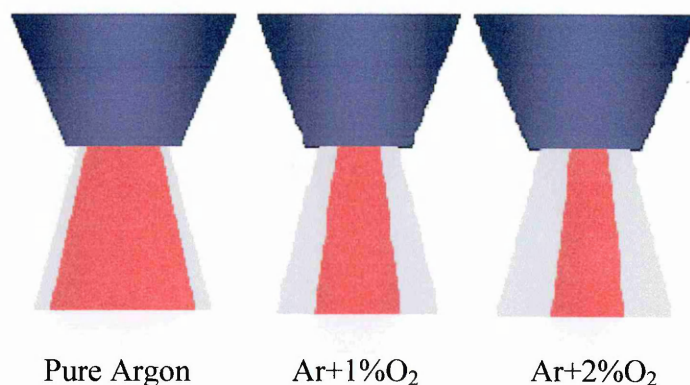


Figure 2.6 - Schematic diagram showing that an increasing oxygen content in the shielding gas leads to an increase in thermal conductivity and a decrease in the conductive core of the arc.

Argon is an inert gas which is 1.4 times as heavy as air²⁹. As a result when used as a shielding gas it forms a blanket over the joint which protects it from the atmosphere. Although argon has a low ionisation potential and it is relatively easy to initiate and maintain an arc, it is a poor conductor of heat which results in a viscous transfer of material leading to an unsatisfactory appearance in the brazing seam. This can be corrected by the addition of an active gas such as oxygen or carbon dioxide.

The addition of active gases containing oxygen can also have detrimental effects on the brazed joint when a copper filler material is used. The copper combines with the oxygen to form Cu_2O , which produces a brittle microstructure³³. This effect can be overcome by using a braze alloy containing a deoxidant such as silicon³³.

Helium is also an inert gas, but in contrast to argon it has a density approximately 0.14 that of air^{29, 42} and as a result requires flow rates of approximately three times that of argon to maintain an equivalent shield²⁹. Helium has a higher thermal conductivity than argon and therefore the arc energy is distributed more uniformly^{29, 40, 42} and is also therefore capable of higher travel speeds. However, helium has a high ionisation potential²⁹ meaning that it is relatively difficult to initiate and maintain a stable arc.

2.2.4.4 Arc Brazing Filler Material

Arc brazing of steel, mainly uses copper based alloys as filler materials due to their favourable melting points and good wetting ability. To further decrease the melting point of the filler material elements such as silicon and manganese can be added³⁰.

One of the most widely used filler materials for arc brazing is BS:2901 C9. This is a copper alloy containing 3% silicon and 1% manganese. As well as lowering the melting point of the filler material, the alloying additions are strong deoxidants. These elements preferentially combine with oxygen and in most cases will be less dense than the molten braze, resulting in the compound containing the oxygen rising to the top of the braze seam⁴³. This can aid the arc in the cleaning of the passive film from the surface of the stainless steel, thereby improving the wetting of the faying

surfaces. One disadvantage of this filler material is that the increased silicon levels lead to increased viscosity⁴⁴ and therefore this may affect the flow characteristics of the braze. Another commercially available brazing alloy is BS:2901 C28. Once again this is a copper based alloy containing 8% aluminium. Aluminium is a stronger deoxidant than silicon or manganese. This filler material also has a higher tensile strength and a higher hardness than BS:2901 C9⁴⁵. Previous unpublished work by Burgin at Sheffield Hallam University, in which a drop of braze alloy was deposited using a GMAW torch onto a sheet of stainless steel, has shown that BS:2901 C28 produces a smaller contact angle than BS:2901 C9⁴⁶. This may be as a result of the reduced silicon content, or the addition of aluminium, or a combination of both factors improving the wetting behaviour of BS:2901 C28.

The following three, copper based, commercially available filler materials will be investigated in this research:

- BS:2901 C9
- BS:2901 C11
- BS:2901 C28

Table 2.2 details the chemical composition, ultimate tensile strength and melting points of these materials.

Filler Material	Chemical Composition	Ultimate Tensile Strength (MPa)	Melting Point (°C)
BS:2901 C9	3%Si, 1%Mn, 96%Cu	350	980-1020
BS:2901 C11	7%Sn, 93%Cu	260	900-1050
BS:2901 C28	8%Al, 92% Cu	430	1030

Table 2.2 – Chemical compositions, ultimate tensile strength and melting point of the filler materials investigated⁴⁵

2.3 *Residual Stress*

As their name suggests residual stresses are stresses present in a material when no external forces are acting upon it. Residual stresses are often seen as a problem to be overcome, however compressive residual stresses can have beneficial effects on fatigue properties⁴⁷ inhibiting crack propagation. An example can be seen in the rapid cooling of toughened glass, producing compressive stresses on the surface⁴⁸. The compressive stress in the surface layers are balanced by tensile stresses in the bulk. Therefore, if a crack reaches the bulk of the toughened glass it will propagate through the material at great speed, shattering the glass⁴⁸.

Residual stresses can be divided into three types⁴⁸:

- *Type 1 – which exist over the distance of a few grains*
- *Type 2 – which exist over one grain*
- *Type 3 – which exist over several atomic distances within a grain*

Type 1 residual stresses are termed as macro stresses whilst type 2 and type 3 are termed micro stresses.

Macro stresses are caused by non uniform plastic deformation or steep temperature gradients⁴⁸. Type two stresses, or intergranular stresses, are caused by differences between the phases in a microstructure⁴⁸. Type three stresses are caused by dislocation stress fields⁴⁸.

2.3.1 Residual Stresses in Welding

Due to the localised heat input involved in welding the parent material expands and contracts unevenly resulting in residual stresses in the material. As the weld pool contracts a residual tensile stress is established in the surrounding material, which is balanced in the bulk of the material by a compressive stress as shown in figure 2.7¹³.

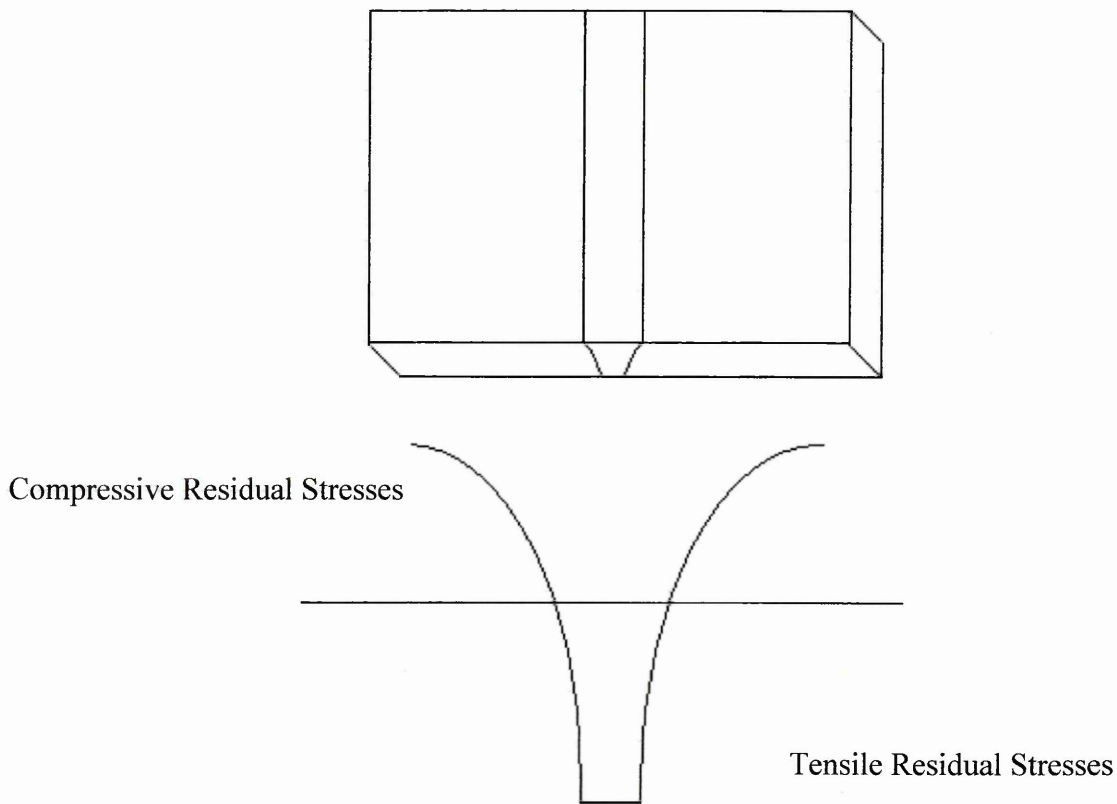


Figure 2.7 – Distribution of Residual Stresses in a Welded Butt Joint

2.4 Fatigue

The word fatigue originates from the Latin “fatigare” meaning to tire and whilst it is normally used to express mental or physical tiredness it is used as an engineering term to describe the damage caused to a material or structure by cyclic loading⁴⁹.

The process of fatigue in a material or structure can be broken down into 3 stages. Firstly a crack is initiated on the microscopic scale. The second stage is crack growth on the macroscopic scale before the specimen finally fails⁵⁰.

The initiation of a crack will often occur as the results of a stress concentration such as a surface defect or may be as a result of the movement of slip bands in the material, on the fracture surface of the specimen this can be seen as a smooth, flat, semicircular or elliptical area⁴⁷. As the crack propagates through the material it extrudes metal from the slip bands forming ridges which appear similar to tide marks on a beach⁴⁷. Finally when the crack reaches a critical size it spontaneously propagates through the specimen causing failure⁵¹.

When assessing the mean fatigue life of a material (or joint) it is not possible to conduct a test such that specimens will break at a specific number of cycles. Therefore, a statistical method such as the staircase fatigue test must be used⁵¹.

2.4.1 Staircase Fatigue Test

To begin the staircase fatigue test an estimate of the mean fatigue strength (a load at which 50% of the samples will survive) and standard deviation must be made. The

first specimen is tested at the estimated value for the mean fatigue strength. If the sample survives the load will be increased by one standard deviation for the next specimen, whereas if the sample fails the load will be decreased by one standard deviation as shown in table 2.3. The procedure continues in this way until sufficient samples are tested⁵² (normally at least 25⁵¹).

	Sample Number														
	1	2	3	4	5	6	7	8	9	10	11	12	13	14	15
Mean Fatigue Load + 2SD											x				
Mean Fatigue Load + 1SD		x								o		x			
Mean Fatigue Load	o		x		x				o				O		x
Mean Fatigue Load - 1SD				o		x		o						o	
Mean Fatigue Load - 2SD							o								

(x=fail, o=pass)

Table 2.3 - Example of Staircase Fatigue Test Results

Once sufficient samples are gathered, the total number of run outs and failures is determined. Only the run outs (or the failures) will be used to calculate the mean fatigue strength and the standard deviation, depending on which has the fewest occurrences (least frequent event)^{53, 54, 55}.

The loads are labelled L_n starting at the lowest load at which a least frequent event occurred (labelled L_0) and the number of least frequent events at each load level are recorded. Two variable quantities A and B can then be calculated^{53, 54, 55} as shown in equations 2.2 and 2.3.

$$A = \sum in_i \text{ Equation 2.2 }^{53, 54, 55}$$

$$B = \sum i^2 n_i \text{ Equation 2.3 }^{53, 54, 55}$$

where n is the number of least frequent events and i is the step number (e.g. at L_0 $i=0$).

The mean fatigue strength μ can then be calculated using equation 2.4

$$\text{If the least frequent event is "run outs" } \mu = L_0 + d \left(\frac{A}{\sum n} + \frac{1}{2} \right)$$

$$\text{If the least frequent event is failures } \mu = L_0 + d \left(\frac{A}{\sum n} - \frac{1}{2} \right)$$

where n is the number of least frequent events

L_0 is the lowest load level at which a least frequent event occurred

d is the chosen step divide

$$\text{Equation 2.4 }^{53, 54, 55}$$

Equation 2.5 can be used to determine the standard deviation (SD).

$$SD = 1.620d \left(\frac{B \sum n - A^2}{(\sum n)^2} + 0.029 \right)$$

where n is the number of least frequent event

d is the chosen step divide

$$\text{Equation 2.5 }^{53, 54, 55}$$

The validity of the standard deviation can be checked by calculating the convergence factor, which will return a result between 0.3 and 1.2 if the results are valid⁵⁶, as shown in equation 2.6.

$$\frac{B \sum n - A^2}{(\sum n^2)} \text{ where n is the number of least frequent events}$$

$$\text{Equation 2.6 }^{56}$$

2.5 Possible Initiation and Failure Modes of Liquid Metal Embrittlement

As stated in section 2.2.2 one of the most significant problems associated with arc brazing is LME. In their paper Joseph, Picat and Barbier discuss several possible mechanisms which have been proposed as a model for LME, but state that despite these studies a qualitative explanation of LME has still to be determined³⁴.

Glickman proposes that instead of being an instantaneous process LME, can in fact be separated into two distinct stages which act in series⁵⁷:

- *Firstly grooving of the grain boundaries by bulk liquid phase diffusion occurs.*
- *Secondly local plastic deformation takes place as a result of dislocation activity at the crack tip.*

Grain boundary grooving was first proposed by Mullins who attributed the phenomenon to the diffusion of solid atoms through the penetrating liquid⁵⁸. Mullins also modelled the process as shown overleaf in equation 2.7.

$$d = 1.01m(A't)^{\frac{1}{3}}$$

$$A' = \frac{C_o \gamma_s \Omega^2 D}{KT}$$

- Where:
- d = Groove depth (cm)
 - t = Time (s)
 - C_o = Concentration at Equilibrium (%)
 - γ_s = Surface Free Energy (J)
 - Ω = Molar Volume (cm³)
 - D = Diffusion Coefficient
 - K = Boltzmann's Constant (JK⁻¹)
 - T = Absolute Temperature (K)

Equation 2.7 – Mullins Model of Grain Boundary Grooving

The value for m is the gradient of the opening angle and is therefore given by the tangent of half the groove opening angle (θ) as shown in figure 2.8 below.

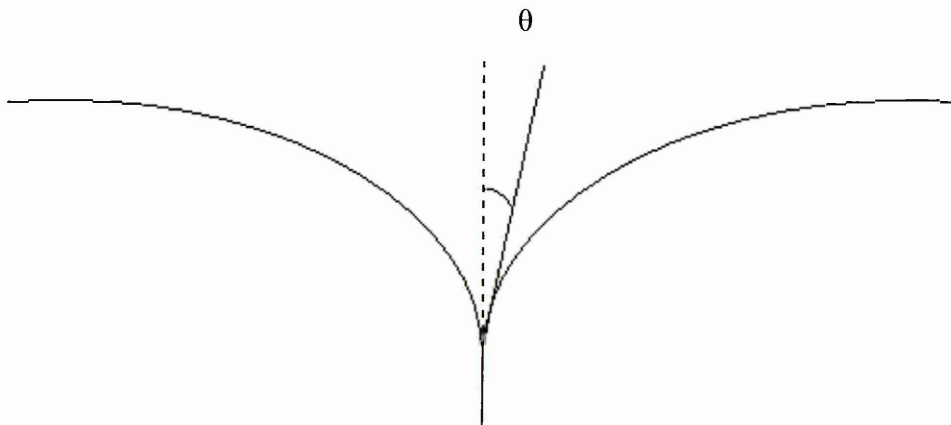


Figure 2.8 – Gradient used as m in Mullins Model

Looking at the other variables within Mullins's model, the most important variable is the surface free energy of the parent material. The process of grooving occurs to reduce the interfacial free energy, whilst this cannot be reduced completely to zero⁵⁸, the higher the surface free energy of the stainless steel at the start of the process the further into the material the groove will penetrate. Time and temperature are also important because it is only possible for grooving to occur during saturation, by a liquid phase, of the grain boundary⁵⁸. Therefore the longer the filler material is liquid the further the groove will penetrate into the material. During the arc brazing process the time that the filler material will be liquid will be dependent on the temperature gradient generated by the process.

Mullins states in his paper that one of the transport mechanisms of the grooving process is surface diffusion. This will be limited by both the molar volume of the copper and the diffusion coefficient of the parent material within the copper. Finally the Boltzmann constant links the temperature in Kelvin with the energy in Joules⁵⁹. Therefore this enables the temperature and energy at which the grooving is occurring to be linked.

Considering the second stage of the process proposed by Glickman for LME, if the opening angle is small, under an externally applied tensile load the groove will act as a stress raiser in the same way as a crack⁵⁷.

2.6 Summary of Literature

In the preceding literature review a summary has been presented of the literature for arc brazing and the parent materials which will be investigated. This includes the evolution of the stainless steel and the reasons for stainless steel's corrosion resistance. As this investigation will use austenitic stainless steel as one of the parent materials the method by which a stainless steel retains an austenitic microstructure at room temperature is discussed. Whilst arc brazing is not a welding process the main issues with welding austenitic stainless steels are considered as the temperature of the arc brazing process may still cause several of these detrimental effects.

The other parent material used in this investigation is rephosphorised mild steel. The material in this study is zinc coated to provide protection from corrosion. The metallurgy of how the zinc coating inhibits corrosion is detailed along with the problems associated with welding zinc coated mild steel, although the lower heat input of the arc brazing process should minimise these issues. Finally the reason why the phosphorous is removed during the initial stages of the steel making process and then added at a later stage is explained.

Whilst arc brazing is not a conventional brazing method, conventional brazing including a description of the process, the differences between welding and brazing and the advantages and disadvantages of the conventional brazing process are detailed, to provide a background for the arc brazing process. The differences between conventional brazing and arc brazing are then discussed along with the advantages and disadvantages of arc brazing with respect to conventional brazing and welding. The effect of the process variables are detailed including which are the most

important with respect to particular properties required by a joint. One of the variables of the process is the composition of the shielding gas and whilst most of the literature refers to welding processes, the information can be read across for arc brazing.

Previous investigations into arc brazing have been concerned with using mild steel as the sole parent material. The results of an investigation into the evolution of the microstructure of these joints are presented and will be compared, in chapter 5 to the microstructure found in the stainless steel to stainless steel joints and stainless steel to mild steel joints, manufactured during this investigation.

The staircase fatigue test will be used to ascertain the fatigue properties of the arc brazed joints manufactured in this investigation. Therefore the method for this test is explained.

Finally LME is an associated problem with arc brazing. A model has been presented which attempts to demonstrate the controlling mechanism of LME. This model will be explored in further detail in Chapter 5. In Chapter 3 the experimental procedure used in this investigation is detailed.

3.0 Experimental Procedure

3.1 *As-Received Material Characterisation: Tensile Testing*

Initially tensile tests were performed on samples of the as-received AISI grades 304 and 316 stainless steel, see table 3.1 for chemical compositions of these alloys. The reason for this was that although information on the mechanical properties could be obtained from mill certificates and reference data sheets, an in-house test of this type would give data which was obtained from the same equipment and material, avoiding problems with batch to batch variations. This test provided a base-line from which later experiments on brazed material could be assessed. The test pieces (dimensions 180mm x 13mm x 2mm as shown in figure 3.1) were cut using a mechanical shear.

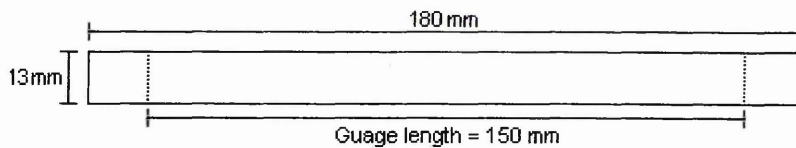


Figure 3.1 - Dimensions of flat test piece

A gauge length was marked on the test pieces using a vernier and the as-sheared actual dimensions were measured and recorded. The sample was then tensile tested with the crosshead moving at a speed of $10\text{mm}\cdot\text{min}^{-1}$.

3.2 Initial Testing of Arc Brazed Similar Metal Butt Joints

The objective of the next element of the experimental work was to ensure that the results from previously unpublished work by Wong were reproducible. To do this 8 sample blanks were cut from AISI 304 and AISI 316 stainless steel (with chemical compositions shown in table 3.1) measuring 90mm x 100mm x 2mm (see figure 3.2a). The blanks were then divided into four pairs for each material and brazed using GMAB *short circuit* transfer (figure 3.2b). Two different filler metals and two different shielding gases were tested. The filler metals used (BS:2901 C9 and BS:2901 C28) were both copper braze alloys with the compositions shown in table 2.2. The two shielding gases used were pure argon and argon containing 2% oxygen producing four sample types for each parent material.

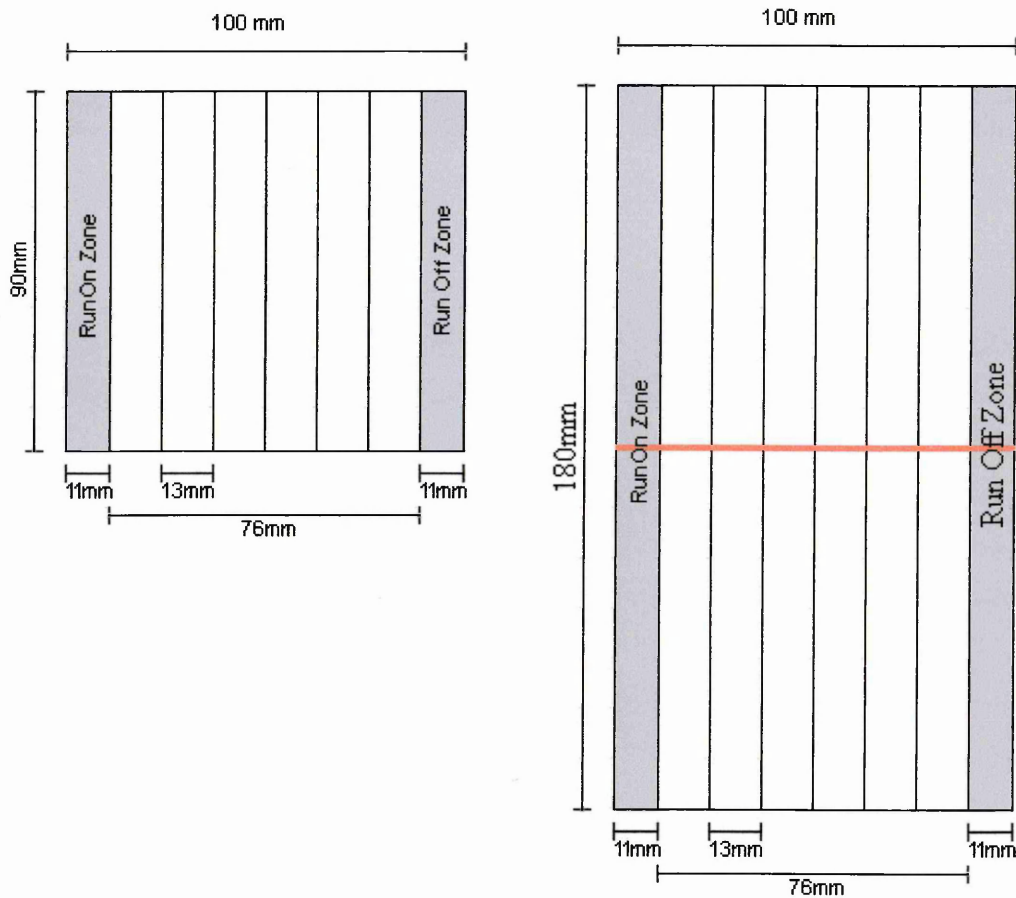


Figure 3.2a – Unbraided sample blanks Figure 3.2b – Braided samples

Grade	Carbon	Chromium	Nickel	Molybdenum
304	0.04	18.1	8.1	---
316	0.04	17.2	10.1	2.1

Table 3.1 - Chemical Compositions of AISI 304 and AISI 316³⁶

It was found necessary to include a run-on and run-off zone at the beginning and end of the braze run because the quality of the braze in these areas was sub standard. Until a steady-state has been achieved it is difficult to maintain a stable arc, therefore an area of acceptable braze will not be produced until the material in the vicinity of the arc has been heated and a steady torch velocity has been established. At the end of the seam, problems occur due to the surface tension of the molten filler material.

As the braze alloy cools and solidifies it contracts causing undercut in a direction longitudinal to the seam. This problem can be rectified in industrial applications by the use of run-on and run-off plates.

Once joined the run-on and run-off zones were removed and each specimen was sectioned into six test pieces, each with the nominal dimensions of 180mm x 13mm x 2mm. The exact dimensions of each test piece were measured and the test pieces were tensile tested in accordance with BS EN 10002-1:2001⁶⁰. The joint efficiency could then be calculated by dividing the ultimate tensile strength of the joint by the ultimate tensile strength of the parent material. A value of unity indicates a 100% joint efficiency, i.e. the joint is as strong as the parent material.

3.3 *Microstructural Characterisation of Arc Brazed Joints with High Joint Efficiency*

In order to establish the microstructure of an arc brazed joint with high joint efficiency, the joints which displayed the highest and lowest tensile strength from each parent material were prepared for microstructural examination. The four samples were examined in the unetched condition to see the distribution of the phases present in the material. Initially the optical light microscope was used to determine if there were any noticeable differences between the two sample types.

Following the examination of the samples in the as-polished condition the samples were etched to develop the microstructure. It was not possible to develop a single etch technique to bring out the microstructures of both the stainless steel and the filler metal because any etchant that worked successfully with regards to the filler material was not strong enough to etch the stainless steel. Similarly any etchant, which developed the microstructure of the stainless steel, over etched the filler material making it impossible to determine any detail from this area. It was therefore necessary to employ a dual etch approach. This meant that firstly the copper based filler material would be etched using alcoholic ferric chloride. The microstructure was then examined and recorded using both the optical light microscope and the Scanning Electron Microscope (SEM) in both secondary and backscattered imaging modes. The Energy Dispersive X-ray analysis (EDX) system on the Scanning Electron Microscope (SEM) was also used to determine the distribution of the

elements within the microstructure. Once this had been achieved the microstructure of the stainless steel was revealed using an electrolytic etch in 10% oxalic acid.

During both etching techniques the progress was checked using the optical light microscope, to ensure that the samples were not over etched. If the microstructure was not sufficiently developed the etching technique was repeated. However, if the sample had been over etched it was re-polished and the procedure was started again. Finally, the samples were examined in the Scanning Electron Microscope (SEM) using secondary electron, backscattered electron and x-ray detectors. These analytical techniques were used to examine the parent metal – braze metal interface to determine whether any of the parent metal had melted or diffused into the braze metal or vice versa.

3.3.1 Immersion Test of Stainless Steel into BS:2901 C28 and BS:2901 C9 Braze Alloys

During optical and SEM microstructural investigation of butt joints with high joint efficiency, iron and chromium rich dendritic structures were identified within the braze material. From these micrographs it was not known whether these structures were found in the braze due to dissolution or localised melting. In order to determine which mechanism was dominant batches of both of the braze alloys under investigation (BS:2901 C9 and BS:2901 C28) were melted and strips of stainless steel were immersed into them at temperatures of 1100°C, 1200°, 1300°C and 1400°C for 5, 10 and 15 seconds. One strip per temperature and time was then prepared for microstructural investigation.

3.3.2 Microstructural Analysis of Simulated Experimental As-Brazed Alloy

S Magowan manufactured an experimental alloy using 10% AISI grade 304 stainless steel and 90% made to the composition of BS:2901 C28. The material was placed in a furnace at a temperature of 1600°C to ensure it was fully molten. The molten material was then removed from the furnace and cast into a chill block to simulate the rapid cooling experienced in the braze seam. The cast sample was then sectioned, ground, polished and examined using an optical microscope. The microstructures produced by this trial (and the immersion test) were then compared to that obtained for the arc brazed joints to establish if melting or diffusion of stainless steel was occurring during the arc brazing process.

3.3.3 Volume Fraction Analysis of Cellular Dendritic Structure

During the microstructural investigation of the as-brazed joints it was noted that the samples exhibiting higher tensile strengths appeared to contain more of the iron and chromium rich cellular dendritic “islands” in the braze seam. To investigate whether these were responsible for the improved strength of the arc brazed joints three butt joints were manufactured all using AISI 304 stainless steel as the base material and BS:2901 C28ⁱⁱ as the filler material and with 3 shielding gases; pure argon, argon containing 1% oxygen and argon containing 2% oxygenⁱⁱⁱ. The joints were then sectioned, ground and polished and a random area was selected and then examined using the backscattered electron detector of the SEM. The volume fraction was then measured using image analysis software and recorded. Another area was chosen at

ⁱⁱ BS:2901 C28 was used in this investigation because it proved to have the highest tensile strength

ⁱⁱⁱ Pure argon and argon containing 2% oxygen was sourced from BOC Gases and argon containing 1% oxygen was sourced from Linde Industrial Gases.

The Brazing of Austenitic Stainless Steel to Similar and Dissimilar Metals Experimental Procedure

random and the process was repeated until five areas had been measured. The average was taken and then compared to the tensile strengths to see if a relationship existed between the tensile strength and the volume fraction of iron and chromium rich cellular dendritic “islands” in the braze seam.

Once it was established that the arc brazing process was capable of manufacturing similar metal butt joints and the microstructure of these joints had been characterised the process variables were investigated in order to optimise them.

3.4 Similar Metal Butt Joints

3.4.1 Optimisation of Process Variables to Maximise Joint Tensile Strength

3.4.1.1 Optimum Torch Height

The first variable to be determined was the height of the torch from the work piece. This was initially set by reference to GMAW of similar materials and then by a process of trial and error. A range of heights between 10mm and 16mm in 1mm increments were investigated. The closer the torch is positioned to the work piece the greater the efficiency with which the heat is transferred to the work piece. Therefore, if the current, voltage and velocity are kept constant and the torch is too close to the work piece there will be an increased risk of excessive heat input. Alternatively, if the torch is positioned too far from the work, the risk increases of unacceptable amounts of spatter being produced.

3.4.1.2 Optimum Torch Velocity

A process of trial and error was also used to set up the torch velocity. Several runs were conducted at different velocities and if there were holes appearing within the braze, due to the velocity being too great in relation to the rate deposition, the velocity was decreased. Conversely if excessive amounts of filler material were produced above the joint the velocity was increased.

As previously shown in equation 2.1 by increasing the torch velocity the total heat input can be reduced. A BOC HW75 Tractor similar to that shown in figure 3.3 was used in order to maintain a constant pass speed and torch height.

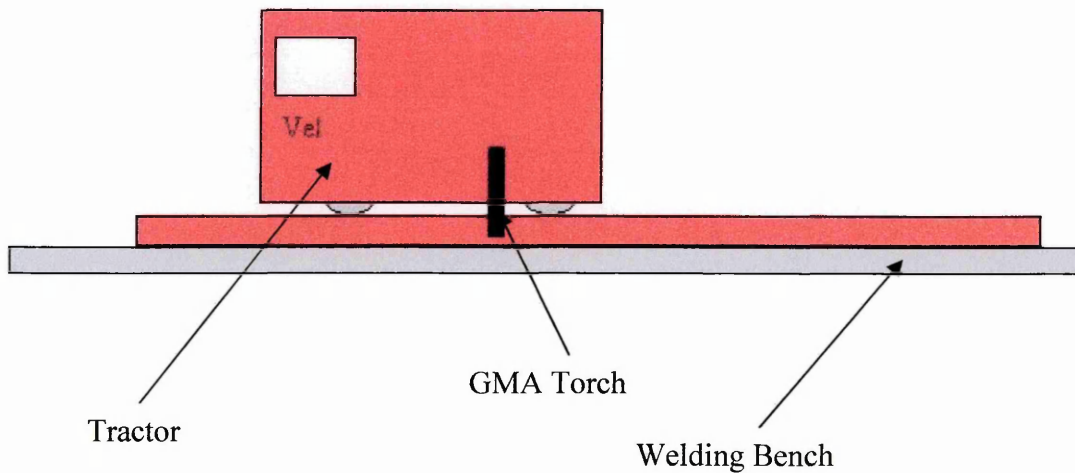


Figure 3.3 – Schematic Diagram of the BOC HW75 Tractor at Sheffield Hallam University

3.4.1.3 Measuring Arc Characteristics

The current, voltage, gas flow and wire feed can be monitored throughout the process using appropriate arc logging equipment. The Arc Logger 10 (ALX), used in this project, is an example of commercially available arc monitoring equipment (see figure 3.4 for a schematic diagram of the system). The waveform produced can be plotted during the process and average values for current, and voltage, the gas flow rate and the total amount of consumable used in the process can be measured.

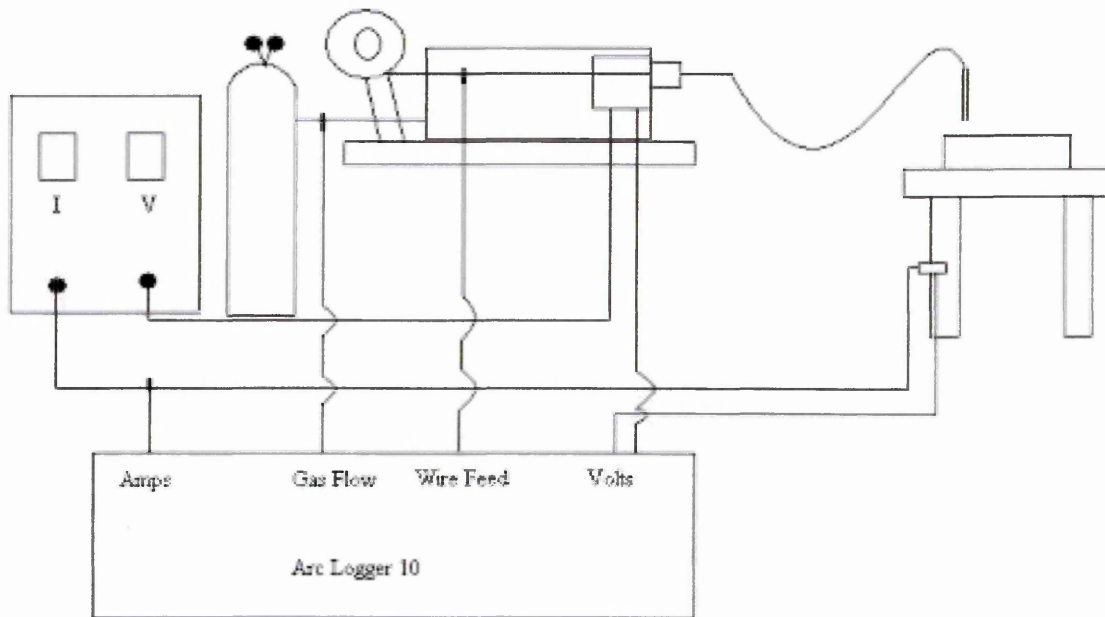


Figure 3.4 – Schematic diagram of the Arc Logger Ten (ALX)

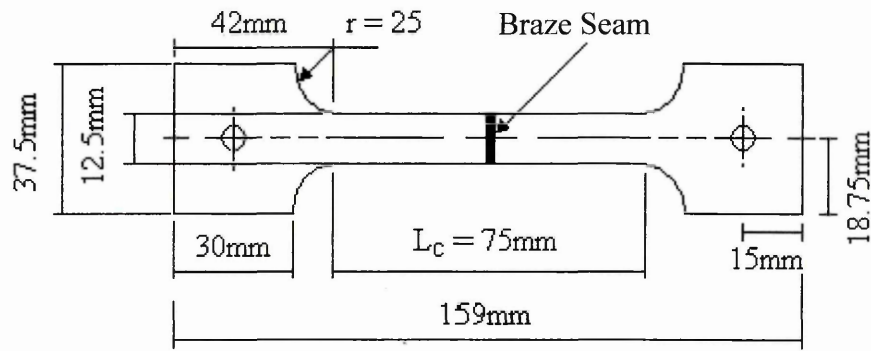
3.4.1.4 Optimisation of Arc Characteristics

In order to determine the correct arc characteristics for each combination of filler material and shielding gas the Fronius TransPluseSynergic 2700 welding equipment was set in synergic mode and the closest equivalent pre set programme for the filler material and shielding gas was selected. The Fronius RCU5000i was then used to manipulate the pulsed current variables until a stable arc was achieved.

3.4.1.5 Optimisation of Butt Joint Root Gap

Although arc brazing does not require capillary action to distribute the filler material the gap between the two plates to be joined it was still felt to be an important variable. If the plates were positioned too close together the braze alloy would not be able to completely penetrate the depth of the joint. Alternatively, if the plates were positioned too far apart the braze alloy would not be able to bridge the gap between the faying surfaces and this would result in lack of fill.

In order to ascertain the optimum width between the faying surfaces two plates were set up and clamped with a 0.1mm gap between them. The plates were then brazed together. The process variables such as current and voltage were dependent upon the composition of the shielding gas. The four combinations of filler material and shielding gas that had been used in the test detailed in section 3.2 were again used. This process was repeated with the gap increasing by 0.1mm until a gap width was found where two consecutive brazes were produced showing evidence of lack of fill. The plates were then examined and only those samples which showed evidence of penetration through the entire joint were accepted. Tensile test specimens in the “dog bone” configuration as shown in figure 3.5 were prepared so that the mechanical properties of the different gap widths could be investigated.



L_c – Parallel Length

Figure 3.5 – Dog bone tensile test piece (butt joint)

3.4.1.6 Selection of Braze Filler Material and Shielding Gas Compositions

The final process parameters to examine and optimise were the composition of the shielding gas and the chemical composition of the braze alloy. To do this, butt joints were constructed using three different filler materials: BS:2901 C9, BS:2901 C28 and BS:2901 C11 with pure argon, argon containing 1% oxygen and argon containing 2% oxygen shielding gases, using a 0.5mm gap between the faying surfaces. After brazing the braze reinforcement was removed by grinding. The plates were laser cut into the dog bone configuration shown in figure 3.5 and tensile tested. 6 dog bone specimens were also laser cut from a 1mm thick unbrazed sheet of AISI grade 304 stainless steel for comparison. These results were then compared to those obtained from the procedure detailed in section 3.4.1.5. Table 3.2 details the combinations of filler material and shielding gas tested.

Sample ID	Filler Material	Filler Material Composition	Shielding Gas Composition
BGT15	BS:2901 C28	92% Cu; 8% Al	Argon + 2%O ₂
BGT25	BS:2901 C28	92% Cu; 8% Al	Pure Argon
BGT35	BS:2901 C9	96% Cu; 1%Mn; 3% Si	Pure Argon
BGT45	BS:2901 C9	96% Cu; 1%Mn; 3% Si	Argon + 2%O ₂
BGT55	BS:2901 C9	96% Cu; 1%Mn; 3% Si	Argon + 1%O ₂
BGT65	BS:2901 C11	93% Cu, 7% Sn	Pure Argon
BGT75	BS:2901 C11	93% Cu, 7% Sn	Argon + 1%O ₂
BGT85	BS:2901 C11	93% Cu, 7% Sn	Argon + 2%O ₂
BGT95	BS:2901 C28	92% Cu; 8% Al	Argon + 1%O ₂

Table 3.2 – Combinations of filler materials and shielding gases tested

3.4.2 Effect of Braze Seam Geometry on Tensile Properties

Removing the braze seam after the joining process offers both advantages and disadvantages for the automotive industry. Firstly, if the brazed joint is in a visible area of the car body (such as the C pillar) there would be an advantage to grind this, as it would provide a better cosmetic finish. However, the grinding process would incur increased cost to the process through the time taken for the operation and the material waste. The grinding process could also produce surface imperfections (notches) in the surface of the material.

Before it could be decided if the braze seam was to be removed (or left intact) it was necessary to establish whether the geometry of the braze seam affected the mechanical properties of the joint. To do this two plates were joined for each combination of filler material and shielding gas (as shown in table 3.2). These plates were then cut into the dog bone configuration shown in figure 3.5 and tensile tested with the braze seam left intact. These results were then compared to those already obtained for samples with their braze seam removed.

3.4.3 Impact Testing

3.4.3.1 Modified Quantitative Chisel Test

It was not possible to manufacture standard Charpy impact samples for the joints created as it would not be possible to braze a sample of sufficient depth in a single pass. Instead it was decided to adapt a quantitative impact test which was designed for resistance spot welds (RSW), and which has been developed at Sheffield Hallam University⁶¹.

The first stage of the investigation was undertaken by D. Mallon. To ensure the arc brazed plug joints would fail in shear in the same way as the resistance spot welds. To do this lap shear specimens were manufactured as shown in figure 3.6 with the dimensions stipulated in table 3.3.

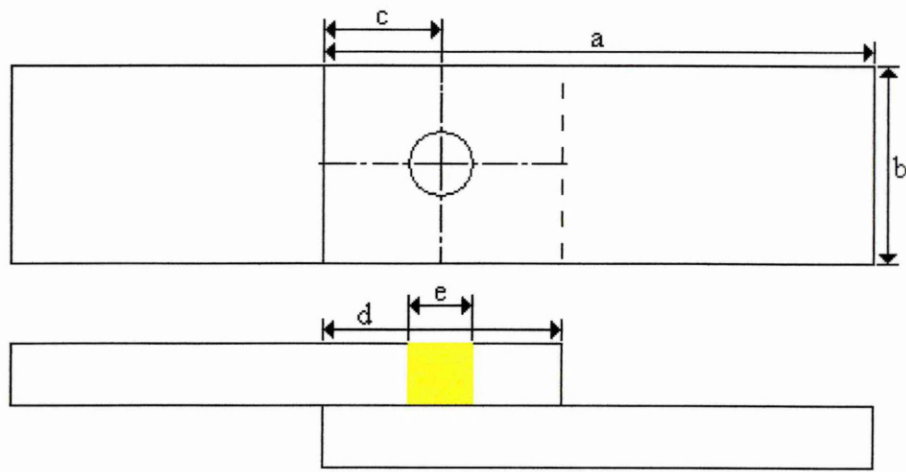


Figure 3.6 - Plug Braze Lap Shear Specimen

Dimension	Description	Size
a	Sheet Length	100mm
b	Sheet Width	30mm
c	Pre Braze Length	15mm
d	Sheet Overlap	45mm
e	Braze Hole Diameter	3, 6 or 8mm

Table 3.3 - Plug Braze Lap Shear Sample Dimensions

Once it was established that the plug braze lap shear samples failed in a similar way to the resistance spot weld impact samples, more plug braze joints were manufactured in the configuration shown in figure 3.7 with the dimensions given in table 3.4.

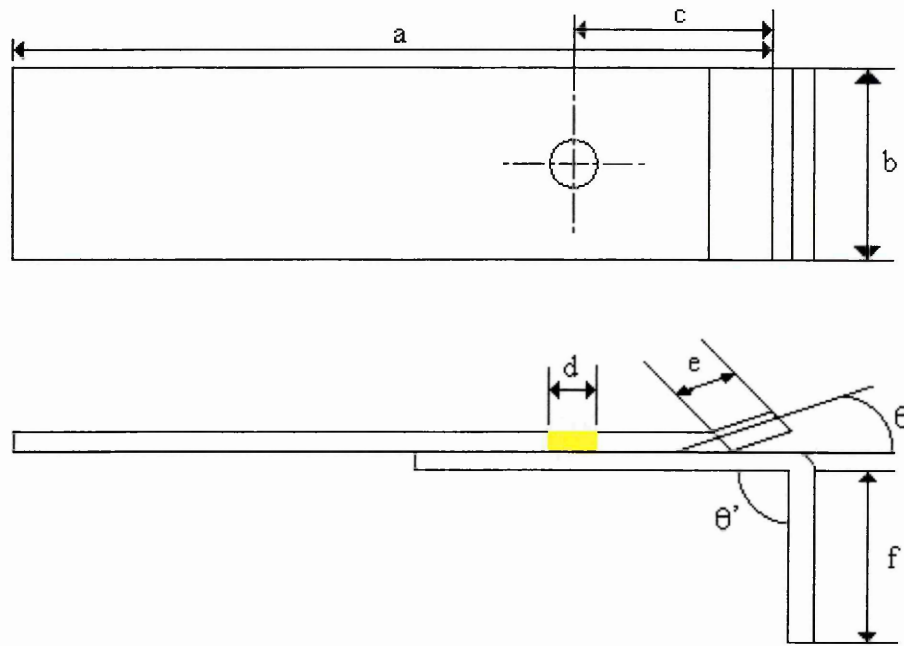


Figure 3.7 – Modified arc brazed joint, diagram modified from⁶¹

Dimension	Description	Size
a	Top Sheet Length	100mm
b	Top Sheet width	30mm
c	Pre Base Length	15mm
d	Braze Diameter	3, 6, 8mm
e	Raised Lap Length	5mm
f	Clamp Lap Length	60mm
θ	Raised Lap Angle	25°
θ'	Clamp Lap Angle	85°

Table 3.4 – Quantitative Arc Braze impact test samples dimensions

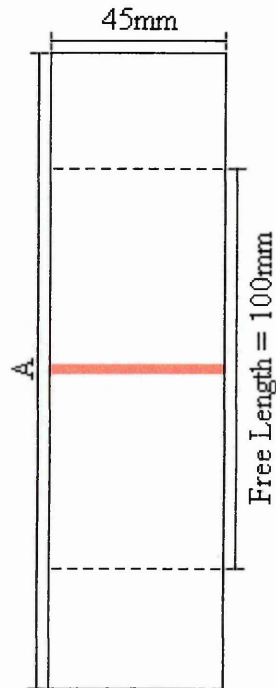
The Gas Metal Arc Spot Welding process also had to be modified to ensure that effective brazing occurred. In the Gas Metal Arc Spot Welding process the plates

would be clamped together and then the arc would be struck on the top sheet. The heat from the process would result in the material under the arc melting and combining with the filler material to form the weld nugget however, this would not be appropriate for arc brazing. To ensure that an adequate braze joint was produced a hole was drilled in the area in the top sheet in which the braze plug was to be deposited, to enable the braze material to wet both the surfaces of the upper sheet and the lower sheet.

Initially, during the investigation by D. Mallon, 6mm holes were drilled into the top sheet of the joint. These joints failed to wet effectively and so a second investigation was undertaken by S Magowan to improve the wetting by drilling different diameter holes. The two hole sizes chosen were 3mm and 8mm, whilst a lack of wetting was again observed using a 3mm hole, the joints made with an 8mm hole wetted sufficiently to allow impact testing to be undertaken.

3.4.4 Fatigue Testing - Similar Metal Butt Joint

A staircase fatigue test was carried out on 25 similar metal butt joints manufactured from 1mm AISI 304 parent material, BS:2901 C28 filler material and argon containing 1 % oxygen shielding gas as shown in figure 3.8. This combination of filler material and shielding gas was chosen due to the superior mechanical properties established in the previous tensile and impact tests.



A = 160mm

Figure 3.8 – Similar Metal Butt Joint Fatigue Test Sample

The load ratio (minimum load/maximum load) was set to 0.1 and the test was conducted at a frequency of 25Hz. If the joint survived 2×10^6 cycles it was considered a run out. The failure criteria was set to a stroke displacement of ± 2.5 mm.

3.5 *Manufacturing Similar Metal Arc Brazed Lap Joints*

Once a suitable combination of filler material and shielding gas had been determined for the manufacture of butt joints (BS:2901 C28 filler material and argon containing 1% oxygen shielding gas) the process variables were again manipulated to manufacture arc brazed lap joints using the same filler material and shielding gas as for the manufacture of butt joints

When suitable process parameters had been determined the effect, if any, of the length of overlap was investigated. To do this 12 sheets of stainless steel were sectioned and split into four pairs. Two pairs were then joined with a 10mm overlap, two pairs joined with a 20mm overlap and two pairs were joined with a 30mm overlap, with a single seam, as can be seen in figure 3.9i. Due to excessive distortion upon heating and cooling the samples manufactured with a 30mm overlap were discarded.

Eight more plates with similar dimensions were also sectioned, this time two pairs were joined with a 10mm overlap and two pairs joined with a 20mm overlap with a double seam, as can be seen in figure 3.9ii.

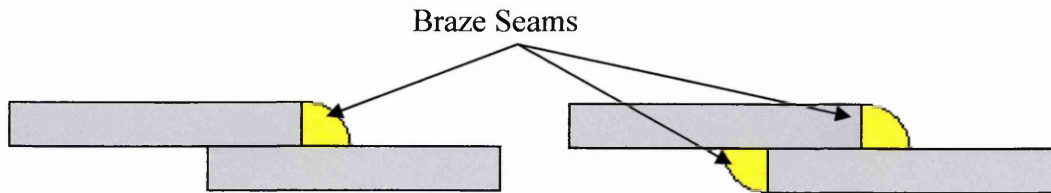
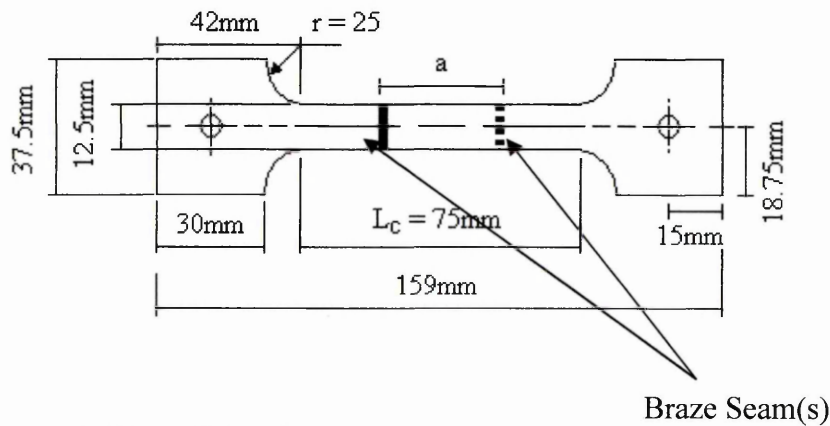


Figure 3.9i – Joint geometry of a single seam lap joint Figure 3.9ii – Joint geometry of a double seam lap joint

These plates were then laser cut into the dog bone configuration shown in Figure 3.10:



a = overlap length (10mm/20mm)

Figure 3.10 – Lap joint dog bone tensile test piece.

Upon microstructural investigation of the lap joints with a 10mm and 20mm single overlap it was noted that the bottom sheet of the lap joint was not wetting in a similar manner to the top sheet or the previously constructed butt joints. For this reason a further series of lap joints were manufactured to investigate the wetting of the bottom sheet and the subsequent mechanical strength could be improved by using the following torch angles as shown in figure 3.11:

- $\theta = 45^\circ$
- $\theta = 60^\circ$
- $\theta = 70^\circ$
- $\theta = 80^\circ$

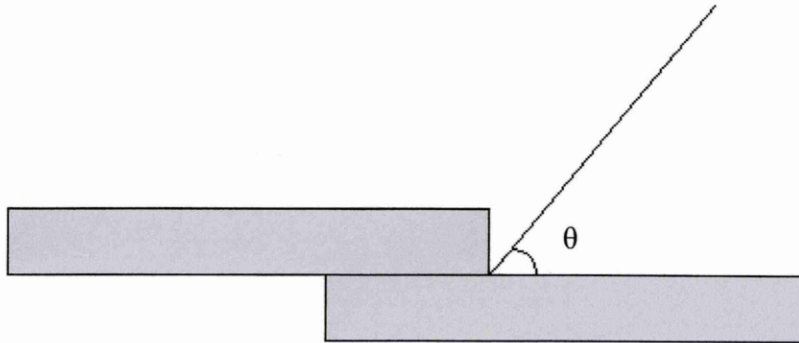


Figure 3.11 - Orientation of GMAB Torch during Manufacture of Similar Lap Joints

3.6 Dissimilar Butt Joints – Dogal 260RP-x Zinc Coated Mild Steel to AISI 304 Stainless Steel

3.6.1 Determination of Process Variables

For the dissimilar metal butt joints AISI 304 grade stainless steel was joined to Dogal 260RP-x, zinc coated rephosphorized mild steel. The average zinc coating thickness was stated as 7 μ m.

The initial trial attempted to manufacture dissimilar metal butt joints using the same process parameters that had been used for the similar metal butt joints, as shown in Appendix 1, however the nature of the short circuit transfer process combined with the zinc vapour led to the braze arc being too unstable. Therefore, the process variables were modified for dissimilar metal joining to achieve spray arc transfer.

3.6.1.1 Optimisation of Torch Height and Torch Angle

Optimisation of the torch height and torch angle was achieved by a process of trial and error. In the case of dissimilar metal joining the height and angle of the torch had to be set to allow the escape of the zinc vapour from the arc, as well as avoiding excessive heat input and spatter as with similar metal butt joints.

3.6.1.2 Optimisation of Torch Velocity

A BOC HW75 Tractor as shown in figure 3.4 was again used to regulate the torch velocity. Manipulation of the process variables was used to establish a pass velocity

which would produce an aesthetically pleasing seam with complete wetting of the joint and without excessive braze reinforcement being deposited.

3.6.1.3 Optimisation of the Arc Characteristics

As outlined in section 3.6.1 it was not possible to manufacture dissimilar metal butt joints using the short circuit transfer method and so the Fronius RCU5000i was used to manipulate the pulsed current variables to achieve spray arc transfer was obtained. The variables were then modified so that a stable arc was established.

3.6.1.4 Optimisation of Butt Joint Root Gap

Again the root gap was thought to be an important variable. This was investigated in the same manner as for the similar butt joints, detailed in section 3.4.1.5. However, due to the experience gained from previous work (see section 4.3.1.4) it was possible to narrow down this to gaps between 0.5mm and 0.7mm.

3.6.1.5 Selection of Filler Material

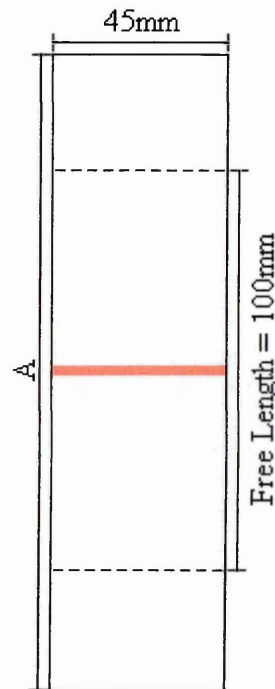
Dissimilar metal butt joints were constructed using BS:2901 C9 and BS:2901 C28 filler materials, argon containing 1% oxygen shielding gas and a 0.6mm root gap between the faying surfaces. The joints were sectioned using a guillotine and machined into the dogbone configuration shown in figure 3.5 and tensile tested to give an initial indication of any differences between the two braze filler materials. BS:2901 C28 gave the better performance in the tensile test and so two more plates of AISI 304 stainless steel were joined to two more plates of zinc coated mild steel using

this filler material. Three dogbones were then water jet cut^{iv} from each of the plates and tensile tested to give the results detailed in section 4.6.5.

^{iv} The second set of dogbones were water jet cut to eliminate the possibility of notches or burrs on the edge of the test pieces influencing the results.

3.6.2 Fatigue Testing - Dissimilar Metal Butt Joints

A staircase fatigue test was conducted on 25 dissimilar metal butt joints. The samples were manufactured from 1mm AISI 304 stainless steel and 1.2mm Dogal 260 RP-x parent materials using BS:2901 C28 braze alloy and argon containing 1% oxygen shielding gas as shown in figure 3.12.



A=150mm

Figure 3.12 – Dissimilar Metal Butt Joint Fatigue Test Sample

As with the similar metal fatigue testing the load ratio was set to 0.1 and the test was conducted at a frequency of 25Hz. If the joint survived 2×10^6 cycles it was considered a run out. The failure criteria was set to a stroke displacement of ± 2.5 mm.

3.7 Scanning Electron Microscopy Measurement of Mullins Grooving

During microstructural investigation of arc brazed joints it was noted that, at the interface of the braze and the stainless steel, copper penetrated the grain boundaries of the stainless steel forming a composite type area. To investigate whether this penetration followed the Mullins model, of grain boundary grooving, two joints were manufactured, one from similar parent materials and one from dissimilar parent materials. During the brazing of the joints the ALX arc measuring equipment was used to monitor the arc variables during the process. The joints were sectioned, ground and polished to a 1 μ m finish and electrolytically etched in 10% oxalic acid. The samples were then examined using the SEM and 20 measurements of the depth of penetration of the copper from the interface were measured. Finally, the groove opening angles were measured using a protractor.

3.8 ***Summary***

In Chapter 3 the methods used to determine the feasibility of the arc brazing process for brazing stainless steel to itself and to zinc coated mild steel are discussed. The methodology for determining the microstructure of an arc braze with high joint efficiency, the process parameters and mechanical testing for similar and dissimilar metal butt joints are detailed. The experimental work to demonstrate the feasibility of manufacturing similar metal arc brazed lap joints and the correlation between Mullins's theory of grain boundary grooving and the work conducted in this investigation is detailed. Chapter 4 details the results of these investigations.

4.0 Results

4.1 Material Characterisation

Table 4.1 shows the results of tensile testing conducted on the as received AISI 316 and AISI 304 grades of stainless steel.

Test Piece	Material	Rm (MPa)	Rp _{0.2} (MPa)
1a	316	641	305
1b	316	609	202
1c	316	645	318
1d	316	646	278
1e	316	643	293
	Range	37	116
	Average	637	279
1g	304	636	240
1h	304	638	292
1i	304	629	259
1j	304	632	295
1k	304	621	282
1l	304	626	342
	Range	17	102
	Average	630	285

Test Piece 1f failed outside of the gauge length

Table 4.1 - Tensile Properties of AISI 316 and 304 Stainless Steel

4.2 Initial Testing of Similar Metal Butt Joints

4.2.1 Comparison of Ultimate Tensile Strengths of Various Combinations of Parent Material, Filler Material and Shielding Gas

Table 4.2 shows the results of tensile testing conducted on similar metal butt joints constructed using combinations of BS:2901 C9 and BS:2901 C28 filler materials; pure argon and argon containing 2% oxygen shielding gasses and AISI 316 and AISI 304 grades of stainless steel as the parent material.

Table 4.2

Test Piece	Parent Material	Shielding Gas	Filler Material	Rm (MPa)
2-316ia	316	Pure Argon	BS:2901 C9	300
2-316ib	316	Pure Argon	BS:2901 C9	311
2-316ic	316	Pure Argon	BS:2901 C9	250
2-316id	316	Pure Argon	BS:2901 C9	182
2-316ie	316	Pure Argon	BS:2901 C9	308
2-316if	316	Pure Argon	BS:2901 C9	296
			Range	129
			Average	274

Table 4.2 Contd.

Test Piece	Parent Material	Shielding Gas	Filler Material	Rm (MPa)
2-316iia	316	Argon + 2%O ₂	BS:2901 C9	430
2-316iib	316	Argon + 2%O ₂	BS:2901 C9	454
2-316iic	316	Argon + 2%O ₂	BS:2901 C9	434
2-316iid	316	Argon + 2%O ₂	BS:2901 C9	433
2-316iie	316	Argon + 2%O ₂	BS:2901 C9	441
2-316iif	316	Argon + 2%O ₂	BS:2901 C9	447
			Range	24
			Average	440
2-316iia	316	Pure Argon	BS:2901 C28	440
2-316iib	316	Pure Argon	BS:2901 C28	392
2-316iic	316	Pure Argon	BS:2901 C28	379
2-316iid	316	Pure Argon	BS:2901 C28	387
2-316iie	316	Pure Argon	BS:2901 C28	373
2-316iif	316	Pure Argon	BS:2901 C28	378
			Range	67
			Average	391

Table 4.2 Contd.

Test Piece	Parent Material	Shielding Gas	Filler Material	Rm (MPa)
2-316iva	316	Argon + 2%O ₂	BS:2901 C28	503
2-316ivb	316	Argon + 2%O ₂	BS:2901 C28	523
2-316ivc	316	Argon + 2%O ₂	BS:2901 C28	322
2-316ivd	316	Argon + 2%O ₂	BS:2901 C28	467
2-316ive	316	Argon + 2%O ₂	BS:2901 C28	460
2-316ivf	316	Argon + 2%O ₂	BS:2901 C28	524
			Range	202
			<i>Average</i>	467
2-304ia	304	Pure Argon	BS:2901 C9	205
2-304ib	304	Pure Argon	BS:2901 C9	240
2-304ic	304	Pure Argon	BS:2901 C9	247
2-304id	304	Pure Argon	BS:2901 C9	236
2-304ie	304	Pure Argon	BS:2901 C9	242
2-304if	304	Pure Argon	BS:2901 C9	271
			Range	66
			<i>Average</i>	240

Table 4.2 Contd.

Test Piece	Parent Material	Shielding Gas	Filler Material	Rm (MPa)
2-304iia	304	Argon + 2%O ₂	BS:2901 C9	483
2-304iib	304	Argon + 2%O ₂	BS:2901 C9	460
2-304iic	304	Argon + 2%O ₂	BS:2901 C9	504
2-304iid	304	Argon + 2%O ₂	BS:2901 C9	409
2-304iie	304	Argon + 2%O ₂	BS:2901 C9	440
2-304iif	304	Argon + 2%O ₂	BS:2901 C9	484
			Range	95
			Average	463
2-304iiaa	304	Pure Argon	BS:2901 C28	435
2-304iiaa	304	Pure Argon	BS:2901 C28	358
2-304iiic	304	Pure Argon	BS:2901 C28	418
2-304iiid	304	Pure Argon	BS:2901 C28	361
2-304iiie	304	Pure Argon	BS:2901 C28	489
2-304iiif	304	Pure Argon	BS:2901 C28	454
			Range	131
			Average	420

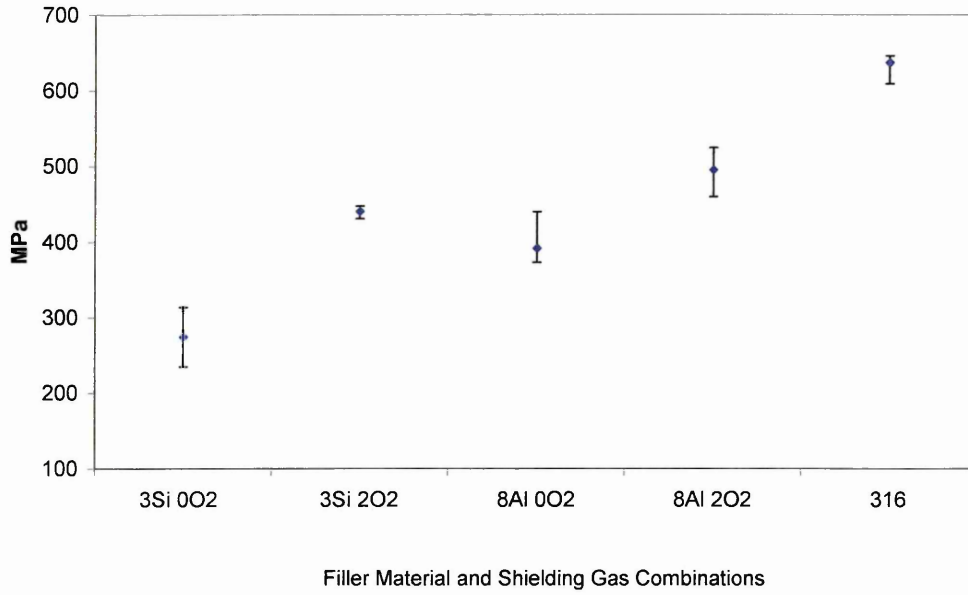
Table 4.2 Contd.

Test Piece	Parent Material	Shielding Gas	Filler Material	Rm (MPa)
2-304iva	304	Argon + 2%O ₂	BS:2901 C28	556
2-304ivb	304	Argon + 2%O ₂	BS:2901 C28	411
2-304ivc	304	Argon + 2%O ₂	BS:2901 C28	563
2-304ivd	304	Argon + 2%O ₂	BS:2901 C28	446
2-304ive	304	Argon + 2%O ₂	BS:2901 C28	421
2-304ivf	304	Argon + 2%O ₂	BS:2901 C28	517
			Range	152
			Average	486

Table 4.2 - Tensile Properties of Arc Brazed Butt Joints

By displaying the average tensile strengths for each set of conditions, see figures 4.1 and 4.2, it is possible to note any variation in strength due to filler material and shielding gas. Figures 4.3 and 4.4 display the average percentage elongations displayed by each combination of filler material shielding gas.

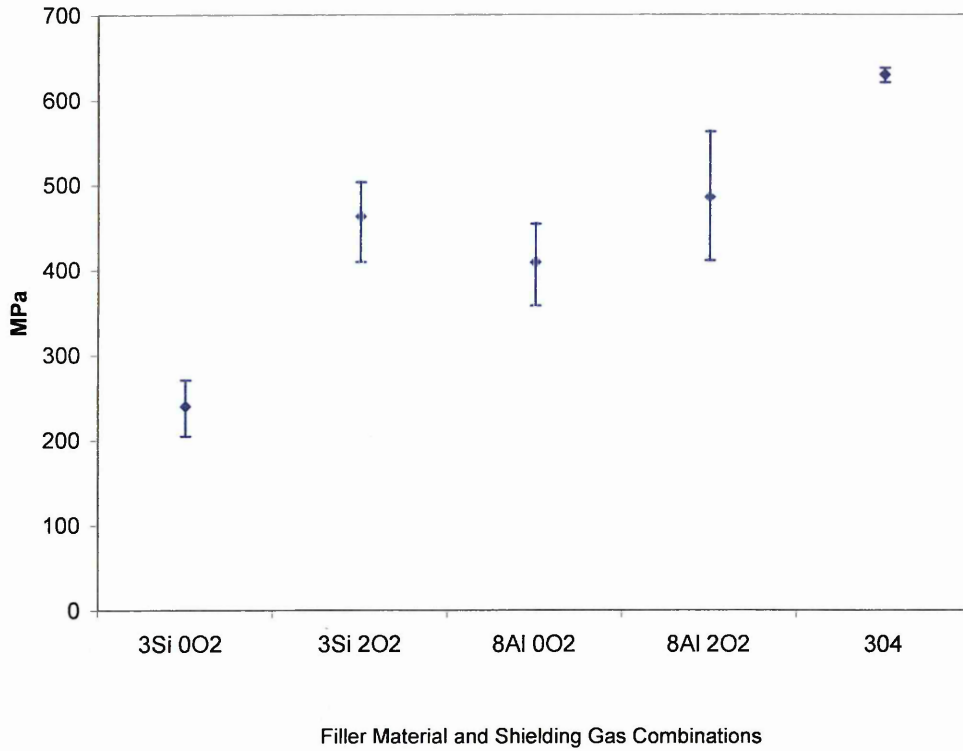
AISI 316 Stainless Steel



3Si	BS:2901 C9
8Al	BS:2901 C28
0O2	Pure Argon
2O2	Argon containing 2% Oxygen

Figure 4.1 - Comparison of tensile strengths for joints constructed from combinations of BS:2901 C9 and BS:2901 C28 filler materials; argon and argon containing 2% oxygen and 316 stainless steel base material.

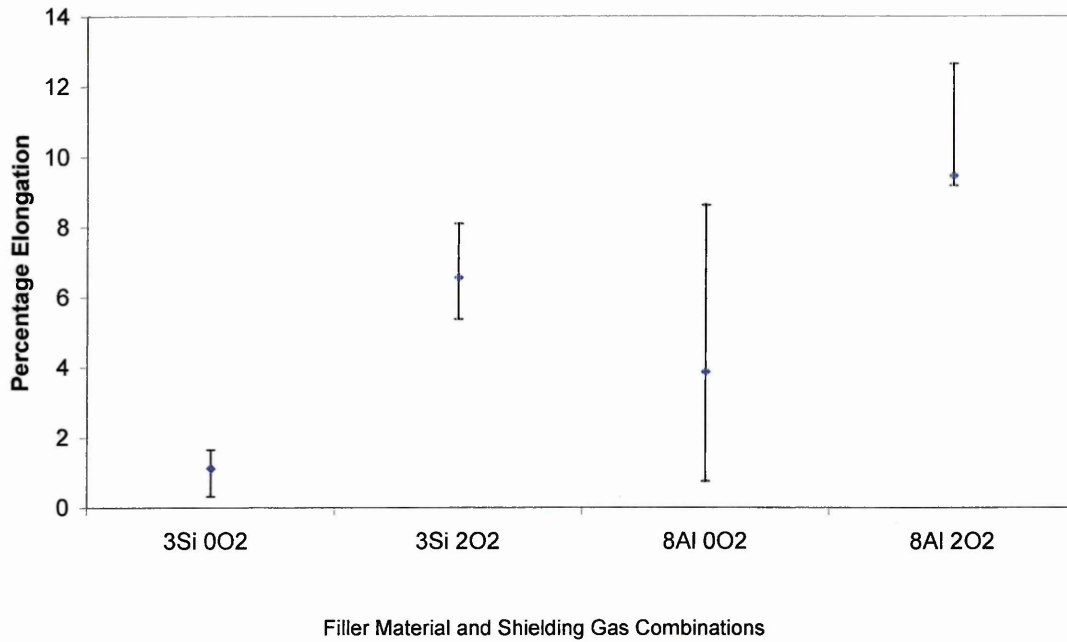
AISI 304 Stainless Steel



3Si	BS:2901 C9
8Al	BS:2901 C28
0O2	Pure Argon
2O2	Argon containing 2% Oxygen

Figure 4.2 - Comparison of tensile strengths for joints constructed from combinations of BS:2901 C9 and BS:2901 C28 filler materials; argon and argon containing 2% oxygen and 304 stainless steel base material.

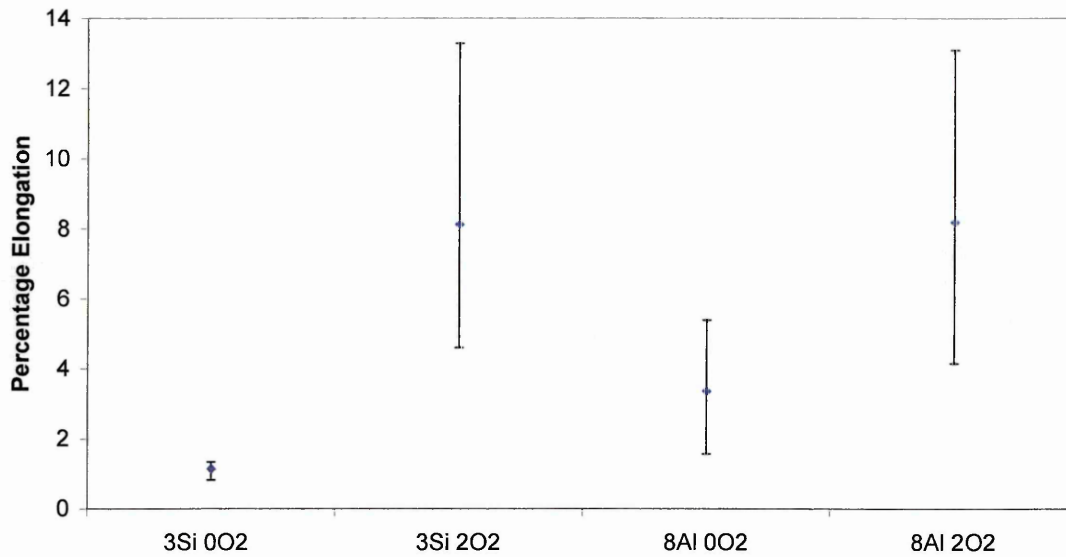
AISI 316 Stainless Steel



3Si	BS:2901 C9
8Al	BS:2901 C28
0O2	Pure Argon
2O2	Argon containing 2% Oxygen

Figure 4.3 - Comparison of percentage elongations of joints constructed from combinations of BS:2901 C9 and BS:2901 C28 filler materials; argon and argon containing 2% oxygen and 316 stainless steel base material.

AISI 304 Stainless Steel



Filler Material and Shielding Gas Combinations

3Si	BS:2901 C9
8Al	BS:2901 C28
0O2	Pure Argon
2O2	Argon containing 2% Oxygen

Figure 4.4 - Comparison of percentage elongations of joints constructed from combinations of BS:2901 C9 and BS:2901 C28 filler materials; argon and argon containing 2% oxygen and 304 stainless steel base material

4.2.2 Microstructural Characterisation of an Arc Brazed Joint with High Joint Efficiency

Figure 4.5 shows optical light micrographs of the interface between the braze and stainless steel from sample 2-304ia (table 4.2) which exhibited a tensile strength of 205MPa. The sample was etched in alcoholic ferric chloride.

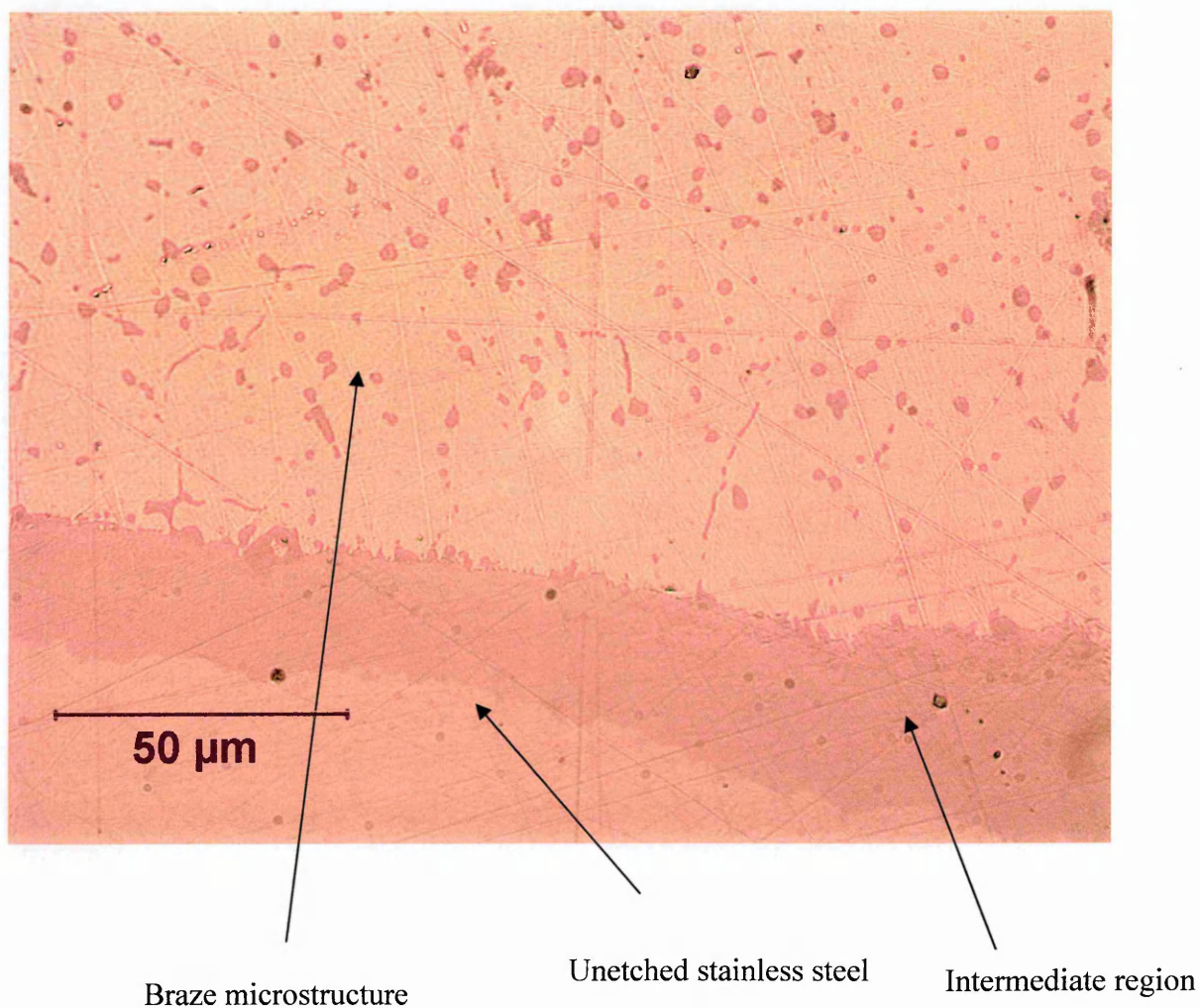
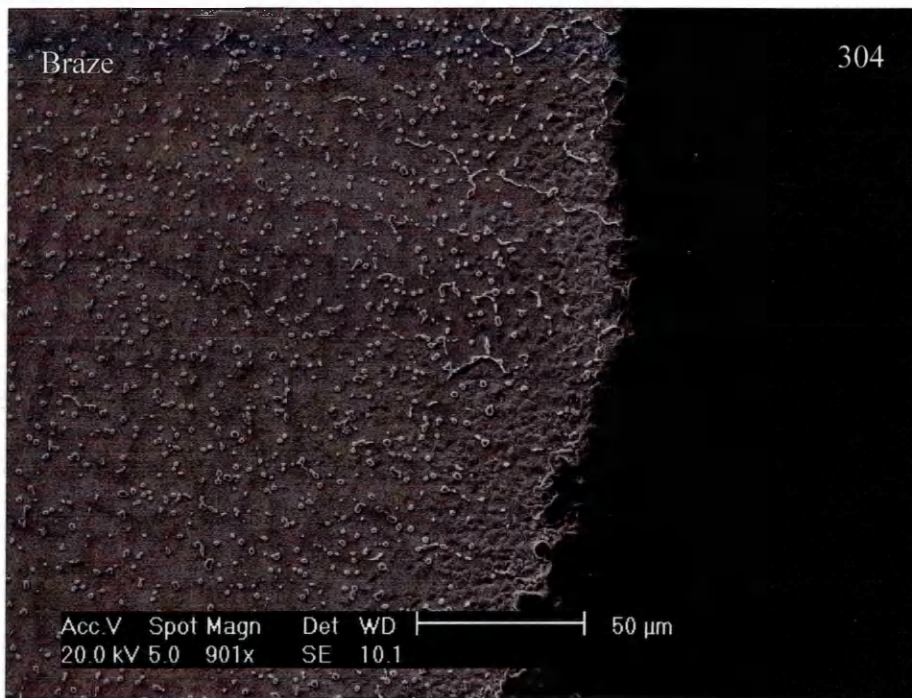


Figure 4.5 - Optical light micrograph taken at the joint interface of a sample manufactured from AISI 304 stainless steel parent material, brazed with BS:2901 C9 braze alloy and pure argon shielding gas etched in alcoholic ferric chloride. Tensile testing results showed no elongation.

In figure 4.5 there appear to be three distinct regions, the braze microstructure, the parent stainless steel and an intermediate region between the two. Whilst it was not possible to establish the identity of this intermediate region using light microscopy the x-ray detectors of the SEM were used to try and identify the chemicals present in this area. In figure 4.6 the secondary electron image, detailing the topographical features, and the x-ray maps, showing the distribution of the main elements, produced from sample 2-304ia are shown.



Iron X-ray Map



Chromium X-ray Map



Nickel X-ray Map



Copper X-ray Map

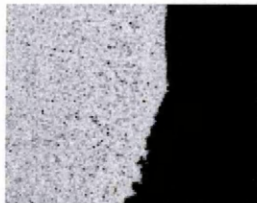


Figure 4.6 - Sample manufactured from AISI 304 stainless steel parent material, brazed with BS:2901 C9 braze alloy and pure argon shielding gas etched in alcoholic ferric chloride. Tensile testing results showed no elongation.

Figure 4.6 shows that there is a definite separation between the main elements from the stainless steel and the braze. Whilst no intermediate region is visible in the secondary electron image, the iron and nickel x-ray maps show a reduction in intensity moving towards the centre of the image from right to left. It may be this which is responsible for the darker intermediate region in figure 4.5.

Figure 4.7 shows an optical light micrograph of the interface between the braze and the stainless steel from sample 2-316ivf (table 4.2) which exhibited a tensile strength of 524MPa. The sample was etched in alcoholic ferric chloride.

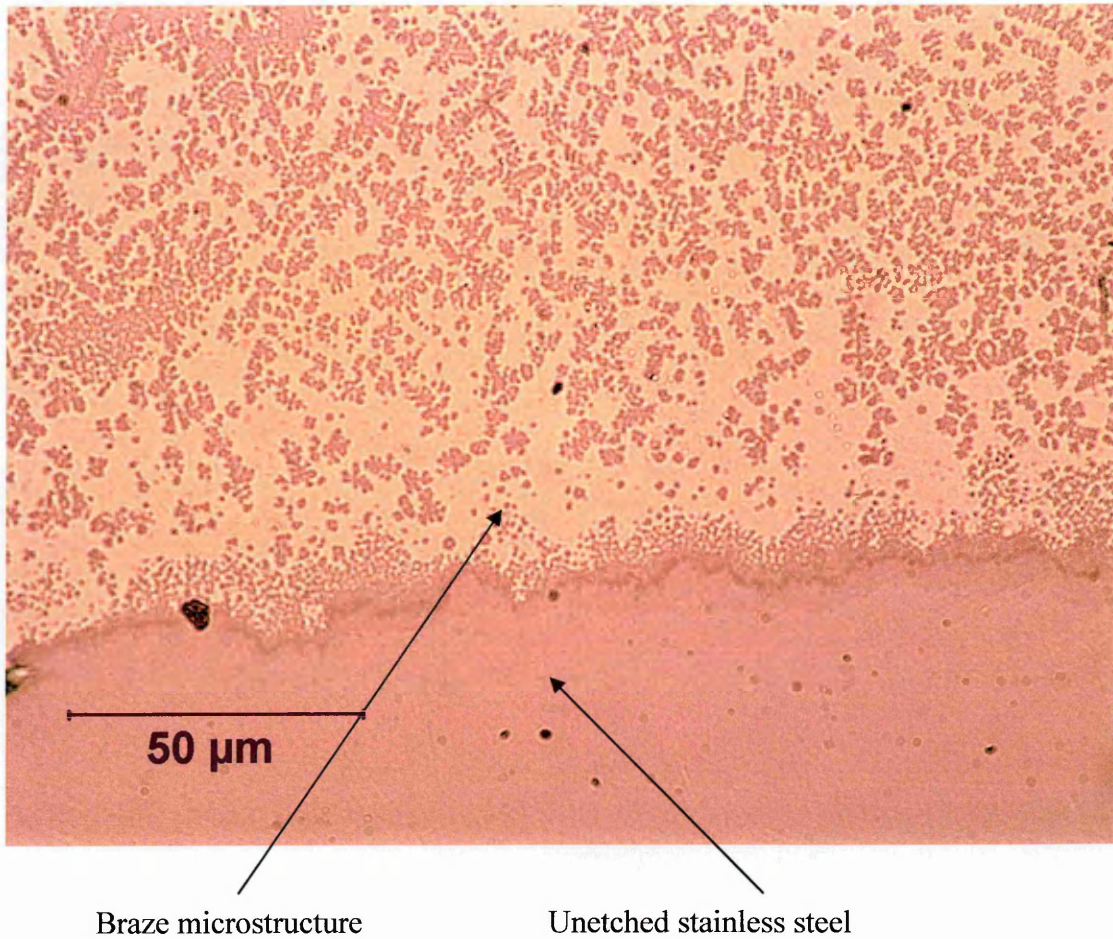
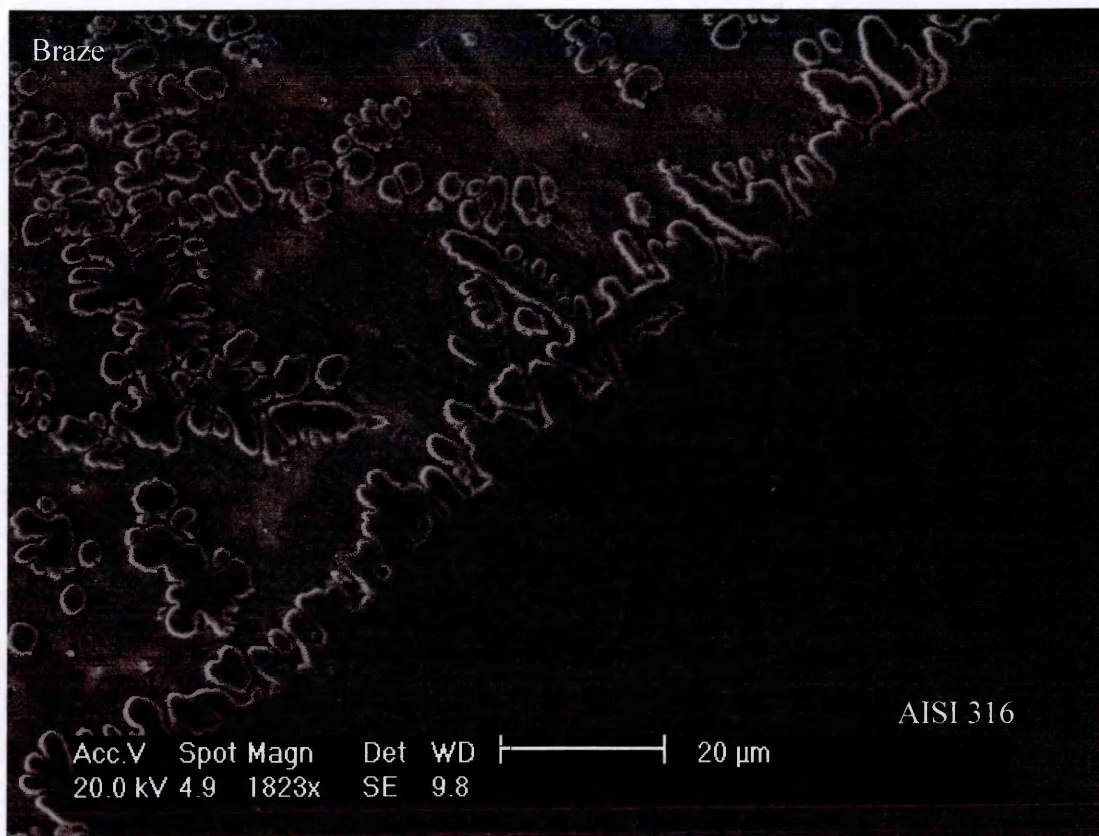
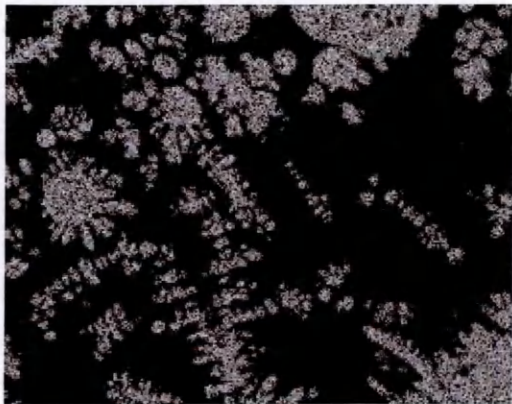


Figure 4.7 – Optical light micrograph taken at the joint interface of a sample manufactured from AISI 304 stainless steel parent material, brazed with BS:2901 C28 braze alloy and argon containing 2% oxygen shielding gas etched alcoholic ferric chloride.

The image in figure 4.7 looks very different to that in figure 4.5. The most obvious difference are the dark structures present in the braze microstructure. To identify these structures the SEM was used. Figure 4.8 shows the SEM secondary electron image and the copper and iron x-ray maps. The interface between the braze and the stainless steel is in the centre of the secondary electron image. This has been moved to the bottom right hand corner of the x-ray maps so that more of the braze microstructure can be seen.



Iron X-ray Map



Copper X-ray Map

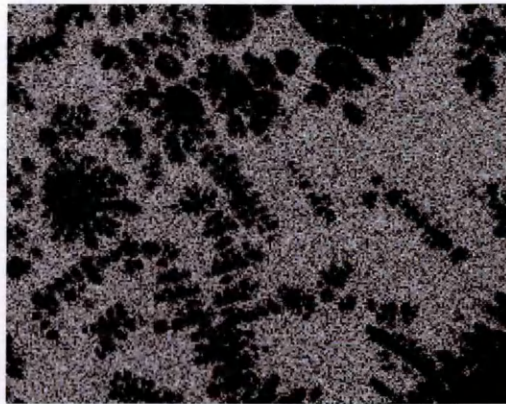


Figure 4.8 – Sample manufactured from AISI 316 stainless steel parent material, brazed with BS:2901 C28 braze alloy and argon containing 2% oxygen shielding gas etched alcoholic ferric chloride, showing a cellular dendritic structure composed of iron within the braze microstructure.

From figure 4.8 it can be seen that the interface of the braze and stainless steel has been altered during the joining process so as the iron from the stainless steel encroaches into the braze microstructure. Figure 4.8 also establishes that the dark structures seen in figure 4.7 were cellular dendritic structures of iron.

Comparison of figures 4.5 - 4.8 shows that the microstructure of arc brazes with a high tensile strength is very different to the microstructure of an arc braze with a low tensile strength. In the joints which exhibit a low tensile strength the iron from the stainless steel and copper from the braze remain separated, with a clear boundary between the two materials. However, the microstructure of an arc braze with high tensile strength shows the iron encroaching into the braze microstructure at the interface as well as cellular dendritic structures of iron within the braze.

Once the braze microstructure was established attention was turned to the stainless steel side of the interface. Samples were prepared and electrologically etched in 10% oxalic acid to reveal the microstructure on the stainless steel side of the interface.

Figures 4.9 – 4.12 show low and high magnification images of a possible intermetallic region in samples 2-304ia and 2-304ivf. Figure 4.9 is a low magnification image of an arc brazed with low joint efficiency

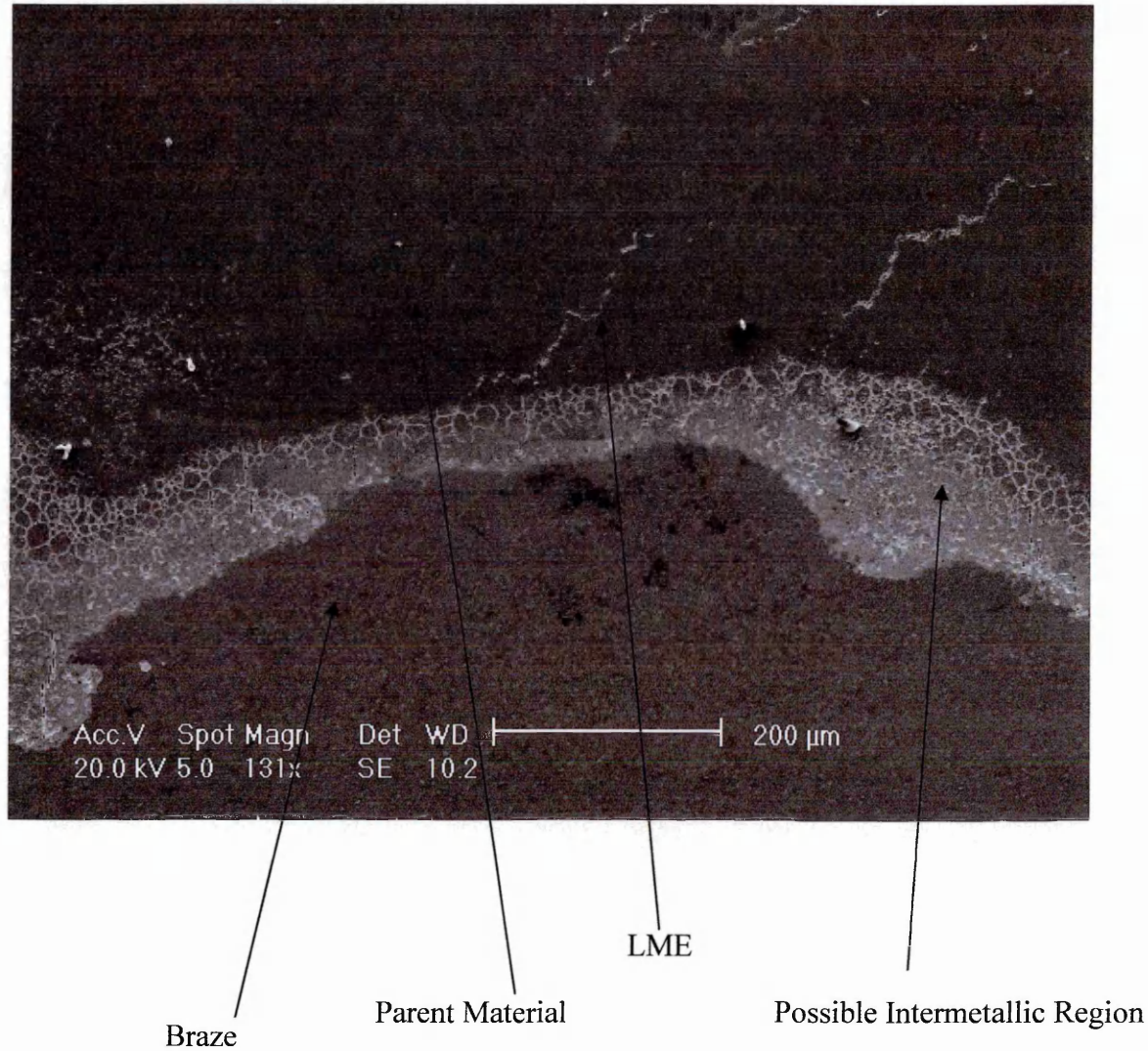


Figure 4.9 - Low magnification image of a sample with low joint efficiency manufactured from AISI 304 stainless steel parent material, brazed with BS:2901 C9 braze alloy and pure argon shielding gas dual etched in alcoholic ferric chloride and electro-etched in 10% oxalic acid.

In figure 4.9 (sample 2-304ia) there is evidence of LME penetrating into the stainless steel as well as what appears to be an intermetallic region between the braze and the parent material. Figure 4.10 has a high magnification image of this area.

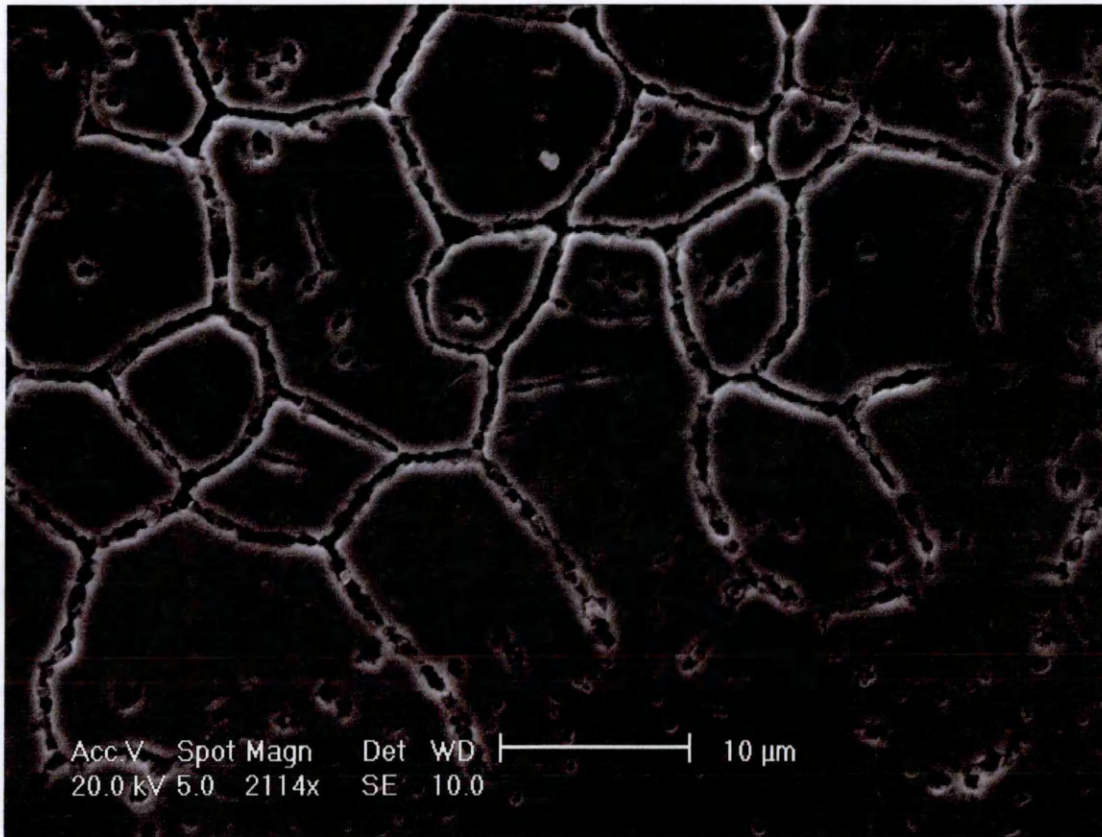


Figure 4.10 - High magnification using secondary electron imaging of the microstructure of the possible intermetallic region in figure 4.9.

Rather than being an intermetallic region the microstructure in figure 4.9, magnified in figure 4.10 has the same appearance as the 304 parent material. Although, the region cannot simply be parent material as it has etched preferentially to the bulk of the stainless steel.

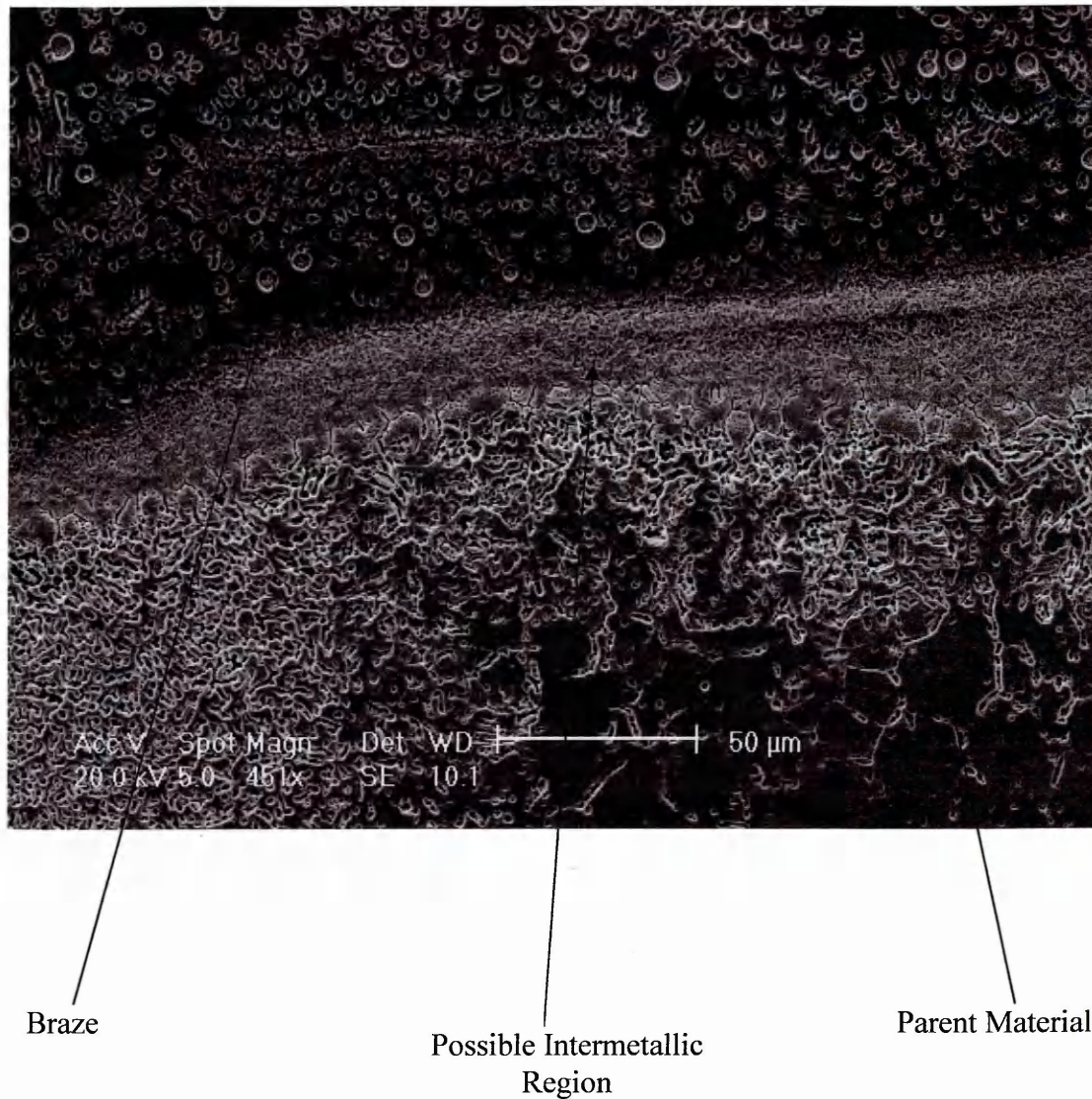
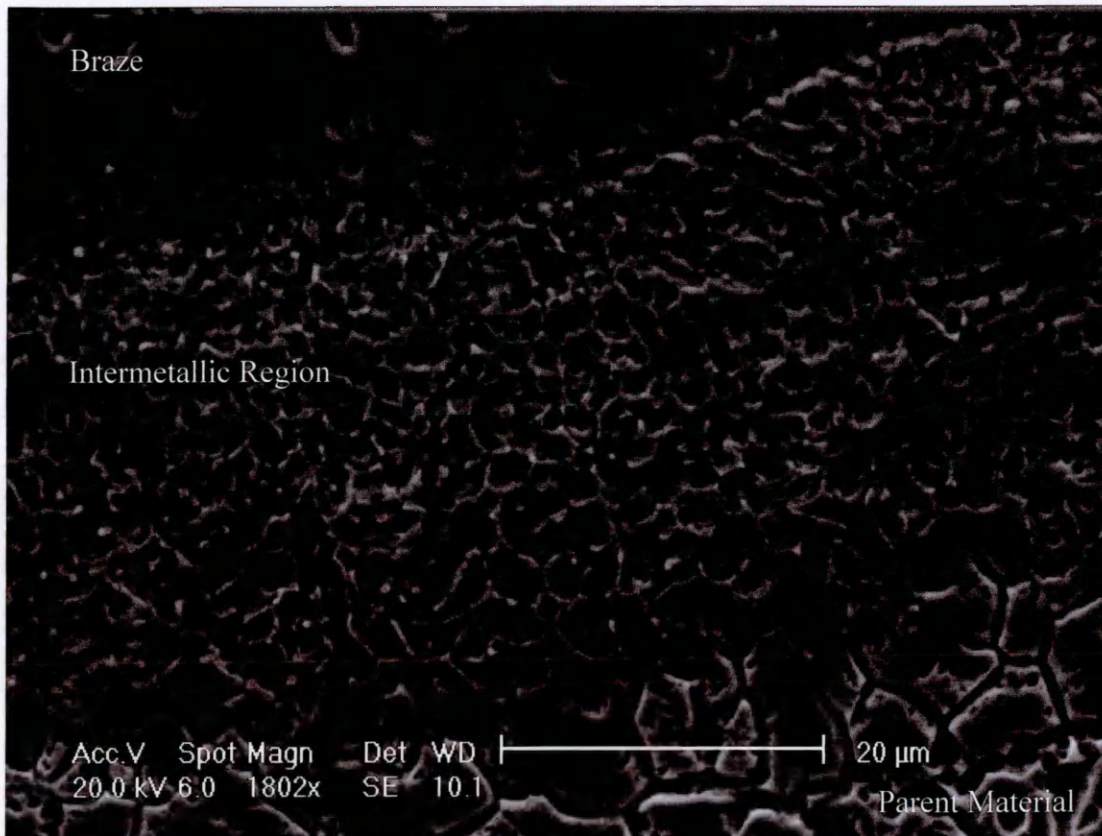


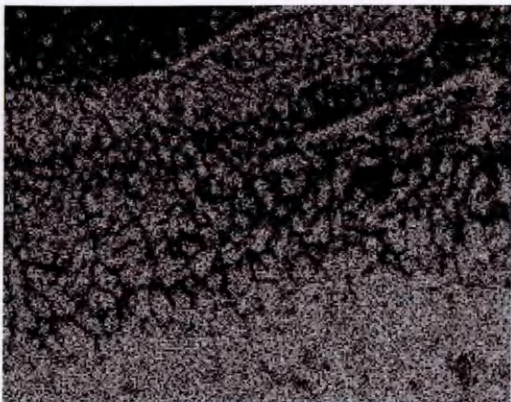
Figure 4.11 - Low magnification scanning electron microscopy secondary electron image of a sample with high joint efficiency manufactured from AISI 304 stainless steel parent material, brazed with BS:2901 C28 braze alloy and argon containing 2% oxygen shielding gas dual etched in alcoholic ferric chloride and electro-etched in 10% oxalic acid.

In figure 4.11 the microstructure of the parent material at the interface of an arc braze with high joint efficiency can be seen. Similar to figure 4.9 an intermetallic region

appears to exist between the stainless steel and the braze. Figure 4.12 is a high magnification image of this area along with the corresponding copper and iron x-ray maps.



Fe X-ray map



Cu X-ray Map



Figure 4.12 - High magnification scanning electron micrograph (secondary electron image) of the intermetallic region in figure 4.11 dual etched in alcoholic ferric chloride and electro-etched in 10% oxalic acid and x-ray maps showing the distribution of copper and iron.

Unlike figure 4.10, in figure 4.12 there is an intermetallic area where the copper appears to penetrate the grain boundaries of the stainless steel. It would normally be expected that this penetration would lead to embrittlement but this sample demonstrated high joint efficiency during tensile testing.

Figures 4.5 – 4.12 show there are marked differences in the microstructures of the braze and stainless steel around the interface of arc brazed joints with high and low joint efficiency. In joints with low joint efficiency the constituent elements of the parent material and braze remain mostly separated following the joining operation, with some copper penetrating the grain boundaries of the stainless steel resulting in embrittlement. The area of stainless steel immediately adjacent to the braze has also undergone some change as it etches far more readily than the bulk of the parent material. By contrast in an arc braze with high joint efficiency there is mixing of the elements from the braze and the parent material with cellular dendritic structures of iron forming in the braze. Copper also penetrates the grain boundaries of the stainless steel but to a much greater extent than that in the brazes with low joint efficiency, forming an intermetallic region at the interface. These observations and reasons for their occurrences will be discussed in more detail in Chapter 5.

4.2.2.1 Immersion Testing of AISI 304 in Molten BS:2901 C9

Braze Alloy

Figure 4.13i below shows a secondary electron image of a sample of AISI grade 304 stainless steel, which was immersed in a copper alloy containing 3% silicon and 1% manganese for 5 seconds at 1100°C. In figure 4.13ii are x-ray maps showing the distribution of copper, silicon, chromium and iron.

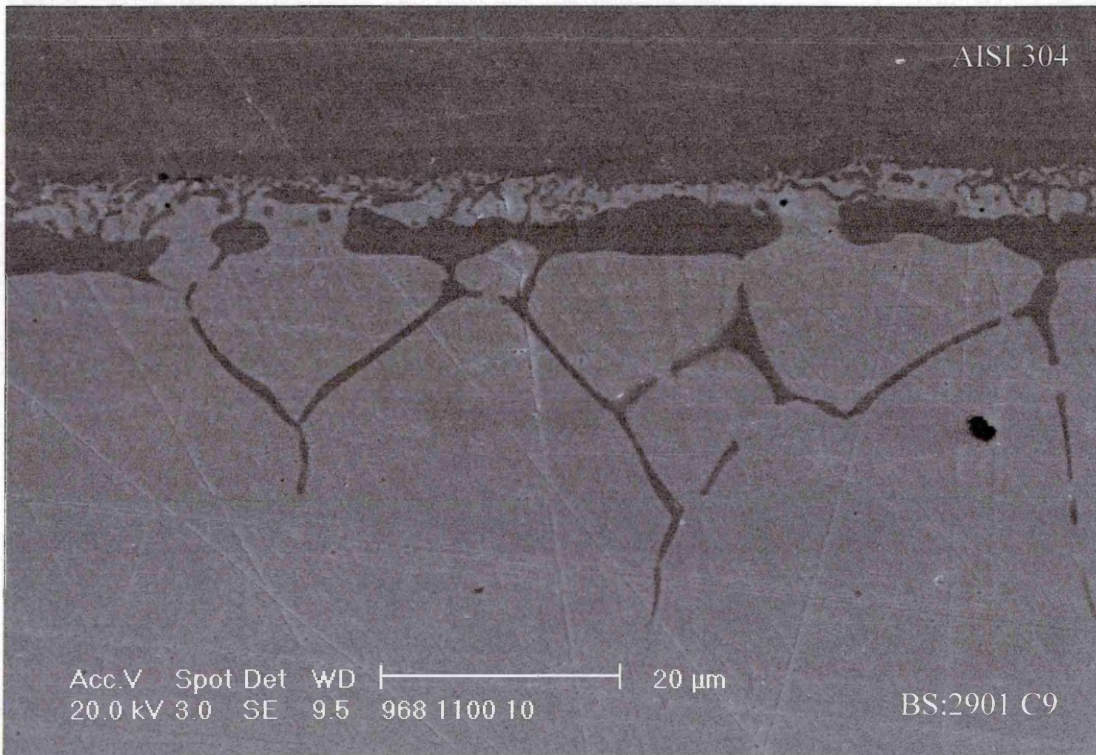
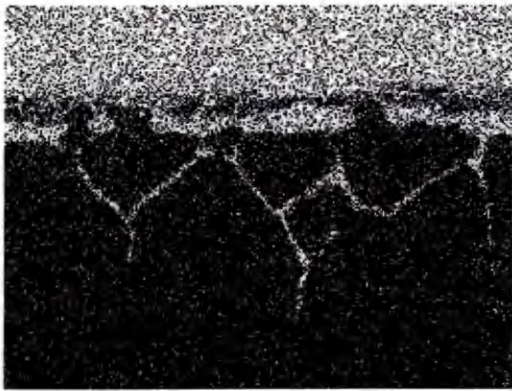
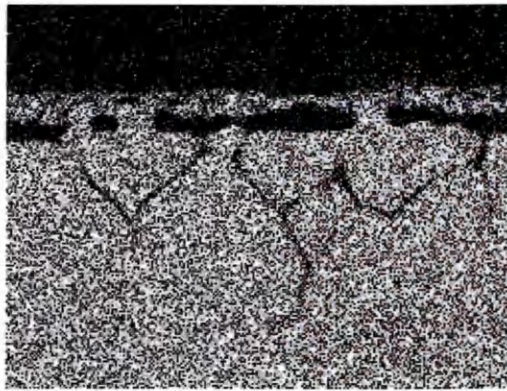


Figure 4.13i – Secondary electron image of AISI 304 stainless steel strip after immersion in BS:2901 C9 braze alloy.



Fe Ka1



Cu Ka1



Cr Ka1



Si Ka1

Figure 4.13ii – X-ray maps produced by EDX of image in figure 4.13i showing diffusion of iron, chromium and silicon into the copper of the braze alloy.

In figure 4.13ii it can be seen that the iron and chromium from the stainless steel have diffused into the copper alloy and that these two elements along with the silicon from the braze alloy have precipitated out of the copper at the grain boundaries.

4.2.2.2 Experimental melt of AISI 304 in BS:2901 C28 Molten Filler Metal at 1600°C

Figure 4.14 below shows the image of a cast sample composed of 10% AISI grade 304 stainless steel and 90% BS:2901 C28.

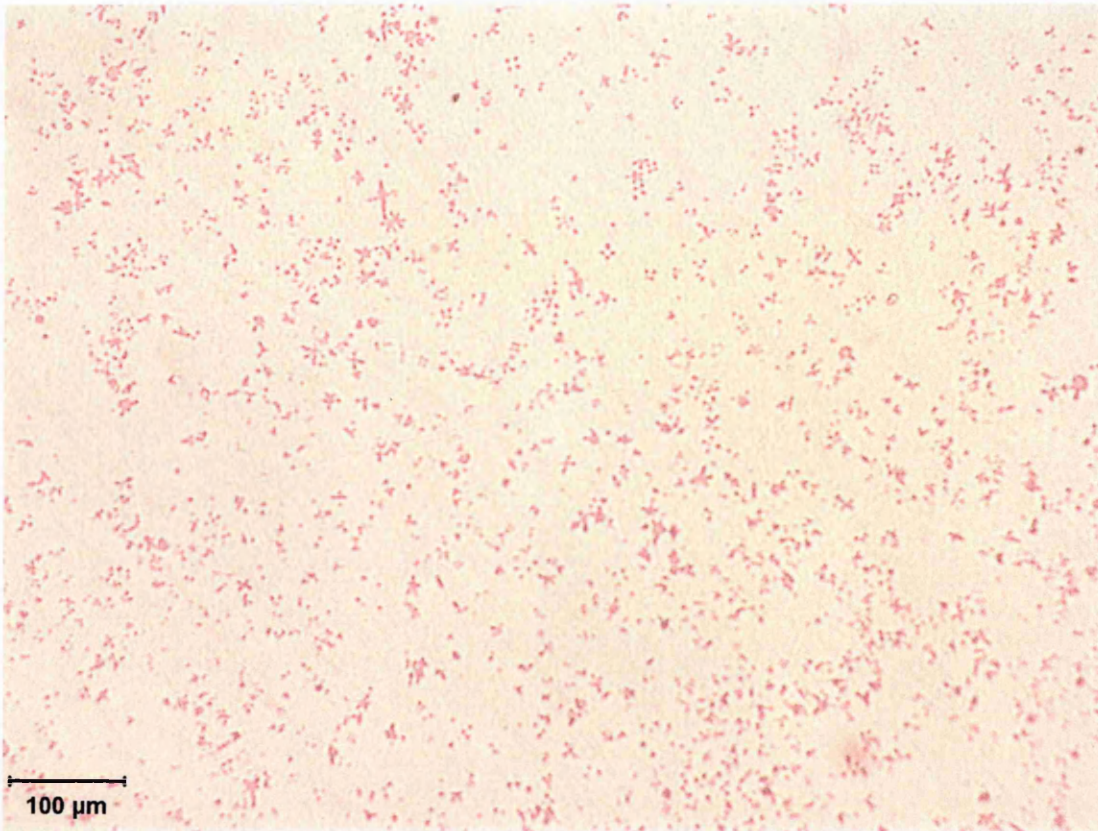


Figure 4.14 - As polished structure of an alloy composed of 10% 304 stainless steel and 90% BS:2901 C28 braze alloy showing similar cellular dendritic structures to those seen in arc brazed joints.

From figures 4.13 and 4.14 it would appear that the elements from the stainless steel may be present in the microstructure of the arc brazed joint though both dissolution and melting. The predominate method resulting in presence of these elements in the microstructures of the brazes in this study will be discussed along with a comparison between these findings and those of Li et al³⁸ in chapter 5.

4.2.2.3 Volume Fraction of Cellular Dendritic Structure in joints produced using BS:2901 C28 filler material and Pure Argon, Argon Containing 1% oxygen and Argon Containing 2% Oxygen Shielding Gases

Table 4.3 below shows the volume fraction of the cellular dendritic iron structures found in arc brazed joints manufactured, using AISI 304 stainless steel base material, BS:2901 C28 filler material with pure argon, argon containing 1% oxygen and argon containing 2% oxygen shielding gases, for each of the five random areas of each sample examined. The images can be found in Appendix 2.

Shielding Gas	Area	Volume Fraction (%)
Pure Argon	a	9.1
Pure Argon	b	2.6
Pure Argon	c	3.5
Pure Argon	d	7.1
Pure Argon	e	9.0
	<i>Average</i>	6.26
	<i>Range</i>	6.5

Shielding Gas	Area	Volume Fraction (%)
Argon Containing 1%O ₂	a	16.5
Argon Containing 1%O ₂	b	21.6
Argon Containing 1%O ₂	c	27.1
Argon Containing 1%O ₂	d	15.5
Argon Containing 1%O ₂	e	23.8
	<i>Average</i>	20.9
	<i>Range</i>	11.6
Argon Containing 2%O ₂	a	11.4
Argon Containing 2%O ₂	b	10.1
Argon Containing 2%O ₂	c	10.0
Argon Containing 2%O ₂	d	9.5
Argon Containing 2%O ₂	e	10.6
	<i>Average</i>	10.32
	<i>Range</i>	1.9

Table 4.3 – Volume Fraction of iron and chromium rich grains found in the microstructures of arc brazed joints.

Figure 4.15 overleaf shows the relationship between the above volume fractions and the tensile strengths of the joints.

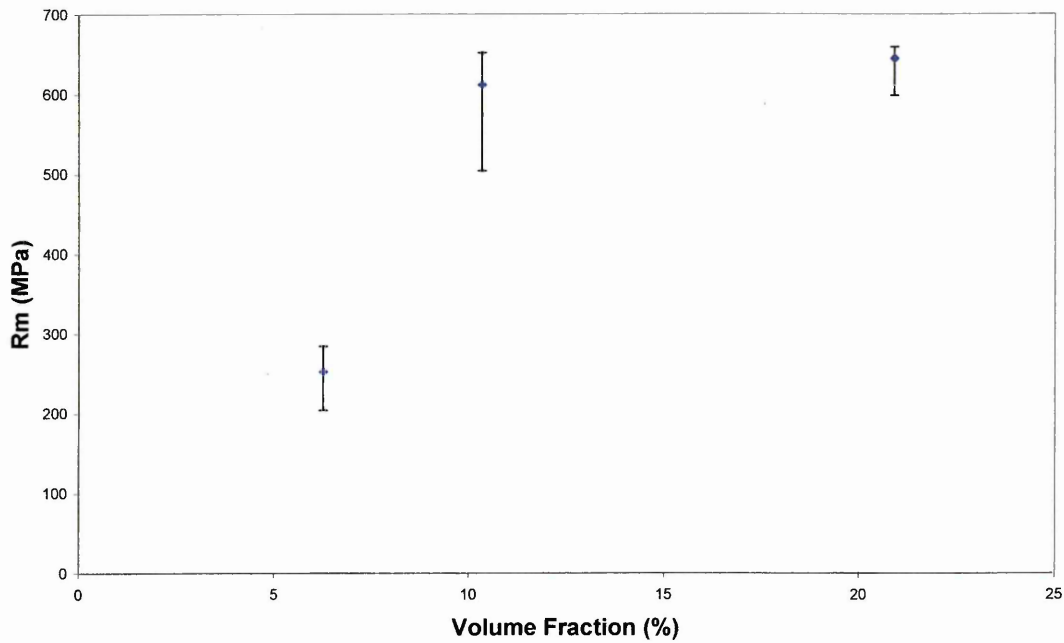


Figure 4.15 – Tensile strength of arc brazed butt joints compared to volume fraction of iron rich cellular dendritic structures present in the microstructure.

Figure 4.15 clearly shows that as there is a significant increase in tensile strength with a rise in the volume fraction of the cellular dendritic iron an chromium structures found in the braze microstructure.

4.3 Similar Metal Butt Joints – AISI 304 to AISI 304

4.3.1 Determination of Optimum Process Variables

4.3.1.1 Optimisation of Torch Height

It was found that the optimum position for the brazing torch was 15mm from the work piece because above this height excessive spatter was produced and below this height too much heat was transferred to the parent material producing increased distortion.

4.3.1.2 Optimisation of Torch Velocity

The torch velocity was found to be dependent upon the shielding gas and joint geometry. The shielding gases and their respective torch velocities for manufacturing butt joints with optimum aesthetic appearance can be seen in table 4.4.

Shielding Gas	Torch Velocity (cm.min ⁻¹)
Argon	101.6
Argon Containing 1%O ₂	114
Argon Containing 2%O ₂	63.5

Table 4.4 – Optimum torch velocities for respective shielding gases when manufacturing butt joints using AISI 304 parent material.

4.1.3.3 Optimisation of Arc Characteristics

The process parameters required to maintain a stable arc for manufacturing arc brazed joints are dependent upon the combination of shielding gas and filler material and the

joint geometry. The parameters for each combination investigated in this study can be found in Appendix 1.

4.3.1.4 Similar Metal Butt Joint Root Gap

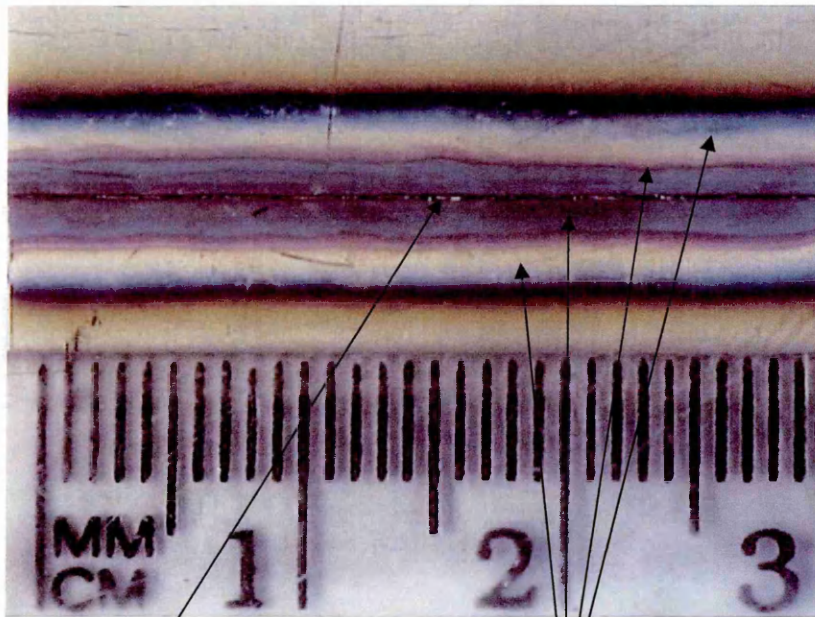
4.3.1.4.1 Penetration and Aesthetic Quality

Figures 4.16 - 4.18 show photographs of the braze seam and the reverse of the joint (demonstrating degree of penetration and heat tint) for butt joints joined with various root gaps between the faying surfaces prior to brazing.



Figure 4.16i - Front view of a joint brazed using BS:2901 C28 filler material and argon containing 2% oxygen shielding gas with a 0.1mm root gap.

In figure 4.16i it can be seen that that a butt joint root gap of 0.1mm produces a braze seam with a neat appearance.



Braze (inadequate penetration)

Discolouration due to heat tint

Figure 4.16ii - Rear view of a joint brazed using BS:2901 C28 filler material and argon containing 2% oxygen shielding gas with a 0.1mm root gap

Figure 4.16ii shows that there is very little evidence of penetration of filler material through to the reverse of a butt joint with a 0.1mm root gap prior to arc brazing.

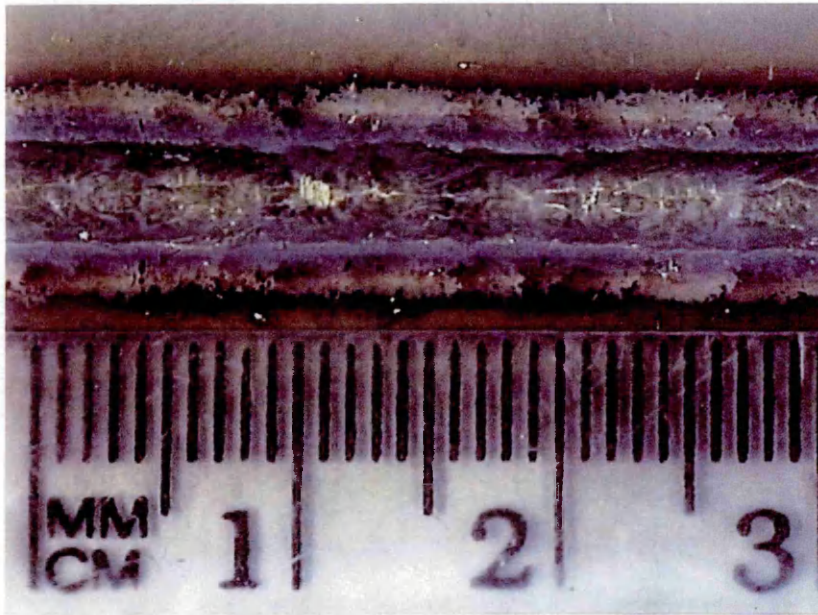
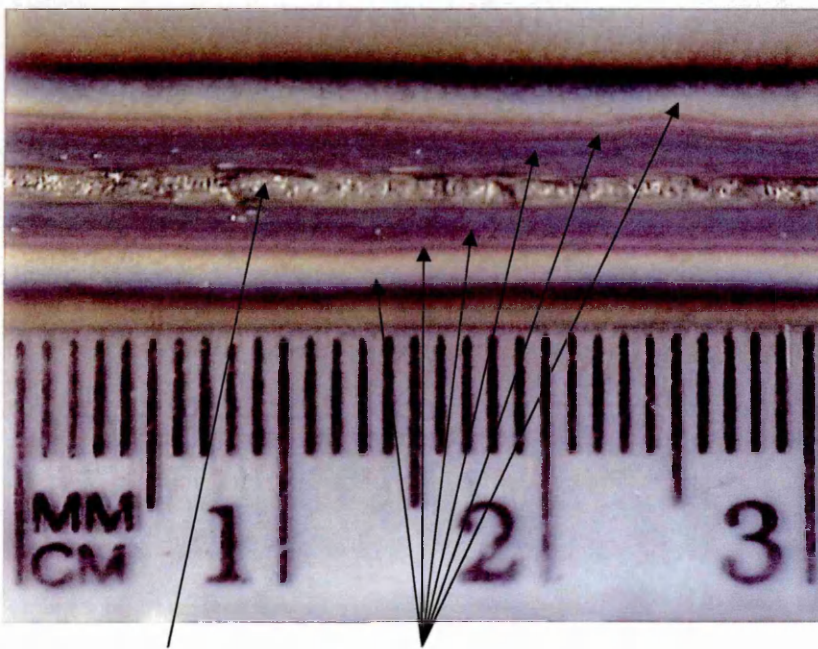


Figure 4.17i - Front view of a joint brazed using BS:2901 C28 filler material and argon containing 2% oxygen shielding gas with a 0.6mm root gap

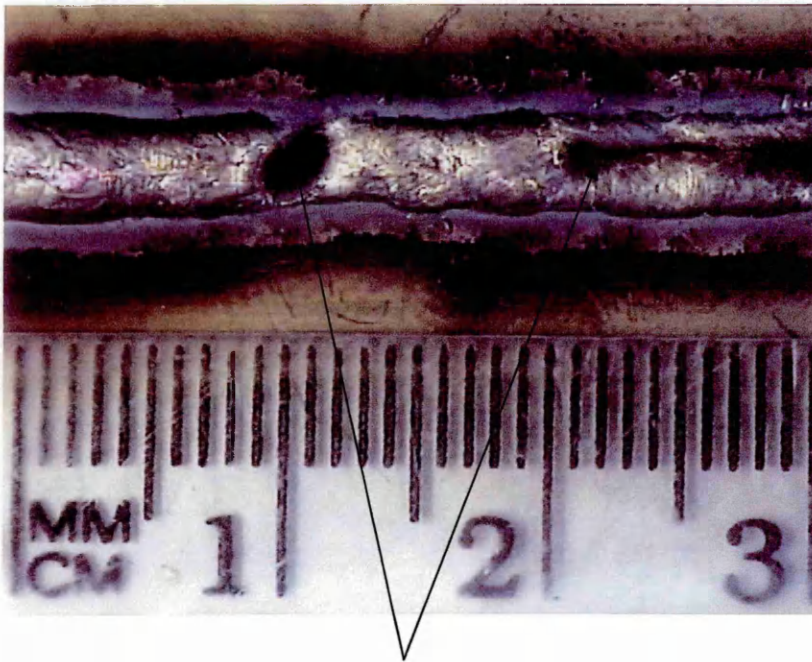


Braze (adequate penetration)

Discolouration due to heat tint

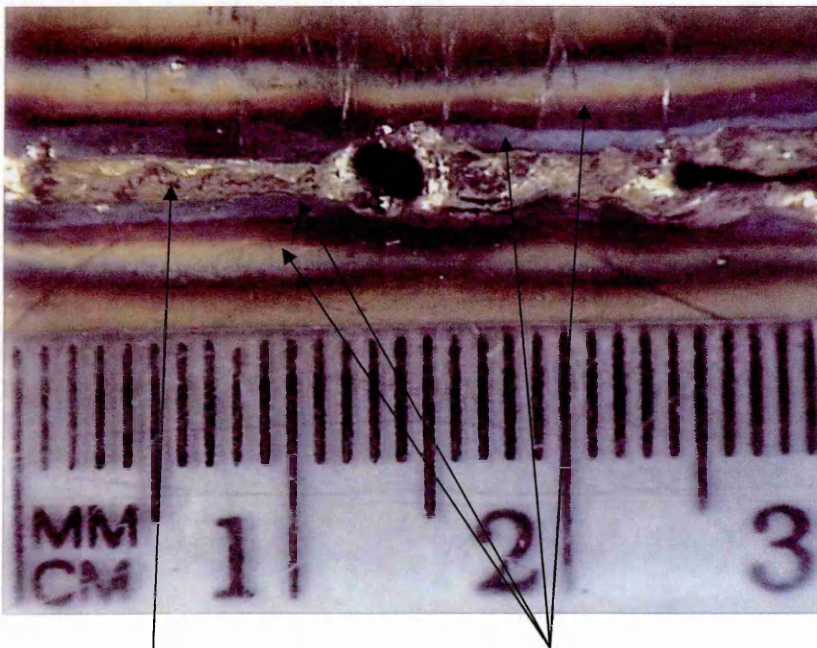
Figure 4.17ii - Rear view of a joint brazed using BS:2901 C28 filler material and argon containing 2% oxygen shielding gas with a 0.6mm root gap

It can be seen in figures 4.17i and 4.17ii that an arc brazed butt joint with a 0.6mm root gap prior to brazing produces a neat braze seam on the top of the joint with penetration of filler material throughout the depth of the joint.



Holes caused by the root gap being too large

Figure 4.18i - Front view of a joint brazed using BS:2901 C28 filler material and argon containing 2% oxygen shielding gas with a 0.8mm root gap.



Brazed Seam

Discolouration due to heat tint

Figure 4.18ii - Rear view of a joint brazed using BS:2901 C28 filler material and argon containing 2% oxygen shielding gas with a 0.8mm root gap

Figures 4.18i and 4.18ii show that a with a root gap of 0.8mm and an electrode diameter of 0.8mm the filler material fails to bridge the gap between the sheets of parent material resulting in holes in the braze seam.

4.3.1.4.2 Effect of Varying Butt Joint Root Gap on Tensile Properties

Table 4.5 shows the results of tensile testing conducted on similar metal butt joints constructed using combinations of BS:2901 C9 and BS:2901 C28 filler materials and pure argon and argon containing 2% oxygen shielding gases and AISI 304 grade stainless steel as the parent material with gaps of 0.4mm, 0.5mm and 0.6mm between the faying surfaces.

Table 4.5

Test Piece	Shielding Gas	Filler Material	Gap (mm)	R _m (MPa)	R _{p0.2} (MPa)
BGT14a	Argon + 2% O ₂	BS:2901 C28	0.4	180	*
BGT14b	Argon + 2% O ₂	BS:2901 C28	0.4	462	302
BGT14c	Argon + 2% O ₂	BS:2901 C28	0.4	249	*
BGT14d	Argon + 2% O ₂	BS:2901 C28	0.4	428	295
BGT14e	Argon + 2% O ₂	BS:2901 C28	0.4	444	275
BGT14f	Argon + 2% O ₂	BS:2901 C28	0.4	504	288
			Range	324	27
			Average	417	290

*Samples did not deform plastically and therefore the R_{p0.2} could not be calculated

Table 4.5 Contd

Test Piece	Shielding Gas	Filler Material	Gap (mm)	Rm (MPa)	Rp _{0.2} (MPa)
BGT15a	Argon + 2% O ₂	BS:2901 C28	0.5	607	321
BGT15b	Argon + 2% O ₂	BS:2901 C28	0.5	633	278
BGT15c	Argon + 2% O ₂	BS:2901 C28	0.5	504	307
BGT15d	Argon + 2% O ₂	BS:2901 C28	0.5	637	294
BGT15e	Argon + 2% O ₂	BS:2901 C28	0.5	637	270
BGT15f	Argon + 2% O ₂	BS:2901 C28	0.5	652	317
			Range	148	51
			Average	612	298
BGT16a	Argon + 2%O ₂	BS:2901 C28	0.6	617	280
BGT16b	Argon + 2%O ₂	BS:2901 C28	0.6	608	271
BGT16c	Argon + 2%O ₂	BS:2901 C28	0.6	548	298
BGT16d	Argon + 2%O ₂	BS:2901 C28	0.6	473	306
BGT16e	Argon + 2%O ₂	BS:2901 C28	0.6	613	324
BGT16f	Argon + 2%O ₂	BS:2901 C28	0.6	589	299
			Range	144	53
			Average	575	297

Table 4.5 Contd

Test Piece	Shielding Gas	Filler Material	Gap (mm)	Rm (MPa)	R _{p0.2} (MPa)
BGT24a	Pure Argon	BS:2901 C28	0.4	260	*
BGT24b	Pure Argon	BS:2901 C28	0.4	253	*
BGT24c	Pure Argon	BS:2901 C28	0.4	545	263
BGT24d	Pure Argon	BS:2901 C28	0.4	240	*
BGT24e	Pure Argon	BS:2901 C28	0.4	286	*
BGT24f	Pure Argon	BS:2901 C28	0.4	305	*
			Range	65	0
			Average	315	263
BGT25a	Pure Argon	BS:2901 C28	0.5	269	*
BGT25b	Pure Argon	BS:2901 C28	0.5	241	*
BGT25c	Pure Argon	BS:2901 C28	0.5	285	*
BGT25d	Pure Argon	BS:2901 C28	0.5	204	*
BGT25e	Pure Argon	BS:2901 C28	0.5	276	*
BGT25f	Pure Argon	BS:2901 C28	0.5	240	*
			Range	81	
			Average	252	

*Samples did not deform plastically and therefore the R_{p0.2} could not be calculated

Table 4.5 Contd

Test Piece	Shielding Gas	Filler Material	Gap (mm)	Rm (MPa)	Rp _{0.2} (MPa)
BGT26a	Pure Argon	BS:2901 C28	0.6	472	302
BGT26b	Pure Argon	BS:2901 C28	0.6	525	304
BGT26c	Pure Argon	BS:2901 C28	0.6	404	300
BGT26d	Pure Argon	BS:2901 C28	0.6	399	301
BGT26e	Pure Argon	BS:2901 C28	0.6	445	335
BGT26f	Pure Argon	BS:2901 C28	0.6	439	329
			Range	126	35
			Average	447	312
BGT34a	Pure Argon	BS:2901 C9	0.4	454	285
BGT34b	Pure Argon	BS:2901 C9	0.4	405	287
BGT34c	Pure Argon	BS:2901 C9	0.4	331	233
BGT34d	Pure Argon	BS:2901 C9	0.4	516	314
BGT34e	Pure Argon	BS:2901 C9	0.4	492	278
BGT34f	Pure Argon	BS:2901 C9	0.4	376	249
			Range	185	81
			Average	429	274

Table 4.5 Contd

Test Piece	Shielding Gas	Filler Material	Gap (mm)	Rm (MPa)	Rp _{0.2} (MPa)
BGT35a	Pure Argon	BS:2901 C9	0.5	505	248
BGT35b	Pure Argon	BS:2901 C9	0.5	451	276
BGT35c	Pure Argon	BS:2901 C9	0.5	429	302
BGT35d	Pure Argon	BS:2901 C9	0.5	419	318
BGT35e	Pure Argon	BS:2901 C9	0.5	383	319
BGT35f	Pure Argon	BS:2901 C9	0.5	435	254
			Range	122	71
			Average	437	286
BGT36a	Pure Argon	BS:2901 C9	0.6	Sample Slipped	
BGT36b	Pure Argon	BS:2901 C9	0.6	346	256
BGT36c	Pure Argon	BS:2901 C9	0.6	445	270
BGT36d	Pure Argon	BS:2901 C9	0.6	384	267
BGT36e	Pure Argon	BS:2901 C9	0.6	450	274
BGT36f	Pure Argon	BS:2901 C9	0.6	391	271
			Range	104	18
			Average	403	267

Table 4.5 Contd

Test Piece	Shielding Gas	Filler Material	Gap (mm)	R _m (MPa)	R _{p0.2} (MPa)
BGT44a	Argon + 2%O ₂	BS:2901 C9	0.4	422	296
BGT44b	Argon + 2%O ₂	BS:2901 C9	0.4	443	296
BGT44c	Argon + 2%O ₂	BS:2901 C9	0.4	453	262
BGT44d	Argon + 2%O ₂	BS:2901 C9	0.4	491	245
BGT44e	Argon + 2%O ₂	BS:2901 C9	0.4	559	285
BGT44f	Argon + 2%O ₂	BS:2901 C9	0.4	550	285
			Range	137	51
			Average	486	278
BGT45a	Argon + 2%O ₂	BS:2901 C9	0.5	312	*
BGT45b	Argon + 2%O ₂	BS:2901 C9	0.5	428	307
BGT45c	Argon + 2%O ₂	BS:2901 C9	0.5	405	310
BGT45d	Argon + 2%O ₂	BS:2901 C9	0.5	189	*
BGT45e	Argon + 2%O ₂	BS:2901 C9	0.5	52	*
BGT45f	Argon + 2%O ₂	BS:2901 C9	0.5	277	*
			Range	376	3
			Average	277	308

*Samples did not deform plastically and therefore the R_{p0.2} could not be calculated

Table 4.5 Contd

Test Piece	Shielding Gas	Filler Material	Gap (mm)	R _m (MPa)	R _{p0.2} (MPa)
BGT46a	Argon + 2%O ₂	BS:2901 C9	0.6	453	305
BGT46b	Argon + 2%O ₂	BS:2901 C9	0.6	502	313
BGT46c	Argon + 2%O ₂	BS:2901 C9	0.6	332	280
BGT46d	Argon + 2%O ₂	BS:2901 C9	0.6	442	267
BGT46e	Argon + 2%O ₂	BS:2901 C9	0.6	387	259
BGT46f	Argon + 2%O ₂	BS:2901 C9	0.6	377	265
			Range	170	54
			Average	415	281

Table 4.5 - Tensile properties of arc brazed butt joints with varying root gaps

between 0.4mm and 0.6mm

Figures 4.19 – 4.26 show the variation, with root gap, in tensile strength and 0.2% proof stress for each combination of filler material and shielding gas.

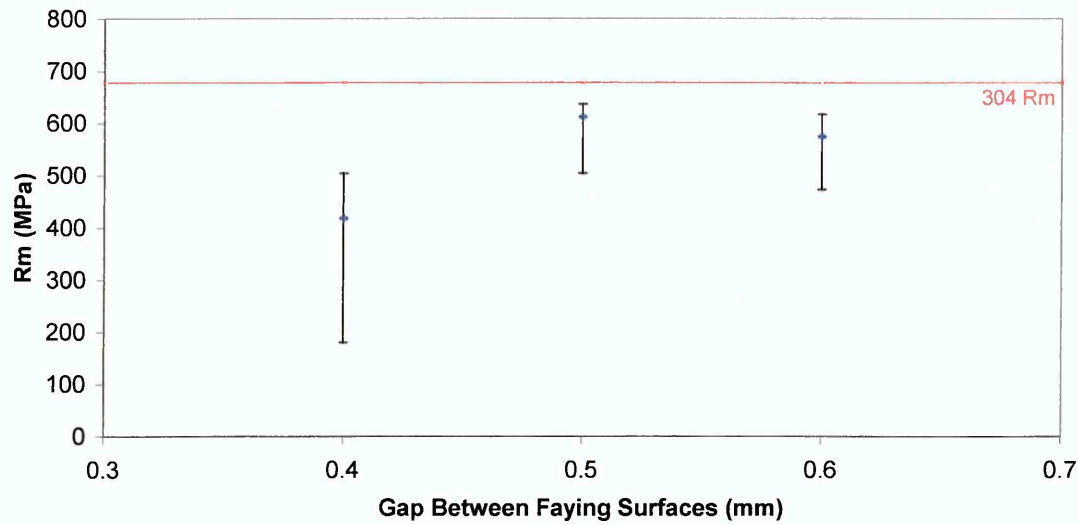
**BS:2901 C28
Argon + 2%O₂**

Figure 4.19 - Comparison of the effect of varying braze root gaps on the tensile strength of butt joints constructed using BS:2901 C28 filler material and argon containing 2% oxygen compared with the as received material tensile strength.

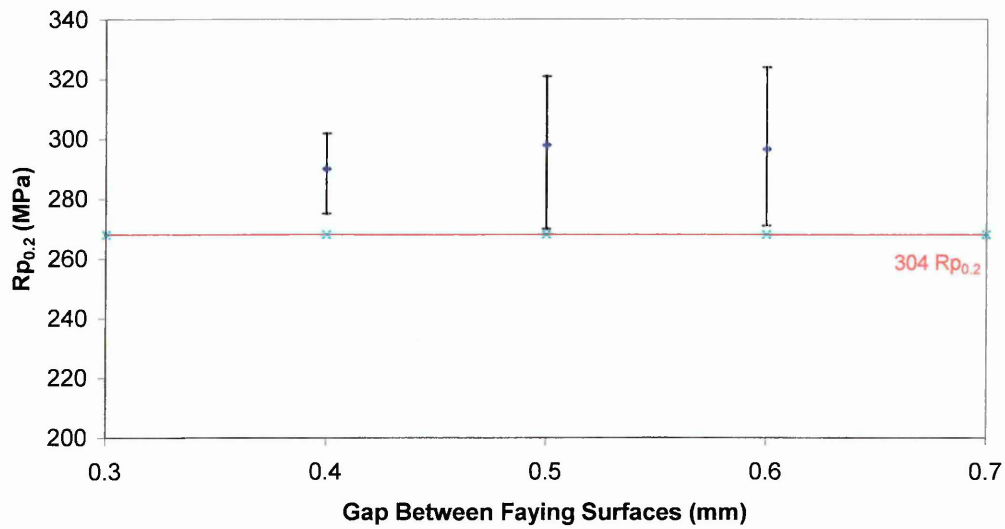
**BS:2901 C28
Argon + 2%O2**

Figure 4.20 - Comparison of the effect of varying braze root gaps on the 0.2% proof stress of butt joints constructed using BS:2901 C28 filler material and argon containing 2% oxygen compared with the as received parent material 0.2% proof stress.

**BS:2901 C28
Pure Argon**

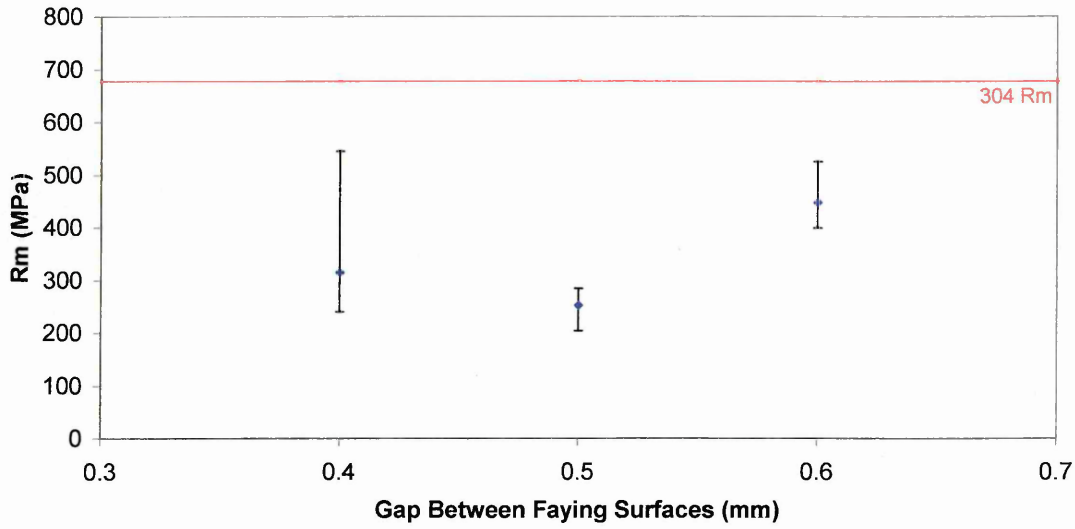


Figure 4.21 - Comparison of the effect of varying braze gaps on the tensile strength of butt joints constructed using BS:2901 C28 filler material and pure argon shielding gas compared with the as received material tensile strength.

Only one sample with a 0.4mm gap deformed plastically prior to failure whilst no samples with a 0.5mm gap deformed plastically prior to failure

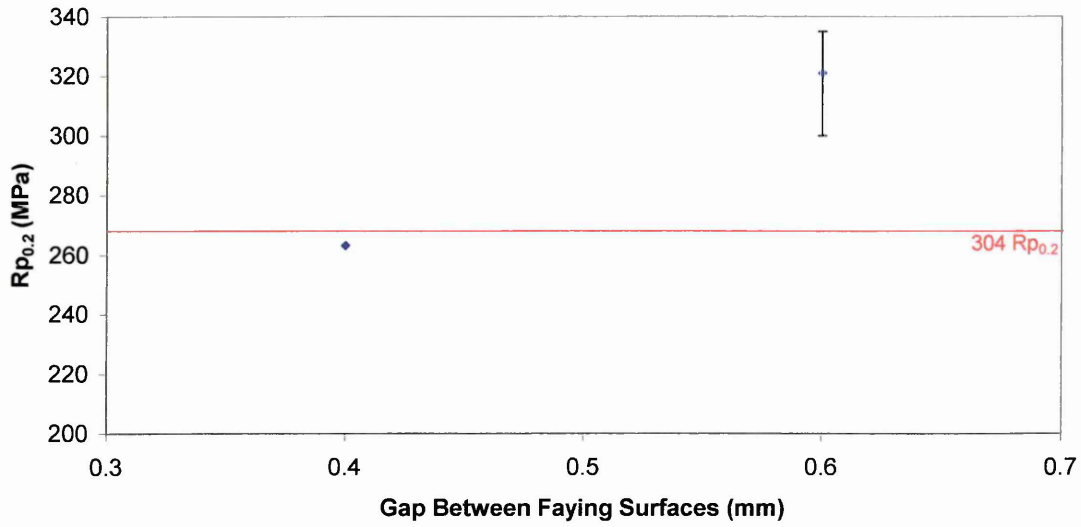


Figure 4.22 - Comparison of the effect of varying braze root gaps on the 0.2% proof stress of butt joints constructed using BS:2901 C28 filler material and pure argon shielding gas compared with the as received parent material 0.2% proof stress.

Only one sample with a 0.4mm gap deformed plastically prior to failure whilst no samples with a 0.5mm gap deformed plastically prior to failure

**BS:2901 C9
Pure Argon**

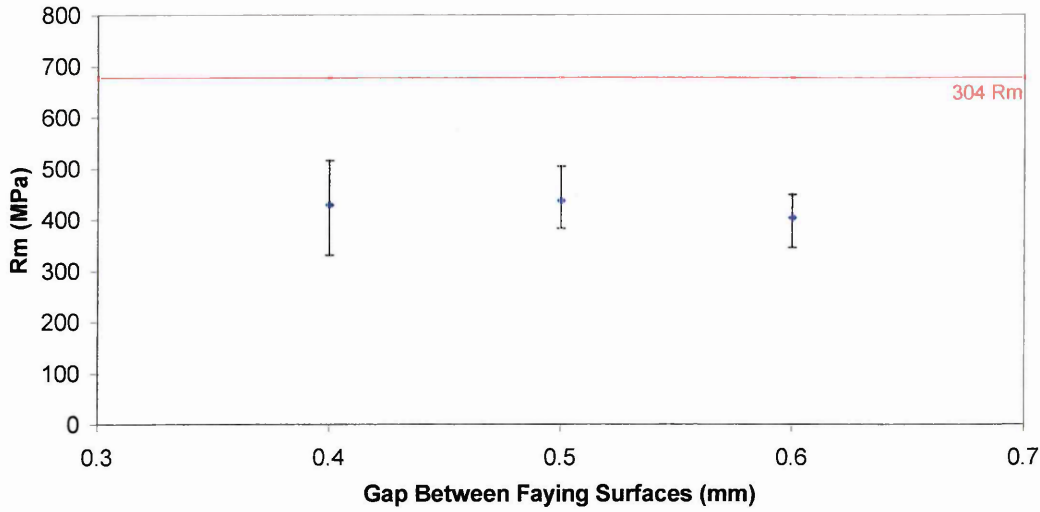


Figure 4.23 - Comparison of the effect of varying braze root gaps on the tensile strength of butt joints constructed using BS:2901 C9 filler material and pure argon shielding gas compared with the as received material tensile strength.

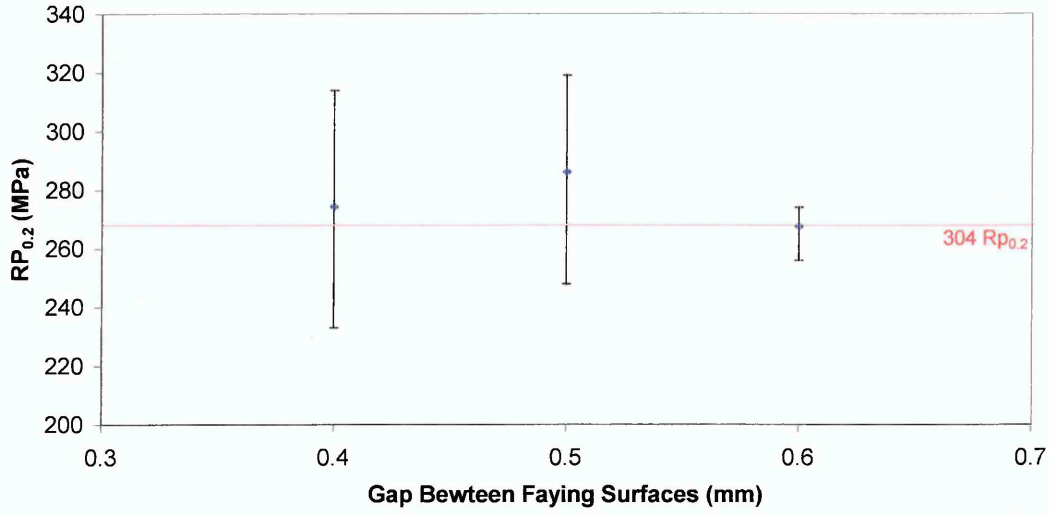


Figure 4.24 - Comparison of the effect of varying braze root gaps on the 0.2% proof stress of butt joints constructed using BS:2901 C9 filler material and pure argon shielding gas compared with the as received parent material 0.2% proof stress.

BS:2901 C9
Argon + 2%O₂

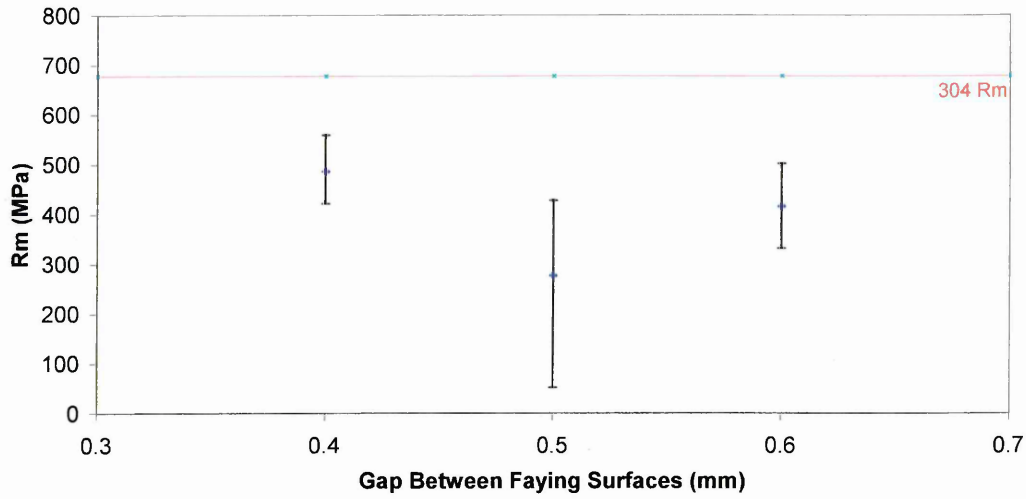


Figure 4.25 - Comparison of the effect of varying braze gaps on the tensile strength of butt joints constructed using BS:2901 C9 filler material and argon containing 2% oxygen compared with the as received material tensile strength.

Only 2 samples with a 0.5mm gap deformed plastically prior to failure

**BS:2901 C9
Argon + 2%O2**

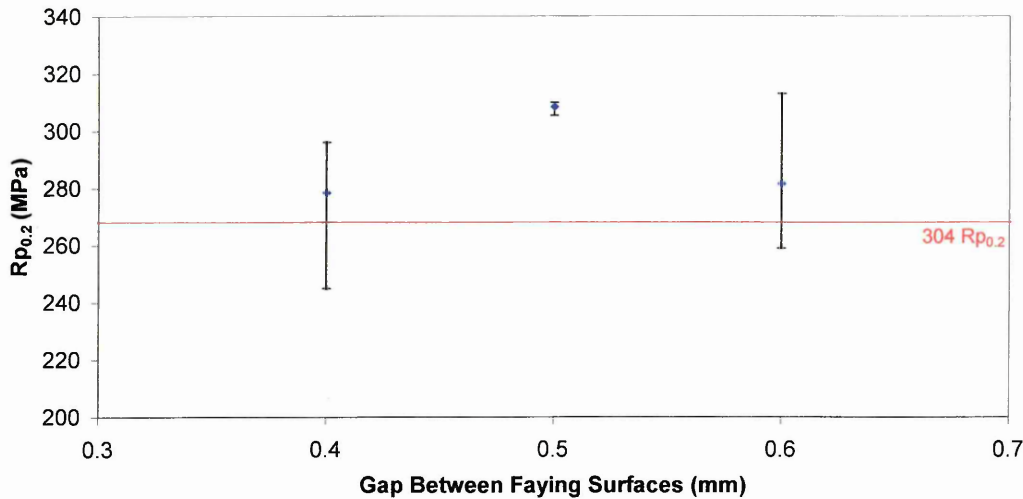


Figure 4.26 - Comparison of the effect of varying braze gaps on the 0.2% proof stress of butt joints constructed using BS:2901 C9 filler material and argon containing 2% oxygen compared with the as received parent material 0.2% proof stress.

Only 2 samples with a 0.5mm gap deformed plastically prior to failure

Figures 4.19 – 4.26 show that for combinations of filler material and shielding gas in which all test pieces deformed plastically the butt joints manufactured with a 0.5 mm root gap prior to brazing displayed the highest tensile strength and 0.2% proof stress. Figures 4.27 and 4.28 compare the tensile strengths of butt joints manufactured with a 0.5mm root gap prior to brazing for each combination of filler material and shielding gas.

0.5mm Gap

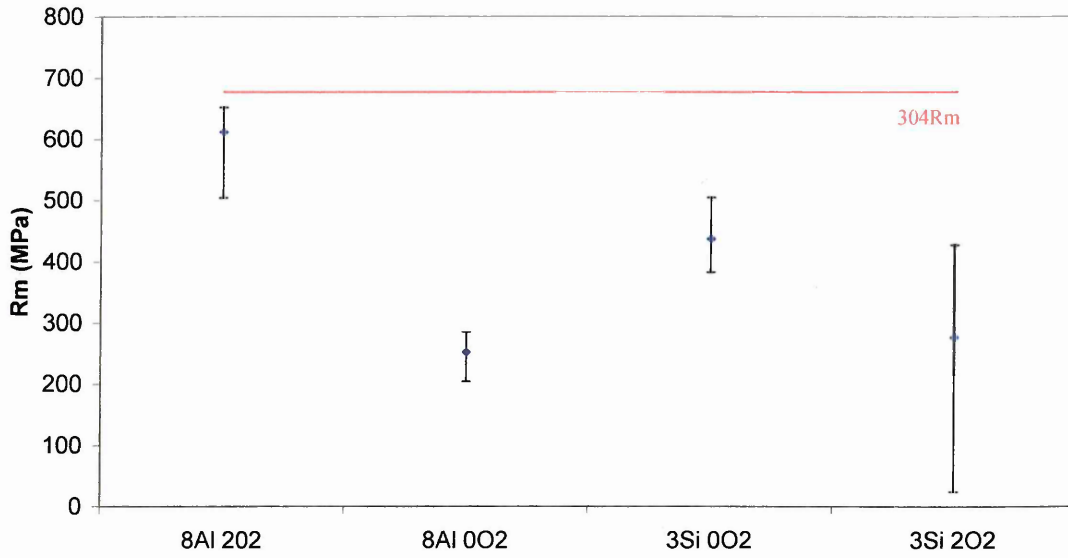


Figure 4.27 - Comparison of Filler Material and Shielding Gas Combinations with a 0.5mm Gap Prior to Brazing

0.5mm Gap

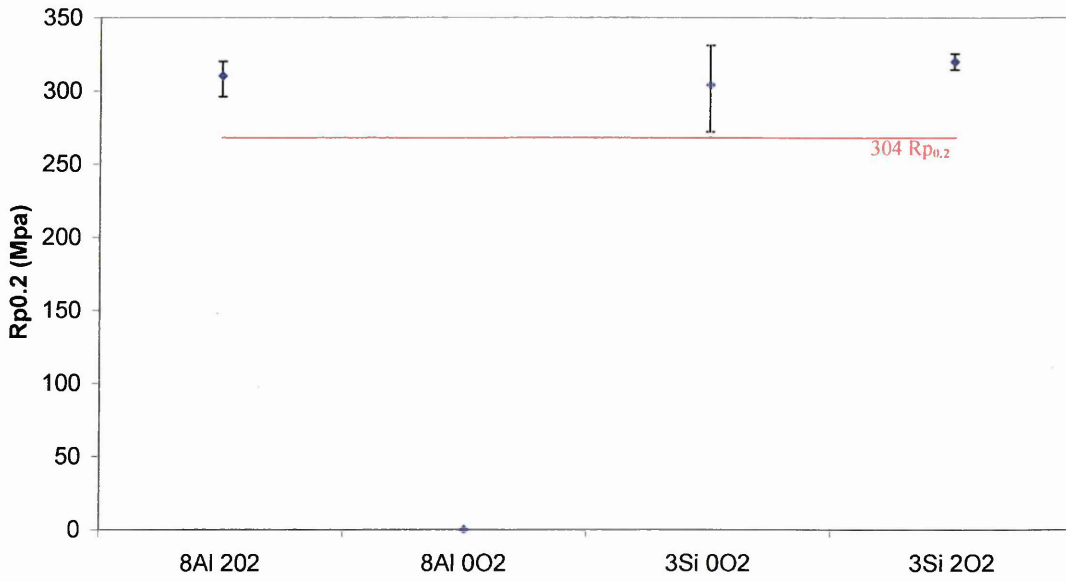


Figure 4.28 - Comparisons of Filler Material and Shielding Gas Combinations with a 0.5mm Gap Prior to Brazing

From figures 4.27 and 4.28 it can be seen that the butt joints which produced the highest tensile strength and 0.2% proof stress were those manufactured from BS:2901 C28 filler material and argon containing 2% oxygen shielding gas with a 0.5mm root gap, prior to brazing.

4.3.1.4.3 Microstructural investigation

Evidence of LME was found in those samples which did not deform plastically prior to failure. Figure 4.29 is a micrograph of the braze seam adjacent to sample BGT25c (see table 4.5) which was joined using BS:2901 C28 filler material and pure argon shielding gas

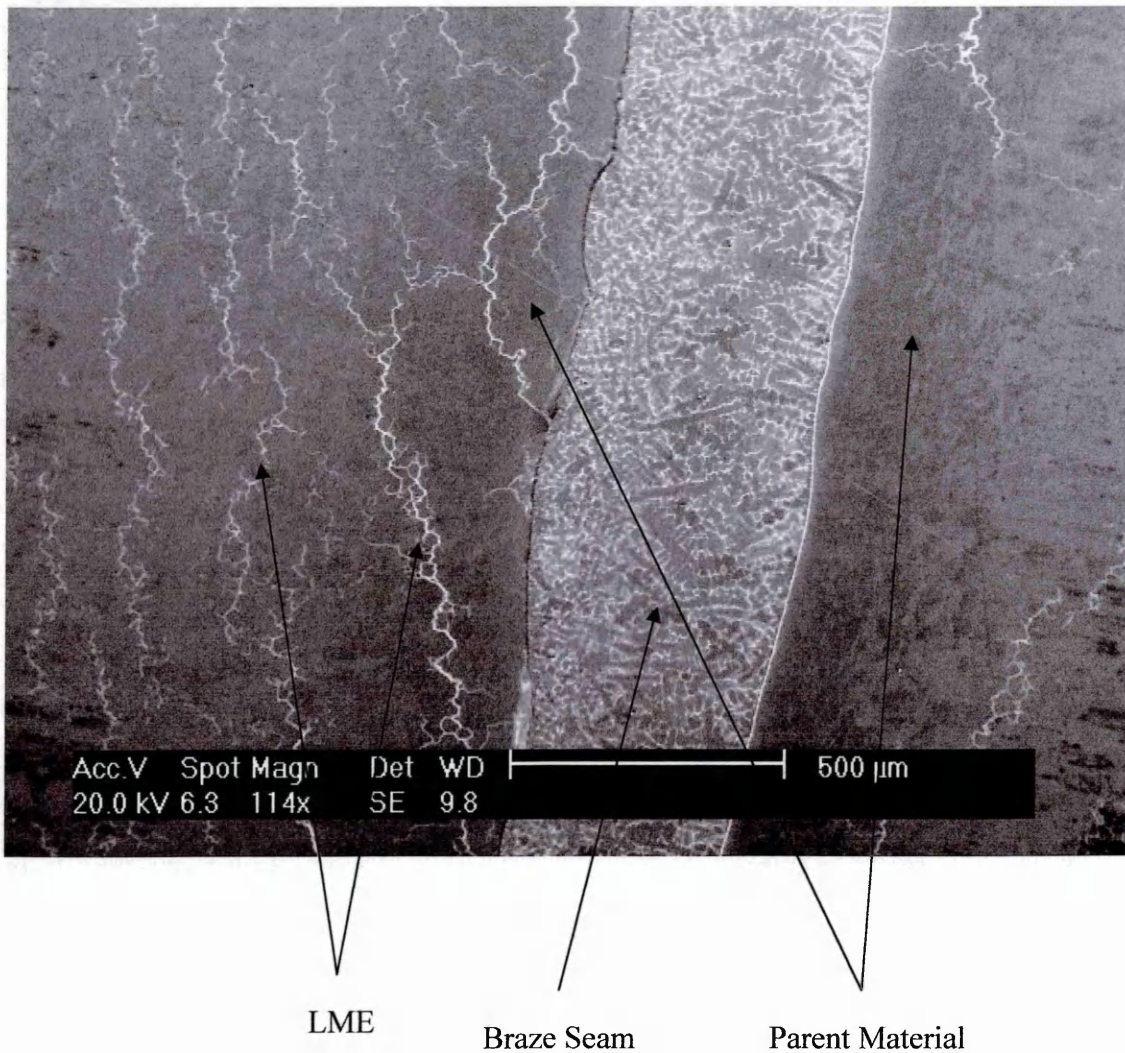


Figure 4.29 - Liquid Metal Embrittlement as found adjacent to sample BGT25c brazed using BS:2901 C28 filler material and pure argon shielding gas.

In figure 4.29 copper from the braze is penetrating the stainless steel, this appears to have weakened and embrittled the joint. In figure 4.12 copper is also seen to be penetrating the parent material resulting in an arc braze with high joint efficiency. The difference between the two images is that in figure 4.12 the copper penetrates the stainless steel close to the interface in every direction, whereas in figure 4.29 the copper is only apparent in the stainless steel in a direction parallel to the joint. The reasons for this difference in mechanical properties and microstructure will be discussed in Chapter 5.

4.3.1.5 Selection of Filler Material and Shielding Gas for Similar Metal Butt Joints.

Table 4.6 shows the results of tensile testing conducted on butt joints constructed using the combinations of BS:2901 C9, BS:2901 C11 and BS:2901 C28 braze alloys and shielding gas compositions of pure argon, argon containing 1% oxygen and argon containing 2% oxygen and AISI 304 grade stainless steel as the parent material with a root gap of 0.5mm.

Table 4.6

Test Piece	Shielding Gas	Filler Material	Rm (MPa)	Rp _{0.2} (MPa)	Max Extension (mm)
BGT15a	Argon + 2% O ₂	BS:2901 C28	607	321	21.18
BGT15b	Argon + 2% O ₂	BS:2901 C28	633	278	27.61
BGT15c	Argon + 2% O ₂	BS:2901 C28	504	307	9.9
BGT15d	Argon + 2% O ₂	BS:2901 C28	637	294	26.85
BGT15e	Argon + 2% O ₂	BS:2901 C28	637	270	26.7
BGT15f	Argon + 2% O ₂	BS:2901 C28	652	317	34.79
		Range	148	51	24,89
		Average	612	298	24.51

Table 4.6 Contd

Test Piece	Shielding Gas	Filler Material	Rm (MPa)	R _{p0.2} (MPa)	Max Extension (mm)
BGT25a	Pure Argon	BS:2901 C28	269	*	1.02
BGT25b	Pure Argon	BS:2901 C28	241	*	0.91
BGT25c	Pure Argon	BS:2901 C28	285	*	1.02
BGT25d	Pure Argon	BS:2901 C28	204	*	0.9
BGT25e	Pure Argon	BS:2901 C28	276	*	1.14
BGT25f	Pure Argon	BS:2901 C28	240	*	0.95
		Range	81		0.24
		Average	252		0.99
BGT35a	Pure Argon	BS:2901 C9	505	248	10.59
BGT35b	Pure Argon	BS:2901 C9	451	276	7.6
BGT35c	Pure Argon	BS:2901 C9	429	302	5.6
BGT35d	Pure Argon	BS:2901 C9	419	318	4.94
BGT35e	Pure Argon	BS:2901 C9	383	319	2.72
BGT35f	Pure Argon	BS:2901 C9	435	254	5.91
		Range	122	71	7.87
		Average	437	286	6.23

*Samples did not deform plastically and therefore the R_{p0.2} could not be calculated

Table 4.6 Contd

Test Piece	Shielding Gas	Filler Material	Rm (MPa)	R _{p0.2} (MPa)	Max Extension (mm)
BGT45a	Argon + 2%O ₂	BS:2901 C9	312	*	1.11
BGT45b	Argon + 2%O ₂	BS:2901 C9	428	307	5.4
BGT45c	Argon + 2%O ₂	BS:2901 C9	405	310	4.22
BGT45d	Argon + 2%O ₂	BS:2901 C9	189	*	1.04
BGT45e	Argon + 2%O ₂	BS:2901 C9	52	*	0.66
BGT45f	Argon + 2%O ₂	BS:2901 C9	277	*	1.13
		Range	376	3	4.74
		Average	277	308	2.26
BGT55a	Argon + 1%O ₂	BS:2901 C9	601	317	19.64
BGT55b	Argon + 1%O ₂	BS:2901 C9	579	306	16.53
BGT55c	Argon + 1%O ₂	BS:2901 C9	569	315	15.85
BGT55d	Argon + 1%O ₂	BS:2901 C9	563	308	15.33
BGT55e	Argon + 1%O ₂	BS:2901 C9	558	295	14.48
BGT55f	Argon + 1%O ₂	BS:2901 C9	567	309	15.29
		Range	43	22	5.16
		Average	573	308	16.19

*Samples did not deform plastically and therefore the R_{p0.2} could not be calculated

Table 4.6 Contd

Test Piece	Shielding Gas	Filler Material	Rm (MPa)	Rp _{0.2} (MPa)	Max Extension (mm)
BGT65a	Pure Argon	BS:2901 C11	416	309	4.85
BGT65b	Pure Argon	BS:2901 C11	363	315	2.49
BGT65c	Pure Argon	BS:2901 C11	390	313	3.41
BGT65d	Pure Argon	BS:2901 C11	573	315	16.01
BGT65e	Pure Argon	BS:2901 C11	543	307	13.76
BGT65f	Pure Argon	BS:2901 C11	417	294	4.66
		Range	210	21	13.52
		Average	450	309	7.53
BGT75a	Argon + 1%O ₂	BS:2901 C11	481	319	7.95
BGT75b	Argon + 1%O ₂	BS:2901 C11	513	318	10.34
BGT75c	Argon + 1%O ₂	BS:2901 C11	458	297	6.48
BGT75d	Argon + 1%O ₂	BS:2901 C11	443	311	5.97
BGT75e	Argon + 1%O ₂	BS:2901 C11	467	295	7.41
BGT75f	Argon + 1%O ₂	BS:2901 C11	458	295	7.49
		Range	70	24	4.37
		Average	470	306	7.61

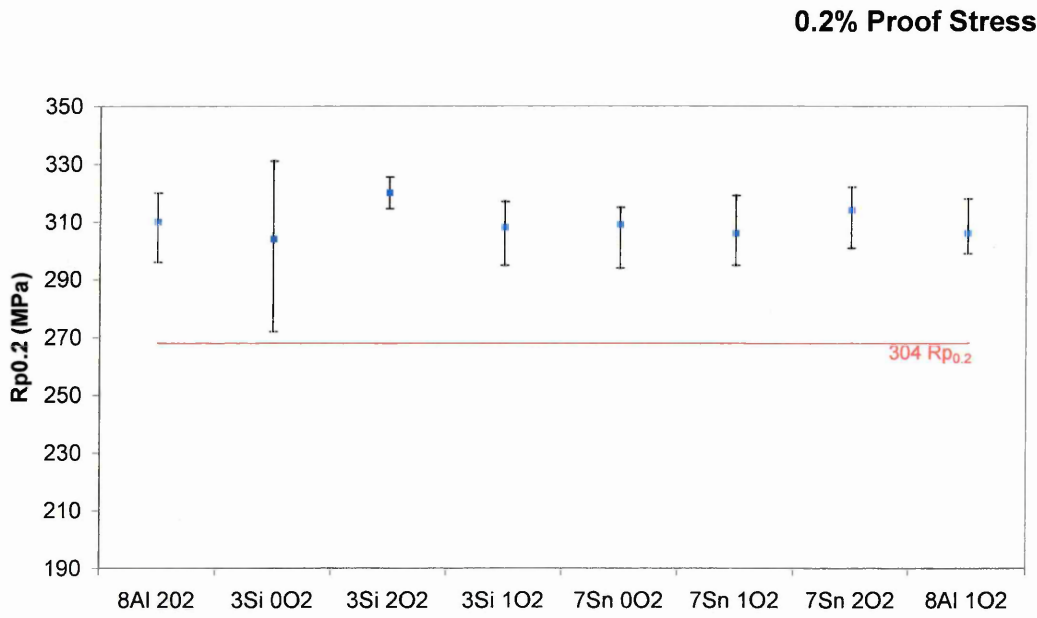
Table 4.6 Contd

Test Piece	Shielding Gas	Filler Material	Rm (MPa)	Rp _{0.2} (MPa)	Max Extension (mm)
BGT85a	Argon + 2%O ₂	BS:2901 C11	417	322	4.23
BGT85b	Argon + 2%O ₂	BS:2901 C11	477	301	7.99
BGT85c	Argon + 2%O ₂	BS:2901 C11	410	309	4.1
BGT85d	Argon + 2%O ₂	BS:2901 C11	484	310	8.72
BGT85e	Argon + 2%O ₂	BS:2901 C11	555	319	13.63
BGT85f	Argon + 2%O ₂	BS:2901 C11	568	320	15.09
		Range	158	21	10.99
		Average	485	314	8.96
BGT95a	Argon + 1%O ₂	BS:2901 C28	598	299	21.8
BGT95b	Argon + 1%O ₂	BS:2901 C28	654	307	36.26
BGT95c	Argon + 1%O ₂	BS:2901 C28	659	300	37.12
BGT95d	Argon + 1%O ₂	BS:2901 C28	660	318	34.27
BGT95e	Argon + 1%O ₂	BS:2901 C28	643	302	37.96
BGT95f	Argon + 1%O ₂	BS:2901 C28	654	309	38.73
		Range	62	19	16.93
		Average	645	306	34.36

Table 4.6 – Comparison of Tensile Properties of Filler Materials and Shielding Gases

By presenting the information in table 4.6 graphically (figures 4.30 – 4.32) it will be possible to determine the optimum combination of shielding gas and filler material

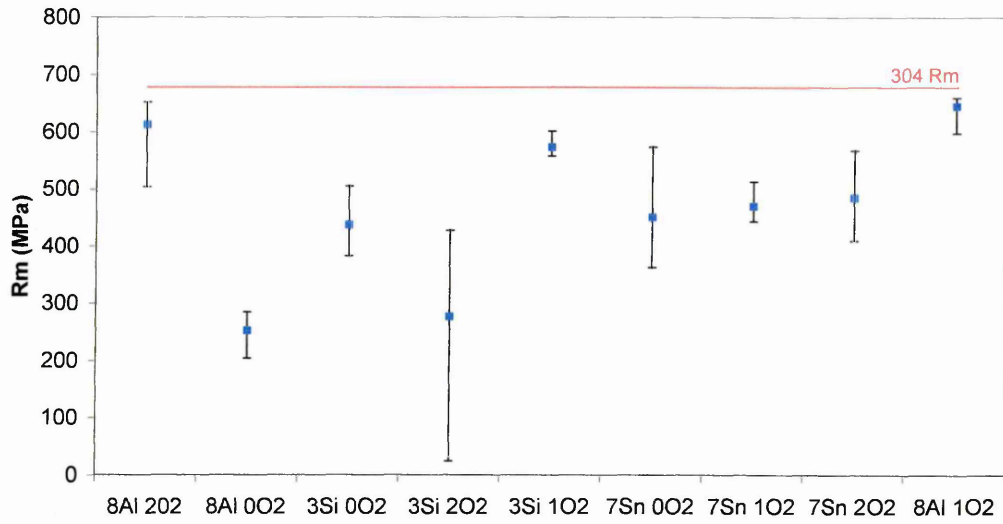
which provides the best compromise of tensile properties in terms of tensile strength, 0.2% proof stress and percentage elongation.



- 3Si BS:2901 C9
- 7Sn BS:2901 C11
- 8Al BS:2901 C28
- 0O2 Pure Argon
- 1O2 Argon containing 1% Oxygen
- 2O2 Argon containing 2% Oxygen

Figure 4.30 - Comparison of 0.2% proof stresses for various combinations of filler material and shielding gas for joints using 304 parent material with a root gap of 0.5mm

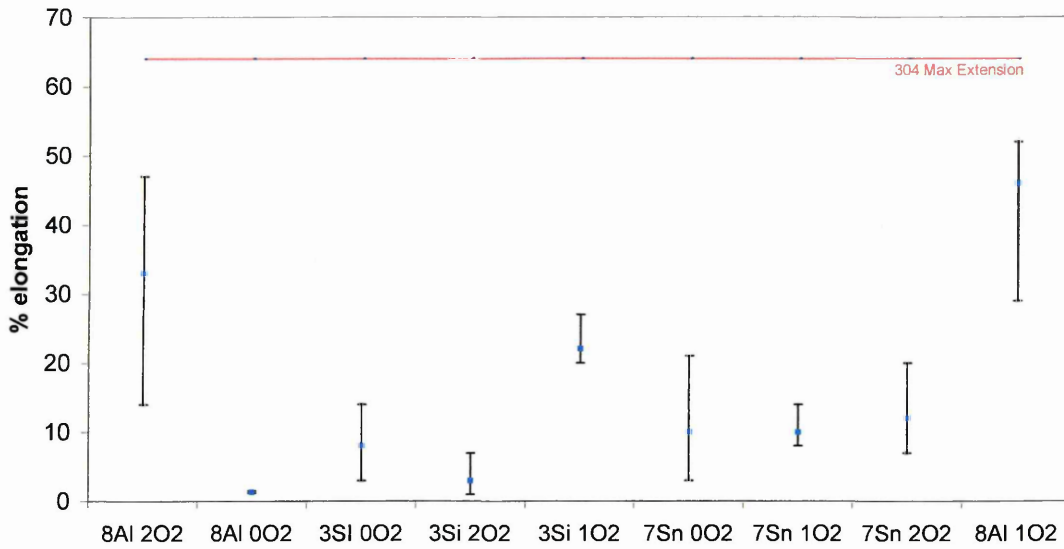
Tensile Strength



- 3Si BS:2901 C9
- 7Sn BS:2901 C11
- 8Al BS:2901 C28
- 0O2 Pure Argon
- 1O2 Argon containing 1% Oxygen
- 2O2 Argon containing 2% Oxygen

Figure 4.31 – Comparison of the ultimate tensile strength for various combinations of filler material and shielding gas for joints using 304 parent material with a root gap of 0.5mm

Max Extension



3Si	BS:2901 C9
7Sn	BS:2901 C11
8Al	BS:2901 C28
0O2	Pure Argon
1O2	Argon containing 1% Oxygen
2O2	Argon containing 2% Oxygen

Figure 4.32 - Comparison of extensions at failure for various combinations of filler material and shielding gas for joints using 304 parent material and a root gap of 0.5mm

Whilst figure 4.30 shows that all samples appeared to yield at approximately the same stress, figures 4.31 and 4.32 show that the combination of BS:2901 C28 filler material and argon containing 1% oxygen shielding gas displayed the highest tensile strength and percentage elongation.

4.3.2 Effect of Braze Seam Geometry on the Tensile Properties of Nine Filler Material and Shielding Gas Combinations

Table 4.7 shows the results of tensile testing conducted on as brazed butt joints constructed using combinations of BS:2901 C9, BS:2901 C11 and BS:2901 C28 braze alloys, shielding gas compositions of pure argon, argon containing 1% oxygen and argon containing 2% oxygen and AISI 304 grade of stainless steel as the parent material with a root gap of 0.5mm. Due to the irregular surface area of the unground joints it was not possible to accurately calculate values for engineering stress, therefore a load at which the material started to yield (at 0.2% offset) and failed was recorded rather than a stress.

Table 4.7

Test Piece	Shielding Gas	Filler Material	Max Load (N)	Proof Load (N)	Max Extension (mm)
4-C9Ara	Pure Argon	BS:2901 C9	8283	3769	34.57
4-C9Arb	Pure Argon	BS:2901 C9	7019	4066	14.90
4-C9Arc	Pure Argon	BS:2901 C9	6753	3800	13.12
4-C9Ard	Pure Argon	BS:2901 C9	7997	3462	26.98
4-C9Are	Pure Argon	BS:2901 C9	8364	3923	46.34
4-C9Arf	Pure Argon	BS:2901 C9	7808	3923	23.29
		Range	1611	604	33.22
		Average	7704	3824	26.53

Table 4.7 Contd

Test Piece	Shielding Gas	Filler Material	Max Load (N)	Proof Load (N)	Max Extension (mm)
4-C9Ar01a	Argon + 1%O ₂	BS:2901 C9	8331	3923	45.08
4-C9Ar01b	Argon + 1%O ₂	BS:2901 C9	8303	3778	45.23
4-C9Ar01c	Argon + 1%O ₂	BS:2901 C9	8239	3944	34.10
4-C9Ar01d	Argon + 1%O ₂	BS:2901 C9	8142	3870	31.35
4-C9Ar01e	Argon + 1%O ₂	BS:2901 C9	8311	4000	45.72
4-C9Ar01f	Argon + 1%O ₂	BS:2901 C9	8347	3926	46.03
		Range	205	222	0.95
		Average	8279	3907	41.25
4-C9Ar02a	Argon + 2%O ₂	BS:2901 C9	8412	3926	47.69
4-C9Ar02b	Argon + 2%O ₂	BS:2901 C9	8355	3962	45.98
4-C9Ar02c	Argon + 2%O ₂	BS:2901 C9	8323	3865	45.04
4-C9Ar02d	Argon + 2%O ₂	BS:2901 C9	8311	3942	45.25
4-C9Ar02e	Argon + 2%O ₂	BS:2901 C9	8271	3926	44.55
4-C9Ar02f	Argon + 2%O ₂	BS:2901 C9	8247	3961	44.82
		Range	165	97	3.14
		Average	8320	3930	45.56

Table 4.7 Contd

Test Piece	Shielding Gas	Filler Material	Max Load (N)	Proof Load (N)	Max Extension (mm)
4-C11Ara	Pure Argon	BS:2901 C11	8049	3889	27.81
4-C11Arb	Pure Argon	BS:2901 C11	7196	3796	16.61
4-C11Arc	Pure Argon	BS:2901 C11	7083	3889	15.21
4-C11Ard	Pure Argon	BS:2901 C11	5404	3900	5.77
4-C11Are	Pure Argon	BS:2901 C11	7393	3900	18.37
4-C11Arf	Pure Argon	BS:2901 C11	8339	4000	46.61
		Range	2935	204	40.84
		Average	7244	3896	21.73
4-C11Ar01a	Argon + 1%O ₂	BS:2901 C11	8013	3880	28.99
4-C11Ar01b	Argon + 1%O ₂	BS:2901 C11	7256	3327	17.78
4-C11Ar01c	Argon + 1%O ₂	BS:2901 C11	6564	3808	12.47
4-C11Ar01d	Argon + 1%O ₂	BS:2901 C11	6938	3846	14.95
4-C11Ar01e	Argon + 1%O ₂	BS:2901 C11	5996	3855	9.33
4-C11Ar01f	Argon + 1%O ₂	BS:2901 C11	6894	3927	14.66
		Range	2017	47	19.66
		Average	6944	3774	16.36

Table 4.7 Contd

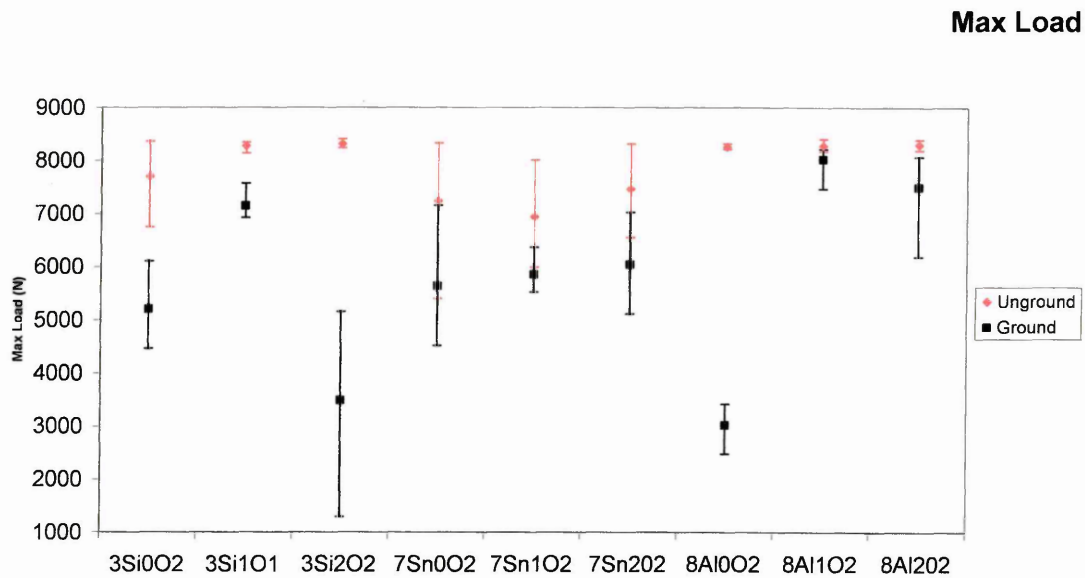
Test Piece	Shielding Gas	Filler Material	Max Load (N)	Proof Load (N)	Max Extension (mm)
4-C11Ar02a	Argon + 2%O ₂	BS:2901 C11	7184	3833	16.51
4-C11Ar02b	Argon + 2%O ₂	BS:2901 C11	6556	3796	12.15
4-C11Ar02c	Argon + 2%O ₂	BS:2901 C11	8138	3917	31.24
4-C11Ar02d	Argon + 2%O ₂	BS:2901 C11	7264	3936	17.54
4-C11Ar02e	Argon + 2%O ₂	BS:2901 C11	8009	3933	28.36
4-C11Ar02f	Argon + 2%O ₂	BS:2901 C11	7643	3825	20.81
		Range	1582	103	19.09
		Average	7466	3873	21.10
4-C28Ara	Pure Argon	BS:2901 C28	8295	3816	44.77
4-C28Arb	Pure Argon	BS:2901 C28	8239	3900	44.63
4-C28Arc	Pure Argon	BS:2901 C28	8227	3853	43.84
4-C28Ard	Pure Argon	BS:2901 C28	8323	3815	44.64
4-C28Are	Pure Argon	BS:2901 C28	8243	3706	44.88
4-C28Arf	Pure Argon	BS:2901 C28	8251	3817	44.85
		Range	96	194	1.04
		Average	8263	3818	44.54

Table 4.7 Contd

Test Piece	Shielding Gas	Filler Material	Max Load (N)	Proof Load (N)	Max Extension (mm)
4-C28Ar01a	Argon + 1%O ₂	BS:2901 C28	8178	3708	45.54
4-C28Ar01b	Argon + 1%O ₂	BS:2901 C28	8178	3892	47.09
4-C28Ar01c	Argon + 1%O ₂	BS:2901 C28	8206	3758	47.19
4-C28Ar01d	Argon + 1%O ₂	BS:2901 C28	8359	3875	44.37
4-C28Ar01e	Argon + 1%O ₂	BS:2901 C28	8376	3688	45.83
4-C28Ar01f	Argon + 1%O ₂	BS:2901 C28	8412	3933	47.31
		Range	234	245	2.94
		Average	8285	3809	46.22
4-C28Ar02a	Argon + 2%O ₂	BS:2901 C28	8400	3654	46.96
4-C28Ar02b	Argon + 2%O ₂	BS:2901 C28	8372	3867	47.86
4-C28Ar02c	Argon + 2%O ₂	BS:2901 C28	8315	3933	48.30
4-C28Ar02d	Argon + 2%O ₂	BS:2901 C28	8198	3813	44.57
4-C28Ar02e	Argon + 2%O ₂	BS:2901 C28	8287	3700	46.42
4-C28Ar02f	Argon + 2%O ₂	BS:2901 C28	8275	3882	47.24
		Range	202	279	3.73
		Average	8308	3808	46.89

Table 4.7 - Comparison of Tensile Properties of Unground Butt Joints

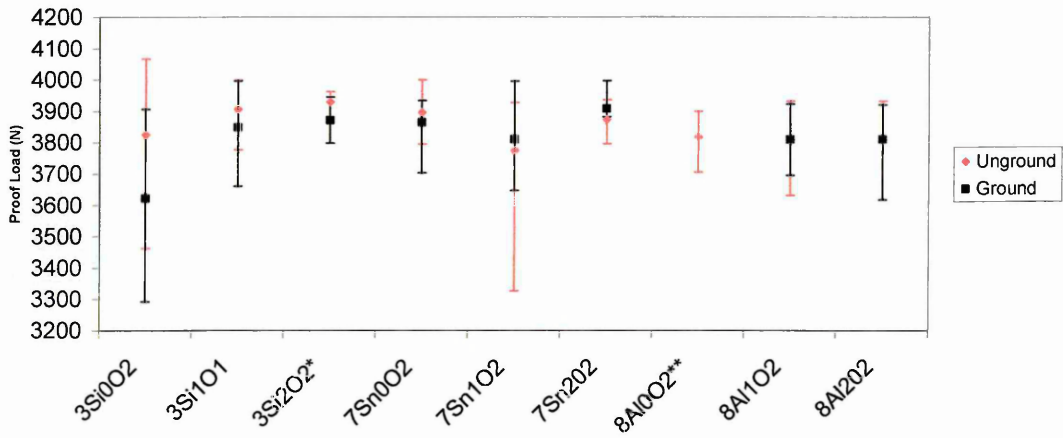
A comparison of the tensile properties of ground and unground butt joints can be seen in figures 4.33 – 4.35.



3Si	BS:2901 C9
7Sn	BS:2901 C11
8Al	BS:2901 C28
002	Pure Argon
102	Argon containing 1% Oxygen
202	Argon containing 2% Oxygen

Figure 4.33 - Comparison of maximum loads experienced prior to failure by ground and unground butt joints manufactured using 304 parent material and various combinations of filler material and shielding gas.

Proof Load



3Si BS:2901 C9

7Sn BS:2901 C11

8Al BS:2901 C28

0O2 Pure Argon

1O2 Argon containing 1% Oxygen

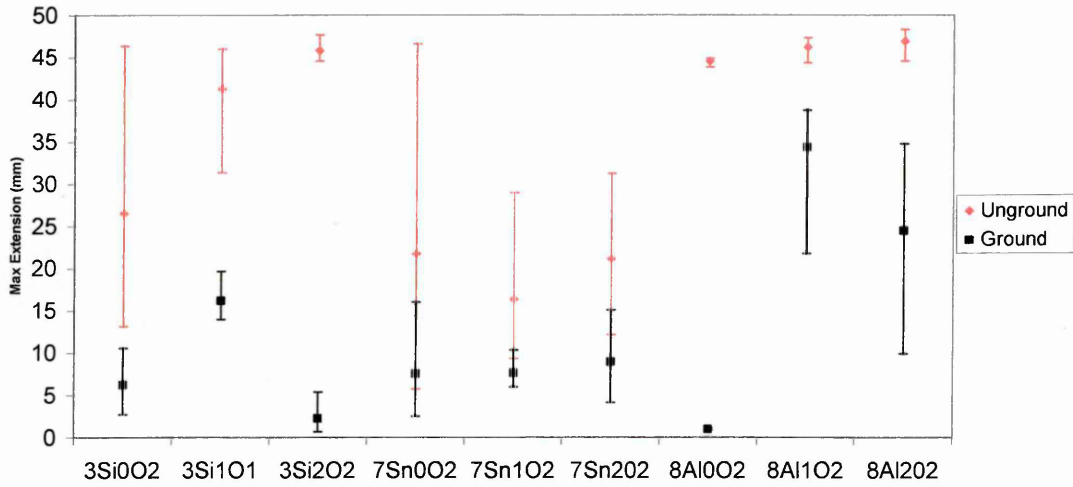
2O2 Argon containing 2% Oxygen

*only 2 ground samples deformed plastically prior to failure

** no ground samples deformed plastically prior to failure

Figure 4.34 – Comparison of loads experienced at yield by ground and unground butt joints manufactured using 304 parent material and various combinations of filler material and shielding gas.

Max Extension



3Si BS:2901 C9

7Sn BS:2901 C11

8Al BS:2901 C28

002 Pure Argon

102 Argon containing 1% Oxygen

202 Argon containing 2% Oxygen

Figure 4.35 – Comparison of total extensions at failure of ground and unground butt joints manufactured using 304 parent material and various combinations of filler material and shielding gas.

Figures 4.33 – 4.35 show that although the unground butt joints withstood a higher load prior to failure and displayed a larger percentage elongation, both ground and unground butt joints yielded at similar loads.

4.4 Impact Testing of Similar Metal Modified Impact Test Samples

4.4.1 Wetting of Parent Material

Macrostructural Investigation

Assessments of the degree of wetting of both the top and the bottom plate were made using low magnification optical light microscopy. Examples of wet and non wet joints can be observed in figures 4.36 and 4.37 respectively

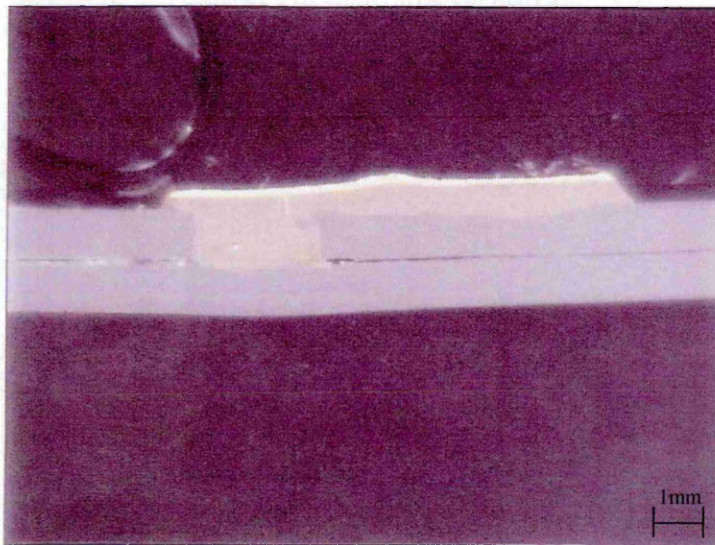


Figure 4.36 - Plug braze manufactured using BS:2901 C28 filler material and pure argon shielding gas showing complete wetting of the upper and lower plate.

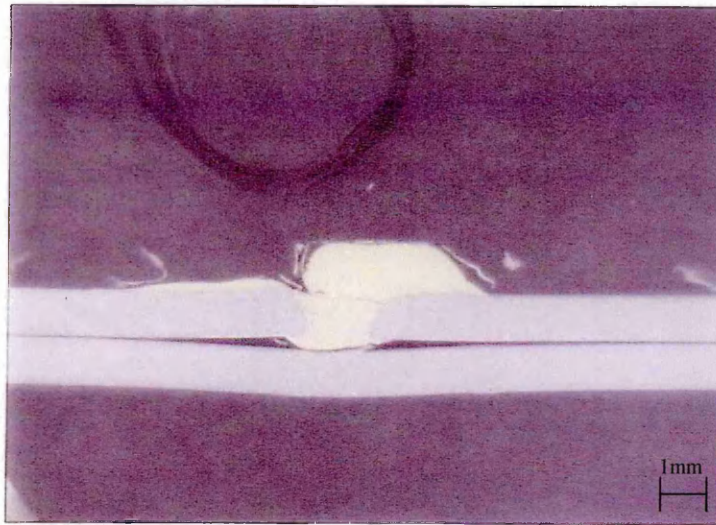


Figure 4.37 - Plug braze manufactured using BS:2901 C11 filler material and argon containing 1% oxygen shielding gas showing incomplete wetting of the lower plate.

Lap Shear Testing of Arc Brazed Plug Joints

Results of the lap shear testing showed that all samples manufactured using an 8mm hole failed by braze pull-out failure as shown in figure 4.38 and figure 4.39.

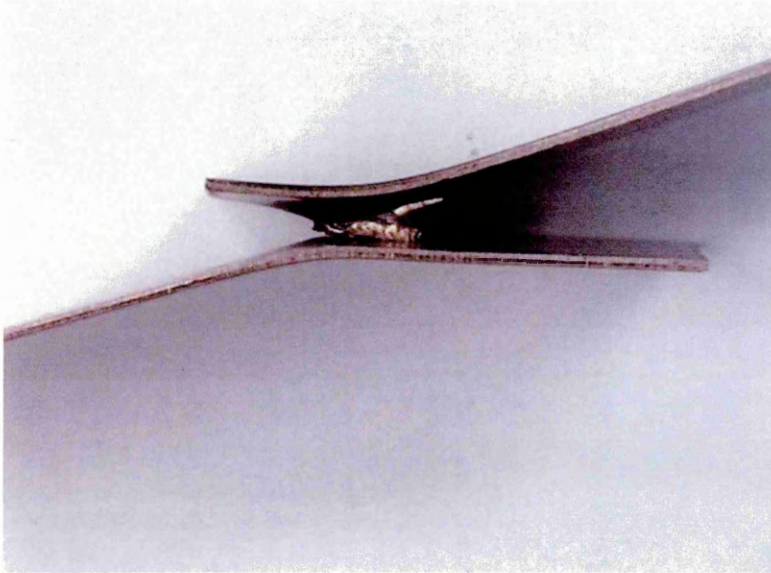


Figure 4.38 - Lap shear sample showing braze pull-out failure of an arc brazed plug joint

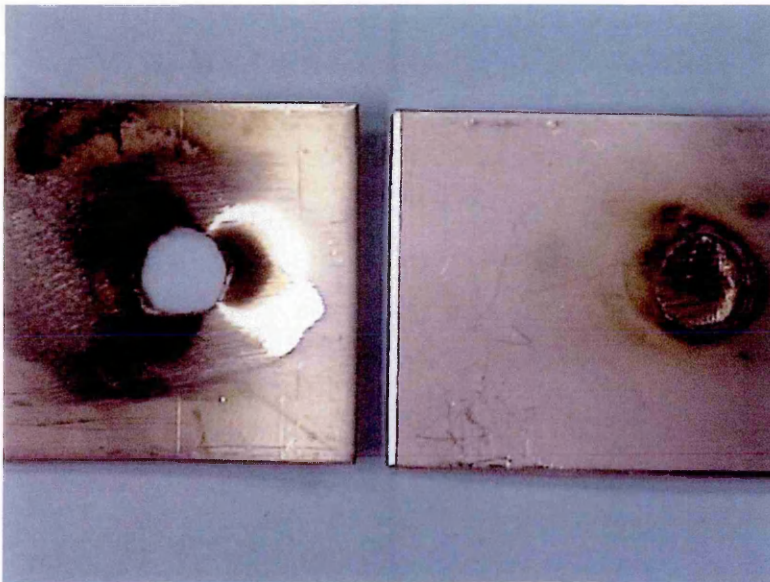


Figure 4.39 - Lap shear sample showing braze pull-out failure of an arc brazed plug joint

4.4.2 Modified Quantitative Impact Test Result

Table 4.8 shows the results of the modified quantitative chisel test to measure impact toughness of the arc plug brazed joints.

Table 4.8

Sample No.	Filler Material	Shielding Gas	Impact Energy (J)
1.1	BS:2901 C28	Pure Argon	20
1.2	BS:2901 C28	Pure Argon	28
1.3	BS:2901 C28	Pure Argon	22
1.4	BS:2901 C28	Pure Argon	22
1.5	BS:2901 C28	Pure Argon	27
1.6	BS:2901 C28	Pure Argon	19
		<i>Average</i>	23
		<i>Range</i>	9
2.1	BS:2901 C28	Argon + 1% O ₂	32
2.2	BS:2901 C28	Argon + 1% O ₂	32
2.3	BS:2901 C28	Argon + 1% O ₂	*
2.4	BS:2901 C28	Argon + 1% O ₂	*
2.5	BS:2901 C28	Argon + 1% O ₂	29
2.6	BS:2901 C28	Argon + 1% O ₂	35
		<i>Average</i>	32
		<i>Range</i>	6

*Result invalid as parent material was impacted prior to braze plug

Table 4.8 Contd

Sample No.	Filler Material	Shielding Gas	Impact Energy (J)
3.1	BS:2901 C28	Argon + 2% O ₂	26
3.2	BS:2901 C28	Argon + 2% O ₂	16
3.3	BS:2901 C28	Argon + 2% O ₂	18
3.4	BS:2901 C28	Argon + 2% O ₂	31
3.5	BS:2901 C28	Argon + 2% O ₂	14
3.6	BS:2901 C28	Argon + 2% O ₂	34
		<i>Average</i>	<i>23.17</i>
		<i>Range</i>	<i>20</i>
4.1	BS:2901 C9	Pure Argon	16
4.2	BS:2901 C9	Pure Argon	29
4.3	BS:2901 C9	Pure Argon	14
4.4	BS:2901 C9	Pure Argon	10
4.5	BS:2901 C9	Pure Argon	15
4.6	BS:2901 C9	Pure Argon	20
		<i>Average</i>	<i>17.33</i>
		<i>Range</i>	<i>19</i>

Table 4.8 Contd

Sample No.	Filler Material	Shielding Gas	Impact Energy (J)
5.1	BS:2901 C9	Argon + 1% O ₂	24
5.2	BS:2901 C9	Argon + 1% O ₂	29
5.3	BS:2901 C9	Argon + 1% O ₂	34
5.4	BS:2901 C9	Argon + 1% O ₂	16
5.5	BS:2901 C9	Argon + 1% O ₂	32
5.6	BS:2901 C9	Argon + 1% O ₂	29
		Average	27.33
		Range	18
6.1	BS:2901 C9	Argon + 2% O ₂	31
6.2	BS:2901 C9	Argon + 2% O ₂	44
6.3	BS:2901 C9	Argon + 2% O ₂	27
6.4	BS:2901 C9	Argon + 2% O ₂	21
6.5	BS:2901 C9	Argon + 2% O ₂	16
6.6	BS:2901 C9	Argon + 2% O ₂	16
		Average	25.83
		Range	28

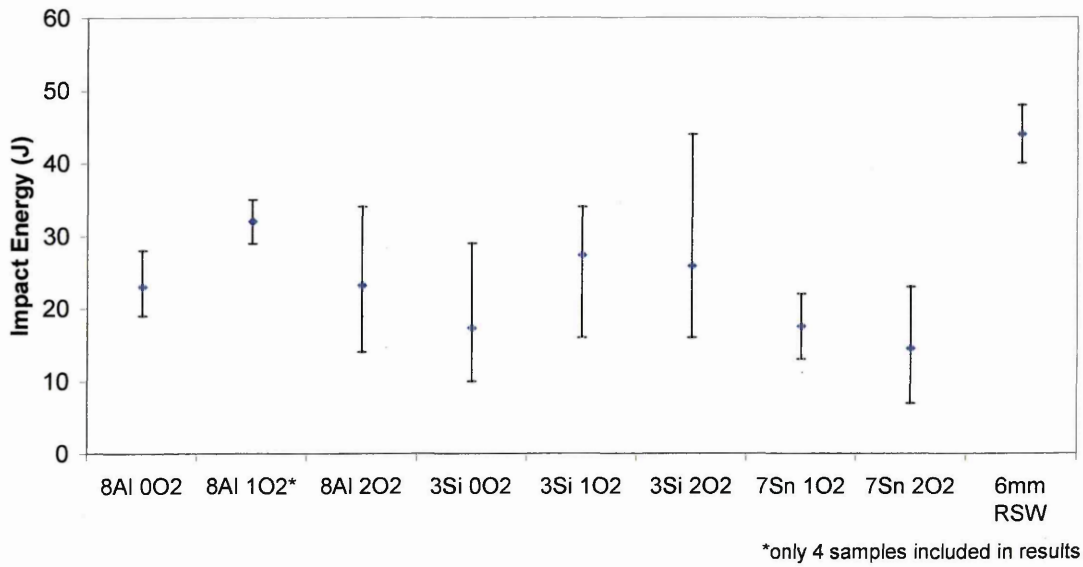
Table 4.8 Contd

Sample No.	Filler Material	Shielding Gas	Impact Energy (J)
8.1	BS:2901 C11	Argon + 1% O ₂	18
8.2	BS:2901 C11	Argon + 1% O ₂	19
8.3	BS:2901 C11	Argon + 1% O ₂	16
8.4	BS:2901 C11	Argon + 1% O ₂	22
8.5	BS:2901 C11	Argon + 1% O ₂	17
8.6	BS:2901 C11	Argon + 1% O ₂	13
		Average	17.5
		Range	9
9.1	BS:2901 C11	Argon + 2% O ₂	13
9.2	BS:2901 C11	Argon + 2% O ₂	7
9.3	BS:2901 C11	Argon + 2% O ₂	23
9.4	BS:2901 C11	Argon + 2% O ₂	10
9.5	BS:2901 C11	Argon + 2% O ₂	14
9.6	BS:2901 C11	Argon + 2% O ₂	20
		Average	14.5
		Range	16

Table 4.8 - Impact Properties of Arc Plug Brazes

Figure 4.40 shows a comparison of the impact properties of the arc brazed plug joints from this investigation and the 6mm resistance spot welded joints investigated by Wray⁶¹.

Impact Strength



3Si	BS:2901 C9
7Sn	BS:2901 C11
8Al	BS:2901 C28
0O2	Pure Argon
1O2	Argon containing 2% Oxygen
2O2	Argon containing 2% Oxygen

Figure 4.40 – Impact energies achieved for similar metal impact test samples which have been joined using 3 different filler metals, 3 different shielding gas combinations and 6mm and 8mm resistance spot welds.

The impact results for the plug brazed impact test pieces are compared to 6mm RSW^v tested using the same equipment and procedure developed by Wray⁶¹. This shows that the 6mm RSW display the highest impact toughness with the combination of BS:2901 C28 filler material and argon containing 1% oxygen shielding gas displaying the highest impact toughness of all the combinations of filler material and shielding gas tested for arc brazed plug joints.

^v The results for the 6mm resistance spot welds were obtained from the work by Wray⁶¹

4.5 Similar Metal Lap Joints

4.5.1 Tensile Properties

Table 4.9 shows the results of tensile testing conducted on lap joints constructed using the BS:2901 C28 filler material, argon containing 1% oxygen shielding gas and AISI 304 grade of stainless steel as the parent material. Overlap lengths of 10mm and 20mm; and single and double braze seams were used. Due to the irregular surface area of the lap joints it was not possible to calculate values for stress, and so results are presented as loads in Newtons.

Table 4.9

Test Piece	Overlap Length (mm)	No. of Braze Seams	Max Load (N)	Proof Load (N)	Percentage Elongation (%)
Lap10sa	10	1	6121	3294	14.56
Lap10sb	10	1	6064	3824	13.49
Lap10sc	10	1	5939	3411	13.17
Lap10sd	10	1	4590	3375	4.75
Lap10se	10	1	5698	3475	10.81
Lap10sf	10	1	5545	3500	10.15
		<i>Average</i>	<i>5660</i>	<i>3480</i>	<i>11.16</i>
		<i>Range</i>	<i>1531</i>	<i>530</i>	<i>9.81</i>

Table 4.9 Contd

Test Piece	Overlap Length (mm)	No. of Braze Seams	Max Load (N)	Proof Load (N)	Percentage Elongation (%)
Lap10da	10	2	8351	3852	55.31
Lap10db	10	2	8323	3667	56.09
Lap10dc	10	2	8343	3722	59.25
Lap10dd	10	2	8335	3854	56.16
Lap10de	10	2	8351	3500	57.24
Lap10df	10	2	8347	3929	58.57
		<i>Average</i>	8342	3754	57.10
		<i>Range</i>	28	429	3.95
Lap20sa	20	1	4760	3550	5.00
Lap20sb	20	1	5311	3275	8.27
Lap20sc	20	1	5126	3500	7.28
Lap20sd	20	1	4973	3475	6.81
Lap20se	20	1	5339	3550	8.77
Lap20sf	20	1	5480	3650	9.36
		<i>Average</i>	5165	3500	7.58
		<i>Range</i>	720	375	4.36

Table 4.9 Contd

Test Piece	Overlap Length (mm)	No. of Braze Seams	Max Load (N)	Proof Load (N)	Percentage Elongation (%)
Lap20da	20	2	8291	3821	46.09
Lap20db	20	2	8307	3893	47.19
Lap20dc	20	2	8295	3640	47.55
Lap20dd	20	2	8376	4074	50.00
Lap20de	20	2	8380	3593	50.73
Lap20df	20	2	8251	3815	40.45
		<i>Average</i>	8317	3806	47.00
		<i>Range</i>	129	481	9.55

Table 4.9 – Tensile Properties of Arc Brazed Lap Joints

By presenting these results graphically (figures 4.41 and 4.42) with the maximum loads withstood by similar metal butt joints arc brazed with BS:2901 C28 filler material and argon containing 1% oxygen shielding gas any differences can be observed.

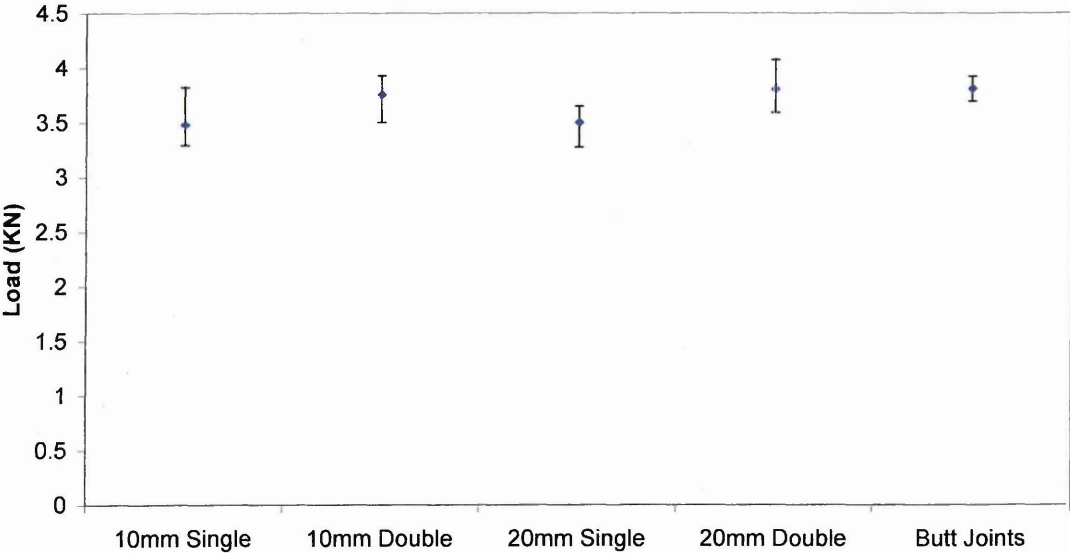


Figure 4.41 - Loads at yield for lap joints manufactured using BS:2901 C28 filler material and argon containing 1% oxygen compared with butt joints manufactured using the same consumables.

Max Load

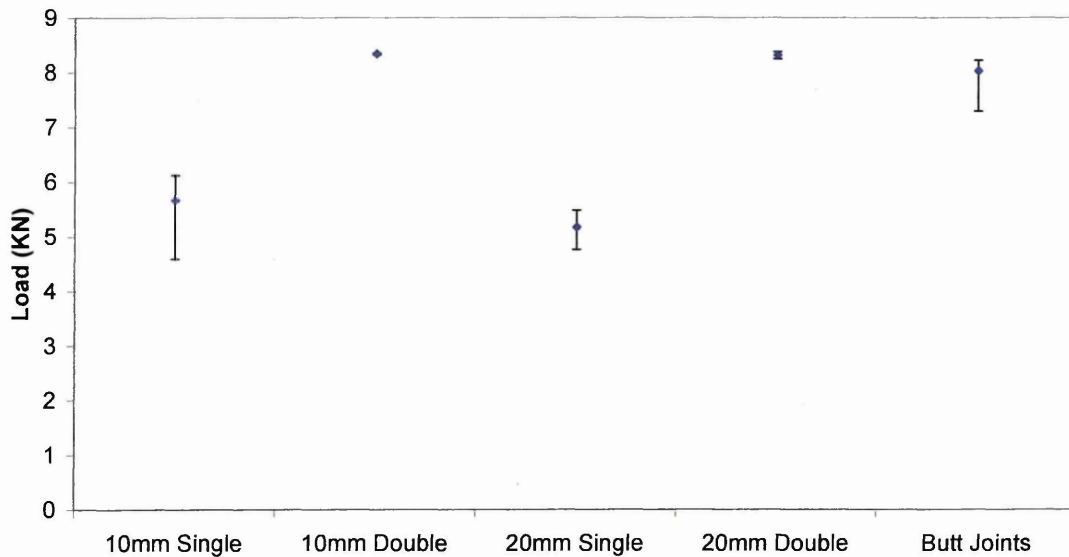


Figure 4.42 - Maximum loads prior to failure supported by lap joints manufactured from BS:2901 C28 filler material and argon containing 1% oxygen shielding gas compared with butt joints manufactured using the same consumables.

From figure 4.41 it can be seen that all arc brazed lap joints yielded at a similar load to the arc brazed butt joints. Figure 4.42 shows that although the double seam lap joints withstood a higher load than the single seam lap joints, the maximum load withstood by the double seam lap joints was comparable to that supported by the arc brazed butt joints.

4.5.2 Microstructural Investigation of Similar Metal Arc Brazed Lap Joints

Figures 4.43 and 4.44 show the interface between the braze material and top and bottom sheet of the similar metal lap joint respectively.

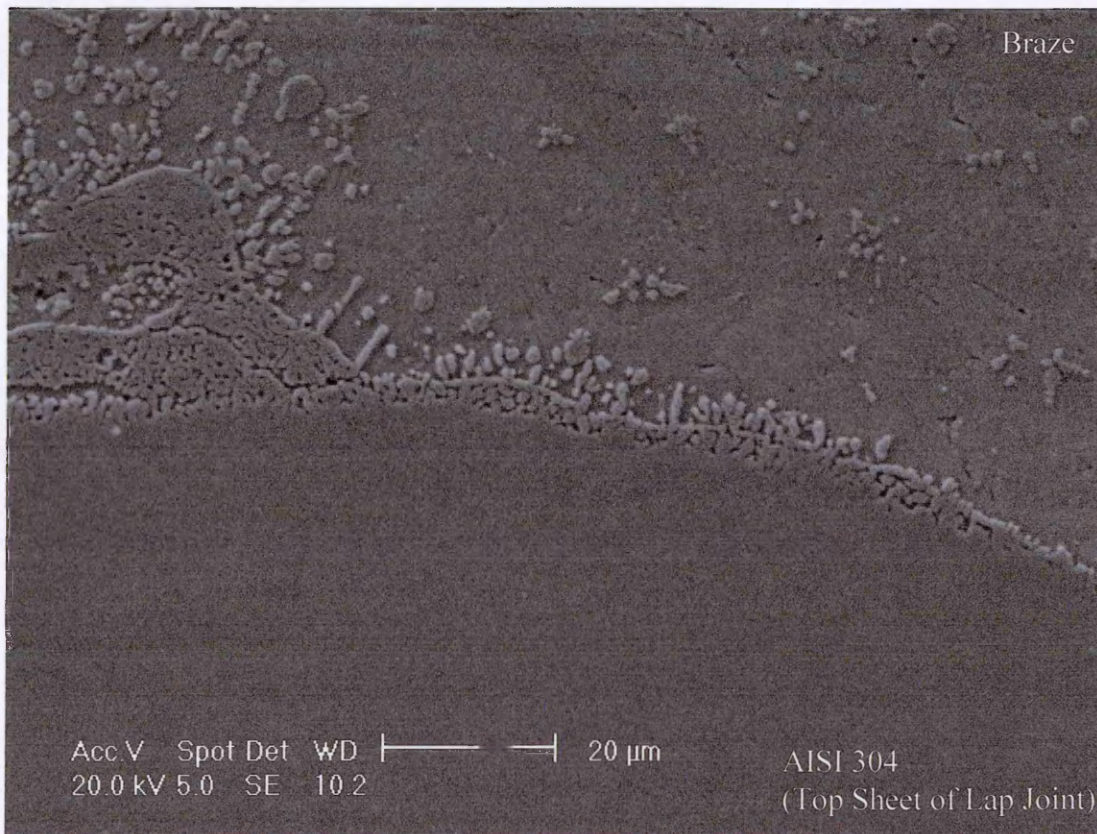


Figure 4.43 - Interface between braze material and top sheet of the similar metal lap joint

The image shows localised melting of the top sheet of the AISI 304 parent material at the interface with the braze.

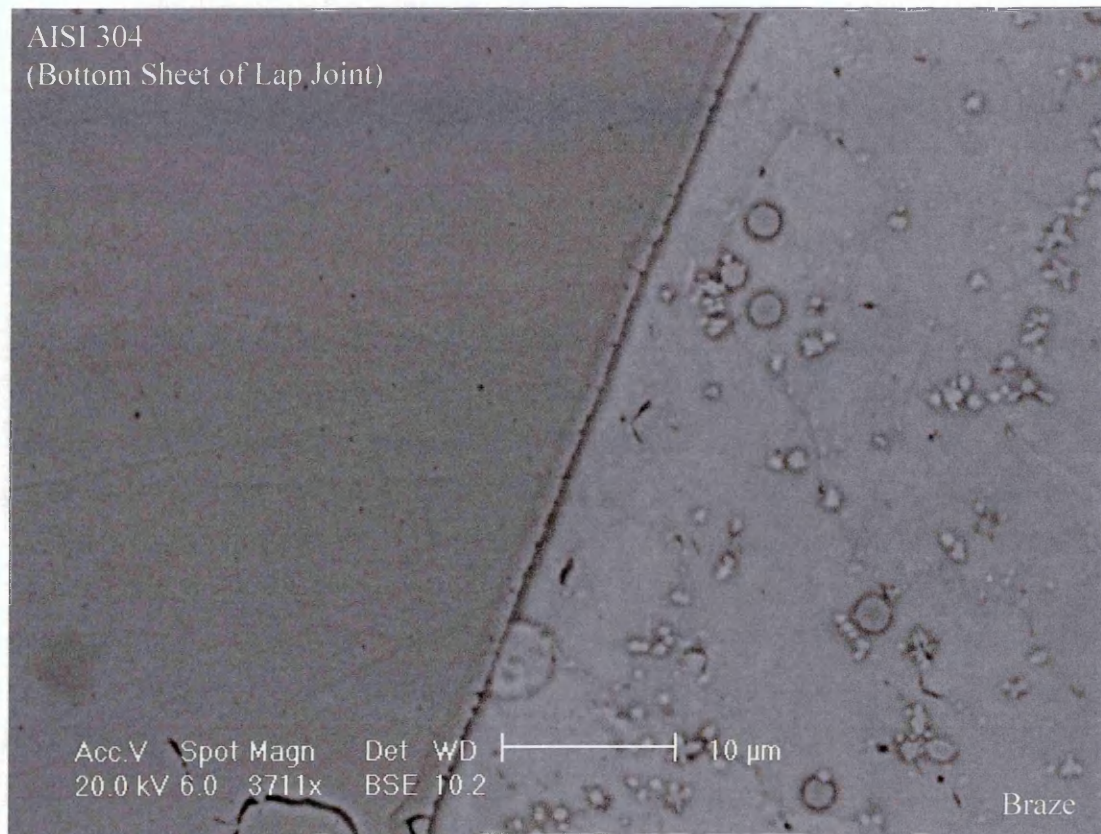


Figure 4.44 - Interface between braze material and bottom sheet of the similar metal lap joint

There is a clear difference between the above image and that seen in figure 4.43. The lack of wetting at the interface of the braze and the parent material, as seen above, reduces the strength of the joint. The reasons for this lack of wetting of the bottom plate will be discussed in Chapter 5.

4.6 Optimisation of Process Parameters for Dissimilar Metal Butt Joints – Dogal 260RP-x to AISI 304

4.6.1 Optimisation of Torch Angle and Torch Height

The torch was positioned at 85° to the work piece at a vertical height of 12.75mm, as shown in figure 4.45. This resulted in the torch being a distance of 12.8mm from the work piece.

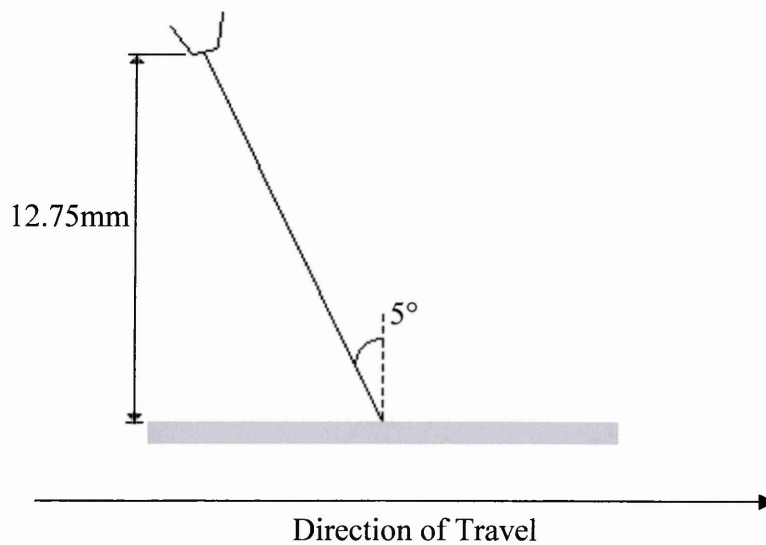


Figure 4.45 - Orientation of GMAB Torch during Manufacture of Dissimilar Butt Joints

4.6.2 Optimisation of Root Gap

Figures 4.46 and 4.47 show photographs of the braze seam reinforcement for dissimilar metal butt joints constructed using a 0.5mm and 0.6mm root gap. Both joints were manufactured using a torch velocity of $63.5\text{cm}\cdot\text{min}^{-1}$.

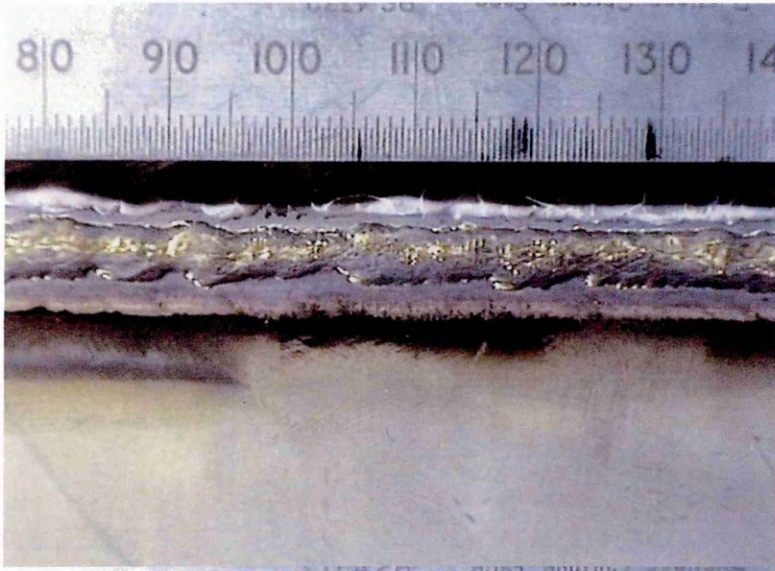


Figure 4.46 - Braze seam reinforcement with 0.5mm root gap joining AISI 304 grade stainless steel to Dogal 260RP-x.

In figure 4.46 the uneven braze seam does not have the aesthetic properties which would be required for the intended application in the automotive industry.

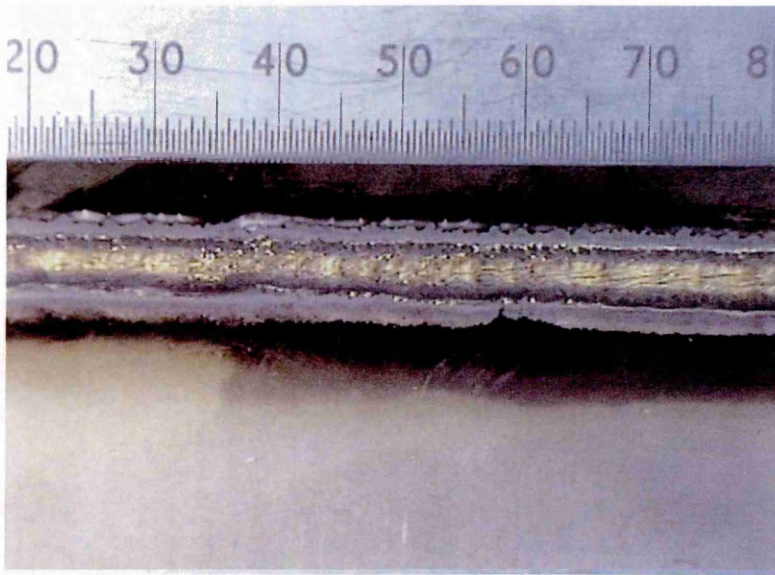


Figure 4.47 - Braze seam reinforcement with 0.6mm gap joining AISI 304 grade stainless steel to Dogal 260RP-x

In contrast with figure 4.46, the braze seam in figure 4.47 has a more uniform appearance.

4.6.3 Optimisation of Torch Velocity

Figures 4.48 - 4.49 show photographs of dissimilar butt joints manufactured using a 0.6mm root gap and pass velocities of $88.9\text{cm}\cdot\text{min}^{-1}$ and $96.5\text{cm}\cdot\text{min}^{-1}$ respectively.

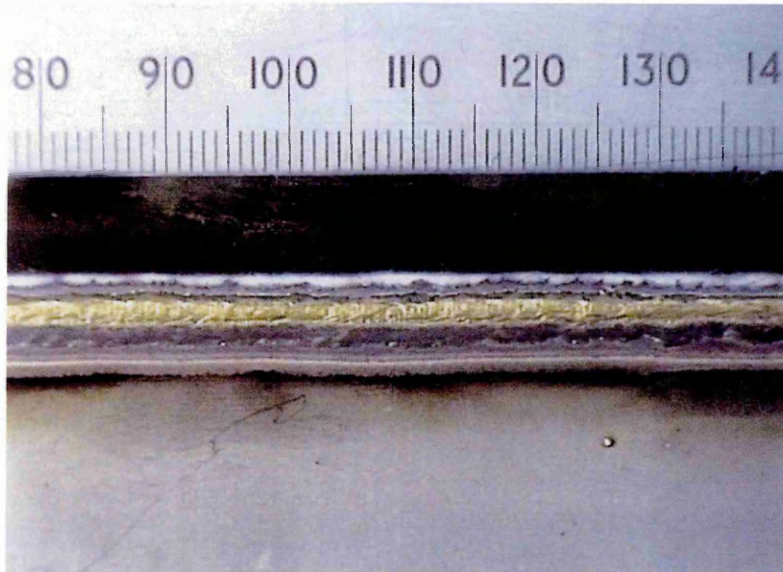


Figure 4.48i - Braze seam reinforcement with $88.9\text{cm}\cdot\text{min}^{-1}$ torch velocity showing a neat, uniform braze seam

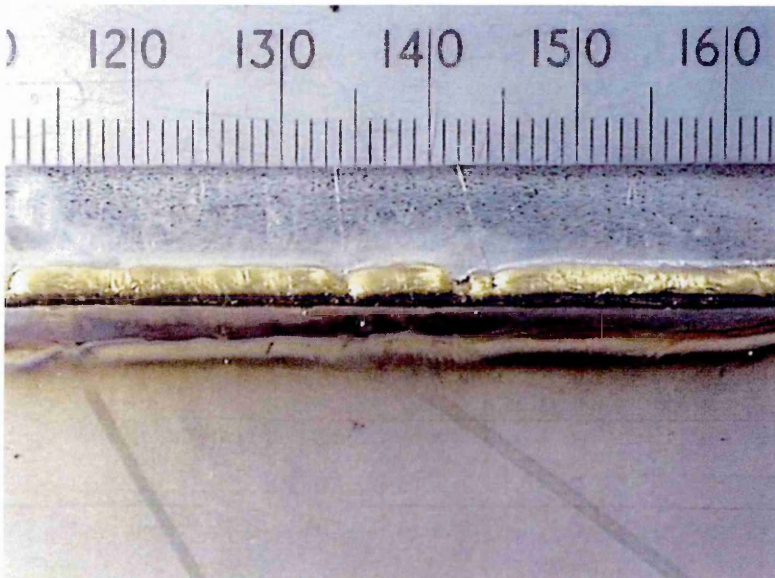


Figure 4.48ii - Rear view of brazed joint with $88.9\text{cm}\cdot\text{min}^{-1}$ torch velocity showing complete penetration by the braze alloy

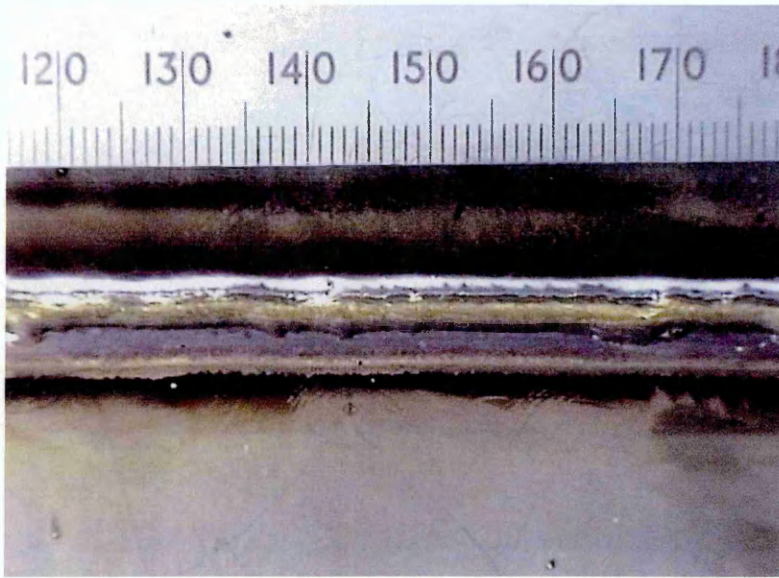


Figure 4.49i - Braze seam reinforcement with $96.5\text{cm}\cdot\text{min}^{-1}$ torch velocity with unacceptable appearance

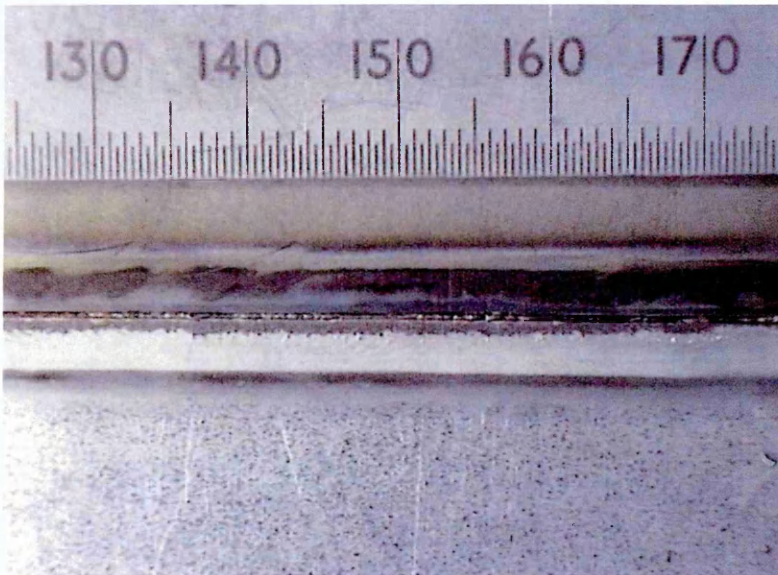


Figure 4.49ii - Rear view of brazed joint with $96.5\text{cm}\cdot\text{min}^{-1}$ torch velocity showing inadequate penetration of the joint.

In figure 4.48i the braze seam has a neat appearance and there is penetration, shown in figure 4.48ii throughout the depth of the joint. When the pass velocity was

increased the appearance of the braze reinforcement deteriorates, as shown in figure 4.49i and the and there is very little penetration to the underside of the joint, figure 4.49ii.

4.6.4 Optimisation of Arc Characteristics

The arc characteristics required to manufacture dissimilar butt joints by spray arc transfer are shown in Appendix 1.

4.6.5 Dissimilar Metal Butt Joints Tensile Properties

Table 4.10 shows the tensile properties for the dissimilar metal butt joints manufactured using a 0.6mm root gap, BS:2901 C28 filler material, argon containing 1% oxygen shielding gas and a pass velocity of 88.9cm.min⁻¹.

Test Piece	Cross Sectional Area (mm ²)		Load at Yield (KN)	Rp _{0.2} (MPa)	Max Load (KN)	Rm (MPa)	Percentage Elongation (%)
	Mild Steel	AISI 304					
DBTa	14.79	12.53	3.4	273	6.028	408	26
DBTb	14.75	12.5	3.4	275	5.964	404	27
DBTc	14.73	12.48	3.8	308	5.915	402	27
DBTd	14.66	12.42	3.5	279	5.891	402	26
DBTe	14.69	12.45	3.4	270	5.956	405	26
DBTf	14.71	12.47	3.5	282	5.972	406	25
		Average	3.5	281	5.954	404	26
		Range	0.4	38	0.137	6	2

Table 4.10 - Tensile properties of dissimilar metal arc brazed butt joints manufactured from AISI 304 and Dogal 260RP-x parent materials, BS:2901 C28 filler material and argon containing 1% oxygen shielding gas

4.7 *Fatigue Testing Results for Similar and Dissimilar Metal Joints Using Optimised Arc Brazing Process Parameters*

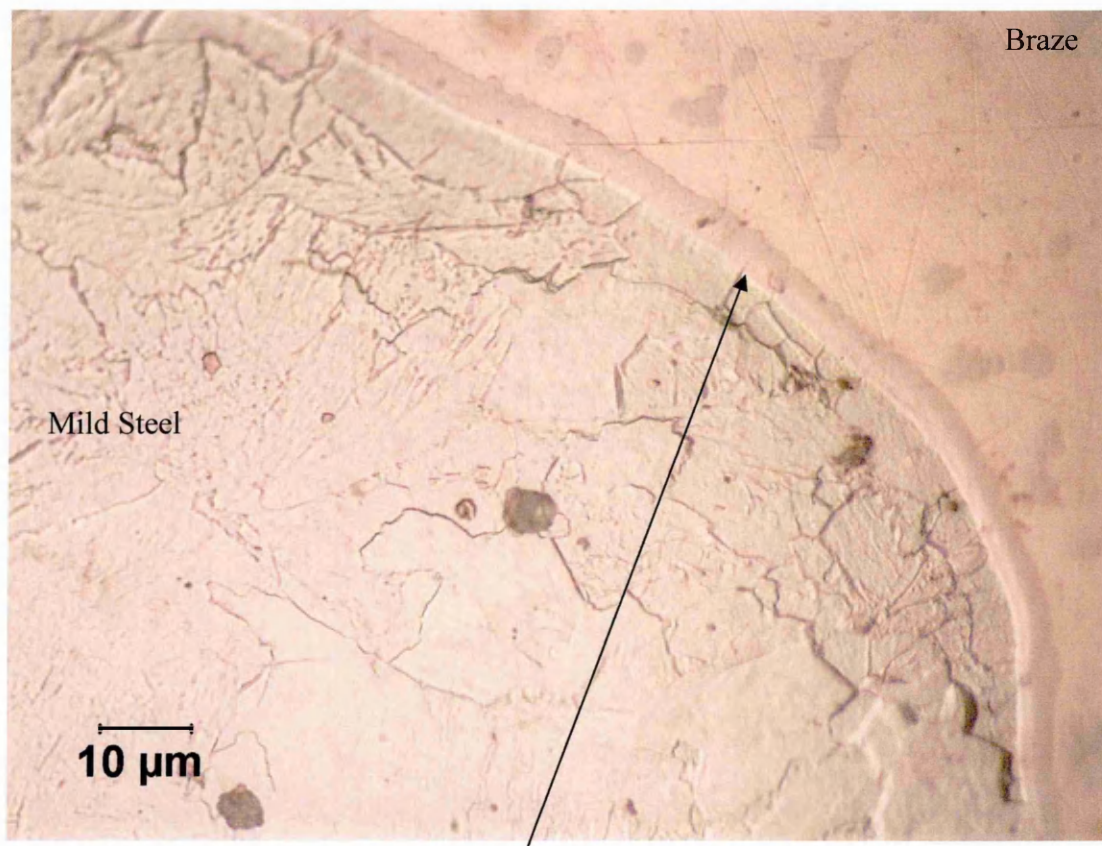
4.7.1 *Similar Metal Butt Joints*

The results from the staircase fatigue test showed that the mean fatigue strength for similar butt joints was 5.72 kN, which equates to a line load of 127 Nmm^{-1} the standard deviation was found to be 0.389 kN with a convergence factor of 1.17.

4.7.2 *Dissimilar Metal Butt Joints*

The staircase fatigue test showed that the mean fatigue strength for dissimilar butt joints was 3.59 kN, which equates to a line load of 78 Nmm^{-1} the standard deviation was found to be 0.77 kN with a convergence factor of 0.769.

In order to establish a reason for the difference in the fatigue properties of arc brazed similar metal and dissimilar metal butt joints, the microstructure of the dissimilar metal joint was investigated using light and scanning electron microscopy and compared to that of the similar metal joint. The results can be seen in figures 4.50 - 4.53.



Band at Interface

Figure 4.50 – Optical microscopy image of a band at the interface between the mild steel and BS:2901 C28 braze alloy joined using argon containing 1% oxygen shielding gas.

This band seen at the interface of the braze and the mild steel was investigated further using the SEM as seen in figures 4.51 and 4.52.



Figure 4.51 – SEM Image of band between the BS:2901 C28 braze alloy and mild steel

The highlighted area in figure 4.51 denotes where the spot analysis shown in figure 4.52 overleaf was taken.

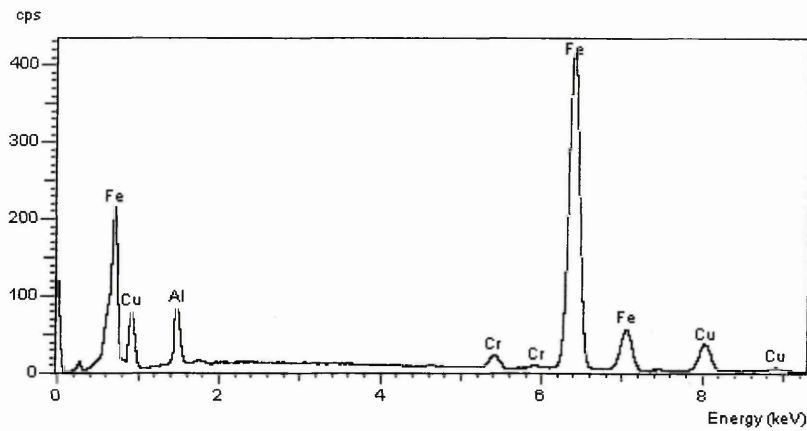


Figure 4.52 – Spectrum of Spot Analysis of Area Highlighted in Figure 4.51.

From the x-ray analysis in figure 4.52 it can be seen that the band at the interface of the braze and the mild steel, figures 4.50 and 4.51, is composed of copper and aluminium from the braze and iron from the steel. The small amount of chromium present suggests that this iron is from both the mild steel and the stainless steel parent materials.

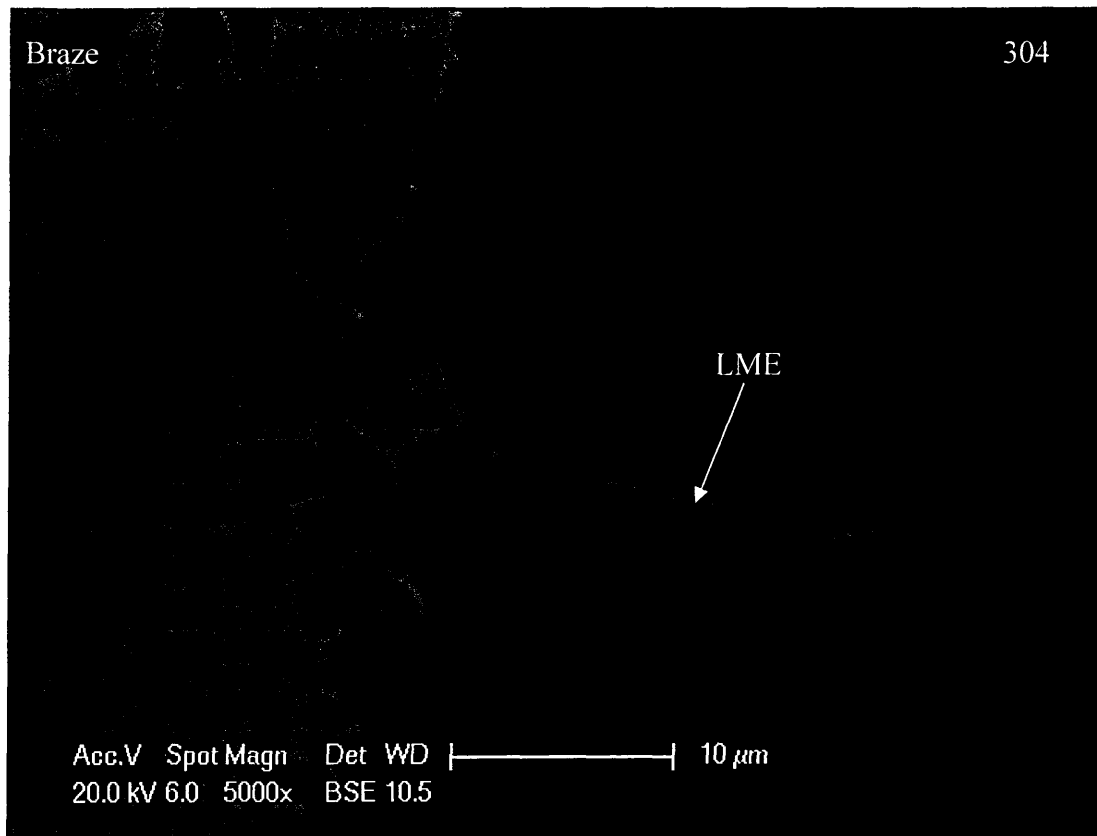


Figure 4.53 – Failed dissimilar metal butt joint showing evidence of LME at the interface of the stainless steel and BS:2901 C28 braze alloy.

Whilst the backscattered electron image in figure 4.53 does show a surface layer present between the braze and the stainless steel it has a different appearance to the band seen at the interface of the braze and the mild steel seen in figures 4.50 and 4.51. The differences between these and why copper can be seen to penetrate the stainless steel, but not the mild steel will be discussed further in Chapter 5.

4.8 Mullins Grooving

4.8.1 Similar Material Joints

Figure 4.54 shows five of the depth measurements taken and the four angles used to calculate the value for m , the gradient of the opening angle in equation 2.7 for similar material joints using BS:2901 C28 filler material and argon containing 1% oxygen shielding gas. It is important to note that the grain boundary grooving has occurred in an area which has a different microstructure to the bulk of the stainless steel. This microstructure is most likely to be similar to the surface layer seen in the backscattered electron image shown in figure 4.53. It can also be seen that these grooved grain boundaries, in figure 4.54, have a smooth appearance whilst the copper penetrating the stainless steel in figure 4.53 have a sharp appearance, associated with LME. These differences will be discussed in Chapter 5.

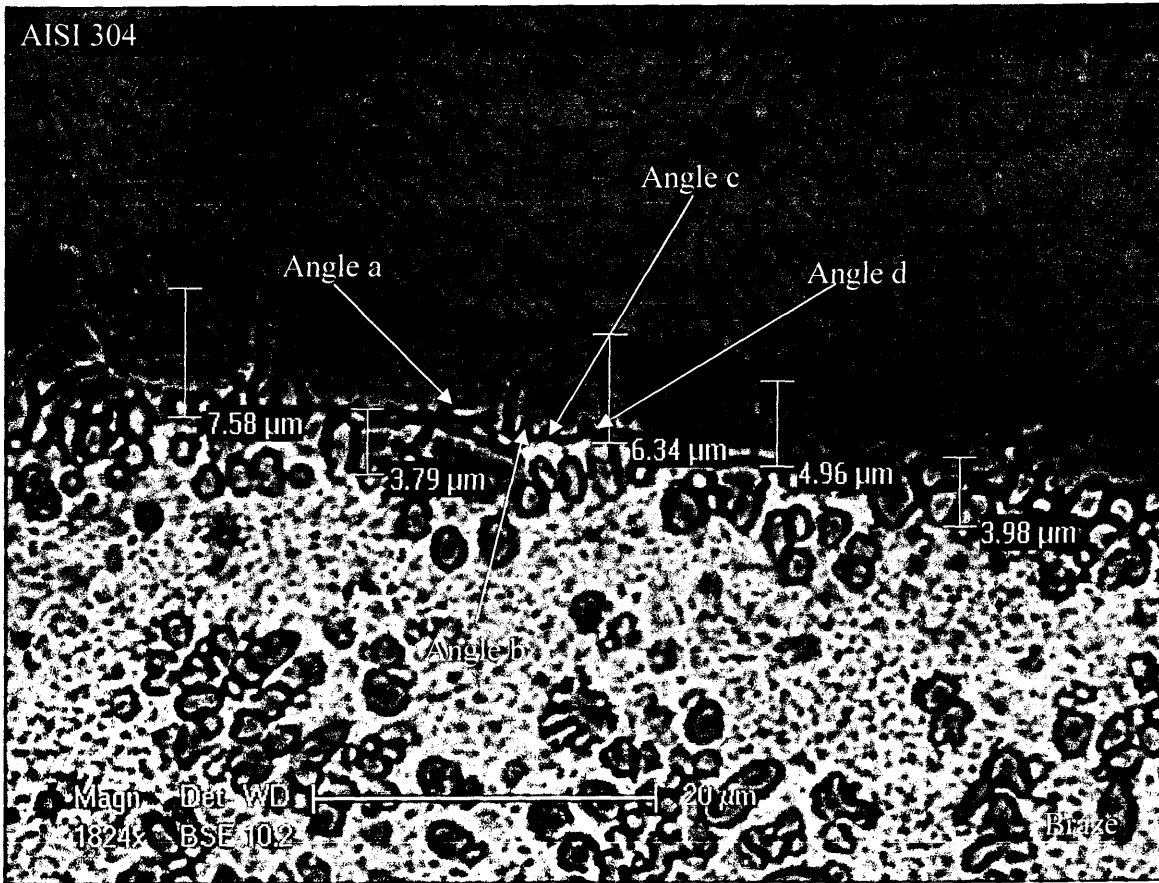


Figure 4.54 - SEM image showing grain boundary grooving of AISI 304 grade stainless steel in a butt joint brazed using BS:2901 C28 filler material and argon containing 1 % oxygen shielding gas.

The angles measured in figure 4.54 are

- a 39°
- b 41°
- c 78°
- d 46°

This gives an average of 51° however this is the average angle for the whole groove opening and therefore the value of m is the tangent of half of this.

Table 4.11 below gives the lengths of each depth measurement from the interface.

Measurement	Length (μm)	Measurement	Length (μm)
a	3.40	k	7.58
b	2.13	l	3.79
c	2.94	m	6.34
d	7.71	n	4.96
e	21.60	o	3.98
f	17.50	p	7.45
g	10.10	q	3.53
h	9.34	r	4.05
i	5.55	s	5.16
j	8.36	t	6.79

Table 4.11 - Depth of penetration of copper from the braze-stainless steel interface for similar material butt joints brazed using BS:2901 C28 filler material and argon containing 1% oxygen shielding gas.

The average depth of penetration was therefore $7.16\mu\text{m}$.

4.8.2 Dissimilar Material Joint Braze / Stainless Steel Interface

Figure 4.55 overleaf shows an image of the interface of the braze and stainless steel from a joint manufactured from dissimilar parent materials. Despite the fact that both the joint shown below and the one shown in figure 4.54 above were brazed using BS:2901 C28 filler material and argon containing 1% oxygen shielding gas the interface of the two joints appear to be different, whereas in figure 4.54 the grain boundaries of the parent material appear to have been grooved by the braze alloy, in the image overleaf it appears that grains of stainless steel have solidified in the molten braze material.

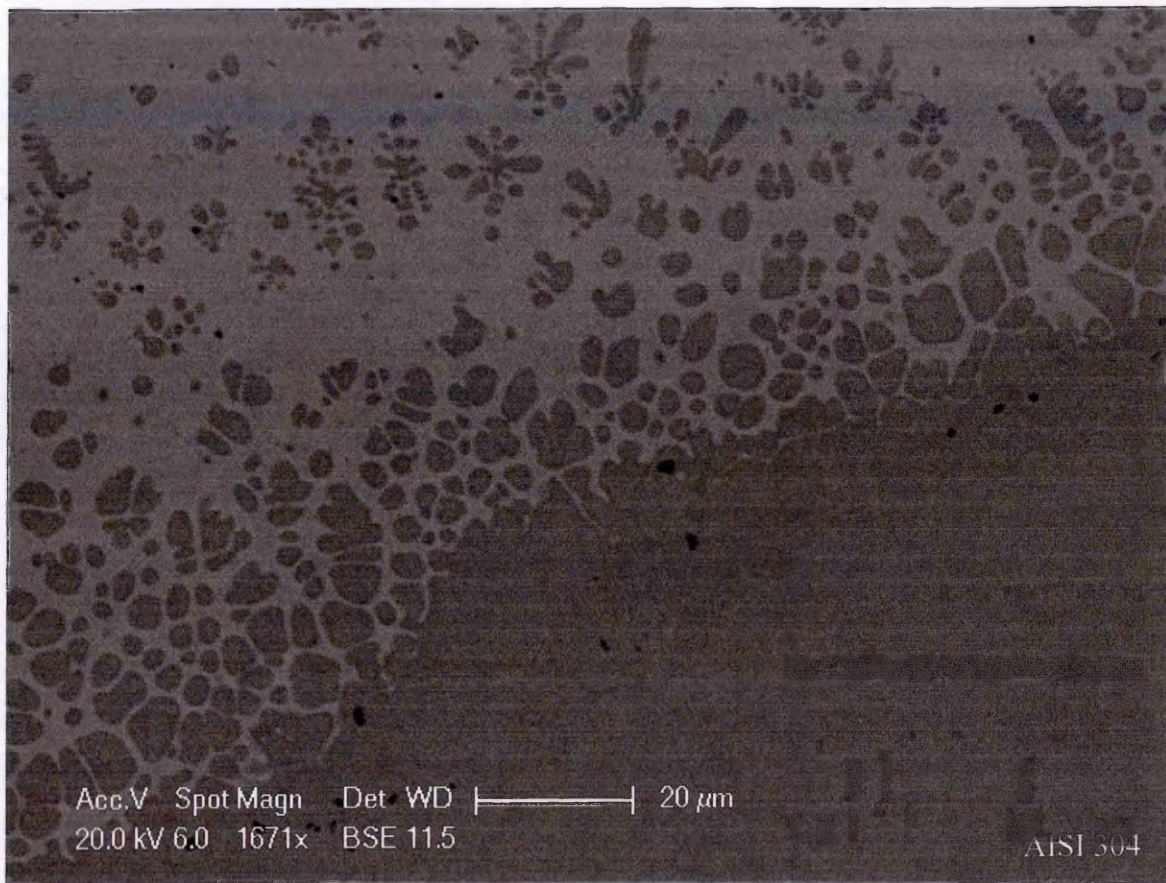


Figure 4.55 - Interface of stainless steel and braze in a dissimilar parent material butt joint manufactured from AISI 304 and Dogal 260RP-x parent materials, BS:2901 C28 filler material and argon containing 1% oxygen shielding gas.

4.9 Summary of Results

Chapter 4 details the results of this investigation including a measure of the tensile strength and maximum extension of arc brazed joints using the same methodology as that by Wong in the previous unpublished work. This demonstrated that Wong's results⁴ were repeatable.

Optical and scanning electron micrographs were used to characterise the microstructure of an arc brazed butt joint with high and low joint efficiency. In the microstructures of arc brazed butt joints with a low joint efficiency the constituent elements from the braze and the parent material remained mostly separated, although in some microstructures copper could be seen penetrating the grain boundaries of the parent material resulting in embrittlement.

In the microstructures of the arc brazed butt joints with high joint efficiency cellular dendritic structures of iron, from the parent material, could be seen within the braze matrix. Volume fraction analysis demonstrated a correlation between the volume fraction of the cellular dendritic structures and the tensile strength of the arc brazed butt joints, although the microstructures of only three joints were examined. This was because the only method of manufacturing arc brazed joints with different volume fractions of the cellular dendritic structures was to change the composition of the shielding gas. The results of the immersion and melt trials showed that iron could be present within the braze material by diffusion below the melting point of the parent material and by melting AISI grade 304 stainless steel in the filler material. Whilst it was possible to regulate the temperature in the immersion and melt trials there was no way of simulating any effects of the arc forces. As with the joints with low joint

efficiency copper was seen penetrating the grain boundaries of the parent material, close to the interface of the braze and the stainless steel, forming an intermetallic region. Although by contrast the intermetallic region appeared to strengthen the joints rather than embrittle them.

The following process parameters for both similar and dissimilar material joining have been optimised

- Torch height
- Torch angle
- Velocity
- Root gap
- Material transfer method
- Current
- Voltage

Combinations of three braze materials and three shielding gases have been tested for both similar and dissimilar butt joints. The combination of BS:2901 C28 filler material and argon containing 1% oxygen was found to give the optimum mechanical properties in terms of ultimate tensile strength and percentage elongation and for similar material arc brazed plug joints, impact strength.

The tensile properties of similar metal arc brazed lap joints and their microstructures are described, including issues encountered with the wetting of the top and bottom plates of arc brazed butt joints.

The fatigue strengths determined by the staircase fatigue test for both similar and dissimilar material butt joints brazed using BS:2901 C28 filler material and argon containing 1% oxygen shielding gas are presented.

Finally in samples where penetration, on the parent material side of the joint interface, of copper is suspected measurements of the groove opening angle have been taken to attempt to understand the grain boundary penetration mechanism. However, assumptions of chemical compositions have had to be made and the accuracy of the groove opening angle measurement was difficult to gauge. Chapter 5 will discuss these results in more detail and consider the reasons behind them.

5.0 Discussion of Results

5.1 Parent Material Characterisation

All of the as received tensile tested samples deformed plastically prior to failure with a minimum percentage elongation of 45%. Whilst the 0.2% proof stress was found to be in reasonable agreement with the supplier's specified figures³⁶, the average values for tensile strengths were found to be significantly higher for both grades of stainless steel. There are two possible reasons for this, firstly the supplier generally gives conservative estimates and this may be an explanation for the higher values obtained. Secondly, the samples were deformed during the cutting process and were straightened prior to testing, this cold working may have work hardened the material. This cutting process induced deformation was overcome in later testing by using thinner material and using other cutting methods such as laser cutting, water jet cutting and CNC machining.

Whilst the microstructures of the parent materials were not studied in this investigation, the chemical compositions of AISI grades 304 and 316 stainless steels, taken from table 3.1, can be plotted on the Shaeffler Diagram to determine the expected microstructures.

AISI Grade 316 Stainless Steel

$$\text{Nickel Equivalent} = 10.1 + (30 \times 0.04) + (0.5 \times 0) = 11.3$$

$$\text{Chromim Equivalent} = 17.2 + 2.1 + (1.5 \times 0) + (0.5 \times 0) = 19.3$$

Plotting the figures for the nickel and chromium equivalents on figure 5.1 shows the expected microstructure for AISI grade 316 stainless steel.

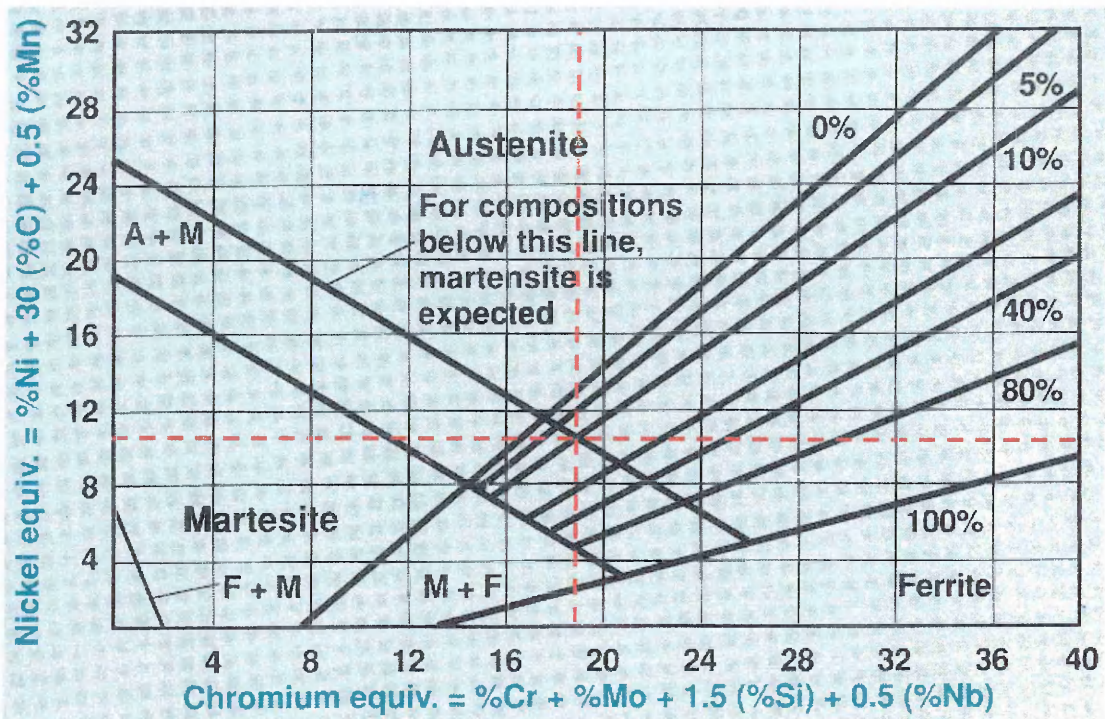


Figure 5.1 - Schaeffler Delong Diagram⁸ showing the expected microstructure for AISI grade 316 stainless steel.

AISI Grade 304 Stainless Steel

$$\text{Nickel Equivalent} = 8.1 + (30 \times 0.04) + (0.5 \times 0) = 9.3$$

$$\text{Chromium Equivalent} = 18.1 + 0 + (1.5 \times 0) + (0.5 \times 0) = 18.1$$

These figures are plotted on figure 5.2 to show the expected microstructure for AISI grade 304 stainless steel.

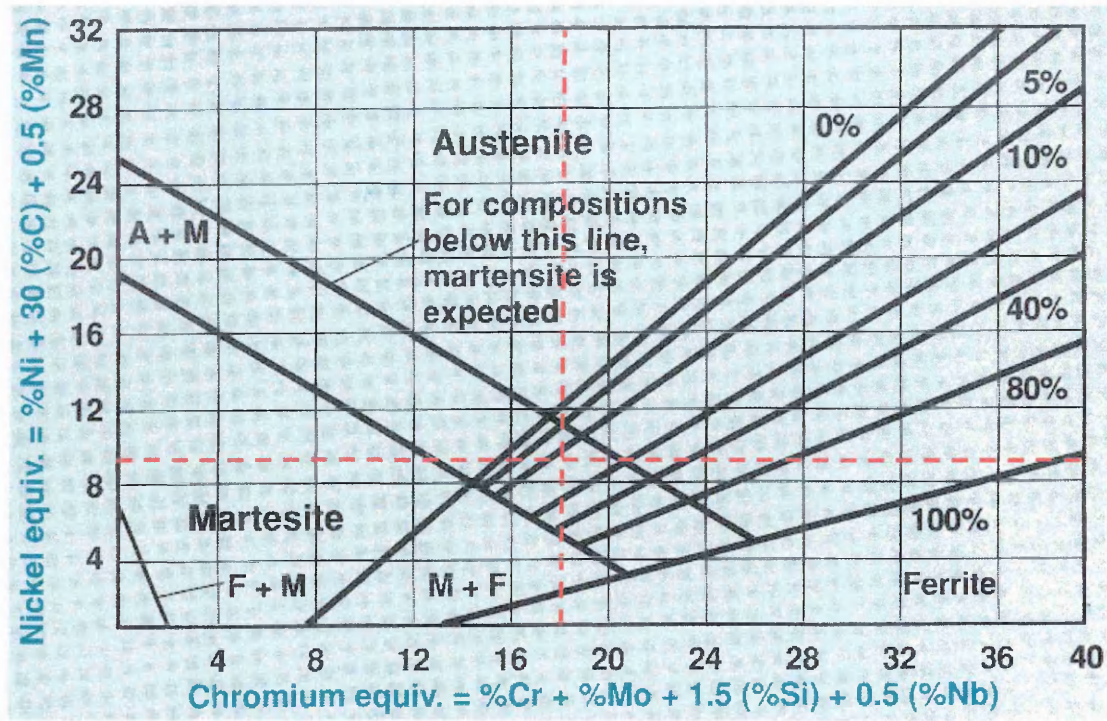


Figure 5.2 - Schaeffler Delong Diagram⁸ showing the expected microstructure for AISI grade 304 stainless steel.

Based on chemical compositions stated in table 3.1, it can be seen from figures 5.1 and 5.2 neither AISI grades 304 or 316 are fully austenitic. From figure 5.1 it can be seen that the microstructure of AISI grade 316 is made up from austenite and 5% ferrite. The presence of the ferrite is due to the high concentrations of chromium and molybdenum, which as well as aiding the passivity of the stainless steel⁶², stabilise the ferritic phase as can be seen from the chromium equivalent equation.

In figure 5.2 it can be seen that AISI grade 304 stainless steel is made up of either austenite and approximately 10% ferrite. The 18% chromium content considerably increases the gamma loop¹² of the stainless steel however, a minimum nickel equivalent of approximately 12% is still required to produce fully austenitic microstructure¹².

ARC BRAZING OF STAINLESS STEELS TO SIMILAR AND DISSIMILAR METALS Discussion of Results

5.2 Initial Mechanical Testing of Similar Metal Arc Brazed Butt Joints

5.2.1 Arc Brazed AISI 304 Grade Similar Metal Butt Joints Using BS:2901 C9 and BS:2901 C28 Filler Materials and Pure Argon and Argon Containing 2% Oxygen Shielding Gases

Following the results from the initial tensile testing, it was established that regardless of parent material used, all samples brazed using BS:2901 C9 filler material and pure argon shielding gas failed in a brittle manner with no evidence of plastic deformation. These results are marginally at odds with the unpublished work by Wong⁴ where it was reported that some samples made from the 304 grade and brazed using BS:2901 C9 and a pure argon shielding gas deformed plastically during tensile testing. However closer examination of the results revealed the average elongation to be 1.84% suggesting that these samples were actually failing in a brittle fashion and possibly suffered from LME.

The effect of adding oxygen to the shielding gas is striking. The results from this investigation showed that the test pieces brazed using BS:2901 C28 filler material and argon containing 2% oxygen shielding gas produced the strongest joint, followed by the combination of BS:2901 C9 and 2% oxygen. These combinations were both stronger and more ductile than the joints manufactured using either filler material and pure argon as the shielding gas. The trend of these results was the same as those found in the investigation conducted by Wong⁴ which showed increased values of tensile strength for either filler material with the addition of oxygen in the shielding

gas. When comparing the two braze alloys BS:2901 C28 was stronger and more ductile, in the as brazed condition. This was to be expected as in table 2.2 it can be seen that the tensile strength of BS:2901 C28 is higher than that of BS:2901 C9.

5.2.2 Arc Brazed AISI 316 Grade Similar Metal Butt Joints Using BS:2901 C9 and BS:2901 C28 Filler Materials and Pure Argon and Argon Containing 2% Oxygen Shielding Gases

As with the 304 grade parent material, the elongation and tensile strength followed the same trend as the unpublished work by Wong⁴ with BS:2901 C28 filler material being the stronger and more ductile of the two filler materials and the addition of oxygen to the shielding gas improving the results for both consumables.

The manufacturers of the filler material quote the tensile strength of the BS:2901 C9 filler material to be 350Nmm^{-2} , whereas the BS:2901 C28 filler material has a tensile strength of 430Nmm^{-2} ⁴⁵. As all joints tested failed in the filler material, it is unsurprising that the joints manufactured using BS:2901 C28 demonstrated a higher ultimate tensile strength.

5.2.3 Microstructural Characterisation of an Arc Brazed Joint with High Joint Efficiency

Once combinations of filler material and shielding gas which produced arc brazed butt joints with high and low joint efficiencies were established it was possible to characterise their microstructures in an attempt to identify what microstructural characteristics contributed to a given joints mechanical properties.

From figures 4.5 and 4.7 it can be seen that, as expected there is a distinct difference between the microstructure of an arc brazed joint with high joint efficiency compared to one with low joint efficiency. Both the images show structures within the braze material. However, in the image of the arc braze with high joint efficiency there is a dramatically higher volume fraction of these structures. The x-ray maps in figure 4.6 show that in an arc braze with low joint efficiency there is a definite separation of iron, chromium and nickel from the stainless steel and the copper from the braze. However there does appear to be a small amount of iron and chromium within the braze material, which suggests that the parent material was either melted during the process or elements of the parent material diffused into the braze alloy. Figure 4.8 shows a much larger amount of iron, in a cellular dendritic structure, is present in the microstructure of an arc braze with high joint efficiency, which suggests that this cellular dendritic structure is responsible in some degree for the increased strength of the joint. Again, in figure 4.8 it can be seen that this cellular dendritic structure appears to be produced at the interface of the parent material and the braze alloy before it migrates to the centre of the braze. The evolution of the arc braze microstructure will be discussed in sections 5.2.3.1 and 5.2.3.2.

Figures 4.9 - 4.12 show the interface of the braze and parent material. In both low magnification images (figure 4.9, BS:2901 C9 filler material and pure argon shielding gas and 4.11, BS:2901 C28 filler material and argon containing 2% oxygen shielding gas) there appears to be an intermetallic region. When a high magnification image was taken of the sample with the lowest joint efficiency (BS:2901 C9 filler material and pure argon shielding gas (figure 4.10)), it can be seen that this region appears to be the microstructure of the parent material, although as this is only apparent at the interface and not throughout the parent material this cannot be the case. The most likely reason why the interface etches more readily than the bulk of the parent material is due to a depletion of chromium in this region. It is possible that sensitisation of the stainless steel has occurred with chromium forming chromium carbides at the grain boundaries. However carbide precipitation is a two part process of nucleation and growth. At high temperatures the growth of carbides is fast but nucleation is slow, and at low temperatures nucleation is fast but growth is slow. The melting point of the filler material is approximately 1000°C and it is therefore reasonable to assume that the etched area was formed at this temperature. The optimum temperature for carbide precipitation is approximately 660°C, so it is unlikely that sensitisation is responsible for the depletion of chromium in this region. A more feasible explanation is that the chromium has migrated into the braze. This is supported by the immersion trials detailed in section 3.3.1. During this trial a strip of AISI grade 304 stainless steel was immersed in a copper alloy at 1100°C for 5 seconds. The x-ray maps from this trial (figure 4.13ii) clearly show chromium present at the grain boundaries of the stainless steel. It is therefore concluded that the depletion of chromium from the parent material is due to migration of the chromium into the braze.

Arc Brazing of Stainless Steels to Similar and Dissimilar Metals Discussion of Results

In the high magnification image of the joint manufactured using the BS:2901 C28 filler material and argon containing 2% oxygen shielding gas (figure 4.12) it can be seen that a region exists where the copper braze alloy has penetrated the grain boundaries of the stainless steel. If the copper were to penetrate in a direction perpendicular to an applied load it could be expected that ductility would be drastically reduced as a result of LME. However the tensile results showed that this was not the case for the joints arc brazed with the BS:2901 C28 filler material and argon containing 2% oxygen shielding gas. The most likely reason for this was that the load was supported by the copper between the grain boundaries parallel to the direction of the applied load in a similar way to the fibres in a composite. However, in a composite the fibres are normally much stronger than the matrix, in this situation the copper is not as strong as the stainless steel which explains why the joints have a joint efficiency of less than 1.

To determine the mechanism by which the iron and chromium were distributed within the braze material the immersion tests and melt tests detailed in sections 3.3.1 and 3.3.2 respectively were conducted.

5.2.3.1 Immersion of AISI 304 Stainless Steel into BS:2901 C9 Braze Alloy

Figure 4.13ii shows that iron and chromium are present within the solidified copper alloy and that the silicon from the braze alloy has migrated to the grain boundaries of the copper. Further examination of the specimen showed traces of iron as deep as 250 μ m into the copper alloy.

Due to the test being conducted at 1100°C, significantly below the melting point of AISI grade 304 stainless steel, the presence of these elements cannot be attributed the melting of the parent material. The x-ray maps show that the iron and chromium appear to be penetrating the grain boundaries of the copper alloy. It is therefore likely that the elements were dissolved within the molten copper. Upon cooling the silicon from the braze and the chromium and iron from the parent material solidified at the grain boundaries of the copper. Although it was shown that dissolution of iron and chromium was occurring it was believed that the cellular dendritic structures were formed in the braze microstructure due to localised melting of the parent material as discussed in section 5.2.3.2.

5.2.3.2 Experimental Melting of Stainless Steel into BS:2901 C28 Braze Alloy

This experiment took place at 1600°C, above the melting point of AISI 304 grade stainless steel and appears to produce a similar microstructure to that seen in the arc brazed joints, with cellular dendritic structures within the microstructure of the braze alloy, as shown in figures 4.7 and 4.14.

In their paper “Growth Mechanisms of Interfacial Compounds in Arc Brazed Galvanised Steel Joints With $\text{Cu}_{97}\text{Si}_3$ Filler”³⁸ Li et al proposed that the structures present within the matrix of an arc brazed joint were produced by the iron from the mild steel being diffused into the braze. However, during the melt trial, in this investigation, the differing melting points of the 10% AISI grade 304 stainless steel and the 90% BS:2901 C9 had the following effect. As the temperature dropped below 1536°C (the melting point of iron)⁷ the iron started to solidify within the still molten

arc brazing of stainless steels to stainless steels

copper. The non-equilibrium cooling caused the iron to form spherical and cellular dendritic structures as seen in figures 4.7 and 4.14. Whilst some diffusion of the iron and chromium may have occurred following the solidification of the spherical and cellular dendritic structures, prior to the solidification of the braze alloy it is concluded that the predominant mechanism in the evolution of an arc brazed microstructure is melting of the parent material at the interface with the filler material, the main elements of the parent material are then distributed throughout the molten braze until they re-solidify. Despite this, the process still meets the criteria for brazing as follows:

- The composition of the filler material is significantly different from that of the parent material²⁶.
- The strength of the filler material is significantly less than that of the parent material²⁶.
- The melting point of the filler material is lower than that of the parent material²⁶.
- The melting of the parent material is highly localised and the elements of the parent and filler material remain separate upon cooling.

To summarise the arc brazing process results in localised melting of the parent material. As well as localised melting of the interface copper from the braze penetrates the grain boundaries of the parent material as shown in figure 4.12, forming a three dimensional network. It is proposed that the copper in this network acts in the same way as the fibres in a composite material supporting any load applied parallel to the direction of the fibres. As the copper penetrates in all directions producing a three dimensional network any load applied must be in a direction

parallel to that of at least one copper “fibre” and therefore failure can only occur if the applied force is greater than the tensile strength of the solidified braze material.

5.2.3.3 Volume Fraction Analysis of Cellular Dendritic Structure

Figure 4.15 suggests that the samples which exhibited the highest tensile strength contained the highest volume fraction of the iron and chromium rich second phase particles in the braze microstructure. This was also one of the finds of Li et al in their investigation “Interfacial structure and joint strengthening in arc brazed galvanized steels with copper based filler”³⁹.

Upon initial inspection it could be seen that the microstructural features took on two forms, spherical and dendritic as shown in figure 5.3. Whilst it was believed that the dendritic structure was produced by the non-equilibrium cooling rate, it was not clear whether the spherical structures were of the same composition or were porosity. If these structures were caused by porosity it would invalidate the results as it was not possible for the image analysis software to distinguish between these and the cellular dendritic structures. Following optical analysis, shown in figure 5.4, these spherical features appeared to be of the same phase as the cellular dendritic structures, but Transmission Electron Microscopy would need to be conducted to confirm this. If the spherical features and the cellular dendritic structures are found to be the same phase then the results presented in figure 4.15 are supported showing that the volume fraction of iron and chromium second phase structures in the matrix of an arc brazed joint is proportional to the strength of that joint.

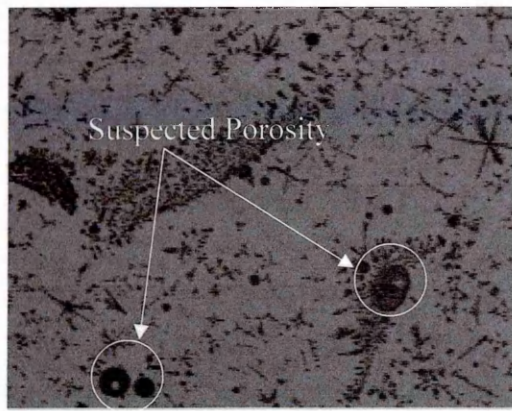


Figure 5.3 – Backscattered electron volume fraction image (at magnification x1000) showing suspected porosity in a braze microstructure manufactured using BS:2901 C28 filler material and argon containing 1% oxygen shielding gas.

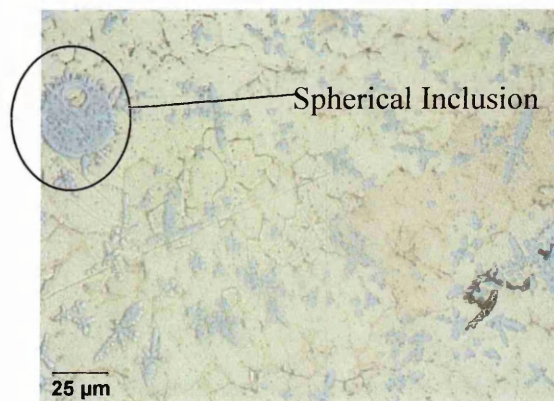


Figure 5.4 – Optical image of spherical inclusion within the braze microstructure of a joint manufactured using BS:2901 C28 filler material and argon containing 1% oxygen shielding gas.

5.3 Determination of Arc Brazing Process Variables

The joints manufactured in the initial trials were brazed manually and the variables adjusted by a process of trial and error until a satisfactory joint was produced. In order for the process to be used in the motor industry, it must be reproducible and automated. To achieve this the process variables for both similar and dissimilar metal joining had to be optimised.

5.3.1 AISI 304 Similar Metal Butt Joints

5.3.1.1 The Affect of Torch Height on the Arc Brazing Process

The torch should be positioned 15mm from the work piece for similar metal butt joints. Above this height excessive levels of spatter are experienced. This is problematic for the motor industry because it will necessitate cleaning of the joint after brazing. Due to the high production volumes in the motor industry this cleaning may lead to the process being too time consuming to be economically viable. If the torch is too close to the work piece the heat transfer efficiency is increased, resulting in increased distortion of the parent material. This distortion may be overcome if the parent material is restrained as would be the case in a car body, however this will result in an increase in the residual stress in the material.

Another problem with positioning the torch too close to the parent material is electrode stubbing. This occurs because the current and the wire feed are linked. For the similar metal butt joints the current was set so it was impossible to achieve spray transfer, and if the torch was too close to the work piece there may have been

insufficient time for the arc to re-initiate before the wire feed caused the electrode to contact the work piece again.

The gas flow can also be affected by the position of the torch. Spatter is an associated problem with short circuit transfer and if the torch is too close to the work piece spatter may solidify inside the nozzle disrupting the gas flow. Also by positioning the torch far from the specimen the gas may not be able to cover the joint effectively and therefore not protect it from atmospheric contamination.

5.3.1.2 Effect of the Changes in the Composition of the Shielding Gas

During the initial trials (detailed in section 3.2) it was noted that the addition of oxygen to argon had a positive effect on the mechanical properties of the joint. To examine this further, a range of gas mixtures were then tested to determine the optimum shielding gas in terms of aesthetic appearance, pass velocity and mechanical properties of arc brazed joints for similar metal butt joints.

Three different gas mixtures were tested, pure argon, argon containing 1% oxygen and argon containing 2% oxygen. Trials showed that, for similar metal butt joints, using argon with 1% oxygen allowed the fastest pass velocity, followed by pure argon, whilst argon with 2% oxygen required the most time to braze an equivalent length. The fastest pass velocity which does not compromise mechanical or aesthetic properties of the joint would be required in the automotive industry in order to maximise production.

The increased oxygen content of the 1% and 2% argon /oxygen gas mixtures led to an oxide layer forming on top of the braze seam. Testing revealed that the braze seams could be ground following brazing without compromising the 0.2% proof stress of the joints. This grinding procedure ensured that the braze was flush with the parent material and completely removed the oxide layer. However, as mentioned in section 5.3.1.1 due to the time involved any post braze cleaning of the joint may result in the process being economically prohibitive for the motor industry. If grinding of the joint is to be used care must be taken not to produce stress concentrations in the form of notches on the surface of the parent material as these would act as initiation sites for both fatigue and tensile failures.

Despite the potential benefits, it was decided not to test helium in comparison to argon as a shielding gas. The main reason for this was the cost of helium gas in Europe. Helium has a density approximately 0.14 times that of air^{29, 42} and as a result does not cover the braze in the same way as a denser gas such as argon, requiring higher flow rates to maintain equivalent protection. It was due to these reasons that helium was thought to make the process prohibitively expensive for its intended application in the automotive industry.

5.3.1.3 The Effect of Butt Joint Root Gap on Mechanical and Aesthetic Properties of Similar Metal Butt Joints

5.3.1.3.1 The Effect of Increasing Butt Joint Root Gap on Aesthetic Appearance of Similar Metal Butt Joints

In figure 4.16ii no braze material can be seen penetrating to the rear of the joint as a result of positioning the faying surfaces too closely together. Although the braze seam reinforcement (figure 4.16i) has an appropriate appearance the rapid heating and cooling cycle of the arc brazing process has resulted in increased distortion of the stainless steel, and a lack of penetration. This can be seen by comparing figure 4.16ii with figure 4.17ii. In contrast, if the faying surfaces are positioned too far apart then lack of fill occurs, as can be clearly seen in figures 4.18i and 4.18ii.

When considering welding, an empirical rule is to leave a gap between the faying surfaces of approximately the size of the electrode being used for the root run. This relationship does not work when considering arc brazing because the parent material will not be melted to the same extent. It was found that using a 0.8mm electrode the parent material in all joints produced with a braze gap between 0.1mm and 0.3mm resulted in overlapping of the plates and insufficient penetration of the joint. It was also found that the largest gap that could be bridged without holes appearing in the braze seam was 0.6mm. Therefore, in purely aesthetic terms, the optimum root gap between the faying surfaces was found to be 0.4mm - 0.6mm.

5.3.1.3.2 The Effect of Increasing Butt Joint Root Gap on Tensile Properties of Similar Metal Butt Joints

Figures 4.19 and 4.23 show that the highest tensile strengths were achieved from joints brazed with a 0.5mm root gap prior to brazing, with the exception of BS:2901 C28 filler material and pure argon shielding gas as all joints manufactured with this combination of filler material and shielding gas showed evidence of LME, as shown in figure 4.29, and as a result displayed the lowest results for tensile strength and percentage elongation for all the combinations of filler material and shielding gas tested.

The filler material seen within the parent material in figure 4.29 is only penetrating in a direction parallel to the braze, this is due to the residual stresses within the parent material, generated by the arc brazing process in the same way as those in a weld. As stated in section 2.3.1, when the weld pool, or arc braze seam solidifies it contracts generating a tensile residual stress in the surrounding material, this is then balanced by a residual compressive stress in the bulk of the parent material¹³. This residual tensile stress pulls open the parent material grain boundaries making it easier for the filler material to penetrate them. Therefore the lines of filler material seen in figure 4.29 identify the locations of the tensile residual stresses within the parent material, caused by the solidification and contraction of the braze seam.

In figure 4.12 again the filler material is seen penetrating the parent material but in this case the penetration is in all directions forming a “composite” type structure, where the copper is acting as the fibres. As the filler material is penetrating the parent material in all directions it is able to support any load applied, up to the tensile

strength of the filler material, as one of the “fibres” will be in the same direction as the applied load. By contrast in figure 4.29, the filler material is only penetrating the stainless steel in a direction parallel to the braze seam. When a force is applied at 90° to the braze, as is the case in the tensile testing, there is nothing to support the load and failure occurs at a lower load than would otherwise be expected.

LME was also seen in the microstructures of four of the samples manufactured from BS:2901 C9 filler material, argon containing 2% oxygen shielding gas and a 0.5mm root gap. The combinations of BS:2901 C28 filler material and argon containing 2% oxygen and BS:2901 C9 filler material and pure argon shielding gas did not appear to suffer from LME and as a result displayed higher joint efficiencies. The combination of BS:2901 C28 filler material and pure argon shielding gas displayed a significantly smaller range of results than the joints brazed using the BS:2901 C9 filler material and argon containing 2% oxygen shielding gas, although this was due to all the BS:2901 C28 testpieces failing in a brittle manner at a strength well below that in table 2.2.

The selection criteria for the project has focused on 0.2% proof stress as a percentage of this is the design criteria used within the automotive industry. As can be seen from figures 4.20, 4.24 and 4.26 the highest values of 0.2% proof stress were obtained for the joints manufactured with a 0.5mm gap between. No proof stress results were obtained for BS:2901 C28 filler material and pure argon shielding gas as these samples were severely embrittled resulting in none of these samples deforming plastically prior to failure.

Figure 4.27 shows that all the ultimate tensile strengths for joints manufactured with a 0.5mm root gap between the faying surfaces was less than that of the parent material with BS:2901 C28 filler material benefiting from the addition of 2% oxygen in the shielding gas. However, an adverse effect was caused when the BS:2901 C9 filler metal was used to braze joints with argon containing 2% oxygen shielding gas. Figure 4.28 shows that all the samples which deformed plastically prior to failure with 0.5mm gap between the faying surfaces had comparable 0.2% proof stress results and all were in excess of the AISI grade 304 parent material and therefore the optimum root gap for butt joints in terms of both aesthetic appearance and tensile properties for similar metal butt joints is 0.5mm.

5.3.1.4 Selection of Shielding Gas and Filler Material Similar Metal Butt Joints with a Root Gap of 0.5mm

It can be seen from figure 4.30 that the average proof stresses for all combinations of filler material and shielding gas were extremely similar with a range of 14MPa in the averaged results. It is also seen that all samples yield above the values quoted in table 2.1 by the steel manufacturer and those found experimentally, it was therefore concluded that the testpieces started to yield in the parent material. As it was not possible to differentiate between samples based on their 0.2% proof stress the average tensile strengths and extensions to failure were examined to see if there were any noticeable differences, which could be attributed to either the shielding gas composition, the chemical composition of the filler material or a combination of both.

Figures 4.31 and 4.32 show the results for tensile strengths and extensions to failure. It can be seen that the addition of oxygen to the shielding gas benefits all filler

materials tested in terms of joint ductility, suggesting that Cu_2O was not formed in any of the brazes produced³³. It can also be seen that the highest tensile strength and elongation was found in the joints manufactured using BS:2901 C28 filler material and argon containing 1% oxygen shielding gas.

Whilst all the filler materials are quoted to have a similar melting point by the manufacturer, the BS:2901 C28 material has an ultimate tensile strength of 430Nmm^{-2} , whereas the BS:2901 C9 materials strength is quoted by the manufacturer as 350Nmm^{-2} and the BS:2901 C11 material as 260Nmm^{-2} . This results in the increased strength of the joints brazed with the BS:2901 C28 material. Although the values of tensile strength for BS:2901 C9 and BS:2901 C11 were comparable, the low values of percentage elongation obtained for the joints manufactured using the BS:2901 C11 filler material resulted in no further investigation of this filler material, except as a comparison for impact properties.

Both the BS:2901 C9 and BS:2901 C28 filler materials benefited from the addition of 1% oxygen in the shielding gas in terms of both mechanical properties and pass velocity. The addition of the active gas increased the thermal conductivity of the shielding gas, reducing the viscosity and improving the wetting of the joint. However, the addition of 2% oxygen to the shielding gas had a negative effect on mechanical properties and the pass velocity when compared with 1% oxygen. The most likely reason for this is that the increased oxygen caused oxides to form on the surface of the parent material, reducing wetting and therefore mechanical properties and pass velocity.

5.3.2 Dissimilar Metal Butt Joints – AISI 304 Stainless Steel to Dogal 260 RP-x Zinc Coated Mild Steel

5.3.2.1 The Affect of Process Variables on the Arc Brazing Process

5.3.2.1.1 The Effect of Torch Angle and Height on the Wetting and Aesthetic Properties of Dissimilar Material Arc Brazed Butt Joints

During the initial trials a torch angle of 90° was used to produce arc brazed dissimilar metal joints. However, this proved to be unsatisfactory because the zinc vapour caused the arc to be too unstable leading to spatter and incomplete wetting of joint. It was therefore found to be necessary to introduce a leading angle of 5° from vertical to the GMAB torch (see figure 4.45). This allowed the zinc vapour to be removed from the area around the solidifying braze alloy by the pressure exerted by the shielding gas, making it easier to maintain a stable arc, minimise spatter and ensure complete wetting of the joint. A vertical torch height of 12.75mm was found to be the optimum in order to reduce the adverse effects detailed in section 5.3.1.1 as far as possible.

5.3.2.1.2 Optimisation of Root Gap for Dissimilar Metal Butt Joints

Following from the results in section 4.3.1.4 a dissimilar butt joint with a 0.5mm gap was manufactured. However, as can be seen in figure 4.46 the braze reinforcement was not uniform and therefore unacceptable to the motor industry where aesthetic appearance is crucial. In contrast figure 4.47 shows that a butt joint manufactured

using a 0.6mm gap produces a uniform braze seam. As with the similar metal butt joints it was not possible to bridge a root gap of more than 0.6mm as at larger root gaps the braze alloy fell through the gap producing holes in the seam.

5.3.2.1.3 Optimisation of Torch Velocity for Dissimilar Metal Butt Joints

Once the root gap had been established at a torch velocity of $63.5\text{cm}\cdot\text{min}^{-1}$ the pass velocity was increased in order to reduce the profile of the braze seam whilst ensuring penetration throughout the joint. Figures 4.48i and 4.48ii show that with a torch velocity of $88.9\text{cm}\cdot\text{min}^{-1}$, at an angle of 5° from vertical, a uniform braze seam is produced with penetration throughout the joint. For increased pass velocities there was insufficient material deposited to produce a uniform braze seam, resulting in the appearance of the braze reinforcement to be adversely affected as shown in figure 4.49i.

5.3.2.1.4 Optimisation of Arc Variables for Dissimilar Metal Butt Joints

At first it was attempted to manufacture butt joints from dissimilar parent materials using the same arc variables as those used for the joints manufactured from similar parent materials. However, the instability of the arc associated with short circuit metal transfer was made worse by the zinc vapour leading to unsatisfactory wetting of the joint. During spray arc transfer the arc is not constantly being short circuited and reinitiated and it is therefore easier to maintain a stable arc. For this reason the arc variables were changed to those stated in Appendix 1 to achieve spray arc transfer.

5.3.2.1.5 Selection of Filler Material for Dissimilar Metal Joints

Tensile Specimens

When tensile testing the machined dogbones, manufactured using BS:2901 C28 filler material and BS:2901 C9 filler materials and argon containing 1% oxygen shielding gas, it was noted that all the test pieces manufactured using BS:2901 C28 filler material and argon containing 1% oxygen shielding gas failed within the mild steel, giving a joint efficiency of 1. However 3 of the 5 samples manufactured using BS:2901 C9 filler material and argon containing 1% oxygen shielding gas failed in the braze alloy meaning that the strength of the alloy was less than that of the mild steel. This followed the results seen in the investigation into similar metal butt joints where BS:2901 C28 filler material was found to produce stronger joints than those manufactured using BS:2901 C9. For this reason it was decided to manufacture all future samples using BS:2901 C28 filler material and argon containing 1% oxygen shielding gas, with a 0.6mm root gap and spray arc transfer.

5.3.2.1.6 Tensile Properties of Dissimilar Metal Joints

All dissimilar metal joint samples brazed with BS:2901 C28 filler material and argon containing 1% oxygen shielding gas failed in the mild steel giving a joint efficiency of 1. The values for the tensile strength (as shown in table 4.10) fall within the limits quoted for the mild steel³⁷. When examining the load extension graphs it was noted that there was no clearly defined yield point, this would be expected if the joints yielded in the face centred cubic stainless steel. When calculating the 0.2% proof stress based on the cross sectional area of the mild steel it was also seen that the

figures were significantly below those quoted³⁷. However, when these were recalculated based on the cross sectional area of the thinner stainless steel (detailed in table 4.10) it could be seen that the values were comparable for those calculated experimentally. It is therefore concluded that the samples yielded in the stainless steel leading to work hardening before failing in the mild steel, meaning the arc brazed joint was stronger than the weakest parent material.

BS:2901 C28 filler material is quoted by the manufacturer as having a tensile strength of 430MPa⁴⁵, the strength of BS:2901 C9 braze alloy is quoted as 350 MPa⁴⁵ and a strength of 380 – 460 MPa³⁷ is quoted for the mild steel. As a result of the tensile properties of the filler materials the arc brazes joined using the BS:2901 C28 filler material displayed an ultimate tensile strength in excess of both the BS:2901 C9 filler material and the mild steel.

5.4 Effect of Braze Seam Geometry on the Tensile Properties of Similar Metal Butt Joints

During the tensile testing stage of the investigation into the affect of the root gap on similar parent material joints, it was noted that some of the samples which had their braze seam removed by grinding failed within the ground area of the parent material. The fracture faces were examined using the SEM and it was found that the initiation site for the fracture started at a grinding notch on the surface of the material. For this reason it would be beneficial for the braze reinforcement to be left intact, providing it did not affect the aesthetic or mechanical properties of the joint.

From figures 4.33 and 4.35 it can be seen that all unground joints tested withstood higher forces prior to failure and extended further than the ground samples for all combinations of filler material and shielding gas. This is because stress is force over area therefore as the volume of braze alloy increases so does the area and the effective stress is reduced.

Figure 4.34 shows the loads at which the similar metal butt joints samples yielded. There is very little difference between the loads for the ground and unground specimens for any given combination of shielding gas and filler material as all samples appeared to yield in the stainless steel. This shows that the geometry of the braze seam does not act as a significant stress raiser during tensile testing and grinding will only be necessary if the joint is in a visible area, for cosmetic reasons.

**5.5 *Impact Testing of Similar Metal Plug Brazed Joints
Manufactured Using BS:2901 C9, BS:2901 C11 and
BS:2901 C28 Filler Materials and Pure Argon, Argon
Containing 1% Oxygen and Argon Containing 2%
Oxygen Shielding Gases***

5.5.1 *Wetting of the Parent Material*

Originally the impact test was to be conducted, by D Mallon, using 6mm diameter holes in the top sheet of the joint configuration (see figures 3.6 and 3.7), as this was the diameter of the spot welds which had been investigated in previous work⁶¹ thus enabling a direct comparison to be made. However, it was found that with a 6mm diameter hole in the top plate the filler material would fail to wet the bottom sheet as shown in figure 4.37, therefore trials were conducted by S Magowan, with hole diameters of 3mm and 8mm to establish if wetting could be improved. Wetting was assessed in terms of macro structural investigation and lap shear testing.

For resistance spot welds there are two types of failure which can occur in lap shear testing⁵⁶:

- Weld Pull-out
- Weld Shear

Weld pull-out of mild steel RSW joints is generally considered as evidence of an acceptable weld, whereas weld shear occurs when the joint is weaker than the base

material⁵⁶. When considering impact testing of arc brazed joints the pass criteria for this investigation is presented in figures 4.38 and 4.39.

Wetting was impeded on the 3mm and 6mm holes because once the first droplet of braze alloy had been deposited it occupied a large proportion of the volume within the hole and so the arc was attracted to this material instead of the parent. As a result the passive layer on the bottom sheet of stainless steel was not removed by the arc. Once the hole was enlarged this problem was overcome because the same amount of braze alloy was deposited and so a smaller proportion of the hole was occupied by the filler material resulting in it being possible for the arc to be directed towards the parent material and remove the passive layer.

Once satisfactory wetting had been achieved (characterised by a similar failure mode in lap shear to that of a satisfactory RSW i.e. braze pull out) impact testing could be conducted. The results could then be compared to previous trials of RSW.

5.5.2 Modified Quantitative Chisel Test of Arc Brazed Plug Joints

Figure 4.40 shows the results of the impact toughness of arc brazed joints fabricated using combinations of BS:2901 C9, BS:2901 C11 and BS:2901 C28 filler materials and pure argon, argon containing 1% oxygen and argon containing 2% oxygen shielding gases, using a modified chisel test. It is evident from these results that all filler materials tested benefited from the addition of oxygen in the shielding gas. There are no results for the combination of BS:2901 C11 filler material and pure argon shielding gas because without the oxygen in the shielding gas it was difficult to

maintain a stable arc without a run-on plate and due to the method of manufacture it was not possible to produce plug brazed joints in this manner. For all filler materials tested the addition of oxygen to the shielding gas benefited the toughness with 1% oxygen producing average toughness figures higher than that of 2%. The highest mean impact strength for the plug brazed joints was found in those joints which were manufactured using BS:2901 C28 filler material and argon containing 1% oxygen shielding gas. These joints also exhibited the smallest range of all joints including the resistance spot welds, however only four samples were included in the results. At first the results for the 8mm, BS:2901 C28 filler material and argon containing 1% oxygen shielding gas plug brazed joints appeared to be comparable to those for the 6mm resistance spot welds.

Whilst impact properties are not fundamental in the same way as tensile strength, the relationship between the 6mm RSW and the 8mm arc brazed plug joints was investigated for the purposes of comparison. The same chisel attachment for the Charpy Impact Testing Machine was used for the RSW and the arc brazed plug joints resulting in the depth of the material impacted being constant, therefore the area of the joints, as opposed to the volume, was compared.

The areas of the RSW and the arc brazed plug joints were 9.42mm^2 and 12.57mm^2 respectively. The impact strength of the RSW was 44J, resulting in an impact strength per unit area of 4.67Jmm^{-2} . The combination of BS:2901 C28 filler material and argon containing 1% oxygen shielding gas produced an average impact strength of 32J, this translates to an impact strength per unit area of 2.55Jmm^{-2} , suggesting that

Arc Brazing of Stainless Steels to Similar and Dissimilar Metals
the arc brazed plug joints were significantly more brittle than the RSW tested by Wray⁶¹.

5.6 Fatigue Testing of Similar and Dissimilar Metal Arc Brazed Butt Joints

All similar material (304 to 304) butt joint fatigue test failures, failed in the braze. As stated in section 4.7.1 the mean fatigue load for butt joints manufactured from AISI grade 304 parent material BS:2901 C28 filler material and argon containing 1% oxygen shielding gas was found to be 5.72kN. The results of the staircase fatigue test on dissimilar material butt joints showed that these failed at a significantly lower load, 3.59kN. The failure location was also different with the dissimilar metal fatigue samples failing at the interface of the stainless steel and the braze.

The SEM was used to establish a reason why the similar material butt joints were able to withstand higher loads under cyclic loading than dissimilar metal joints. It can be seen in figure 4.53 that there is evidence of LME within the failed dissimilar metal fatigue sample at the interface of the braze and the stainless steel. This was not seen in the similar material joints manufactured using BS:2901 C28 filler material and argon containing 1% oxygen shielding gas.

Once it had been established that LME was present in the dissimilar material joints (and therefore a possible reason why the mean fatigue strength was less than that for the similar parent materials) it was necessary to determine a reason why no evidence of LME was found in those samples manufactured using AISI 304 stainless steel parent material and BS:2901 C28 filler material and argon containing 1% oxygen shielding gas. As stated in section 5.3.2 the arc variables had to be changed to attain spray arc, in the dissimilar metal joints, by increasing the voltage and the current.

Also, to ensure complete wetting of the joint and a satisfactory appearance the pass velocity had to be decreased to $89\text{cm}\cdot\text{min}^{-1}$. If the average values for current and voltage and the pass velocities for spray arc transfer and short circuit transfer using BS:2901 C28 filler material and argon containing 1% oxygen shielding gas are put into equation 2.1 the effect on heat input can be seen^{vi}.

Short Circuit Transfer

$$H_{net} = \frac{\eta EI}{v}$$

$$H_{net} = \frac{1 \times 15.9 \times 40}{18.75}$$

$$H_{net} = 33.92\text{J}\cdot\text{mm}^{-1}$$

Spray Arc Transfer

$$H_{net} = \frac{\eta EI}{v}$$

$$H_{net} = \frac{1 \times 63 \times 18.9}{14.58}$$

$$H_{net} = 81.67\text{J}\cdot\text{mm}^{-1}$$

It can be seen from the above equations that the heat input for the dissimilar metal joints is significantly higher than that for the similar metal joints. Unpublished work by Burgin⁴⁶ shows that there is a critical stress level and arc duration, below which embrittlement by a particular combination of filler material and shielding gas will not occur.

From the work reported in sections 4.3.1.2 and 4.6.3 it is known that spray arc transfer requires a slower pass velocity, therefore the arc duration per unit area is increased increasing the tendency to embrittle. The tendency to embrittle may also be increased if the time it takes for the copper to solidify is increased. Equation 5.1 is the estimate of solidification time equation.

^{vi} As both processes were conducted using the same welding equipment the arc efficiency (η) will be assumed to be 1.

$$S_t = \frac{LH_{net}}{2\pi k \rho c (T_m - T_o)^2}$$

Equation 5.1

- Where
- S_t = Solidification Time (s)
 - L = Heat of Fusion (1.869J.mm⁻³ for copper⁶³)
 - k = Thermal Conductivity of Material (399 W.m⁻¹.K⁻¹ for copper⁶⁴)
 - ρc = Volumetric Specific Heat (0.003 J.mm⁻³.°C⁻¹ for copper⁶⁴)
 - T_m = Melting Temperature (°C)
 - T_o = Initial Plate Temperature

Embrittlement can only occur once the stainless steel is solid but while the copper is still liquid, therefore if T_m is taken as the solidus of AISI 304 grade stainless steel and T_o is taken as the melting point of the filler material. The time taken for the copper to solidify, for both short circuit transfer and spray arc transfer, can now be calculated.

Short Circuit Transfer

$$S_t = \frac{LH_{net}}{2\pi k \rho c (T_m - T_o)^2}$$

$$S_t = \frac{1.869 \times 33.92}{2\pi \times 0.399 \times 0.003 \times 136900}$$

$$S_t = 0.054s$$

Spray Arc Transfer

$$S_t = \frac{LH_{net}}{2\pi k \rho c (T_m - T_o)^2}$$

$$S_t = \frac{1.869 \times 81.67}{2\pi \times 0.399 \times 0.003 \times 136900}$$

$$S_t = 0.129s$$

From these results it is concluded that the reason LME was found in samples manufactured using spray arc transfer, but not in the samples manufactured using

short circuit transfer, is that the slower pass velocity of the spray arc transfer process increased the arc duration per unit length of material passed the critical level as proposed in the unpublished work by Burgin⁴⁶, for BS:2901 C28 filler material and argon containing 1% oxygen shielding gas, whilst the increased solidification time meant that the molten braze had more time to penetrate the parent material.

5.7 Arc Brazed Similar Metal Lap Joints

5.7.1 Effect of Overlap on the Tensile Properties of Similar Metal Arc Brazed Lap Joints

Figure 4.41 shows that irrespective of overlap length or number of braze seams all joints yielded at a load comparable to the unground butt joints. Figure 4.43 shows that the lap joints manufactured with the single seams failed at a considerably lower ultimate tensile load than the butt joints. As expected, the lap joints manufactured with the double seams tolerated a higher load to failure than the single seams, however the load was comparable to that of butt joints which use half the filler material. No discernible difference could be seen between the 10mm and 20mm overlap lengths. This is as expected as the load to failure of a brazed joint is proportional to the cross sectional contact area which, whilst not being affected by the overlap length, is obviously higher for double seam lap joints than it is for single seam lap joints.

5.7.2 Microstructural Investigation of Wetting of the Parent Material of Arc Brazed Similar Metal Lap Joints

A microstructural investigation was undertaken to establish the reason why similar metal arc brazed butt joints were significantly stronger than similar metal arc brazed lap joints. The wetting of the parent was found to be responsible for the low joint efficiency of the arc brazed lap joints. Figure 4.43 shows the interface between the braze material and the top sheet of the lap joint with a 10mm overlap and a single braze seam. The secondary electron image shows that there has been localised

melting of the parent material as with the butt joints seen in figure 4.8. However, in figure 4.44 it can be seen that the localised melting has not occurred on the bottom plate, as there is localised melting of the parent material of both plates of the similar metal butt joints, there is a greater surface contact area than in the similar metal lap joints resulting in the butt joints tolerating a higher load prior to failure.

In order to improve the wetting of the bottom plate a further series of lap joints were manufactured to establish if the wetting of the bottom sheet and the mechanical strength could be improved by varying the torch angle used.

5.7.3 Effect of Torch Angle On The Wetting of Parent Material of Similar Metal Arc Brazed Lap Joints

When it was attempted to manufacture lap joints with varying torch angles from 45° to 80° the braze did not wet both plates. At first it was thought that the unstable arc associated with the short circuit transfer process was causing this and so the variables were changed to deposit the braze alloy using spray arc transfer, however the same results were experienced.

Previous workers have reported that it is possible to manufacture similar metal arc brazed lap joints with mild steel as the parent material. The main differences, in terms of brazing, between austenitic stainless steel and mild steel are the thermal conductivity of the materials and the presence of the passive oxide layer⁶⁵ on the surface of the stainless steel. To discover which was responsible for the lack of wetting it was attempted to manufacture a similar metal lap joint using duplex stainless steel as the parent material. This has a similar thermal conductivity to that of

The Brazing of Stainless Steels to Carbon Steel
mild steel⁶⁵. The results from this trial showed, that as with the austenitic stainless steel lap joints there was a lack of wetting of the joint.

The relative difference in torch height, in relation to the top and bottom plates (due to the joint configuration) resulted in it not being possible for the arc to remove the passive layer from both plates simultaneously. It was concluded that it was the passive layer on the surface of the stainless steel which prevented the wetting of the bottom plate of the lap joint rather than the thermal conductivity of the parent material. This is supported by figure 4.49ii where the excess braze alloy which has penetrated the depth of the joint has wet the mild steel but not the stainless steel.

5.8 *Liquid Metal Embrittlement - Mullins Grooving*

By comparing figures 4.50, 4.51, 4.53, 4.54 and 4.55 it can be seen that the interfaces appear to be very different for similar and dissimilar joints. In figure 4.50 and 4.51 a distinct band can be seen at the interface of the braze and mild steel preventing penetration of the filler into the parent material. This band is composed of iron and the elements from the filler material as seen in the spot analysis in figure 4.52. In figures 4.53 – 4.55 there is no evidence of a similar band at the interface of the stainless steel and the braze and instead a non uniform intermediate phase is present.

The grain boundaries of the intermediate phase between the parent and filler material, in figure 4.54, appear to have been enlarged by some process, whereas copper can be seen penetrating the intermediate phase and then propagating into the bulk of the parent material in figure 4.53.

In the microstructure on the AISI 304 side of the dissimilar metal butt joint in figure 4.55 there appear to be, iron grains which have solidified in the molten copper.

The enlarged grain boundaries in figure 4.54 may be due to a process referred to as grain boundary grooving, proposed by Mullins⁵⁸ where by atoms from the parent material have diffused into the molten copper, effectively enlarging the grain boundaries of the intermediate phase. Although this is not known for certain because in figure 4.54 there is no copper present, unlike in figure 4.12 where it can be seen from the x-ray maps that copper is penetrating the grain boundaries. The most likely reason for the difference in appearance is that the copper in figure 4.54 was removed during the etching process. To establish whether this was the case it was attempted to

examine an unetched sample using the SEM in backscattered electron mode. However, it was difficult to locate the grain boundaries due to the smearing caused by polishing.

To test the hypothesis that grooving of the grain boundaries was occurring in the similar material butt joints was the same as that proposed by Mullins the appropriate data was placed in equation 2.7. As the full chemistry of the intermediate phase is not known the assumption that is made that it is iron atoms which are diffusing into the molten braze and therefore the diffusion co-efficient of iron into copper and the concentration of iron in copper at equilibrium are used for the calculations. The figures used also assume the braze to be pure copper as opposed to BS:2901 C28 which is composed of copper containing 8% aluminium.

$$d = 1.01m(A't)^{\frac{1}{3}}$$

$$A' = \frac{C_o\gamma_s\Omega^2 D}{KT}$$

Equation 2.7

From the Cu - Fe phase diagram it can be seen that the concentration at equilibrium (C_o) of iron in copper is 3%⁶⁴. The surface free energy (γ_s) of AISI 304 is stated as 39.62 mJm⁻²⁶⁶. The molar volume (Ω) of copper can be calculated from its density as 7.09cm³. The diffusion coefficient (D) of iron in copper is stated as $(4.2 \pm 0.3) \times 10^{-13}$ ⁶⁷. Temperature (T) is taken as 1313K because this is 10K above the melting point of the filler material and the time (t) is taken as 0.54. These figures can be used in the Mullins Model to see if grain boundary grooving was responsible for the composite area between the stainless steel and the braze in similar metal butt joints

$$A' = \frac{0.03 \times 39.62 \times 10^{-3} \times (7.09 \times 10^{-6})^2 \times 4.2 \times 10^{-13}}{1.38 \times 10^{-23} \times 1313}$$

$$A' = 1.39 \times 10^{-6}$$

$$\therefore d = 1.01 \times (\tan 25.5) \times (1.39 \times 10^{-6} \times 0.054)^{\frac{1}{3}}$$

$$d = 2.03 \times 10^{-3} \text{ cm}$$

$$d = 20.3 \mu\text{m}$$

It can be seen that there is a discrepancy between the figure for d achieved theoretically and the average value for the depths of the grooves, $7.16 \mu\text{m}$. However the following errors are present within the work. Firstly the intermediate phase is assumed to be pure iron and the filler material is assumed to be pure copper where as in reality these are both alloys containing more than one element. Secondly the measurement of the opening angles of the grooves was made using a protractor on a backscattered electron image taken at approximately 1800x magnification.

Considering the above errors it is conceivable that the composite area between the parent material and the braze in arc brazed butt joints (as shown in figure 4.12 and figure 4.54) manufactured using AISI grade 304 parent material BS:2901 C28 filler material and argon containing 1% oxygen, and argon containing 2% oxygen shielding gases were formed as a result of grain boundary grooving as described by Mullins⁵⁸.

In the proposed mechanism for LME Glickman stated that if the entrance angle of the groove is small then it will act as a stress raiser in the same way as a crack tip⁵⁷. The dissimilar metal fatigue samples failed at the interface of the braze and the AISI 304 parent material. In figure 5.53 the filler material can be seen penetrating the

intermediate phase between the braze and the parent material to a depth of approximately 10 μ m, following this the penetrating filler material appears to narrow slightly and then change direction to one which is parallel to the braze seam in a similar manner to that seen in figure 4.29.

In conclusion the braze alloy penetrated the grain boundaries of the intermediate phase between the filler and parent materials of both similar and the dissimilar metal arc brazed butt joints. In the dissimilar metal joints the increased heat input and time to solidification allowed the filler material to penetrate slightly further into the bulk of the stainless steel, at this point grooving as proposed by Mullins ceased to be the mechanism by which the filler material was penetrating and instead was drawn into the parent material as a result of the residual tensile stress which was present in this area because of the solidification of the arc brazed seam. The end point of this penetration by the filler material produced a sharp angle which, as proposed by Glickman, acted as a stress raiser in the same way as a crack tip. However the penetration of the filler material into the grain boundaries of the intermediate phase between the braze and the parent material of the similar metal joints produced a three dimensional network, which did not penetrate into the bulk of the parent material. As a result of not propagating into the bulk of the parent material and not producing a sharp angle at the tip of the penetration embrittlement did not occur.

To summarise, when AISI 304 stainless steel is arc brazed using a copper based alloy, the filler material penetrates the grain boundaries of the intermediate phase present between the braze and the parent material, on the stainless steel side of the joint, as proposed by Mullins⁵⁸. If the filler material is contained within this intermediate

phase, embrittlement will not occur. However if the copper penetrates into the bulk of the stainless steel the propagation of filler material is no longer controlled by grain boundary grooving and will propagate in a direction normal to any residual stresses generated by the contraction of the braze seam. If the filler material at the end of the propagation forms a sharp angle at its tip, the tip will act as a stress raiser in the same way as a crack⁵⁷ and embrittle the material. Penetration of the mild steel parent material does not occur as the iron from the mild steel combine with the elements from the filler material to form a distinct band at the interface.

5.9 Summary of Discussion of Results

The tensile testing of the parent material showed results above those quoted by the supplier. However, due to the thickness of the material and the sectioning method used the testpieces required straightening prior to testing which may have lead to work hardening of the material. Also suppliers often provide conservative estimates for the mechanical properties of their products. One of these reasons or a combination of both may have resulted in the observed discrepancies.

Whilst the microstructure of the stainless steel parent materials was not investigated the chemical compositions have been plotted on the Shaeffler diagram. This has shown that neither AISI grades 316 or 304 are fully austenitic. The figures used for this were from the supplier's literature and not from the mill certificates for the material and any variation in the nickel, chromium, molybdenum or carbon content, along with trace elements of silicon, niobium or manganese will have an effect on the observed microstructure.

The microstructure of the brazed joints showed that the constituent elements of the arc brazed butt joints with low joint efficiency tended to remain within the braze or the stainless steel where as the in the joints with high joint efficiency there was a mixing of the elements with cellular dendritic structures of iron being present within the braze. Immersion and melt tests conducted demonstrated that solid iron and chromium could dissolve into the braze material, but when AISI grade 304 was melted in BS:2901 C28 braze alloy and then rapidly cooled a similar microstructure to that seen in the arc brazed butt joints with high joint efficiency was observed.

As well as migration of iron into the braze alloy, copper was seen penetrating the grain boundaries of the intermediate phase at the interface with the stainless steel parent material in the arc brazed butt joints with high joint efficiency. The reason for these joints not embrittling following contact with liquid copper is that the copper penetrated in all directions forming a "composite" type structure with the copper acting as the fibres any applied load would then be supported by one of these "fibres".

In the parent material of the arc brazed butt joints with low joint efficiency an area of microstructure was seen to etch more readily than the bulk of the material. This was as the result of depleted chromium in this region which had migrated to the braze as seen in the immersion trials.

The results of the volume fraction analysis suggested there was a correlation between the strength of an arc brazed joint and the cellular dendritic iron structures within the microstructure of the braze. However, only three joints were examined because the only method of fabricating brazes with varying volume fraction of cellular dendritic structures was to change the composition shielding gas. Spherical structures, which may have been porosity, were also included in the volume fraction analysis following optical microscopy which revealed that these appeared to be the same phase as the cellular dendritic structures. Transmission electron microscopy analysis of the joints would be required to ensure this assumption is correct.

When optimising the process parameters of similar material arc brazed butt joints it was found that, with a 0.8mm filler wire, a root gap of 0.7mm or greater would cause holes to be produced in the braze seam as the filler material could not bridge the gap.

Arc Brazing of Stainless Steels to Similar and Dissimilar Metals Discussion of Results

This demonstrates that less melting of the parent material is occurring than in welding, as in GMAW an empirical rule is that the root gap should be the same as the filler wire diameter. In joints manufactured using a root gap of 0.3mm or less the thermal expansion of the parent material prevented full penetration of the joint. Following tensile testing of arc brazed butt joints it was found that a 0.5mm root gap provided the optimum mechanical properties of all combinations of filler material and shielding gas which were not affected by LME. Following this it was initially attempted to manufacture dissimilar material butt joints using a 0.5mm root gap, however the braze seam did not have the required aesthetic properties required for the intended application in the automotive industry. By increasing the root gap to 0.6mm the braze seam of dissimilar material butt joints had the required aesthetic properties. As with the similar material joints it was not possible for the filler material to bridge a root gap in excess of 0.6mm.

The combination of BS:2901 C28 filler material and argon containing 1% oxygen shielding gas provided the optimum tensile properties for arc brazed butt joints for both similar and dissimilar parent material joints. From table 2.2 it can be seen that BS:2901 C28 filler material has the highest tensile strength. The addition of oxygen to argon increased the thermal conductivity of the shielding gas, reducing the viscosity and improving the wetting of the joint, however the addition 2% oxygen caused oxides to form on the surface of the parent material, reducing wetting and therefore the tensile properties of the joint.

Short circuit material transfer was used for similar material butt joints. However, when this was attempted with dissimilar material butt joints the instability of the arc

associated with short circuit transfer was increased by the presence of the zinc vapour. To improve the stability of the arc the arc variables were manipulated to achieve spray arc and a leading angle of 5° was introduced on the torch to remove the zinc vapour from the vicinity of the arc using the gas flow.

The values for the 0.2% proof stress of the similar and dissimilar material butt joints indicated that the samples yielded in the parent material. However, whilst the similar material joints failed in the braze material indicating a joint efficiency of less than 1 the dissimilar parent material joints failed in the mild steel meaning that the braze was stronger than the weakest parent material.

As could be expected from previous tensile testing indicating that the arc brazed joints yielded in the stainless steel, the ground and unground arc brazed butt joints yielded at similar loads. The difference in the maximum loads withstood, by ground and unground joints, prior to failure was attributed to the increased volume of material present in the unground joint, concluding that the braze reinforcement did not act as a stress raiser. However, if the joint reinforcement is to be ground for aesthetic purposes care must be taken to avoid producing notches in the material, which will act as stress raisers.

On initial inspection it appeared that arc brazed plug joints manufactured using BS:2901 C28 and argon containing 1% oxygen had similar impact properties to resistance spot welded joints. However, 6mm diameter resistance spot welded joints were trialled by Wray⁶¹ whilst in order to obtain correct wetting it was necessary to manufacture 8mm arc plug brazes. Whilst impact properties are not fundamental in

the same way as tensile strength comparing the impact resistance per unit area arc brazed plug joints were significantly more brittle than resistance spot welds.

The dissimilar metal butt joints failed in fatigue at a significantly lower load to the similar metal butt joints. It was concluded that this was due to the presence of LME in the dissimilar metal butt joints which was not present in the similar metal butt joints. When attempting to arc braze dissimilar metal butt joints the material transfer method was changed from short circuit transfer to spray arc transfer to aid the stability of the arc. This change increased the heat input per unit area increasing the residual stress in the material and provided more time for the molten braze to penetrate the stainless steel parent material. This resulted in LME of the dissimilar material butt joints.

When manufacturing similar metal arc brazed lap joints difficulty with wetting both sheets of stainless steel was experienced. The passive layer of the stainless steel is removed by the arc during the arc brazing process², due to the configuration of the lap joint the passive layer could not be removed simultaneously from both the top and the bottom plate, resulting in poor wetting of the bottom sheet of stainless steel.

Finally it has been found that if AISI grade 304 stainless steel is arc brazed an intermediate phase is produced at the interface of the braze and the parent material. The braze will then penetrate the grain boundaries of this phase by grain boundary grooving as proposed by Mullins⁵⁸. If the filler is contained within the intermediate phase embrittlement will not occur. However if the filler material penetrates into the bulk of the parent material the propagation is no longer controlled by grain boundary

grooving and will instead propagate in a direction normal to any applied or residual stress. If the filler material at the end of the propagation then forms a sharp angle it will act as stress raiser⁵⁷ causing the material to fail prematurely under an applied or residual stress. Penetration of the mild steel is inhibited by the formation of a band at the interface made up of iron from the mild steel and the continuant elements of the filler material.

6.0 Conclusions

- There is a significant difference in the fatigue properties of similar metal and dissimilar metal arc brazed butt joints due to the different metal deposition methods and pass velocities used in their manufacture.
- Both similar metal and dissimilar metal arc brazed joints can suffer from LME reducing the percentage elongation, although this can be reduced by using the appropriate arc variables and combination of filler material and shielding gas (BS:2901 C28 filler material and argon containing 1% oxygen shielding gas).
- The arc variables detailed in Appendix 1 produce braze seams with appropriate aesthetic appearance and minimal spatter for similar and dissimilar metal butt joints.
- By using a combination of BS:2901 C28 filler material and a shielding gas of argon containing 1% oxygen similar metal (AISI 304) butt joints can be produced with a 0.2% proof stress in excess of that of the parent material. Dissimilar metal butt joints can be produced again using BS:2901 C28 filler material and a shielding gas of argon containing 1% oxygen with a 0.2% proof stress in excess of that of AISI 304 grade stainless steel and an ultimate tensile strength in excess of Dogal 260 RP-x.
- A root gap of 0.5mm should be left between the faying surfaces of similar metal butt joints and a 0.6mm root gap should be used for dissimilar metal butt joints to optimise the aesthetics and mechanical properties of the joint when using BS:2901 C28 and argon containing 1% oxygen.
- Partial melting of the parent material must occur to produce a cellular dendritic structure within the matrix of the braze material in arc brazed joints

to achieve high joint efficiency. The volume fraction of these cellular dendritic structures is proportional to the strength of the similar metal butt joints.

- The braze reinforcement does not adversely affect the tensile properties of the joint.
- The BS:2901 C11 filler material produced the worst impact properties. BS:2901 C9 and BS:2901 C28 filler material produced comparable results and the addition of oxygen in the shielding for both these filler materials benefited the toughness, with 1% oxygen producing the highest impact properties.
- The addition of oxygen in the shielding gas improved the tensile properties of the three filler materials investigated in this study. For the BS:2901 C28 and BS:2901 C9 alloys the highest tensile strengths were found in joints manufactured using argon containing 1% oxygen and for BS:2901 C11 the highest tensile strengths were found in those joints manufactured using argon containing 2% oxygen.
- Of the filler material and shielding gas combinations investigated in this study BS:2901 C28 filler material and argon containing 1% oxygen shielding gas produces butt joints with the highest tensile and impact properties for similar metal butt joints.
- The zinc vapour produced during dissimilar metal joining results in a leading torch angle and spray arc metal transfer being necessary to maintain a stable arc.
- The passive oxide layer of stainless steel and the difference in torch height, in relation to the top and the bottom plate of a lap joint, due to the joint geometry, leads to problems with wetting of the joint.

- During the similar metal arc brazing using AISI grade 304 parent material and BS:2901 C28 filler material and argon containing 1% oxygen shielding gas grain boundary grooving as described by Mullins⁵⁸ occurs which appears to produce a composite type region in which the copper takes the role of the fibres and the iron grains taking the role of the matrix.

6.1 Summary

Gas metal arc brazing has been used to join stainless steel to stainless steel and zinc coated mild steel. Process parameters including arc variables, material transfer method and root gap have been optimised in terms of aesthetic appearance and tensile properties for a number of filler material and shielding gas combinations. The combination of BS:2901 C28 filler material and argon containing 1% oxygen shielding gas provided the best compromise of aesthetic appearance and tensile properties.

Similar metal butt joints have a joint efficiency of less than 1 in tensile testing but demonstrate a 0.2% proof stress in excess of the parent material. Dissimilar metal butt joints have a joint efficiency of 1 with the arc brazed joint being stronger than the zinc coated mild steel. The combination of BS:2901 C28 filler material and argon containing 1 % oxygen shielding gas produced the highest impact toughness although this was still significantly less than that achieved for resistance spot welded joints.

Difficulty is experienced with wetting when trying to manufacture, stainless steel to stainless steel, arc brazed lap joints. As the arc passes along the stainless steel it

removes the passive layer. However the arc will only contact one sheet in the lap joint and so the other sheet will retain its passive layer preventing wetting.

The microstructure of arc brazed joints has been examined. During the process partial melting of the parent material occurs and cellular dendritic structures of iron form within the braze material, with the volume fraction of these cellular dendritic structures appearing to be proportional to the strength of the joint. An intermediate phase is formed at the interface of the braze and the stainless steel which is penetrated by braze material. The mechanism by which this penetration takes place is Mullin's Grooving. If the penetration continues into the bulk of the parent material Mullin's grooving ceases to be the mechanism for propagation and instead the molten braze material is drawn in a direction normal to any applied load or residual stress. If the end of the filler material solidifies into a sharp angle it will act as a stress raiser embrittling the material. When manufacturing dissimilar metal butt joints the arc variables were manipulated to achieve spray arc transfer in order to maintain a stable arc in the presence of zinc vapour. This led to a greater heat input, increasing residual stress in the material and resulting in a longer time to solidification, allowing the molten braze to penetrate through the intermediate phase and into the parent material. This embrittled the joint resulting in fatigue properties which were significantly lower than the similar parent material results.

7.0 Further Work

- An investigation into the residual stresses caused by the restraint within the assembly of a car body of panels that are to be arc brazed.
- An investigation into the problems, if any, of primer adhesion of arc brazed joints.
- Further manipulation of the arc brazing variables in order to reduce the braze profile and limit distortion for dissimilar butt joints.
- Further studies are required into the wetting of arc brazed lap joints to assess the feasibility of this joint geometry.
- Verification of the correlation between volume fraction to tensile strength for arc brazed joints manufactured using BS:2901 C28 filler material and argon containing 1% oxygen shielding gas.
- An investigation using Transmission Electron Microscopy to establish whether the spherical features in figures 5.1 and 5.2 were the same phase as the cellular dendritic structures.
- Measurement of the increase in surface area caused by the localised melting of the interface between the stainless steel and the braze material.
- An investigation into the fatigue properties of similar metal butt joints produced using spray arc transfer for comparison to the dissimilar metal butt joints.
- Further studies to see if the fatigue properties of dissimilar parent material joints can be improved.

- Development of a model to ascertain if the Mullins' grooving occurring at the interface of the stainless steel and braze alloy was acting in a similar manner to a composite.

APPENDIX 1

***Optimal Process Parameters For the Manufacture of Similar
and Dissimilar Metal Butt Arc Brazed Butt Joints Using AISI
304 Parent Material and Various Combination of Filler Material
and Shielding Gases***

Similar Metal Butt Joints:

BS:2901 C28 Filler Material and Pure Argon Shielding Gas

Wire Feed	2.5 m/min
Voltage	26V
Base Current	23 A
Current Rise	1000 A/ms
Pulsing Current	325 A
Pulsing Current Time	1.1 ms
Current Drop	1000 A/ms
Droplet Detachment Current	40 A
Droplet Detachment Time	1.1 ms
Pulsing Frequency	20 Hz
Torch Angle	90° to work piece
Pass Velocity	102 cm.min ⁻¹

BS:2901 C28 Filler Material and argon containing 1% oxygen Shielding Gas

Wire Feed	2.5 m/min
Voltage	22.09V
Base Current	18.7 A
Current Rise	1000 A/ms
Pulsing Current	310 A
Pulsing Current Time	1.5 ms
Current Drop	1000 A/ms
Droplet Detachment Current	40.9 A
Droplet Detachment Time	1.5 ms
Pulsing Frequency	23.9 Hz
Torch Angle	90° to work piece
Pass Velocity	114 cm.min ⁻¹

BS:2901 C28 Filler Material and Argon Containing 2% Oxygen Shielding Gas

Wire Feed	3.8 m/min
Voltage	24.3V
Base Current	34.5 A
Current Rise	650 A/ms
Pulsing Current	360 A
Pulsing Current Time	1.2 ms
Current Drop	1000 A/ms
Droplet Detachment Current	56 A
Droplet Detachment Time	1.34 ms
Pulsing Frequency	42.5 Hz
Torch Angle	90° to work piece
Pass Velocity	64 cm.min ⁻¹

BS:2901 C9 Filler Material and Pure Argon Shielding Gas

Wire Feed	2 m/min
Voltage	21V
Base Current	15 A
Current Rise	650 A/ms
Pulsing Current	360 A
Pulsing Current Time	1.2 ms
Current Drop	1000 A/ms
Droplet Detachment Current	30 A
Droplet Detachment Time	2 ms
Pulsing Frequency	20 Hz
Torch Angle	90° to work piece
Pass Velocity	102 cm.min ⁻¹

BS:2901 C9 Filler Material argon containing 1% oxygen Shielding Gas

Wire Feed	4.2 m/min
Voltage	24.3V
Base Current	34.5 A
Current Rise	650 A/ms
Pulsing Current	360 A
Pulsing Current Time	1.2 ms
Current Drop	1000 A/ms
Droplet Detachment Current	56 A
Droplet Detachment Time	1.34 ms
Pulsing Frequency	42.5 Hz
Torch Angle	90° to work piece
Pass Velocity	114 cm.min ⁻¹

BS:2901 C9 Filler Material and Argon Containing 2% Oxygen Shielding Gas

Wire Feed	4.2 m/min
Voltage	24.3V
Base Current	34.5 A
Current Rise	650 A/ms
Pulsing Current	360 A
Pulsing Current Time	1.2 ms
Current Drop	1000 A/ms
Droplet Detachment Current	56 A
Droplet Detachment Time	1.34 ms
Pulsing Frequency	42.5 Hz
Torch Angle	90° to work piece
Pass Velocity	64 cm.min ⁻¹

BS:2901 C11 Filler Material and Pure Argon Shielding Gas

Wire Feed	3.7 m/min
Voltage	27.5V
Base Current	22 A
Current Rise	1000 A/ms
Pulsing Current	330 A
Pulsing Current Time	1 ms
Current Drop	1000 A/ms
Droplet Detachment Current	45 A
Droplet Detachment Time	1.05 ms
Pulsing Frequency	30 Hz
Torch Angle	90° to work piece
Pass Velocity	102 cm.min ⁻¹

BS:2901 C11 Filler Material and argon containing 1% oxygen Shielding Gas

Wire Feed	4 m/min
Voltage	23V
Base Current	20 A
Current Rise	1000 A/ms
Pulsing Current	300 A
Pulsing Current Time	0.7 ms
Current Drop	1000 A/ms
Droplet Detachment Current	45 A
Droplet Detachment Time	2.5 ms
Pulsing Frequency	30 Hz
Torch Angle	90° to work piece
Pass Velocity	114 cm.min ⁻¹

BS:2901 C11 Filler Material and Argon containing 2% Oxygen Shielding Gas

Wire Feed	3.5 m/min
Voltage	25V
Base Current	20 A
Current Rise	1000 A/ms
Pulsing Current	300 A
Pulsing Current Time	0.7 ms
Current Drop	1000 A/ms
Droplet Detachment Current	45 A
Droplet Detachment Time	2.5 ms
Pulsing Frequency	30 Hz
Torch Angle	90° to work piece
Pass Velocity	64 cm.min ⁻¹

Dissimilar Metal Butt Joints

BS:2901 C28 Filler Material and argon containing 1% oxygen Shielding Gas

Wire Feed	4.3 m/min
Voltage	27.5V
Base Current	25 A
Current Rise	1000 A/ms
Pulsing Current	310 A
Pulsing Current Time	0.8 ms
Current Drop	1000 A/ms
Droplet Detachment Current	38 A
Droplet Detachment Time	1.5 ms
Pulsing Frequency	40 Hz
Torch Angle	85° to work piece
Pass Velocity	89 cm.min ⁻¹

BS:2901 C9 Filler Material and argon containing 1% oxygen Shielding Gas

Wire Feed	4.4 m/min
Voltage	27.5V
Base Current	42.7 A
Current Rise	650 A/ms
Pulsing Current	360 A
Pulsing Current Time	1.2 ms
Current Drop	1000 A/ms
Droplet Detachment Current	67 A
Droplet Detachment Time	1.24 ms
Pulsing Frequency	55 Hz
Torch Angle	85° to work piece
Pass Velocity	89 cm.min ⁻¹

APPENDIX 2

Volume Fraction Images

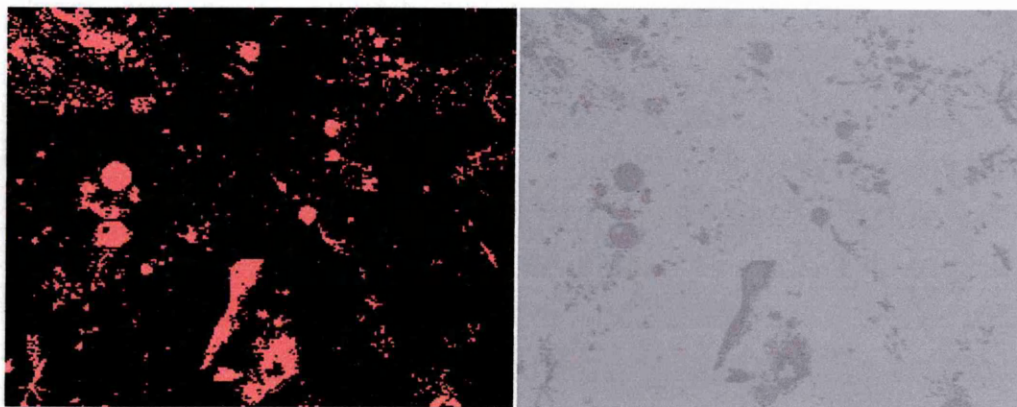
Sample 65 (BS:2901 C28 filler material argon containing 1% oxygen)

Area a

AREA MEASUREMENT RESULTS

Image: (untitled)

Class	:	%total	%classified
Band 1	:(118-137)	09.1	100.0
Unclassified	:	90.9	

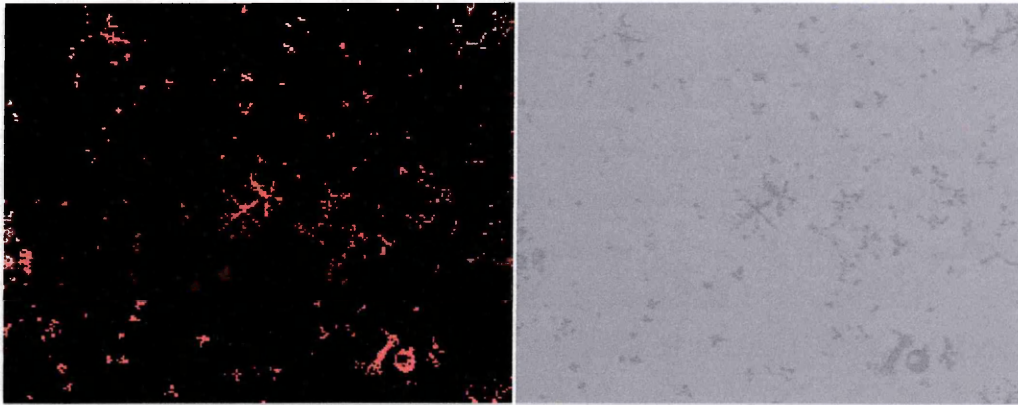


Area b

AREA MEASUREMENT RESULTS

Image: (untitled)

Class	:	%total	%classified
Band 1	:(124-137)	02.6	100.0
Unclassified	:	97.4	

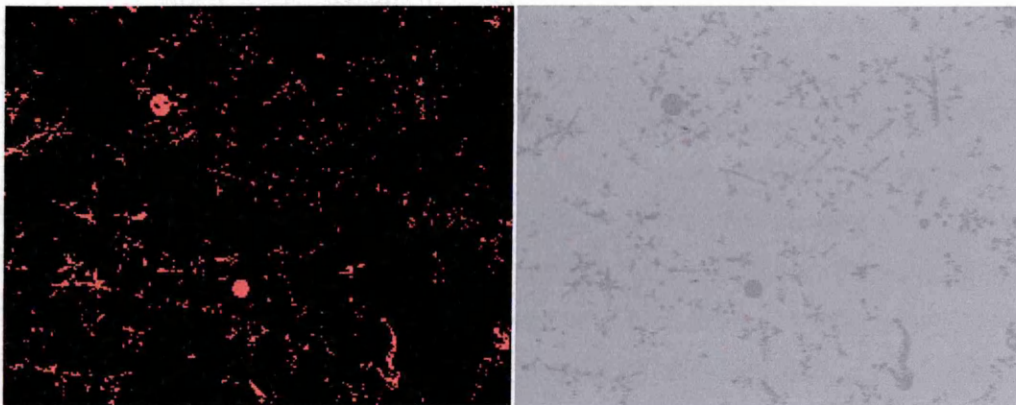


Area c

AREA MEASUREMENT RESULTS

Image: (untitled)

Class	:	%total	%classified
Band 1	:(124-137)	03.5	100.0
Unclassified	:	96.5	

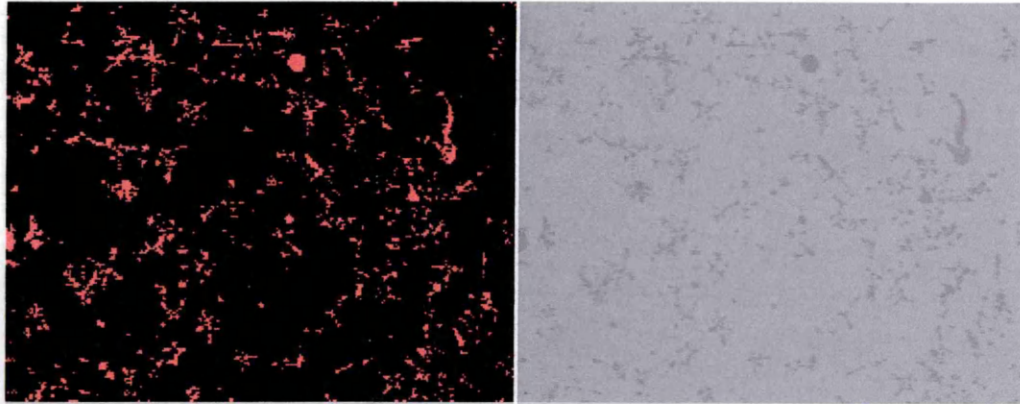


Area d

AREA MEASUREMENT RESULTS

Image: (untitled)

Class	:	%total	%classified
Band 1	:(127-147)	07.1	100.0
Unclassified	:	92.9	

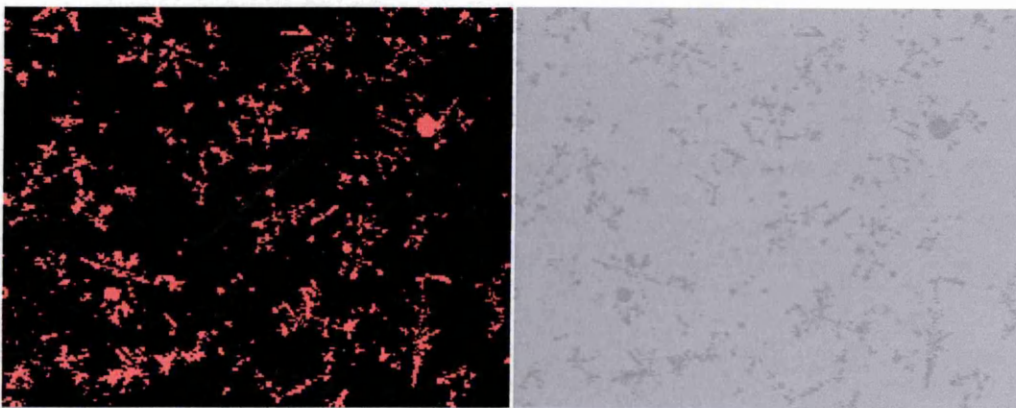


Area e

AREA MEASUREMENT RESULTS

Image: (untitled)

Class	:	%total	%classified
Band 1	:(130-154)	09.0	100.0
Unclassified	:	91.0	



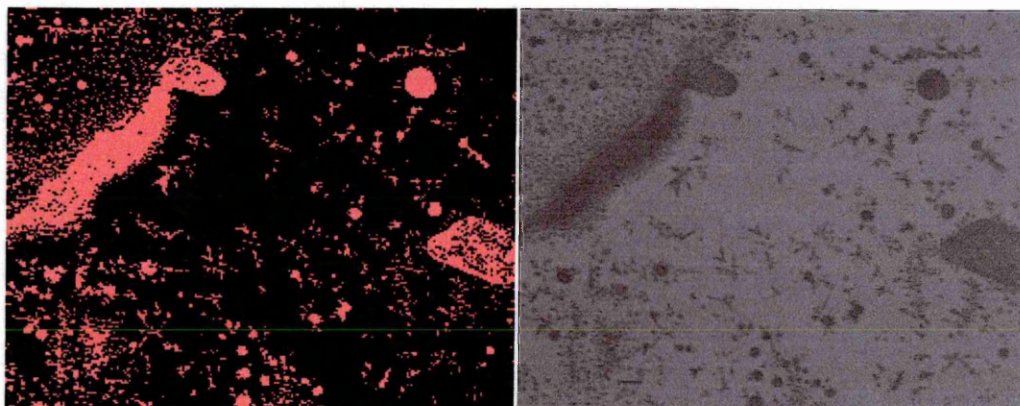
Sample 67 (BS:2901 C28 filler material argon containing 1% oxygen)

Area a

AREA MEASUREMENT RESULTS

Image: (untitled)

Class	:	%total	%classified
Band 1	:(077-093)	16.5	100.0
Unclassified	:	83.5	

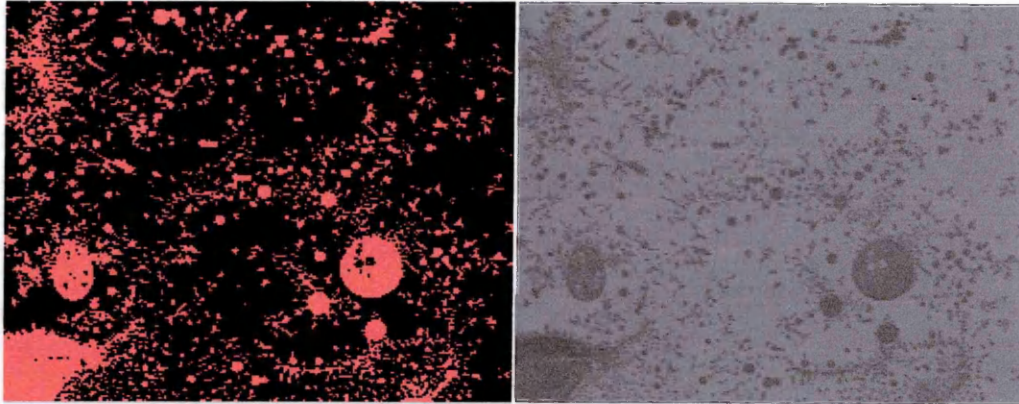


Area b

AREA MEASUREMENT RESULTS

Image: (untitled)

Class	:	%total	%classified
Band 1	:(000-112)	21.6	100.0
Unclassified	:	78.4	

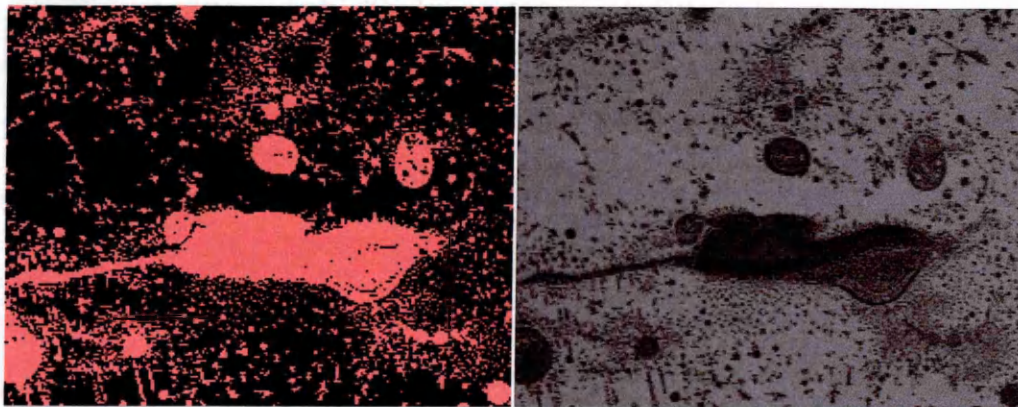


Area c

AREA MEASUREMENT RESULTS

Image: (untitled)

Class	:	%total	%classified
Band 1	:(028-080)	27.1	100.0
Unclassified	:	72.9	

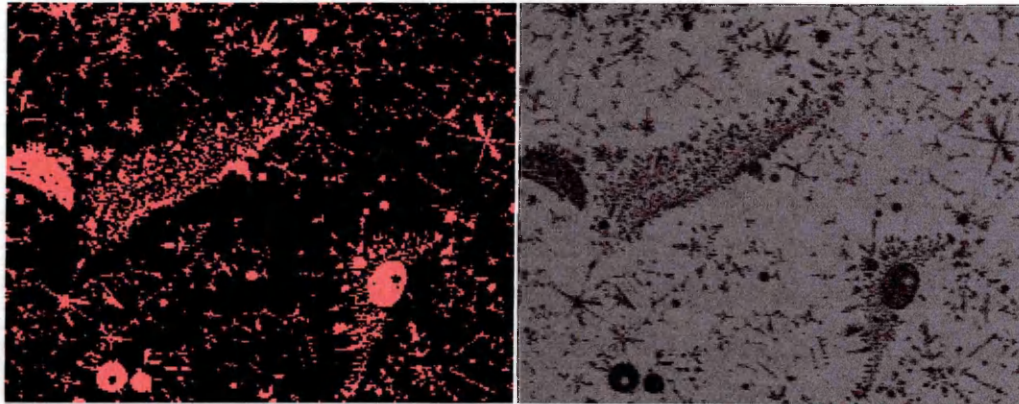


Area d

AREA MEASUREMENT RESULTS

Image: (untitled)

Class	:	%total	%classified
Band 1	:(028-080)	15.5	100.0
Unclassified	:	84.5	

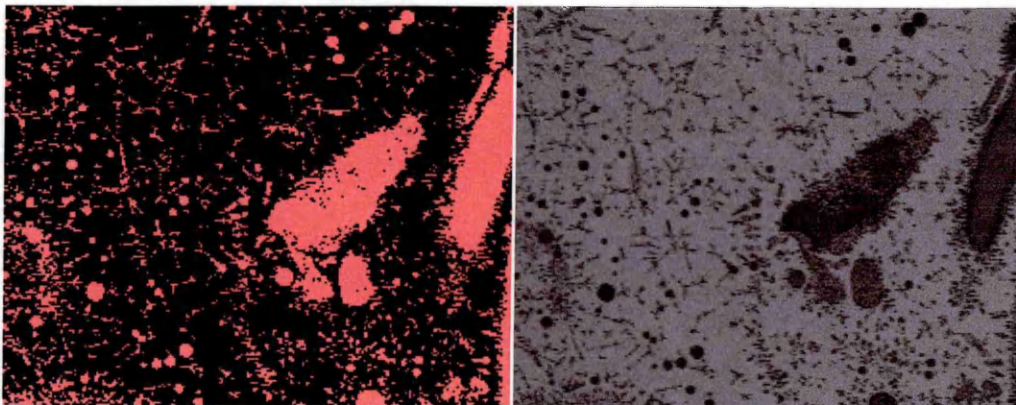


Area e

AREA MEASUREMENT RESULTS

Image: (untitled)

Class	:	%total	%classified
Band 1	:(028-081)	23.8	100.0
Unclassified	:	76.2	



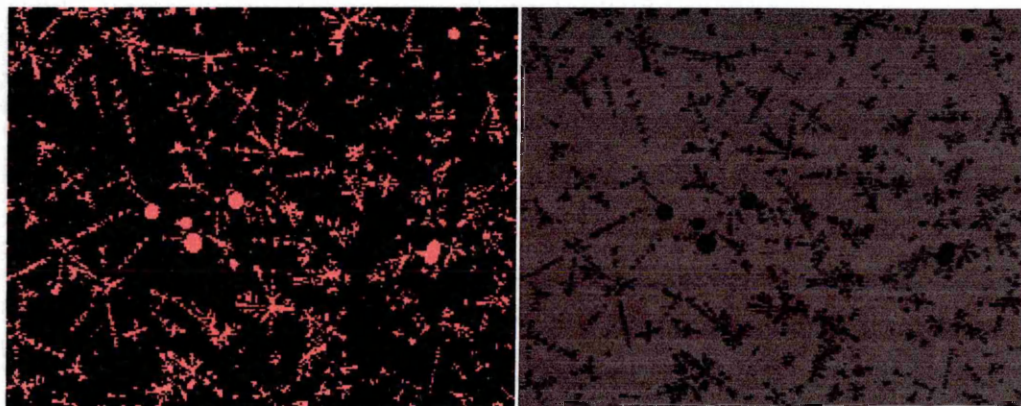
Sample 69 (BS:2901 C28 filler material and argon containing 2% oxygen)

Area a

AREA MEASUREMENT RESULTS

Image: (untitled)

Class	:	%total	%classified
Band 1	:(033-055)	11.4	100.0
Unclassified	:	88.6	

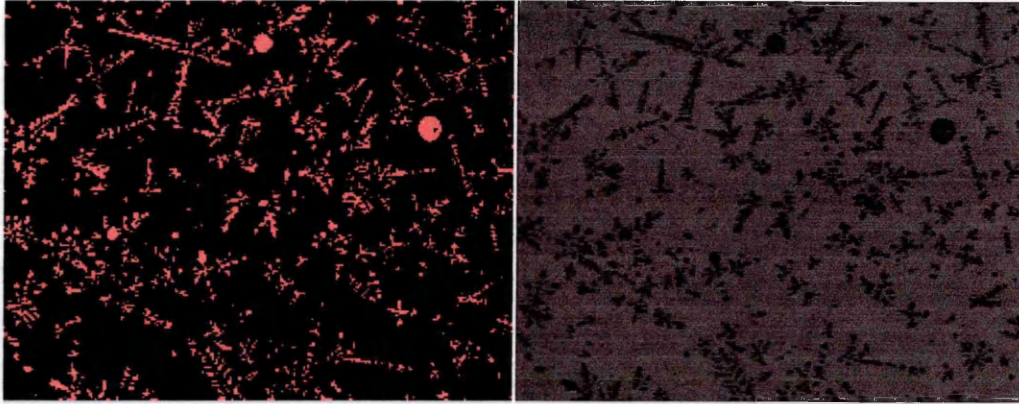


Area b

AREA MEASUREMENT RESULTS

Image: (untitled)

Class	:	%total	%classified
Band 1	:(033-055)	10.1	100.0
Unclassified	:	89.9	

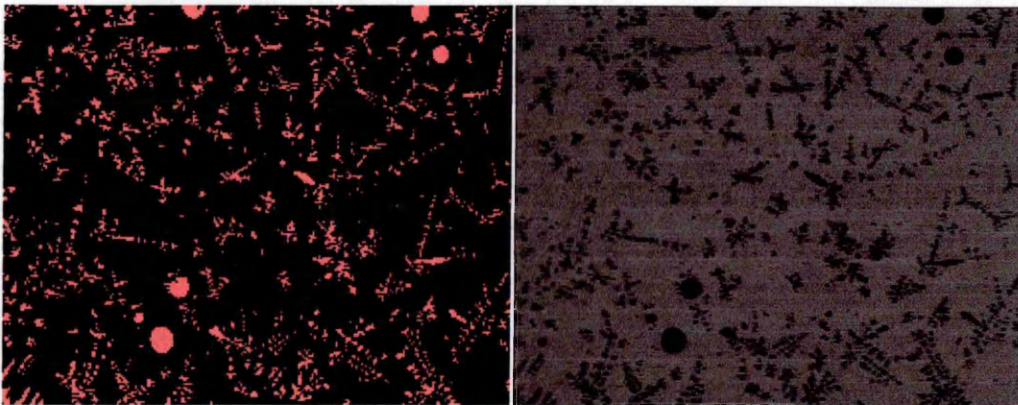


Area c

AREA MEASUREMENT RESULTS

Image: (untitled)

Class	:	%total	%classified
Band 1	:(036-055)	10.0	100.0
Unclassified	:	90.0	

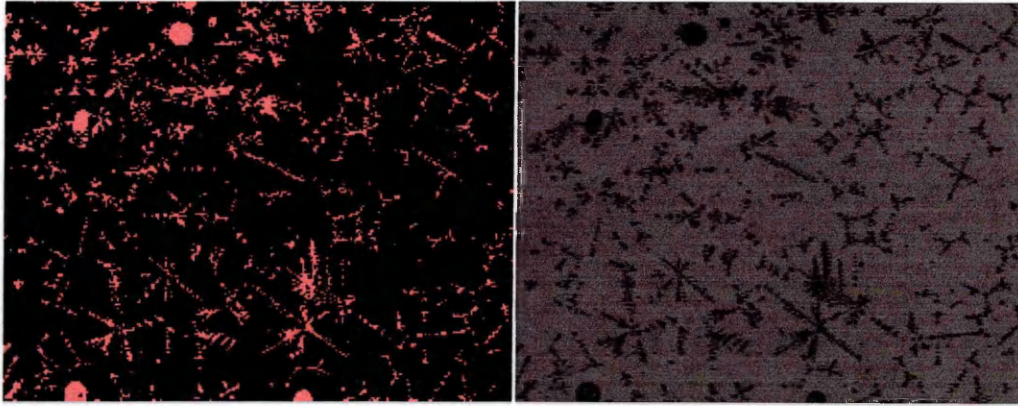


Area d

AREA MEASUREMENT RESULTS

Image: (untitled)

Class	:	%total	%classified
Band 1	:(036-056)	09.5	100.0
Unclassified	:	90.5	

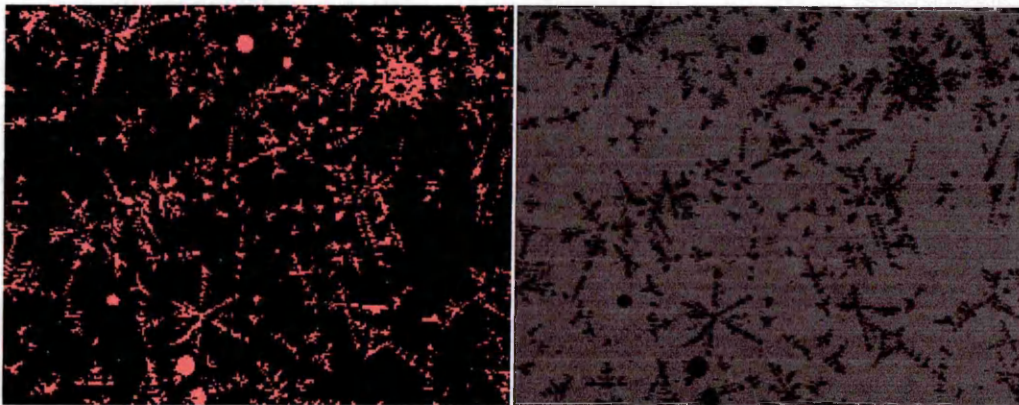


Area e

AREA MEASUREMENT RESULTS

Image: (untitled)

Class	:	%total	%classified
Band 1	:(036-056)	10.6	100.0
Unclassified	:	89.4	



References

- ¹ R. V. Hughes, G Dryburgh and S Garbett “Plasma Braze Welding In Autobody Production at Jaguar Cars” *Welding and Metal Fabrication*, March 1995, **Vol 3**, pp110-111
- ² Peter Nerman and Elisabeth Öhman, “Arc and laser brazing of steel sheets – a literature study”, *Swedish Institute of Metals Research Report*, October 2002.
- ³ W Gawrysiuk, M Rozanski and M Wojcik, “Braze Welding. Examples of the bonding of difficult to weld material systems”, *Welding International*, 2007, **Vol 21** (3) pp180 – 184
- ⁴ Jason Wong Soon Wai “Arc Brazing Of Stainless Steels”, *MSc dissertation available in the Sheffield Hallam University Library and Learning Resource Centre*, (2002/2003).
- ⁵ *Steels Metallurgy and Applications*, Chapter 4. 3rd Edition By D. T. Llewellyn, Roger C. Hudd. ISBN: 0-7506-3757-9.
- ⁶ *Stainless Steels and Their Properties* by Avesta Sheffield AB Research Foundation
- ⁷ *Austenitic Stainless Steel: Microstructure and Mechanical Properties*, Chapter 1. By P. Marshall (1984). ISBN 0-85334-277-6.

⁸ Diagram sourced from: New Hampshire Materials Laboratory Inc, 22 Interstate Drive, Somerworth, NH. 03878. USA.

⁹ Steels Microstructure and Properties, Chapter 12. 3rd Edition by H. K. D. H. Bhadeshia and R. W. K. Honeycomb (2006). ISBN13: 978-0-750-68084-4

¹⁰ Austenitic Stainless Steel: Microstructure and Mechanical Properties, Chapter 3. By P. Marshall (1984). ISBN 0-85334-277-6.

¹¹ Engineering Materials Technology, Chapter 9. By W Bolton. Third Edition (1998). ISBN: 0-7506-3917-2.

¹² The Metallurgical Evolution of Stainless Steels, Page 30. Edited by F.B. Pickering (1979). ISBN 0-87170-077-8.

¹³ Metallurgy of Welding, Chapter 9. By J. F. Lancaster Sixth Edition (1999) ISBN: 1-85573-428-1

¹⁴ Introduction to Stainless Steels, Chapter 7. By Jonathan Beddoes and J Gordon Parr. Third Edition (1999). ISBN 0-87170-673-3.

¹⁵ Welding Handbook, Volume 2, Welding Processes, Chapter 4. By The American Welding Society Eighth Edition (1991). ISBN 0-87171-354-3

16 The Metallurgical Evolution of Stainless Steels, Page 276. Edited by F.B. Pickering (1979). ISBN 0-87170-077-8.

17 A.S. Guimaraes, M. T. Mendes, H. R. M. Costa, J. Da Silva Mchado, N.K. Kuromoto, “An evaluation of the behaviour of a zinc layer on a galvanised sheet, joined by MIG brazing” *Welding International*, 2007, **Vol 21** (4), pp271-278.

18 AF Rangel, LA Manlakhova, RP Da Rocha Paranhos and AN Matlakhov, “Evaluation of MIG – brazing welded joints by means of metallographic techniques” *Welding International*, 2006, **Vol 20** (11), pp889-893.

19 Information sourced from: United States Steel Corporation, 600 Grant Street, Pittsburgh, PA. 15219. USA

20 Information sourced from: American Iron and Steel Institute (AISI), 680 Andersen Drive, Pittsburgh, PA. 15220. USA.

21 D. W. Dickinosn, “Bumper Component Welding state-of-the-art survey” *ISI Bumper Project Group*, Dec 2000.

22 Pocket book of Steel – Corus Automotive. Available from Corus Automotive Engineering. International Automotive Research Centre, University of Warwick, Coventry. CV4 7AL. UK.

23 Steels Metallurgy and Applications, Chapter 1. By D. T. Llewellyn, Roger C. Hudd. Third Edition (1998) ISBN: 0-7506-3757-9.

24 The Making, Shaping and Treating of Steel, Chapter 44. Edited by Harold E. McGannon. Ninth Edition (1971).

25 A. Winiowski, "Brazing of metals – consumables, technologies and standardisation", *Welding International*, April 2008, **Vol 22** (3), Pages 245 – 248

26 Materials and Processes In Manufacturing, Chapter 37. By E. Paul DeGarmo, J. T. Black, and Ronald A. Kohser. Eighth Edition (1997). ISBN 0-02-328621-0

27 Brazing for the Engineering Technologist, Chapter 2. By M. Schwartz (1995). ISBN 0 412 59510 9.

28 Soldering and Brazing Technology. Part 2. Brazing, Chapter 11. By S. Collard Churchill. (1963).

29 Z.-S. Yu, Y. Qian, M.-F. Wu, F.-J. Wang and K. Qi, "Interfacial Distribution of Elements and Fracture Behaviour of Metal Inert Gas Brazed Joint with Copper Based Filler Metals", *Materials Science Technology*, September 2002 **Vol 18** (9), pp1045-1048

³⁰ M Menzel, "The Influence of Individual Components of an Industrial Gas Mixture on the Welding Process and the Properties of Welded Joints", *Welding International*, 2003 **Vol 17** (4), pp262-264.

³¹ *Welding and Cutting: A Guide to Fusion Welding and Associated Cutting Processes*, Chapter 5. By P. T. Houldcroft, Robert John ISBN:1 85573 578 4

³² Luisa Quintino, Gervasio Pimenta, Danut Iordachescu, R. M. Miranda and N.V. Pepe, "MIG Brazing of galvanised thin sheet joints for the automotive industry", *Materials and Manufacturing Processes*, 2006, **Vol 21**, pp63-73.

³³ Daunt Iordacescu, Luisa Quintino, Rosa Miranda, Geervasio Pimenta, "Influence of shielding gases and process parameters on metal transfer and bead shape in MIG brazed joints of the thin zinc coated steel plates", *Materials and Design*, 2006, **Vol 27**, pp381-390.

³⁴ B. Joseph, M. Picat and F. Barbier, "Liquid Metal Embrittlement: A state-of-the-art appraisal" *The European Physical Journal*, October 1998, no 5 pp19-31.

³⁵ ASM ready reference: Thermal properties of metals Chapter 2. By Fran Cverna, ASM International. Materials Properties Database Committee. ISBN: 0-87170-768-3

³⁶ Data Sourced from Outokumpu Stainless Oyj, Riihitontuntie 7, PO Box 140, FIN-02201 Espoo.

³⁷ Data Sourced from SSAB Swedish Steel Ltd. Tel +44 1905 795794

³⁸ R.-F. Li, Z.-S. Yu, K. Qi, F.-M. Zhou, M.-F. Wu and C. Yu, "Growth Mechanisms of Interfacial Compounds in Arc Brazed Galvanised Steel Joints With Cu₉₇Si₃ Filler" *Materials Science and Technology*, Apr 2005, **Vol 21** (4), pp 483 - 487. ISSN 0267-0836.

³⁹ R.-F. Li, Z.-S. Yu and K. Qi, "Interfacial structure and joint strengthening in arc brazed galvanized steels with copper based filler", *Transactions of the Non-ferrous Met. Soc. China*, 2006, **Vol 16**, pp397-401.

⁴⁰ K. A. Lyttle and W.F.G. Stapon, "Select the best Shielding Gas Blend for the Application", *Welding Journal*, November 1990, **Vol 69** (11), pp21-27. ISSN: 0043-2296.

⁴¹ John Medforth, "Shielding Gases for Stainless Steels", *The Australian Welding Journal*, 1993, **Vol 38**, pp12, 14-15. ISSN: 1039-0642.

⁴² A. Kersche and S. Trube, "Shielding Gases for Gas-Shielded Metal Arc Brazing", *originally presented at "Thin Sheet Metal Conference" 28th March 2000.*

⁴³ Chemical Metallurgy, Chapter 4. By J. J. Moore. Second Edition (1990). ISBN 0-408-05369-0.

44 William Cording, "Go With the Flow: How shielding gas affects welds, productivity" *Practical Welding Today*, November/December 2002, **Vol 6 (6)**, pp26-28. ISSN: 1092-3942.

45 Data sourced from Weldability/SIF, Petere House, The Orbital Centre, Ickenfield Way, Letchworth Garden City, Hertfordshire, SG6 1ET.

46 Private Communications with F. Burgin

47 Engineering Materials Technology, Chapter 21. By W Bolton. Third Edition (1998). ISBN: 0 7506 3917 2

48 P. J. Withers and H. K. D. H. Bhadeshia, "Residual Stresses Part 1 - Measurement Techniques", *Material Science and Technology*, 2001, **Vol 17**, pp355-365.

49 Fatigue of Materials, Chapter 1. By S Suresh. Second Edition (1998). ISBN: 0-521-57847-7

50 Fatigue of Structures and Materials, Chapter 2. By Jaap Schijve. Second Edition (2009). ISBN: 978-1-4020-6807-2

51 Metal Fatigue, Chapter 6. By N.E. Frost, K.J. Marsh and L.P. Pook (1974). ISBN: 0-198-56114-8

52 Private communications with A. Clifton

⁵³ Sheng-Kuei Lin; Yung-Li Lee and Min-Wei Lu, "Evaluation of the Staircase and the Accelerated Test Methods of Fatigue Limit Distributions", *International Journal of Fatigue*, 2003, **Vol 23**, pp75 – 83.

⁵⁴ Fatigue Testing and Analysis of Results, Chapter 9. By W. Weibull. (1961). Library of Congress Card no. 59-14498.

⁵⁵ R. Pollak; A. Palazotto and T. Nicholas, "A Simulation-Based Investigation of the Staircase Method of Fatigue Testing", *Mechanics of Materials*, 2006, **Vol 38**, pp1170 - 1181.

⁵⁶ A Statistical Analysis Of The Fatigue Behaviour Of Single And Multi-Spot Welded Joints by Andrew Clifton. PhD Thesis, Sheffield Hallam University

⁵⁷ E.E Glickman, "Grain Boundary Grooving Accelerated by Local Plasticity as a Possible Mechanism for Liquid Metal Embrittlement", *Interface Science*, 2003, **Vol 11**, pp451-459.

⁵⁸ W. W. Mullins, "Grain Boundary Grooving by Volume Diffusion", *Transactions of the Metallurgical Society of AIME*, April 1960, **Vol 218**, pp354-361.

⁵⁹ Fisher et al, "Preparative Steps Towards the New Definition of the Kelvin in Terms of the Boltzmann Constant" , *International Journal of Thermodynamics*, Dec 2007, **Vol 28** (6),. ISSN 0195-928X (Print) 1572-9567 (Online) Pages 1753-1765.

60 BS EN 10002-1:2001

61 Resistance Spot Welding of Duplex Stainless Steel by Timothy Marc Wray 2004
PhD Thesis, Sheffield Hallam University.

62 Extractive Metallurgy of Molybdenum Chapter 1. By C. K. Gupta.
ISBN: 0-8493-4758-0

63 Smithells Metals Reference Book, Chapter 8. 6th Edition. Edited by Eric A
Brandes. ISBN 0-408-71053-5.

64 Smithells Metals Reference Book, Chapter 14. 6th Edition. Edited by Eric A
Brandes. ISBN 0-408-71053-5.

65 Private communications with Prof. S Hertzman.

66 Y. Lui and Q. Zhao, "Influence of Surface Energy of Modified Surfaces on
Bacterial Adhesion", *Biophysical Chemistry*, 2005, **Vol 117**, pp39-45.

67 K.H. Stienmetz et al, "Diffusion of Iron in Copper Studied by Mössbauer
Spectroscopy on Single Crystals", *Physical Review B*, July 1986, **Vol 34** (1),
pp107-116.